



**TUS**

**Technological University of the Shannon:  
Midlands Midwest**

Ollscoil Teicneolaíochta na Sionainne:  
Lár Tíre Iarthar Láir

**BIOCOMPATIBLE POLYMER SYSTEM  
DEVELOPMENT WITH ENHANCED  
ANTIMICROBIAL PROPERTIES USING THE  
ADDITIVE EFFECT OF TRIANGULAR  
SILVER NANOPATES AND CURCUMIN**

Thesis Report

For PhD Polymer Engineering

Submitted by Eduardo Lanzagorta Garcia

Supervisor: Dr. Margaret E. Brennan-Fournet

Co-supervisors: Dr. Declan Devine and Dr. Marija Mojicevic

## Declaration of Authorship

I hereby certify that this material, which I now submit for assessment on the program of study leading to the award of PhD by Research program in Materials Research Institute, Technological University of the Shannon – Athlone Campus is entirely my own work and has not been taken from the work of others and to the extent that work has been cited and acknowledged within the text of my own work.

I confirm that:

- This work was done wholly or mainly while in candidature for a research degree at Technological University of the Shannon – Athlone Campus.
- Where any part of this thesis has been previously been submitted for a degree or any other qualification at this University or any other institution, this has been clearly stated.
- Where I have consulted the published work of others, this is always clearly attributed.
- Where I have quoted from the others, the source is always given.
- With the exception of such quotations, this thesis is entirely my own work.
- I have acknowledged all main sources of help.

Signed: Eduardo Lanzagorta Garcia Date: 21/10/22

## **Acknowledgements**

I would like to extend my heartfelt gratitude and appreciation to all those who have contributed to the completion of this thesis. Without their support, encouragement, and guidance, this endeavor would not have been possible.

First and foremost, I express my deepest gratitude to my supervisors, Dr. Margaret Brennan-Fournet, Dr. Marija Mojicevic and Dr. Declan Devine for their invaluable support throughout this research. Their expertise, patience, and encouragement have been instrumental in shaping this thesis and my overall growth as a researcher.

My heartfelt thanks go to the faculty members and staff of Technological University of the Shannon, Athlone Campus, whose dedication and commitment to education have provided me with an enriching academic experience.

I am indebted to my friends and fellow students who have been a constant source of motivation and support. Your encouragement and camaraderie have made this journey enjoyable and memorable. A special mention goes to my dear friend and colleague, Laura G. Rodriguez Barroso. We embarked on our PhD journey together in a new country, and our constant mutual support was fundamental in successfully overcoming the personal and academic challenges that this process entailed. Now, we are also finishing this remarkable journey together.

I am deeply grateful to my family for their unwavering love, understanding, and encouragement throughout my academic pursuit. Their belief in me has been the driving force behind my accomplishments.

I would also like to express my gratitude to the institutional President's Seed Fund for their financial support, which made it possible for me to focus on my research without additional worries.

Last but not least, I extend my heartfelt appreciation to all the participants and respondents who generously shared their time and insights for this study. Your contributions have been invaluable.

In conclusion, this thesis is a collective effort, and I am sincerely grateful to everyone who has played a part in its realization. Your support and encouragement have been crucial, and I am forever thankful for your presence in my life.

Thank you all.

Sincerely,

Eduardo

## TABLE OF CONTENTS

LIST OF FIGURES .....	8
LIST OF TABLES .....	12
ABBREVIATIONS .....	13
RELEVANT PUBLICATIONS.....	16
ABSTRACT.....	17
CHAPTER 1 – INTRODUCTION .....	18
1.1 Research Challenge .....	18
1.2 Solution Proposed .....	19
1.3 Objectives.....	20
1.4 Research Question.....	20
CHAPTER 2 – LITERATURE REVIEW .....	21
2.1 Overview .....	21
2.2 Silver nanostructures .....	22
2.2.1 Synthesis of Silver Nanoparticles .....	23
2.3 Triangular Silver Nanoplates (TSNP).....	25
2.3.1 Synthesis of TSNP .....	26
2.3.2 TSNP as Nansosensors .....	27
2.3.3 Antimicrobial Activity .....	30
2.3.4 Toxicity Concerns of AgNPs for Humans .....	34
2.3.5 TSNP-Polymer blending .....	37
2.4 Curcumin.....	38
2.4.1 Curcumin-Polymer blending.....	40
2.4.2 Curcumin-Silver Combined Effect .....	40
2.5 Embedding of Silver Nanoparticles (AgNP) into Polymers and Biopolymers.....	42
2.5.1 Polypropylene .....	42
2.5.2 Polycarbonate.....	43
2.5.3 Polycaprolactone.....	44
2.5.4 Polylactic acid.....	45
2.5.5 Bacterial Cellulose .....	47
CHAPTER 3 – MATERIALS AND METHODS .....	50
3.1 TSNP .....	50
3.1.1 Materials .....	50

3.1.2 Synthesis of TSNP .....	50
3.1.2.1 Optimised Method for TSNP Synthesis .....	51
3.1.2.2 Scale-Up of TSNP Production .....	52
3.1.2.3 UV-Vis Spectroscopy for Monitoring of the Optical Properties of TSNP .....	53
3.1.3 TSNP Gold Coating .....	53
3.1.3.1 AuTSNP Sucrose Sensitivity Test .....	54
3.1.3.2 AuTSNP for Fibronectin (Fn) Detection .....	54
3.1.4 TSNP Thermal Evaluation .....	54
3.1.4.1 TSNP Concentration by Water Evaporation .....	55
3.1.5 TSNP protection using halloysite nanotubes .....	55
3.1.6 Transfer of TSNP to Chloroform .....	56
3.2 Integration of TSNP in Polymers .....	57
3.2.1 Materials .....	57
3.2.2 Bacterial Cellulose (BC) production method .....	57
3.2.3 Extrusion .....	58
3.2.3.1 Post-Extrusion Incorporation on PCL .....	58
3.2.4 Solvent casting .....	59
3.2.5 Ex-situ incorporation of TSNP .....	60
3.2.5.1 Incorporation into BC .....	60
3.2.5.2 Incorporation into PCL and PLA .....	61
3.2.6 Stability Assay .....	62
3.2.6.1 Stability on Water and NaCl .....	62
3.2.6.2 Stability in Potassium Chloride .....	62
3.2.7 Materials characterisation .....	63
3.2.7.1 Scanning Electron Microscope (SEM) Analysis .....	63
3.2.7.2 Thermal properties .....	63
3.2.7.2.1 Differential Scanning Calorimetry (DSC) Analysis .....	63
3.2.7.2.2 Thermogravimetric (TGA) Analysis .....	64
3.2.7.3 Mechanical Properties .....	64
3.2.7.4 Evaluation of Antimicrobial Activity .....	64
3.2.7.5 Cytotoxicity of derived films .....	65
3.3 Further enhancement of BC antimicrobial properties .....	65
3.3.1 Materials .....	65
3.3.2 Cultivation with curcumin .....	66

3.3.3 Estimation of curcumin absorption from media .....	66
3.3.4 Fourier-transform infrared (FTIR) spectroscopy of BC films .....	66
3.3.5 Evaluation of BC films stability via weathering tests.....	66
3.3.5 Evaluation of Water Absorption and Water Retention .....	67
3.3.6 Biological Evaluations .....	67
3.3.6.1 Antibacterial Evaluation of BC films.....	67
3.3.6.2 <i>Danio rerio</i> Embryotoxicity Assay .....	68
3.3.6.3 <i>Caenorhabditis elegans</i> Survival Assay .....	68
3.3.7 BC Blends preparation and antimicrobial activity evaluation .....	69
3.4 Statistical Analysis .....	70
<b>CHAPTER 4 – TSNP FORMULATION FOR INCORPORATION WITHIN POLYMERIC MATERIALS.....</b>	<b>70</b>
4.1 Preface.....	70
4.2 Synthesis of TSNP .....	71
4.2.1 Optimised Method for TSNP Synthesis.....	72
4.2.2 TSNP Scale-Up.....	73
4.3 TSNP Gold Coating & Protection Check.....	74
4.3.1 AuTSNP Sucrose Sensitivity Test .....	75
4.3.2 AuTSNP for Fibronectin Detection .....	77
4.4 TSNP Temperature Test.....	78
4.4.1 TSNP Thermal Evaporation.....	80
4.5 TSNP protection using halloysite nanotubes .....	82
4.6 Transfer of TSNP to Chloroform .....	83
4.7 Summary .....	84
<b>CHAPTER 5 – TSNP INTEGRATION WITHIN POLYMERIC SYSTEMS.....</b>	<b>85</b>
5.1 Preface.....	85
5.2 Extrusion .....	85
5.2.1 Integration of TSNP in Polypropylene through Extrusion Process .....	85
5.2.2 Post-extrusion incorporation on PCL.....	86
5.3 Solvent Casting .....	88
5.3.1 Polyethylene Glycol Solvent Casting .....	88
5.3.2 Polycarbonate (PC), Polycaprolactone (PCL) and Polylactic Acid (PLA) Solvent Casting .....	90
5.4 Ex-situ incorporation on PCL and PLA .....	92

5.5 Stability Assay.....	93
5.5.1 Stability on Water and Sodium Chloride (NaCl).....	93
5.5.2 Stability on Potassium Chloride (KCl) .....	95
5.6 Summary .....	99
<b>CHAPTER 6 – CHARACTERISATION AND ANTIMICROBIAL EVALUATION OF SOLVENT CASTED FILMS .....</b>	<b>101</b>
6.1 Preface.....	101
6.2 Scanning Electron Microscope (SEM) Analysis.....	101
6.3 Differential Scanning Calorimetry (DSC) analysis.....	103
6.4 Thermogravimetric (TGA) Analysis .....	104
6.5 Evaluation of Mechanical Properties .....	105
6.6 Antimicrobial Evaluation of Solvent Casted Films.....	107
6.7 Cytotoxicity of Solvent Casted Films .....	109
6.8 Summary .....	111
<b>CHAPTER 7 – BACTERIAL CELLULOSE/CURCUMIN + TSNP FILMS; CHARACTERISATION AND ANTIMICROBIAL EVALUATION.....</b>	<b>112</b>
7.1 Preface.....	112
7.2 Curcumin-supplemented Production of Bacterial Cellulose (BC) and integration of TSNP .....	113
7.2.1 BC Production using curcumin as a supplement .....	114
7.2.1.1 Estimation of curcumin absorption from media.....	115
7.2.2 Preparation of TSNP incorporated BC films .....	115
7.2.3 Characterisation of produced BC films.....	116
7.2.3.1 Morphological characterisation and estimation of TSNP absorption.....	116
7.2.3.2 Thermogravimetric Analysis .....	118
7.2.3.3 Fourier-transform infrared spectroscopy .....	119
7.2.3.4 Evaluation of BC films stability via weathering tests .....	123
7.2.3.5 Evaluation of Water Absorption and Water Retention .....	125
7.2.4 Biological Evaluations .....	128
7.2.4.1 Antibacterial Evaluation of BC films.....	128
7.2.4.2 Cytotoxicity Assay .....	130
7.2.4.3 <i>Danio rerio</i> Embryotoxicity Assay .....	133
7.2.4.4 <i>Caenorhabditis elegans</i> Survival Assay .....	135
7.2.4.5 <i>Discussion of Results of Biological Evaluation</i> .....	136
7.3 Fabrication of BC Blends and incorporation of Curcumin and TSNP.....	137

7.3.1 Antibacterial Evaluation of BC Blends.....	138
7.4 Summary .....	139
CHAPTER 8 – CONCLUSION .....	140
CHAPTER 9 – COMPLETED TRAINING AND WORK DISSEMINATION.....	143
9.1 Completed Training.....	143
9.2 Work Dissemination.....	144
9.5 Conferences and Presentations .....	145
REFERENCES .....	146
APPENDICES .....	165
Appendix 1. Stress-strain Graphs from Tensile Tests of Solvent Casted PCL, PLA, PCL-TSNP and PLA-TSNP films .....	165
Appendix 2. Poster for AIT Research Seminar, April 2019 .....	169
Appendix 3. Abstract for Bioengineering in Ireland (BiNI), January 2020.....	170
Appendix 4. Poster for AIT Online Research Seminar, June 2020.....	171
Appendix 5. Poster for BioICEP Poster Event, October 2020.....	172
Appendix 6. Abstract presented in FEMS 2020 Online Conference, and Certificate of Participation .....	173
Appendix 7. Poster presented in EFB 2021 Virtual conference .....	174
Appendix 8. Poster presented in FEMS 2022 Microbiology Conference, and Certificate of Attendance.....	175
Appendix 9. Participation certificate for AIT Poster and Research Seminar, June 2020 ..	176
Appendix 10. Completion certificate of Research Integrity Module for Engineering and Technology.....	177
Appendix 11. Attendance certificate of “Medical Polymers and Processing Technology” course, at First Polymer Training Skillnet, October 2019.....	178
Appendix 12. MSSM 2019 Conference paper in Key Engineering Materials.....	179
Appendix 13. Research paper published in MDPI Coatings 2020.....	184
Appendix 14. Research paper published in MDPI Materials 2021 .....	204
Appendix 15. Review paper published in MDPI Polymers 2021 .....	218
Appendix 16. Review paper published in MDPI International Journal of Molecular Sciences 2022.....	243



## LIST OF FIGURES

Figure 1. Graphical Abstract for "Enhanced Antimicrobial Activity of Biocompatible Bacterial Cellulose Films via Dual Synergistic Action of Curcumin and Triangular Silver Nanoplates." Paper. ....	16
Figure 2. Graphical Abstract for "Antimicrobial active bioplastics using triangular silver nanoplate integrated polycaprolactone and polylactic acid films." Paper. ....	16
Figure 3. Project schedule for proposed solution.....	19
Figure 4. TEM image of TSNP (Charles et al., 2010). ....	26
Figure 5. Graphical representation of a red shift in LSPR of TSNP, occurring as a result of molecules binding to the particle surface.....	28
Figure 6. Antibacterial action mechanisms of AgNPs. 1) Adhesion to bacterial membrane and wall, 2) Penetration inside the cell, 3) Generation of ROS, 4) Modulation of cell signalling pathways. Adapted from (Marambio-Jones & Hoek, 2010).....	31
Figure 7. Chemical structure of curcumin. Adapted from (Adamczak et al., 2020), with chem-space.com.....	38
Figure 8. Structure of PP (Maddah 2016). ....	42
Figure 9. Structure of PC (Takeuchi 2012). ....	43
Figure 10. Structure of PCL (McKeen 2012). ....	45
Figure 11. Structure of PLA (Auras et al. 2004). ....	46
Figure 12. Structure of BC, consisting of linear chains of glucose units linked by $\beta$ -1,4-glycosidic bonds (Manoukian et al. 2019). ....	47
Figure 13. Seed solution (left) and TSNP solution (right). ....	52
Figure 14. Transfer of TSNP from water to chloroform. From left to right: tube before centrifugation, after centrifugation and after removing the aqueous phase and re-suspending the TSNP. ....	56
Figure 15. Spraying TSNP solution as the PCL exits the extrusion dye and goes through the rolls. ....	59
Figure 16. BC materials immersed in TSNP solution for overnight incubation. Bare BC films and Curcumin-BC films are included. Top row: Bare BC, middle row: BC-Cur2%, bottom row: BC-Cur10%. ....	61
Figure 17. Films of PCL (top) and PLA (bottom), before adding the solvent. ....	61
Figure 18. Drops of TSNP in chloroform solution placed on the surface of extruded PCL films (left) and PLA films (right). ....	62
Figure 19. UV-Vis Spectrum of Ag Seeds and TSNP (200 $\mu$ l seeds). ....	72
Figure 20. UV-Vis Spectrum of Ag Seeds and TSNP (Optimized method). ....	73
Figure 21. UV-Vis Spectrum of Scaled Up TSNP (300 mL). ....	74
Figure 22. UV-Vis Spectrum of seeds, TSNP, AuTSNP and protection check. ....	75

Figure 23. A) UV-Vis Spectrum of AuTSNP as a result of increasing refractive index of the solution. B) $\lambda_{max}$ values of AuTSNP changing as a result of increasing the refractive index of the solution.....	76
Figure 24. UV-Vis Spectra of Fn-coated AuTSNP exposed to basic and acid pH.....	78
Figure 25. UV-Vis Spectrum of TSNP after exposure of a single sample to different temperatures, for 5 minute periods under each temperature.....	79
Figure 26. UV-Vis Spectra of two different sets of samples of TSNP and concentrated TSNP before and after exposure to A)120 °C and B)150 °C, showing practically no shifts in spectrum even after being exposed to higher temperatures, compared to the sample shown in Figure 25. ....	79
Figure 27. Effect on UV-Vis spectrum of TSNP after evaporating water at 150 °C by two different methods, where sample A was exposed to 150 °C on 5-minute cycles, and sample B was exposed to the same temperature on 10-minute cycles. ....	80
Figure 28. Colour of TSNP solution before and after evaporation process: Left) Initial colour of TSNP solution; Centre) Final colour of sample A; Right) Final colour of sample B. ....	81
Figure 29. UV-Vis spectra of TSNP before and after evaporation at 40 °C.....	82
Figure 30. Mixed TSNP+HNT: A) Pure HNT Powder; B) TSNP+HNT solution; C) Dried and ground TSNP+HNT; D) Centrifuged TSNP+HNT. ....	83
Figure 31. UV-Vis spectra of non-concentrated TSNP, concentrated TSNP, SH-PEG coated TSNP and TSNP after transfer to chloroform.....	84
Figure 32. Extruded PP (Left) and PP+TSNP (Right).....	86
Figure 33. Post-extrusion addition of TSNP (in water solution). The blue spots show drops of TSNP solution which could not be absorbed by the polymer even in a melted state, due to its hydrophobicity. ....	87
Figure 34. PCL containing TSNP (in chloroform solution), incorporated post-extrusion, where purple spots represent the areas where the TSNP solution was absorbed into the polymer....	88
Figure 35. Solvent Casted PEG 3%: A) Solutions before ethanol evaporation; B) Solvent casted PEG+HNT; C) Solvent casted PEG+HNT+TSNP; D) Solvent casted PEG; E) Solvent casted PEG+TSNP.....	89
Figure 36. Solvent casted PEG 5%, after evaporating the solvent (left) and after scrapping the polymer off the petri dish (right). Showing that this method did not allow the formation of a PEG film. ....	90
Figure 37. Solvent casted PC (A and B) and PCL (C and D). The films were folded in B and D to display the flexibility of the materials. ....	91
Figure 38. Solvent Casted PLA (Grades 4043 and 4044). Left picture against a white background allows to observe the blue colour present in the films, whilst right picture shows that the film presents a higher transparency, compared to films shown in Figure 37. ....	91
Figure 39. PCL (top) and PLA (bottom) films after incorporation of TSNP on the surface of the polymers by the ex-situ method. ....	92

Figure 40. Photographs of TSNP-Incorporated PCL and PLA films for stability test in distilled water. Top row shows PCL films before and after 1 minute in distilled water. Middle row shows PLA films before and after 1 minute in distilled water. Bottom row shows, on the left side, a PCL film before and after 2 hours in distilled water, and on the right side, a PLA film before and after 2 hours in distilled water.....	94
Figure 41. Photographs of TSNP-Incorporated PCL and PLA films after being washed in NaCl for 1 minute and 2 hours. Pictures on the top row show the films before and after the 1-minute wash in NaCl, PCL on the left and PLA on the right. Pictures on the bottom row show the films before and after the 2-hour wash in NaCl, PCL on the left and PLA on the right.....	95
Figure 42. Colour of the TSNP solution before adding the KCl solution (left picture) and after adding the KCl solutions (right picture) in the concentrations of 1 M, 0.1 M, 0.01 M, 1 mM and 0.1 mM, shown in the same order from left to right. ....	96
Figure 43. UV-Vis Spectra of TSNP solution before and after adding KCl solution in the respective concentrations.....	97
Figure 44. Photographs of PCL (top) and PLA (bottom) solvent casted films before and after being submerged in KCl solution. ....	98
Figure 45. Photographs of PCL (top) and PLA (bottom) TSNP treated films before and after being submerged in KCl solution. ....	99
Figure 46. SEM images of: [a] PCL, [b] TSNP/PCL, [c] PLA and [d] TSNP/PLA films ....	102
Figure 47. DSC curves for second heating of a) bare and treated PCL films and b) bare and treated PLA films.....	103
Figure 48. TGA curves of a) bare and TSNP treated PCL films, and b) bare and TSNP treated PLA.....	105
Figure 49. A) Tensile strength (TS) and elongation at break ( $\epsilon$ ) of bare and TSNP-integrated solvent casted PLA and PCL films. B) Results from paired t-test statistical analysis for TS and $\epsilon$ of the PLA and PCL films (N=6).....	106
Figure 50. A) Elastic modulus (EM) of bare and TSNP-integrated solvent casted PLA and PCL films. B) Results from paired t-test statistical analysis for EM of the PLA and PCL films (N=6).....	107
Figure 51. Antimicrobial Activity of Solvent Casted PCL and PLA films, bare and with TSNP, for both tested strains. Survival % obtained with OD measurements at 630 nm, considering the OD of the bacterial control as the 100%.....	108
Figure 52. Survival percentage of MRC5 Lung Fibroblasts upon exposure to different concentrations of PLA and PCL extracts, with and without TSNP. The extract with the maximum concentration 100%, was prepared by incubating 10mg/mL of the corresponding PCL and PLA materials, which were then diluted up to 12.5%.....	111
Figure 53. Left: Difference between BC pellicles in HS and curcumin-modified HS media after 14 days of incubation. Right: BC produced in HS medium (Left), in 2% curcumin supplemented (Center) and in 10% curcumin supplemented HS medium (Right).....	114
Figure 54. Dry weight of BC and curcumin-supplemented BC with 2% and 10%.....	115

Figure 55. Top) BC produced in regular HS medium (Left), in 2% curcumin supplemented (Center) and in 10% curcumin supplemented (Right). (Bottom) Regular BC (Left), BC with 2% supplemented curcumin (Center) and BC with 10% supplemented curcumin (Right) after TSNP.....	116
Figure 56. SEM micrographs of BC film 100x (A) and 10kx (B); BC-Cur2% 100x (C) and 3.5kx (D); BC-Cur10% 100x (E) and 1.2kx (F); BC-TSNP 115x (G) and 1.29kx (H).....	117
Figure 57. SEM micrographs of examined materials with spots selected for EDS analysis: BC-TSNP-Cur2% (A) and BC-TSNP-Cur10% (B) .....	118
Figure 58. TGA curves of BC, Cur treated BC and Cur-TSNP treated BC films. ....	119
Figure 59. FTIR Spectra for BC, Curcumin, BC-Cur10%, BC-TSNP and BC-TSNP-Cur10%. .....	120
Figure 60. Samples before (A) and after (B) weather testing. From left-to-right, top-to-bottom: BC-Cur10%, BC-TSNP-Cur10%, BC-Cur2%, BC-TSNP-Cur2% and BC. ....	124
Figure 61. Water absorption (Top) & Water retention (bottom) of BC and BC-Cur samples in distilled water.....	125
Figure 62. Water absorption (Top) & Water retention (bottom) of BC and BC-Cur samples in buffer pH 4.....	126
Figure 63. Water absorption (Top) & Water retention (bottom) of BC and BC-Cur samples in buffer pH 7.4.....	127
Figure 64. Water absorption (Top) & Water retention (bottom) of BC and BC-Cur samples in buffer pH 9.....	127
Figure 65. A) Antimicrobial activity of derived BC films measured as absorbance rate at 630 nm, considering the bacterial growth control as the 100%. B) Dunnett statistical analysis ( $\alpha=0.05$ ) for bacterial growth in presences of BC specimens compared against <i>S. aureus</i> growth control. C) Dunnett statistical analysis ( $\alpha=0.05$ ) for bacterial growth in presences of BC specimens compared against <i>E. coli</i> control (n=3). ....	129
Figure 66. Survival rate of cell line (MRC5) after exposure to BC film extracts of different concentrations (n=4). ....	131
Figure 67. One-way ANOVA comparison of means from cell survivability of MRC5 fibroblasts, in the presence of 100% extract of each BC specimen (n=4). ....	132
Figure 68. One-way ANOVA comparison of means from cell survivability of MRC5 fibroblasts, in the presence of 50% extract of each BC specimen (n=4). ....	132
Figure 69. Diagrams for each tested material extract with the percentages of alive, dead and teratogenic embryos. ....	134
Figure 70. Effect of BC materials on development of zebrafish embryos, images of zebrafish embryos at 120 hpf treated with different extracts concentrations and untreated as a control. Blue arrows point to head abnormalities, red arrows point to liver abnormalities and black arrows point to heart abnormalities. ....	134
Figure 71. <i>C. elegans</i> survival rate (24h). ....	135

Figure 72. BC-blends without curcumin (white films), with curcumin (yellow films) and with incorporated TSNP (Blue films) made with A) PHB, B) PLA and C) PCL.....	138
Figure 73. Results of Antimicrobial evaluations for blends of BC with PLA, PCL and PHB, incorporated with Curcumin and TSNP, as well as bare materials used as control.....	139
Figure 74. Stress-Strain graphs from tensile testing of bare PCL samples. Testing was performed with 6 replicates. ....	165
Figure 75. Stress-Strain graphs from tensile testing of PCL-TSNP samples. Testing was performed with 6 replicates. ....	166
Figure 76. Stress-Strain graphs from tensile testing of bare PLA samples. Testing was performed with 6 replicates. ....	167
Figure 77. Stress-Strain graphs from tensile testing of PLA-TSNP samples. Testing was performed with 6 replicates. ....	168

## LIST OF TABLES

Table 1. Shift of LSPR peak wavelength of AuTSNP as a result of refractive index increase. ....	77
Table 2. Changes in LSPR wavelength, Ag Concentration and Volume for TSNP solution after treatments at 150 °C.....	80
Table 3. Thermal Characteristics of pure and TSNP treated films. ....	103
Table 4. Antimicrobial effect (AE) values* for TSNP treated films .....	109
Table 5. Result of EDS Analysis performed on 5 different points of BC-TSNP-Cur10% film. ....	118
Table 6. FTIR peak assignments for BC, Curcumin, BC-Cur10%, BC-TSNP, BC-TSNP-Cur10%. Part 1, from 4000 cm <sup>-1</sup> to 1425 cm <sup>-1</sup> . ....	121
Table 7. FTIR peak assignments for BC, Curcumin, BC-Cur10%, BC-TSNP, BC-TSNP-Cur10%. Part 2, from 1425 cm <sup>-1</sup> to 650 cm <sup>-1</sup> .....	122
Table 8. Colour change, $\Delta E^*$ for each sample case due to weather testing.....	124

## ABBREVIATIONS

AA	Ascorbic Acid
Ag	Silver
Ag <sup>+</sup>	Silver Ions
Ag <sup>0</sup>	Silver Atoms
AgNO <sub>3</sub>	Silver Nitrate
AgNPs	Silver Nanoparticles
AMP	Antimicrobial Peptides
AMR	Antimicrobial Resistance
ATP	Adenosine triphosphate
Au	Gold
AuTSNP	Gold-coated Triangular Silver Nanoplates
BC	Bacterial Cellulose
CFU	Colony Forming Units
CuO	Copper Oxide
Cur	Curcumin
DNA	Deoxyribonucleic Acid
DSC	Differential Scanning Calorimetry
EDS	Energy Dispersive X-rayspectroscopy
EM	Elastic Modulus
Fe <sub>3</sub> O <sub>2</sub>	Iron Oxide
FTIR	Fourier-Transform Infrared Spectroscopy
FtsZ	Filamenting temperature-sensitive mutant Z

FWHM	Full Width at Half Maximum
GTP	Guanosine Triphosphate
H <sub>2</sub> O <sub>2</sub>	Hydrogen Peroxide
HAuCl <sub>4</sub>	Gold (III) chloride
Hg	Mercury
HNO <sub>3</sub>	Nitric Acid
HNT	Halloysite Nanotubes
HS	Hestrin–Schramm Broth
LB	Luria-Bertani Broth
LSPR	Localized Surface Plasmon Resonance
MW	Molecular Weight
Na <sub>2</sub> HPO <sub>4</sub>	Sodium phosphate dibasic
NaBH <sub>4</sub>	Sodium Borohydride
NADH	Nicotinamide Adenine Dinucleotide
NPs	Nanoparticles
OD	Optical Density
PC	Polycarbonate
PCL	Polycaprolactone
PEG	Polyethylene Glycol
PLA	Polylactic Acid
PP	Polypropylene
Ppm	Parts per million
PSSS	Poly(Sodium Styrene Sulphonate)
PVA	Polyvinyl Alcohol

PVP	Polyvinylpyrrolidone
RNA	Ribonucleic Acid
ROS	Reactive Oxygen Species
Rpm	Revolutions per minute
SEM	Scanning Electron Microscopy
SH-PEG	Thiol-Terminated Polyethylene Glycol
SPR	Surface Plasmon Resonance
TGA	Thermal Gravimetric Analysis
TiO <sub>2</sub>	Titanium Dioxide
TS	Tensile Strength
TSC	Trisodium Citrate
TSNP	Triangular Silver Nanoplates
UV-VIS	Ultraviolet-Visible
ε	Elongation at Break (%)



## RELEVANT PUBLICATIONS

- **Garcia EL**, Mojicevic M, Milivojevic D, Aleksic I, Vojnovic S, Stevanovic M, Murray J, Attallah OA, Devine D, Fournet MB. Enhanced Antimicrobial Activity of Biocompatible Bacterial Cellulose Films via Dual Synergistic Action of Curcumin and Triangular Silver Nanoplates. *International Journal of Molecular Sciences*. 2022; 23(20):12198. <https://doi.org/10.3390/ijms232012198>

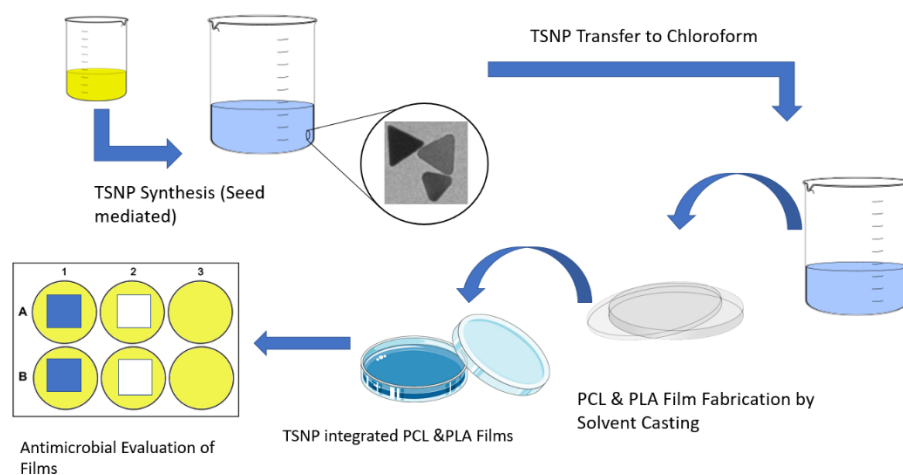


Figure 1. Graphical Abstract for "Enhanced Antimicrobial Activity of Biocompatible Bacterial Cellulose Films via Dual Synergistic Action of Curcumin and Triangular Silver Nanoplates." Paper.

- **Garcia, E. L.**, Attallah, O. A., Mojicevic, M., Devine, D. M., & Fournet, M. B. (2021). Antimicrobial active bioplastics using triangular silver nanoplate integrated polycaprolactone and polylactic acid films. *Materials*, 14(5), 1–15. <https://doi.org/10.3390/ma14051132>



Figure 2. Graphical Abstract for "Antimicrobial active bioplastics using triangular silver nanoplate integrated polycaprolactone and polylactic acid films." Paper.

## ABSTRACT

New antimicrobial interventions are urgently required to combat rising global health and medical infection challenges. Here, an innovative antimicrobial technology, providing price competitive alternatives to antibiotics and readily integratable with currently technological systems is presented. In a design for medical plastics, where bacterial adhesion to medical packing, textiles and implants such as catheters, cannulas, and orthopaedic implants, is a growing reason for failure, triangular silver nanoplates (TSNP) and curcumin are demonstrated for surface integration on medical materials. Using polymer solvation, the TSNPs are integrated within Polycarbonate (PC), Polycaprolactone (PCL) and Polylactic acid (PLA). TSNP encapsulation method is afterwards applied for processing biopolymers such as Polylactic Acid (PLA). TSNP-incorporated materials showed a significant growth inhibition against *Escherichia coli* (ATCC 11775) and *Staphylococcus aureus* (ATCC 25923) strains, where PLA-TSNP exhibited the highest antimicrobial activity. On the other hand, bacterial cellulose (BC) is a biomaterial of growing importance with a rising application spectrum for which developments which improve its properties are very significant. BC films integrated with Cur and TSNP showed an enhanced antimicrobial effect compared to films containing only TSNP, especially against the Gram-positive strain, *S. aureus*. Furthermore, the toxicological evaluation demonstrated the biosafety of the materials during *in vitro* (MRC5 lung fibroblasts) and *in vivo* (*Caenorhabditis elegans* and *Danio rerio*). The combination of curcumin and TSNP in the bacterial cellulose matrix provides a novel mechanism for the sustained antimicrobial action of biopolymeric thin films. This study has effectively demonstrated that integrating curcumin in production medium with *ex situ* TSNP incorporation leads to safe, biocompatible, antimicrobial BC films. Further studies will include the exploration of TSNP-curcumin additive mechanism and improvement of mechanical characteristics of BC materials that will potentially result in designing products suitable for various packaging and biomedical applications.

## CHAPTER 1 – INTRODUCTION

### 1.1 Research Challenge

Environmental surfaces are a common source for contamination and/or transmission of microbiological organisms. This can be especially problematic in places such as health care facilities, food industries, hygienic public environments, among others, where pathogens can easily spread and lead to disease acquisition and infection transmission (Kramer and Assadian 2014). Furthermore, antibiotic resistance in microorganisms is rising and spreading worldwide, and threatening our ability to prevent and treat common infectious diseases (Prestinaci, Pezzotti, and Pantosti 2015). The development of new sustainable technologies that facilitate the protection of surfaces from microorganisms, while at the same time keeping the risk of resistance generation at minimum is a priority. A number of approaches are currently under development, or already in use. The need for improved and more versatile, effective and cost competitive solutions remains an important target as the range of applications continues to increase (Mahira et al. 2019).

Research efforts have focused on finding alternative anti-infective compounds that are capable of exhibiting strong and rapid broad-spectrum antimicrobial activity. Among the list of potential material options for such tasks, Ag<sup>+</sup> ions and curcumin, present as widely available and widely studied compounds and which are also applicable to several other applications. Their action mechanisms are effective against a variety of microorganisms, including bacteria, fungi and viruses, with the important advantage of inducing limited or even null resistance. Therefore, Ag<sup>+</sup> releasing silver nanostructures and curcumin hold great potential to be integrated in innovative technologies to control or prevent microbiological colonisation on specific surfaces. The integration of these compounds in an active format within the structure of materials is a challenging process and depends on various factors such as: target microorganisms, material type, its mechanical properties and selected method for their incorporation. Selection of these parameters can vastly affect resulting antimicrobial properties and performance.

Plastics are a primary material requiring high antimicrobial performance. Taking into consideration the fact that commonly used pervasive plastics are leaving an indelible imprint on our planet, an additional challenge would be to substitute these materials with

environmentally friendly alternative biopolymer, such as PLA or BC which have enabled antimicrobial activity.

## 1.2 Solution Proposed

In this project, the integration of triangular silver nanoplates (TSNP) as Ag<sup>+</sup> nanoreservoirs within polymeric materials and biomaterials intended for wide spectrum of applications is developed, demonstrating effective antimicrobial action and a cost-competitive fabrication process. Moreover, curcumin was introduced into the best performing polymers as a supplementary antimicrobial compound. Combination of these antimicrobials was shown to potentially lead to increased antimicrobial effectiveness compared to currently commercially available antimicrobial systems. A detailed analysis of polymers incorporating anti-microbial agents was performed in order to assess the induced antimicrobial effect and also their biocompatibility using various *in vitro* and *in vivo* systems. The proposed solution and project timeline are presented on Figure 3.



Figure 3. Project schedule for proposed solution.

### 1.3 Objectives

- a) To optimise the synthesis and formulation of TSNP for integration into plastics and bioplastics.
- b) To achieve the functional incorporation of antimicrobial TSNPs in biodegradable and/or recyclable biopolymers.
- c) Assessment of derived materials' antimicrobial activities, effect and mechanical properties.
- d) Effectively integrate antimicrobial active curcumin during the fabrication process of biodegradable polymers.
- e) Demonstrate improved antimicrobial performance of materials including incorporated curcumin and TSNP.
- f) Detailed biocompatibility analysis of derived films using *in vitro* and *in vivo* tests.

### 1.4 Research Question

Can advanced antimicrobial technologies be developed to address the rising bio contamination and infection challenges in the food and medical plastics sectors? Specifically:

- i) Can TSNP and/or curcumin be functionally integrated into biodegradable and/or recyclable polymers, with the potential of being used as antimicrobial packing bioplastics or biomedical materials?
- ii) Can various antimicrobial compounds and agents acting in combination lead to more effective performance in the development of antimicrobial biocompatible plastics?

## CHAPTER 2 – LITERATURE REVIEW

### 2.1 Overview

Since the discovery of penicillin and the diverse variety of antibiotics that followed, humanity found in these compounds, a powerful tool to fight infections from pathogenic microorganisms, which helped save a large number of lives (Adedeji 2016). However, such antibiotics have been responsible for causing evolutionary stress in bacteria, leading to the appearance of antibiotic-resistant mutants (Flasche and Atkins 2018). Although the development of resistance is a naturally occurring response, it has been accelerated in recent years due to the overuse and misuse of antibiotics. Furthermore, these adaptive resistance genes can be mobilized within and between species, further accelerating the appearance of multi-resistant strains (Michael, Dominey-Howes, and Labbate 2014). Another high impact factor is the urbanization rate of modern times, as large numbers of people living in close proximity, together with our ability to rapidly travel across the planet, which provides greater opportunities for interpersonal contact, facilitating the spread of resistant bacteria and resistance genes across the globe (Bruinsma et al. 2003; Michael et al. 2014). Therefore, antimicrobial resistance (AMR) is a serious and growing problem that threatens our ability to treat infectious diseases. AMR also represents a risk for millions of lives in the upcoming years and if not addressed properly and promptly, represents one of the greatest challenges of the 21<sup>st</sup> century.

The development of new antibiotic drugs is a long and costly process, with an average investment of approximately US\$1,300 million for 10 years or longer (Conly and Johnston 2005; Wouters, McKee, and Luyten 2020) with no guarantee for successful drug to be approved or for the generation of high income. These factors make it unattractive for pharmaceutical companies and has resulted in a notable decrease of approved antibiotics developed during the last decades. Therefore, to face the growing problem of AMR, there is an urgent need for the development of novel alternatives. These alternatives will allow us to reduce the dependence on antibiotic drugs and to reduce risks of infection in certain specific situations, such as healthcare facilities, food industries and shared public spaces. As a result, researchers are increasingly focusing on new strategies such as; including novel molecules and using informatics for the development of novel antibiotics.

Highly promising novel antimicrobial molecules include antimicrobial peptides (AMP) and peptide related molecules, pathogen-specific monoclonal antibodies, engineered bacteriophages and CRISPR-Cas (Clustered regularly interspaced short palindromic repeats – associated enzymes) systems, as well as pathogen-specific enzymes, inhibitors, and vaccines (Mantravadi et al. 2019). Nanomaterials are also attractive options as antimicrobial agents, particularly nanostructures, due to the antimicrobial effects some types possess and their ability to be used as vectors for drug delivery applications (Baptista et al. 2018). Silver nanoparticles (AgNPs) are considered the most effective antibacterial nanomaterial, but other metallic nanoparticles (NPs), such as copper oxide (CuO), titanium dioxide (TiO<sub>2</sub>), gold (Au), and iron oxide (Fe<sub>3</sub>O<sub>2</sub>) NPs have also demonstrated antimicrobial activity (Baptista et al. 2018). Further strategies include the research of novel targets for antimicrobial agents, including cell wall and cell membrane, different biosynthetic pathways, transfer of ribosome RNAs (Ribonucleic Acid), cell division machinery, and inhibition of pathogenesis through anti-virulence strategies (Belete 2019). Many of these strategies are intended to work as adjunctive therapies to increase effectiveness of antibiotics and reduce the risk of generating resistance, which means that integration with traditional antimicrobial agents will also be essential.

## **2.2 Silver nanostructures**

Nanotechnology is a science focused on the study of the properties of materials at the nanoscale, including their manipulation and engineering. It is of general agreement that NPs are clusters of atoms ranging between 1-100 nm on size, and particles within this size range exhibit a large surface area to volume ratios and specific quantum effects encountered at these dimensions (Williams 2008). NPs are of great interest to the scientific community due to the peculiar properties they possess, in contrast with their bulk material versions. Bulk materials maintain constant physical properties regardless of any different size or shape they can take, while at the nanoscale materials, physical, chemical, biological and optical properties can exhibit changes induced by size, shape or composition (Chouhan 2018).

Humans began using metallic NPs in ancient times, though were not fully aware of their nature. Earliest examples of NPs in a practical application date back to Mesopotamian and Egyptian cultures, when they used metals in the fabrication of glass. Through history, this technique was used and improved, mainly for decorative purposes, allowing glass staining in a variety of colours due to the plasmonic properties of the NPs (Jeevanandam et al. 2018). Perhaps one of the most representative examples of ancient employment of metal NPs is the Lycurgus cup,

manufactured in Rome during the 4<sup>th</sup> century. The peculiarity of this cup resides in the optical effects displayed by the glass, as it appears green when light is reflected but changes to red when light is transmitted through it. This phenomena is possible due to the presence of silver-gold alloy NPs (7:3 ratio and 50-100 nm in diameter) within the glass of the cup (Freestone et al. 2007). Several cultures exploited the attractive properties of NPs even before acknowledging their existence or understanding the principles dictating their optic behaviour.

Silver (Ag) is one of the most attractive metals for the synthesis of nanoparticles, because of the wide applications derived from the properties it possesses. Attributes such as its malleability, conductivity, ductility, resilience, rareness and antimicrobial properties, made it valuable and convenient for several everyday life purposes through ancient and modern times. The most common applications of Ag include jewellery, ornaments, currency, photography, electrical contacts, among others. Other applications include optoelectronics, water disinfection, diagnostics, anti-cancer therapeutics, biomedical technologies, drug-gene delivery, energy science and clinical anti-bacterial purposes, etc. (Lee and Jun 2019; Remziye Güzel and Erdal 2016). The increasing list of practical uses found for Ag and its NPs, present it as a highly valuable for current and future technologies and applications.

### **2.2.1 Synthesis of Silver Nanoparticles**

There are several methods for the synthesis of AgNPs. Broadly, these methods can be divided into two categories; top-down and bottom-up approaches. Top-down methods constitute the disincorporation of bulk materials into smaller particles, eventually resulting in the formation of the required nanostructures. Bottom-up approach involve techniques to assemble single atoms and molecules into the desired nanostructures. However, it is easier and more common to classify the methods as either physical, chemical or biological. (Chugh et al. 2018; Lee and Jun 2019)

The most important physical methods are evaporation-condensation and laser ablation, both of which are capable of synthesising large amounts of high purity NPs, with the advantage of not using hazardous chemicals. Evaporation-condensation methods generate NPs by evaporating a solid silver source in a furnace, and as the vapour is cooled down, it nucleates into NPs (Vodop'yanov et al. 2017). For laser ablation techniques, the bulk metal source is placed in a liquid environment and irradiated with a pulsed laser, forming the NPs and releasing them into the liquid environment (Chen and Yeh 2002). However, as capping agents are not used,



agglomeration is a common problem while using this approach, as well as a higher operation cost due to the complex equipment, high amount of power and longer time required (Iravani et al. 2014; Lee and Jun 2019).

The most widely used chemical approach involves the reduction of silver salts using agents such as ascorbate, sodium borohydride ( $\text{NaBH}_4$ ), elemental hydrogen or citrate, that reduce  $\text{Ag}^+$  to silver atoms ( $\text{Ag}^0$ ), followed by formation of oligomeric clusters by agglomeration. The formed clusters allow the formation of colloidal AgNPs (Abou El-Nour et al. 2010). During the preparation of the NPs, it is important to use protective agents that can be adsorbed or bind to their surface, helping stabilize their growth and avoid sedimentation, agglomeration or the loss of their surface properties. Some examples include surfactants (such as thiols, amines, acids, alcohols) or polymeric compounds like poly (vinyl alcohol) (PVA), poly (vinylpyrrolidone) (PVP), poly (ethylene glycol), Poly (methacrylic acid) and polymethylmethacrylate, that are used as effective agents for protection and stabilization of NPs (Iravani et al. 2014). Chemical methods can also include the use of additional techniques such as laser irradiation, electrochemistry, photochemistry, lithography, cryochemical synthesis, sono-decomposition and thermal decomposition. These methods usually offer high yield and ease of production, however, the general disadvantage is the use of toxic and hazardous chemicals that not only represents an environmental risk, but also limits the use of AgNPs in applications related to living organisms (Zhang et al. 2016).

Due to the disadvantages of physical and chemical methods, biological synthesis presents itself as an interesting alternative. Biosynthesis methods use biological agents, including plant or algal extracts, bacteria, fungi and yeast. These methods offer the possibility of synthesising the NPs in an environmentally friendly, cost effective and easily scalable manner (Benakashani, Allafchian, and Jalali 2016). A large number of approaches for the biosynthesis of AgNPs already exist, taking advantage of fats, proteins, nucleic acids, pigments, carbohydrates and secondary metabolites produced by plants and holding the capability of reducing Ag from silver salts. In the same way, microorganisms produce several proteins, enzymes and other biomolecules that can act as reducing agents, which allow them to synthesise intracellular or extracellular NPs (Siddiqi, Husen, and Rao 2018).

As methods for synthesis of AgNPs can be very different, the resulting NPs can also show significant variations in their properties, determined by parameters such as shape, size, surface

area, pore size, crystallinity and fractal dimensions (Abou El-Nour et al. 2010). These parameters are strongly influenced by experimental conditions, including factors involving the kinetics of interactions between Ag ions and reducing agents and the activity of the stabilizing agent, making the design of the synthesis method of great importance for the final application of the NPs (Ghorbani et al. 2011). Given that antibacterial activity, optical, magnetic, electronic and catalytic properties are strongly influenced by size and shape, several techniques are directed for the synthesis of non-spherical NPs, including nanorods, nanowires, nanobars nanoprisms, cubic, triangular, hexagonal and flower-shaped NPs (Khodashenas and Ghorbani 2015). The techniques used to identify and characterise NPs include transmission and scanning electron microscopy, dynamic light scattering, Fourier transform infrared spectroscopy and UV-Vis spectroscopy, among others (Abou El-Nour et al. 2010).

### **2.3 Triangular Silver Nanoplates (TSNP)**

It has been established that optical properties of metallic NPs can be highly dependent on shape, size and composition. Triangular Silver Nanoplates (TSNP) (Figure 4) and other non-spherical nanostructures with sharp geometries have been postulated to possess highly controllable optical properties, related to their amenability to greater electric-field enhancement, mainly occurring in the particle tips (Kelly et al. 2003). TSNP have also been reported to exhibit higher antimicrobial activity, attributed to a rate of Ag<sup>+</sup> ion release which is five times larger, compared to spherical TSNPs. As Ag<sup>+</sup> ion release is caused by oxidation, the increased ion release of TSNP is a consequence of its sharp edges and corners, which make them more susceptible to oxidation (Lu et al. 2015).

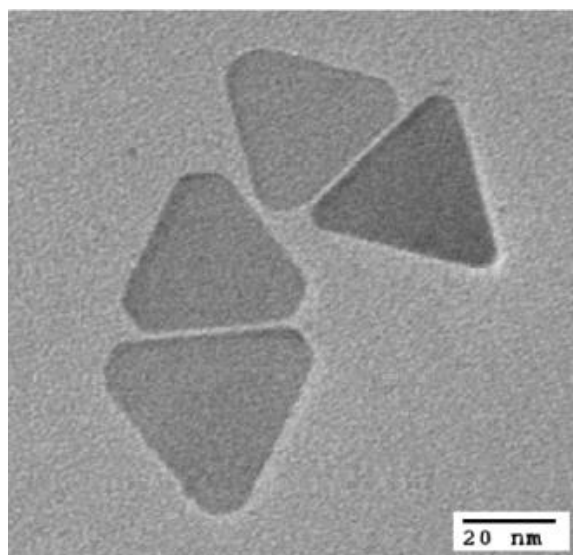


Figure 4. TEM image of TSNP (Charles et al., 2010).

Triangular-shaped nanoplates or nanoprisms started appearing on the picture as by-products of methods that predominately produce spheres (Kirkland et al. 1993; Klaus et al. 1999). Then, the first method found in literature directly intended for the synthesis of triangular silver nanoprisms, reported by Jin et al. (2001), consisted in a photoinduced method that would allow the conversion of large quantities of silver nanospheres into triangular nanoprisms (Jin et al. 2001). Following that, upon observation of their distinctive optical properties and potential in biosensing applications, interest started to arise to further study this morphology and to develop more efficient and consistent methods to synthesise them.

### 2.3.1 Synthesis of TSNP

Different approaches can be followed for the synthesis of TSNP, although seed-catalysed chemical reduction of silver nitrate ( $\text{AgNO}_3$ ) is one of the most common used. Typically,  $\text{AgNO}_3$  is reduced using  $\text{NaBH}_4$ , in the presence of sodium or trisodium citrate (TSC) as a stabilizer to form seeds. Afterwards, for TSNP growth, the seeds serve as a catalysing (nucleating) source for the reduction of more  $\text{AgNO}_3$  using ascorbic acid (AA) and a stabilizing polymer such as PVA (Kelly, Keegan, and Brennan-Fournet 2012), PVP (Singh et al. 2009; Wu, Zhou, and Wei 2015) or by adding TSC at the end of the reaction (Aherne et al. 2009). Some reported methods do not mention the use of stabilizer polymers in the growth step (Brennan-Fournet et al. 2015; Charles et al. 2010; D'Agostino et al. 2017; Zhang et al. 2014), or they use the polymer in the seed synthesis instead, for example PEG (Vinayagam et al. 2018)

or Poly(sodium styrene sulphonate) (PSSS) (Aherne et al. 2008). A method involving PVP as a seed stabilizer, and hydrogen peroxide ( $H_2O_2$ ) as reducing agent in the growth step, instead of AA, has also been reported (Cai et al. 2017; Van Dong et al. 2012; Torres et al. 2007). Other alternatives include the fabrication of TSNP by plasmon-mediated synthesis, by irradiating the seeds with a sodium lamp. Another difference on this reported method is the addition of sodium hydroxide (NaOH) to the seed synthesis step (Ahmad et al. 2019).

The use of a seed-mediated approach offers the advantage of allowing to change the average edge size and thickness by adjusting the volume of seed solution used for the growth reaction of TSNPs. This was demonstrated by Liu et al. (2014), where the edge length of TSNP was precisely tuned from 150 nm and up to 1.50  $\mu m$ , and their thickness varied in a range between  $\sim 5$  nm for the smaller nanoplates, to  $\sim 14$  nm for the largest ones (Liu et al. 2014). Another example was reported by Kelly et al. (2012), where TSNPs were also synthesised with variations in the volume of seeds, resulting in particles with mean edge lengths between 10-200 nm and thickness between  $\sim 5$  and  $\sim 14$  nm (Kelly et al. 2012).

Several methods for TSNP synthesis, using chemical reduction but without seeds as catalysts are also reported. In one method, a single-step approach is proposed adding  $AgNO_3$  to a solution of  $NaBH_4$ , TSC and AA, while using a larger amount of AA compared to other methods. It was found that by increasing the amount of AA, the number of spherical NPs was reduced and the formation of TSNP increased (Etacheri et al. 2010). Additionally, a combination of sodium citrate, PVP,  $H_2O_2$  and  $NaBH_4$  added to  $AgNO_3$  allowed the formation of colloidal TSNP solutions (Fang et al. 2017; Furlotov et al. 2017; Zhang et al. 2011).

The synthesis was also achieved by modifying a procedure used to prepare spherical NPs, by substituting  $NaBH_4$  for hydrazine hydrate as a reducing agent (Li et al. 2012). Moreover, a synthesis employing an ionic liquid-water interfacial methodology allowed the formation of the TSNP, by taking advantage of the tunability of ionic liquids, and keeping the growth under kinetic control due to the high viscosity and ionicity of the ionic liquids (Lu et al. 2015).

### **2.3.2 TSNP as Nansosensors**

Surface plasmon resonance (SPR) is an optical property possessed by some materials, where excitation by incident light results in the collective oscillation of conduction electrons in the surface of the material (Willets and Van Duyne 2007). When light waves interact with

conductive NPs with a much smaller size than the wavelength of the incident light, waves are trapped within the NPs, leading to local plasmonic oscillations with a resonant frequency known as localized surface plasmon resonances (LSPR) (Paridah et al. 2016; Petryayeva and Krull 2011; Willets and Van Duyne 2007). LSPR wavelength is strongly dependent on shape, size, composition, dielectric environment, local refractive index and separation distance of NPs (Aherne et al. 2009; Petryayeva and Krull 2011; Willets and Van Duyne 2007). The resonance wavelength of LSPR and SPR is sensitive to small changes in the local refractive index, transducing these changes to a measurable wavelength shift, giving plasmonic materials and NPs a great potential as powerful biosensors for small-sized analytes (Brennan-Fournet et al. 2015; Chang et al. 2018; Manzano et al. 2016; Unser et al. 2015). Aforementioned shifts can occur towards shorter wavelengths in the spectrum, which is known as a blue shift, and a red shift when it occurs towards longer wavelengths (Figure 5).

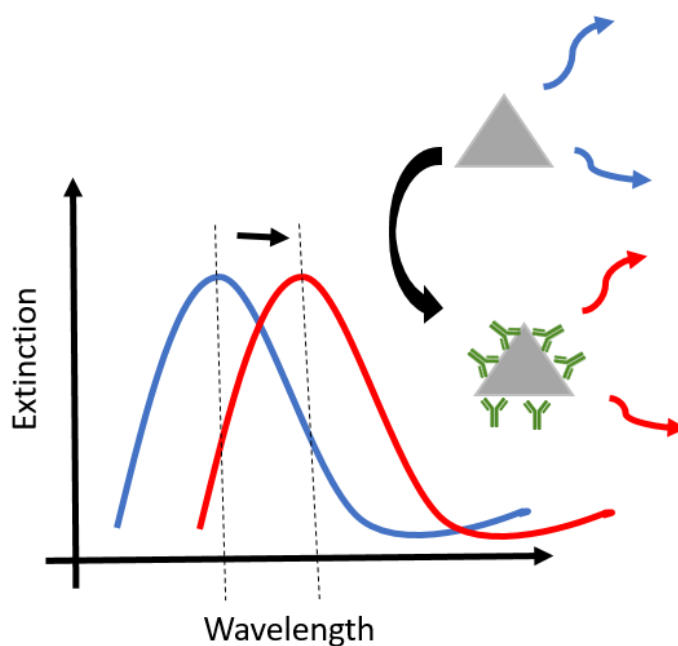


Figure 5. Graphical representation of a red shift in LSPR of TSNP, occurring as a result of molecules binding to the particle surface.

Noble metal nanoparticles such as Ag and Au exhibit LSPR in the visible region of the electromagnetic spectrum, making them attractive for sensing applications, as changes can be even detected with the naked eye in some cases, making detection faster, easier and inexpensive (Unser et al. 2015). AgNPs are particularly attractive because among all metals, silver

possesses the greater scattering cross-section, which means a higher probability of interaction between radiation and the target (Michael Kotlarchyk 1999). Consequently, AgNPs show the most intense plasmonic interaction with incident light, compared to other metallic NPs (Wu et al. 2015).

Changes in refractive index cause detectable shifts in LSPR resonance wavelength, according to the Equation (Eq 1) for the sensitivity ( $\frac{\Delta\lambda_{max}}{\Delta n}$ ) of the resonance wavelength to the refractive index of the medium. “Where  $\epsilon_r$  is the real dielectric constant for silver,  $(\frac{\Delta\epsilon_r}{\Delta n})$  is the real dielectric constant determined by the plasmon resonance condition and  $(\frac{\Delta\epsilon_r}{\Delta\lambda})\lambda_{max}$  is the slope of the real part of the nanoparticle’s dielectric function with changing wavelength” (Charles et al. 2010)

$$\frac{\Delta\lambda_{max}}{\Delta n} = \frac{\frac{\Delta\epsilon_r}{\Delta n}}{(\frac{\Delta\epsilon_r}{\Delta\lambda})\lambda_{max}} \quad (\text{Eq 1})$$

This response can occur as analytes or molecules, which have an adequately different refractive index bind at or near the surface of metallic NPs. This property is significant in TSNP due to the sharp tips and edges of TSNP geometry, making them attractive for use as nanosensors or biosensors. This was confirmed by using the biotin-streptavidin system to demonstrate their high sensitivity and selectivity, and proving their suitability to act as powerful biosensors (Haes and Duyne 2002). Another successful demonstration of sensing efficiency, was performed by changing the refractive index of the TSNP surroundings, through variation in sucrose concentration (Charles et al. 2010).

TSNP are already being used as biosensors in research. For instance, Zhang et al (2014) used cytidine 5'-diphosphocholine coated TSNP and AuTSNP (Gold coated TSNP) for detection of C-reactive protein. Brennan-Fournet et al (2015) successfully detected conformational changes of fibronectin using AuTSNP. Vinayagam et al (2018) built a nanoprobe by conjugating single strand DNA to the TSNP surface, for specific detection of dengue virus. Cai et al (2017) proposed a TSNP-AuNP nanoconjugate which allows detection of glucose due to LSPR changes caused by TSNP etching. Fang et al (2017) also applied TSNP etching colour changes in the design of a colorimetric method for the detection of dopamine, which possesses high affinity to Ag and formed a protective coating against chlorine. A similar approach for the

detection of mercury (Hg(II)) has been reported, taking advantage of Ag/Hg amalgam formation to protect the TSNP from the effects of chlorine (Li et al. 2018). A slightly contrasting method reported by Furletov et al (2017), measured the reduction of TSNP colour intensity after the addition of Hg(II) alone, attributing such changes to both oxidation by Hg<sup>+2</sup> ions and amalgam formation.

### **2.3.3 Antimicrobial Activity**

Antimicrobial compounds can exhibit activity through two different mechanisms; bactericidal or bacteriostatic effects. Bactericidal compounds directly target and destroy bacterial cells, leading to their death. These compounds typically disrupt vital cellular functions, such as inhibiting cell wall synthesis or interfering with essential metabolic pathways, ultimately resulting in the irreversible destruction of the bacteria (Kohanski, Dwyer, and Collins 2010). In contrast, bacteriostatic compounds inhibit bacterial growth and multiplication without causing immediate cell death. They interfere with critical bacterial processes, such as protein synthesis or DNA replication, effectively impeding bacterial reproduction (Loree and Lappin 2022). However, the antibacterial effect of a certain compound can vary under different conditions, and is usually not consistent against all bacteria. Therefore, it is more accurate to describe most antibacterial agents as potentially being both bactericidal and bacteriostatic (Bernatová et al. 2013). In the case of AgNPs, they are capable of exhibiting a potent bactericidal effect against a wide variety of microorganisms, but this activity is dependant of several factors, including size, shape, concentration, aggregation, capping agents, among others (Anees Ahmad et al. 2020).

AgNPs have demonstrated effectiveness against a broad number of microorganisms, including Gram-positive and negative bacteria, viruses and fungi. Even though their broad-spectrum antimicrobial activity has been proven, the precise mechanism of action is not yet fully understood. However, four mechanisms are postulated for the antimicrobial action of Ag NPs, as illustrated in Figure 6. These include; 1) AgNP adhesion to bacterial membrane and cellular wall, altering structure and permeability. 2) Penetration inside cell, destabilizing and denaturing proteins and lipids, causing mitochondrial and ribosomal dysfunction and interacting with DNA. 3) Causing the generation of reactive oxygen species (ROS) and free radicals and therefore inducing cellular toxicity and oxidative stress. 4) Modulating cell signalling pathways, which affect bacterial growth and other molecular and cellular activities (Dakal et al. 2016). Nevertheless, several studies suggest that ROS generation and increase of

oxidative stress, caused by  $\text{Ag}^+$  release, is the most drastic antimicrobial mechanism associated with AgNPs (Sotiriou and Pratsinis 2010; Xiu et al. 2012).

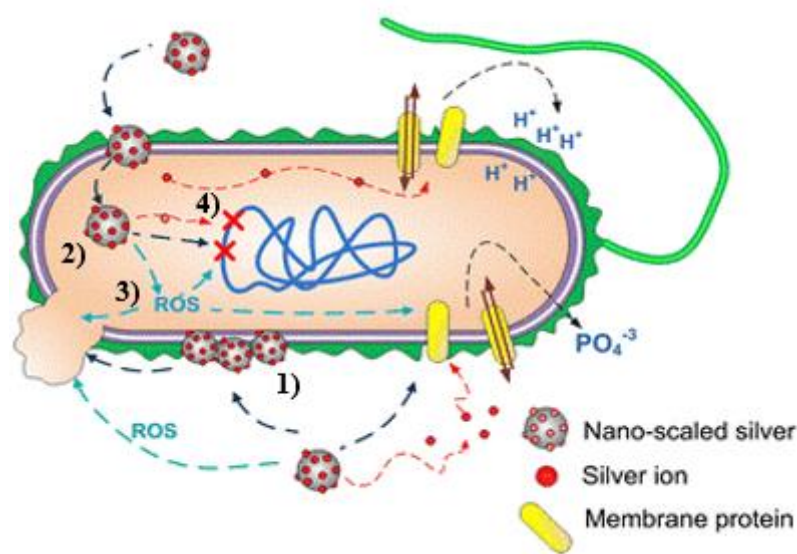


Figure 6. Antibacterial action mechanisms of AgNPs. 1) Adhesion to bacterial membrane and wall, 2) Penetration inside the cell, 3) Generation of ROS, 4) Modulation of cell signalling pathways. Adapted from (Marambio-Jones & Hoek, 2010).

The adhesion of AgNPs to the cell wall and membrane of bacteria is facilitated by their positive surface charge, conferring electrostatic attraction to the negatively charged components present in both wall and membrane (Abbaszadegan et al. 2015). As the AgNPs interact with the sulfur-containing proteins of the bacterial membrane, affecting the integrity of the lipid bilayer and increasing permeability of the membrane, causing irreversible changes in the membrane structure and resulting in its disruption (Ghosh et al. 2012). This alterations in the membrane morphology disturb the ability of the bacteria to properly regulate transport activity through the membrane, affecting vital mechanisms such as the uptake of ions and causing loss by the leakage of cellular contents, including proteins, ions and ATP (Adenosine triphosphate) (Dakal et al. 2016). Although AgNPs have demonstrated effectiveness against both Gram-positive and Gram-negative bacteria, Gram-positive bacteria are less susceptible due to the thickness of their negatively charged peptidoglycan layer, leaving the  $\text{Ag}^+$  ions stuck in the cell wall and impeding their entry. On the other hand, the membrane of Gram-negative bacteria is rich in negatively charged lipopolysaccharide molecules, promoting the adhesion of AgNPs and making the bacteria more susceptible to several cellular dysfunctions (Slavin et al. 2017).



Penetration of the AgNPs inside the bacterial cell is another possibility after their adhesion to the cell membrane, and consequently, interfering with vital cellular functioning. This mechanism is size-dependent, as smaller NPs have been observed to reach the cytoplasm at greater rates, than larger ones (Qing et al. 2018). However, when AgNPs penetrate inside the microbial cell, they may interact with intra-cellular structures and biomolecules, including proteins, lipids and DNA, resulting in their disruption or denaturation (Dakal et al. 2016). Particularly, the interaction of AgNPs with ribosomes, which results in their denaturation, causes inhibition of translation and therefore interrupts protein synthesis (Dakal et al. 2016; Qing et al. 2018) It has been observed that  $\text{Ag}^+$  ions can interact with the functional groups of proteins and cause their inactivation, for example, protein thiol (-SH) groups (Rai et al. 2014). Moreover,  $\text{Ag}^+$  are likely to interact with phosphorus-containing compounds, such as DNA, preventing its replication and even causing denaturation. Another effect on DNA is the formation of conglomerates or condensed regions, which occurs as a defence mechanism when the bacteria sense a disturbance in the membrane as a result of attack by toxic compounds. Condensed forms of DNA also result in loss of replication ability, inhibiting cell division (Dakal et al. 2016; Morones et al. 2005).

Cellular oxidative stress increases as a toxic effect derived from the presence of heavy metal ions, such as  $\text{Ag}^+$  ions. Consequently, the presence of  $\text{Ag}^+$  released by AgNPs will lead to the production of ROS and free radicals, such as superoxide anion ( $\text{O}_2^-$ ), hydroxyl radical ( $\text{OH}\cdot$ ), singlet oxygen ( $\text{O}_2$ ), hydrogen peroxide ( $\text{H}_2\text{O}_2$ ) and hypochlorous acid ( $\text{HOCl}$ ). It has been reported that ROS can exist naturally in intracellular and extracellular locations, however, under certain conditions, elevated levels of ROS increase the oxidative stress in cells. This results in the damage of cell membrane, proteins, DNA, and intracellular systems such as the respiratory system (Kim et al. 2011). ROS are considered as a major mechanism for induced bacterial apoptosis in AgNP treatments, as DNA damage is a common apoptotic mark (Zhang et al. 2018). The dysfunction of the respiratory electron transport chain is thought to occur as a result of  $\text{Ag}^+$  ions interacting with thiol groups in essential enzymes or components of the chain, such as nicotinamide adenine dinucleotide (NADH) and succinate dehydrogenase, therefore obstructing adequate electron transfer to oxygen (Park et al. 2009). It is postulated that AgNPs and  $\text{Ag}^+$  have independent but similar modes of action, with  $\text{Ag}^+$  ions exhibiting stronger antibacterial activity than AgNPs. The aforementioned  $\text{Ag}^+$  antibacterial activity is directly proportional to the environmental concentration of ions, but due to oligodynamic effect (A biocidal effect that some heavy metals present against bacteria, which is produced even

from low amounts of metal) they show high efficacy even in low concentrations (Kędziora et al. 2018).

Cell signalling pathways such as the cycle of phosphorylation and dephosphorylation cascade are essential for microbial growth and activity. Reversible phosphorylation of tyrosine residues acts as an activator for several important protein substrates, such as RNA polymerase, DNA binding proteins and UDP-glucose dehydrogenase. These enzymes play an essential role in replication and recombination of DNA, as well as bacterial metabolism and cell cycle. Therefore, decreasing phosphorylation of such enzymes would result in the inhibition of their activity, which represents critical implications on bacterial growth cycle (Dakal et al. 2016; Shrivastava et al. 2007). Upon penetration of the nanoparticles inside the bacterial cytoplasm, interaction with bacterial cellular components occurs, including dephosphorylation of mentioned enzymes, hence modulating the phosphorylation signalling pathway and disrupting bacterial cycle (Shrivastava et al. 2007).

TSNP have been observed to exhibit enhanced antibacterial action, when compared to spherical AgNPs (Van Dong et al. 2012; Lu et al. 2015; Pal, Tak, and Song 2007; Vo et al. 2019). Sharp edges and corners are associated with the improved activity. P. Van Dong et al (2012) suggested that edges and vertexes could enable TSNP easy penetration into the cell, causing higher toxicity. Lu et al (2015) found that the triangular shape of AgNPs releases five times more  $\text{Ag}^+$  than spherical AgNPs, as a result of the sharp corners and larger areas of reactivity enabled by the {111} plane geometry, making them more susceptible to oxidation. This mechanism is a similar to that presented by Vo et al (2019). Pal et al (2007) also attributed the difference in antibacterial efficiency between triangular and spherical shapes to the available surface area that is in contact with the bacteria, concluding that NP size and the presence of a {111} plane are determining factors in promoting biocidal efficacy. Cheon et al (2019) reached a similar conclusion about surface area being an important factor directly influencing  $\text{Ag}^+$  release and therefore affecting the antimicrobial activity.

Raza et al (2016) also demonstrated that size is an important factor to consider. In their study, they compared the bacterial inhibition of different sizes of spherical AgNPs and TSNP, where the smallest sized AgNPs (15-50 nm) had the strongest antimicrobial effect, while TSNP had the second best. They concluded that larger surface to volume ratio possessed by smaller NPs compared to larger ones, allows smaller particles to release more silver ions. Furthermore, it

was demonstrated that antimicrobial activity of silica-coated TSNP can be modulated by laser irradiation, where an increase or decrease on the activity can be observed depending on the laser intensity (Takeda et al. 2022) Such results support the idea that TSNP are not only suitable for nano-sensing applications, but also for antimicrobial devices and surfaces. In addition, it is possible to control the antimicrobial activity of AgNPs by controlling their size and shape (Cheon et al. 2019; Raza et al. 2016).

### **2.3.4 Toxicity Concerns of AgNPs for Humans**

The multiple advantageous characteristics of AgNPs have been discussed, including their unique optical properties, tunability, conductivity and antimicrobial properties, leading to broad research and utilization in a wide range of applications. Nonetheless, the extended use of AgNPs raises a series of unpredictable concerns involving the risks of their interaction with biological systems, especially in the case of human exposure. It is generally assumed that AgNPs will have higher toxicity towards prokaryotic cells than towards eukaryotic cells; however, this might not always be the case. Under certain conditions, the toxic effect of silver towards bacteria and *in vitro* human cells could manifest within the same concentration range (Greulich et al. 2012). It is implied that factors such as morphology, size, chemical composition and surface charge are important factors influencing their toxicity. It has been observed that the toxic effect of AgNPs is largely dependent on the amount of Ag<sup>+</sup> released, with higher Ag<sup>+</sup> concentrations showing greater *in vitro* toxic effects (Beer et al. 2012). Some of the toxicity mechanisms induced by AgNPs include phagocytosis or endocytosis leading to mitochondrial damage and ROS generation, which in turn causes disruption of proteins, nucleic acids and lipids, provoking apoptosis (Akter et al. 2018). Several factors influence the cytotoxic level of AgNPs, including size of the nanoparticle, concentration, coatings and agglomeration.

The toxicity threshold (Minimum dose of any substance on which toxicity is first encountered) of AgNPs is dependent on particle size for specific cell types. However, this is not always the case, as it might depend on several factors rather than only one, including possible variations of the interaction of the AgNPs according to the type of organism (Akter et al. 2018). Findings also show that smaller AgNPs tend to exhibit higher cytotoxicity, due to generation of greater levels of ROS (Carlson et al. 2008; Liu et al. 2010; Dos Santos et al. 2014). The shape of the AgNPs is another factor that can influence their toxicity, as different shapes can have different interaction mechanisms with the cells. For example, Stoehr et al (2011) showed that spherical

NPs had no effect on human alveolar A549 cells, but Ag wires significantly reduced their viability (Stoehr et al. 2011).

On the other hand, it is critical to determine the minimum concentration for AgNPs to induce toxicity and the variation under different conditions and for different subjects. Similarly to size and shape, induction of cytotoxicity can vary with different concentrations of AgNPs on different cell lines (Akter et al. 2018). It is also important to consider the concentration of Ag<sup>+</sup> ions, as they will also have an effect on cytotoxicity. Different factors influence the concentration of Ag<sup>+</sup>, these include particle size, surface functionalization, particle crystallinity, temperature, nature of immersion medium and storage time (Kittler et al. 2010). It has been observed that minimum or maximum concentration for AgNPs to induce toxicity is not fixed and will depend on the morphology of the NPs, the organism exposed and several other factors.

As the toxicity limits for silver can vary depending on the specific context and application, the regulatory standards and permissible exposure limits for silver toxicity may have variations among different organizations and agencies. The Occupational Safety and Health Administration (OSHA), established that the airborne limit for silver is 0.01 mg/m<sup>3</sup> during an 8-hour work shift and 40-hour work weeks (Occupational Safety and Health Administration (OSHA) 2021). On the other hand, the European Commission recommends that the approximate amount of silver that can be safely consumed by humans is 5 µg/kg/day, and the critical dose is estimated to be 14 µg/kg/day, and the maximum concentration allowed in drinking water is <0.1 mg/L (European Commission 2000).

Coating of AgNPs is generally used to prevent their aggregation, typically producing electrostatic and electrosteric repulsions between the NPs, allowing their stabilization. Commonly used capping agents for coating include organic capping agents such as polysaccharides, citrates, polymers, proteins, etc. and inorganic capping agents such as sulphide, chloride, borate and carbonate. The capping material plays a role in preserving the surface chemistry of the AgNPs by stabilizing, providing a specific shape and reducing Ag<sup>+</sup> emission, hence, they hold a significant potential for modulating their bioactivity (Akter et al. 2018). There have been reports where coating did not show any toxic effect to eukaryotic cells and did not prevent antibacterial activity (Travan et al. 2009), where cytotoxicity was reduced compared to non-coated AgNPs (Kawata, Osawa, and Okabe 2009; Nguyen et al. 2013), where

no significant changes were observed between coated and non-coated AgNPs (Shoultz-Wilson et al. 2011) and where the coating of NPs enhanced the cytotoxic mechanism (Zhang et al. 2014). Therefore, depending on the nature and chemistry of the capping agent, it is possible to use coating as a strategy to reduce cytotoxicity, although this does not apply for every capping agent and it may also depend on additional factors.

Contrary to soluble chemicals, NPs can settle, diffuse or aggregate distinctively depending on factors such as their size, density and physicochemical properties. These conditions can have a significant influence on the cellular dose, therefore making the definition of dose for NPs in an *in vitro* system more dynamic, more complex, and less comparable across Np types, than it is in the case of soluble chemicals (Teeguarden et al. 2007). Agglomeration processes can also be affected by the conditions of the culture medium, including pH, electrolyte or salt content and protein composition (Vippola et al. 2009). Agglomeration may sometimes induce toxicity rather than ion-induced toxicity, as it can play a role in several intracellular responses. Therefore, it is important to assess how different states of aggregation or agglomeration affect different biological responses, as easy penetration of agglomerated cells into mesenchymal stem cells and the nuclei has been observed (Hackenberg et al. 2011).

Humans are generally exposed to Ag from several sources, including jewellery, functional textiles, coins, tableware, deodorants, catheters, antibacterial treatments and coatings in refrigerators, etc. (Hadrup, Sharma, and Loeschner 2018). However, more information is still required to correctly assess the hazards of chronic exposure to nano-silver and its ions, both for humans and for the environment. As has been described previously, the cytotoxicity level of AgNPs depends on the combination of several factors. The toxicity towards unicellular organisms (*in vitro*) and multicellular organisms (*in vivo*) could be very different due to the structural and physiological differences, including specialized tissues acting as defence structures. Furthermore, higher organisms such as plants and animals possess diverse defence mechanisms that allow them to tolerate higher levels of heavy metals, including silver (Vazquez-Muñoz et al. 2017). After exposition, intact skin has proven to be an effective barrier against absorption of AgNPs, while on the other hand, mucosal tissue is a less efficient barrier (Hadrup et al. 2018). Argyria (skin coloration) is one of the effects that has been observed after prolonged accumulation of silver in the human body, while other potential risks also include dermatitis and eye irritation (low potential), genotoxicity and carcinogenesis (non-conclusive), hepatic toxicity, neurotoxicity, renal toxicity and hematological toxicity (Hadrup et al. 2018).

Given all these criteria, proper evaluation of potential risks of new AgNPs-containing products should be conducted, to ensure toxicity is minimal or non-existing for the intended application.

### **2.3.5 TSNP-Polymer blending**

AgNPs amalgamated materials are now used in a range of different applications, including improving electrical and thermal conductivity, water treatment, antimicrobial medical materials, sensing materials for diagnosis, among others (Abbas et al. 2018). In the specific case of TSNP, there are only a limited number of reports of their incorporation into other materials for several applications, and the exploration of the antimicrobial activity of said materials is even more limited.

Dispersion of triangular silver nanoprisms in an aqueous acrylamide matrix was reported. The dispersion showed highly tuneable optical properties, and was used as a carrier liquid for a fluorescent dye in the fabrication process of poly(acrylamide) microparticles (Knauer et al. 2013). Additionally, dispersion of triangular silver microplates in a polyvinylidene fluoride matrix for improvement of electrical conductivity was reported by (Audoit et al. 2016). Zhang et al. (2013) fabricated a composite of a TSNP and chitosan, which significantly enhanced the sensitivity as a SPR biosensor (Zhang et al. 2013). Dithiocarbamate-stabilized silver nanotriangles were used to obtain nanocomposites with nanoparticles of polythiophene-derived nanoparticles, trying to obtain a stable system that could be of interest for applications in catalysis, biosensing, electronics and optics (Reynoso-García et al. 2018). The synthesis of solid silver/polyvinylpyrrolidone/polyacrylonitrile nanocomposite films with triangular silver nanoprisms was also reported, taking advantage of their optical absorption spectra to increase the efficiency of photothermal conversion in the polymer matrix, expecting this material to be used in applications such as absorbing materials for solar collectors (Kudryashov et al. 2020).

Another approach for the formation of TSNP composites includes the coating of their surface with polymers, such as silica, PVP or mercaptohexadecanoic acid (Djafari et al. 2019). Djafari et al. (2019) compared the antimicrobial activity of TSNP with different polymeric coatings, and it was found that surface charge of the selected polymeric coating has an effect on the antimicrobial efficacy of TSNP towards Gram-positive or Gram-negative strains. Similarly, Vo et al. (2019) studied the feasibility of a gelatin-chitosan coating on the synthesis of TSNP and evaluated their antimicrobial activity, which was higher compared to other AgNP morphologies. A method for synthesis of TSNP and posterior *ex situ* incorporation into

Polyvinyl alcohol (PVA) was also reported. Potential applications of this method include dichroic materials and antimicrobial materials, but the antimicrobial effect was not evaluated during this study (Velgosova et al. 2022.) As the applications for TSNP can be diverse, their incorporation into polymers for purposes such as improvement of electrical conductivity, thermal conductivity and biosensing have been explored, but there is still a lack of research about their integration into plastics for antimicrobial purposes.

## 2.4 Curcumin

Turmeric (*Curcuma longa*) is a rhizomatous herbaceous tropical plant, widely used in South Asian and Middle Eastern cuisines, and also traditionally used as an anti-inflammatory, antiseptic, antibacterial, choleric, and carminative agent, as well as in the treatment of wounds, respiratory diseases, rheumatism and gastrointestinal disorders. These properties found in turmeric have been mainly attributed to curcumin as its principal bioactive compound (Adamczak, Ożarowski, and Karpiński 2020). Curcumin (1,7-bis(4-hydroxy-3-methoxyphenyl)-1,6-heptadiene-3,5-dione) (Figure 7) is a naturally occurring polyphenol found in the rhizome of *C. longa* and other *Curcuma* spp., being the main component of the characteristic yellow pigment (Hewlings and Kalman 2017). Several studies have corroborated the anti-inflammatory and anti-oxidant properties of curcumin (Hatcher et al. 2008; Hewlings and Kalman 2017), as well as its anti-infective properties, including antibacterial, antiviral and antifungal activity (Praditya et al. 2019; Zorofchian Moghadamtousi et al. 2014).

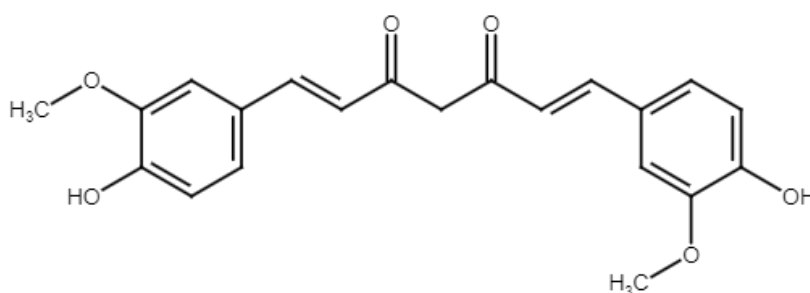


Figure 7. Chemical structure of curcumin. Adapted from (Adamczak et al., 2020), with chem-space.com

Given its numerous bioactive properties, curcumin has become a natural compound of high interest. This is particularly the case due to the consequences caused by the occurrence of the COVID-19 pandemic, which has led to an increased need for products with anti-infective

properties. As a result, in recent years, there has been a significant increase in the number of studies on the methods to obtain curcumin and the research of its bioactivity properties (Raduly et al. 2021). The global curcumin market size was valued in USD 73.41 million in 2021. However, the demand for curcumin has experienced a higher-than anticipated growth (8.13% higher in 2020 compared to 2019) globally, compared to pre-pandemic levels. Consequently, the curcumin global market is now projected to grow from USD 79.94 million in 2022 to USD 155.24 million by 2029 (Fortune Business Insights 2022). This highlights the need for further research on curcumin and to further explore its potential applications.

Curcumin has shown to possess broad-spectrum antibacterial activity against Gram-positive and Gram-negative strains. This activity has been observed to occur through different mechanisms, including interaction and damage of bacterial membrane, bacterial wall, DNA, proteins and other cellular structures (Tyagi et al. 2015; D. Zheng et al. 2020). Curcumin has been observed to downregulate bacterial gene expression, as well as inhibit the bacterial DNA damage response, which is an important protective mechanism involved in the development of drug resistance (D. Zheng et al. 2020). In vitro studies have also shown that curcumin inhibits the bacterial proliferation by disrupting the assembly of FtsZ (Filamenting temperature-sensitive mutant Z) protofilaments and affecting the GTPase activity in the cytoskeleton of *Bacillus subtilis*, *E. coli*, and *S. aureus* strains (Adamczak et al. 2020). Another relevant mechanism of curcumin activity is the disruption of the localization of membrane-associated proteins, leading to an increase in the permeability of bacterial cell membranes, increasing the sensitivity of the bacterial cell towards external harmful compounds. Thinning, cell lysis and cell cracking have also been observed as a result of curcumin interaction with bacterial membranes (Tyagi et al. 2015; Zheng et al. 2020).

Furthermore, curcumin has reportedly exhibited inhibition of bacterial growth through interference with the quorum system. The quorum system is a chemical communication process between microbial cells that allows them to regulate gene expression in response to cell density, act as cohesive group and coordinate collective behaviors. This system is key in the regulation of a wide array of physiological bacterial activities, including virulence, competence, sporulation and biofilm formation (Miller and Bassler 2001). Therefore, this interference has been postulated as a crucial factor in the ability of curcumin to prevent biofilm formation (Packiavathy et al. 2014; Di Salle et al. 2021).



### **2.4.1 Curcumin-Polymer blending**

It has been established that curcumin possess several biological activities, such as antimicrobial and anti-oxidant which render it suitable for biomedical applications. Hence, there has been multiple studies to evaluate the incorporation of curcumin into different materials that can be used for medical purposes, or even for food packing purposes.

Incorporation of curcumin into different polymers and biopolymers is a strategy that has been explored to be used for a variety of therapeutical purposes. One of the principal bioactivities of curcumin is the antioxidant effect, which can help control the oxidative stress of damaged tissue, therefore helping to speed-up the healing process. For instance, curcumin was successfully encapsulated in chitosan nanoparticles by Nair et al. (2019), as a strategy for transdermal delivery (Nair et al. 2019). Curcumin was also loaded into electro-spun nanofibers made of PCL and PLA by Jahanmardi et al. (2021) and Di Salle et al. (2021) respectively, which is another strategy that can be used for controlled drug release, therefore potentially useful to be employed as scaffolds in tissue engineering regeneration (Jahanmardi, Tavanaie, and Tehrani-Bagha 2021; Salle et al. 2021).

Curcumin has also been widely used in combination with materials intended for wound dressing applications, which not only helps the healing process by reducing oxidative stress, but also by preventing infections on the wound area (Alven, Nqoro, and Aderibigbe 2020). A wide variety of polymeric materials have been loaded with curcumin and evaluated for such purposes. These polymers can be used in the form of hydrogels, films/membranes, sponges/bandages, nanofibers or scaffolds (Alven et al. 2020). Some of the commonly used polymers and biopolymers include cellulose (Huang, Liu, and Zhou 2017; Shefa et al. 2020), bacterial cellulose (Gupta et al. 2020), chitosan (Pham et al. 2019; Zhao et al. 2018), polymethacrylic acid (Anjum et al. 2016), PEG (Cirillo et al. 2017; Gong et al. 2013), dextran (Alibolandi et al. 2017), alginate (Kamar, Abdel-Kader, and Rashed 2019; X. Li et al. 2012), poly-acrylamide (Ravindra et al. 2012), Poly(vinyl alcohol) (Anjum et al. 2016; Rezvan, Pircheraghi, and Bagheri 2018; Shefa et al. 2020), PCL, PLA among others.

### **2.4.2 Curcumin-Silver Combined Effect**

Despite of the wide spectrum of antimicrobial action present in compounds like curcumin, it is necessary to implement strategies that allow reducing the risk of resistance generation in the

long term of use of the agent. There are three possible outcomes when antimicrobial agents are combined: they can act additively, where the resulting antimicrobial effect is the sum total of both agents acting together; they can behave synergistically, where the resulting activity is greater than the sum of their individual activities: or they can be antagonistic, when the activity of one of the agents is hindered by the other one (Doern 2014). Studies suggest that the combined use of two antimicrobial agents that have the ability to act synergistically can significantly reduce the mutant selection window and therefore prevent the development of antimicrobial resistance (Xu et al. 2018).

Curcumin and AgNPs have a significant antimicrobial effect by diverse mechanisms. As a result, several research groups have considered the combined use of both, either in separate or combined formulations (Mohammadi et al. 2021). This combined effect can be achieved through diverse strategies thanks to the easy interaction between these two antimicrobial agents. Curcumin can be used to assist the AgNP synthesis and also as a capping agent to stabilise the AgNPs, while increasing the antimicrobial effect at the same time (Mohammadi et al. 2021). For example, curcumin-capped AgNPs showed an increased antimicrobial activity compared to Polyvinylpyrrolidone-capped AgNPs, against *E. coli* and *Bacillus subtilis* (Song et al. 2019). Furthermore, Jaiswal & Mishra (2017) synthesised AgNPs using curcumin as a reducing and capping agent, which exhibited good antimicrobial and antibiofilm activity, as well as selective toxicity towards bacteria over mammalian keratinocytes (Jaiswal and Mishra 2017). These examples demonstrate that there is a strong potential warranting the exploration of combined formulations of AgNPs and curcumin, for diverse antimicrobial applications.

The combination of curcumin and AgNPs has also been tested for incorporation into nanocomposites, to provide materials with antimicrobial properties. For instance, curcumin-loaded AgNP hydrogels were developed for antibacterial and drug delivery applications, demonstrating antimicrobial activity against *E. coli* (Ravindra et al. 2012). A similar approach was undertaken by Alves et al. (2017), with the formulation of a thermoresponsive gel with antimicrobial and antioxidant properties, by combining the incorporation of curcumin in a solid dispersion, with the addition of AgNPs, which resulted in an improvement of the antimicrobial efficacy, compared to curcumin alone (Alves et al. 2018). Another example is the synthesis of AgNPs with the use of curcumin-cyclodextrins as a reducing and capping agent, and their posterior incorporation into bacterial cellulose hydrogels, performed by Gupta et al. (2020) for wound dressing applications (Gupta et al. 2020).

## 2.5 Embedding of Silver Nanoparticles (AgNP) into Polymers and Biopolymers

### 2.5.1 Polypropylene

Polypropylene (PP) is a synthetic resin from the family of polyolefins, which was discovered in 1954 and gained popularity rapidly due to ease of processing and its lowest density among commodity plastics (Maddah 2016). It is currently widely moulded or extruded into several plastic products on a global basis, where toughness, flexibility, light weight and heat resistance are required characteristics. PP is prepared catalytically through the polymerization of propylene, a gaseous compound obtained by the thermal cracking of ethane, propane, butane and the naphtha fraction of petroleum (Encyclopaedia Britannica 2016). The structure of PP is shown in Figure 8. The major advantage of PP as a thermoplastic is high temperature resistance, making it particularly suitable for the fabrication trays, funnels, pails, bottles, carboys and clinical instruments that require to be sterilized frequently and several other items. Due to its crystalline structure PP exhibits a high level of stiffness and a high melting point compared to other commercial thermoplastics (Maddah 2016).

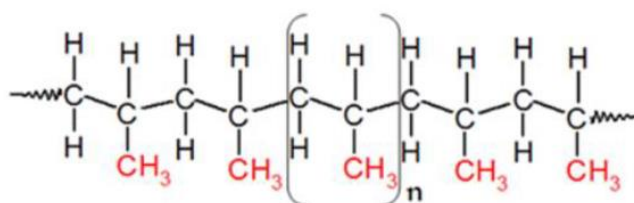


Figure 8. Structure of PP (Maddah 2016).

Given the high demand and wide applications of PP, several examples of integration of AgNPs into this plastic for antimicrobial purposes already exist. For instance, PP fabric loaded with *in situ* synthesised AgNPs demonstrated effective antimicrobial activity against *S. aureus*, *E. coli* and *C. candida* after 24 hours of contact (Gawish and Mosleh 2020). A coating strategy of PP films with AgNPs was developed with the purpose of obtaining surfaces with antifouling properties. Results demonstrated a reduction of 4 log units in viable *S. aureus* concentration and inducing *E. coli* death, even with a low content (0.08 wt %) of AgNPs (Mosconi et al. 2020). Nanocomposite films of PP were prepared through the addition of AgNPs in PVP solution during processing in the extruder, where resulting films presented antimicrobial effects against *S. aureus* and *E. coli*, while no cytotoxicity towards mammalian cells was observed

(Oliani et al. 2015). In another approach, the hydrophobic surface of PP was modified to allow the attachment and reduction of AgNPs and compared to another method called heat softening that consisted on immersing PP in boiling water to make the plastic soft and facilitate the attachment of the in-situ synthesised AgNPs. Both methods demonstrated antimicrobial action towards *E. coli* and *S. aureus*, but the activity was observed to last longer on heat-softened samples due to reduced loss of NPs after repeated disinfection (Wu et al. 2012). Although several examples of AgNPs being integrated to PP can be found in the literature, apparently no attempt to integrate TSNP have yet been reported, leaving a gap to evaluate the effectiveness of this nanoparticle morphology for antimicrobial purposes in PP composites.

### 2.5.2 Polycarbonate

Polycarbonate (PC) is a high-performance amorphous and transparent thermoplastic that offers toughness, high impact strength, high dimensional stability and good electrical properties. It is a class of polymers made of organic functional groups linked together by carbonate groups, which can be classified into aliphatic or aromatic PCs, depending on the structure of the connected R groups, as shown in Figure 9 (Takeuchi 2012). Some of PC's most interesting properties, include an extreme clarity with great transmittance, lightweight, protection from UV radiations, optical nature, and good chemical and heat resistance (Omnexus n.d.). Thanks to these properties, PC and their blends have a wide number of applications in domestic appliances, automotive headlamps and lenses, as a glass alternative in building and construction, food and beverage containers, ophthalmic lenses, safety goggles, medical applications such as surgical instruments, drug delivery systems, haemodialysis membranes, blood reservoirs, among many others (Takeuchi 2012).

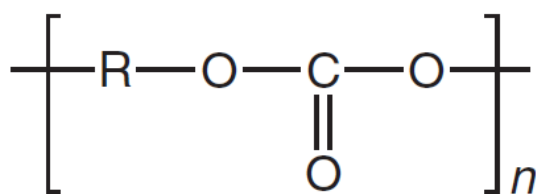


Figure 9. Structure of PC (Takeuchi 2012).

Compared to PP, fewer efforts have been made to integrate AgNPs into PC for antimicrobial purposes, but still, some examples can be found. Green synthesis of AgNP using extract of *Callistemon viminalis* as reducing agent for silver nitrate was performed prior to their integration into a polycarbonate membrane through two different approaches: centrifugation

and sonication. Both approaches resulted in membranes exhibiting inhibition towards *E. coli* and *Bacillus cereus* (Sackey et al. 2020). In a different approach, AgNPs were synthesised in a toluene solution, then separated from the solution through centrifugation and dried in vacuum to obtain a powder that was easily redispersed in organic solvents. Afterwards, PC films were mixed with the AgNPs in a methylene chloride solution, poured in a mould at room temperature to allow the solvent to be evaporated and form a composite of PC films containing the AgNPs. Although the report does not describe clearly how the antibacterial evaluation was performed, they report a reduction of 99.99% of viable colony forming units of *E. coli* by the films containing 0.5 wt% of AgNPs (Lee et al. 2008).

### **2.5.3 Polycaprolactone**

Polycaprolactone (PCL) is a biodegradable polyester prepared by ring opening polymerization of  $\epsilon$ -caprolactone. PCL has a very low melting point compared to other polymers, which is around 60 °C (Lackner 2015; McKeen 2012). Structure of PCL is shown in Figure 10. PCL's ester linkages are degraded by hydrolysis in physiological conditions, making it a highly suitable polymer to be used for the preparation of implantable devices and to encapsulate drugs for controlled release and targeted delivery (McKeen 2012). Due to its high toughness, superior rheological and viscoelastic properties, and its low melting point, PCL is very easy to manufacture and manipulate, making it attractive for applications that require rapid prototyping and a wide range of three-dimensional platforms (Guarino et al. 2017; Lackner 2015). Furthermore, its biodegradability makes it attractive for other industrial applications such as films for packaging, where comparable functionalities to traditional commodity plastics have been found (Guarino et al. 2017), as well as medical applications that require the use of biocompatible and/or bioresorbable materials (Espinoza et al. 2020). However, pure PCL is not used in applications where structural performances are required due to its low elastic modulus, therefore it requires to be blended with other polymers or reinforced with fillers to improve the elastic properties and be suitable for such applications (Guarino et al. 2017).

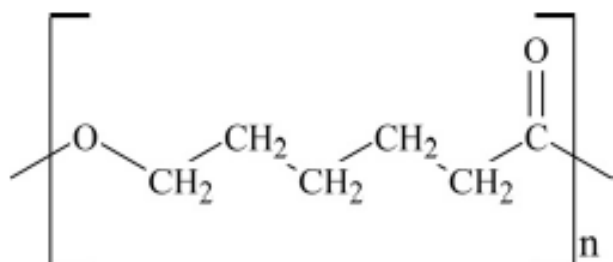


Figure 10. Structure of PCL (McKeen 2012).

Due to the vast biomedical applications of PCL, where antimicrobial properties can be highly desirable to help prevent infections, the integration of AgNPs into this polymer has been researched. For instance, PCL electrospun nanofiber scaffolds doped with AgNPs were fabricated through an air plasma reduction method, successfully inhibiting growth of *Streptococcus pneumoniae* after 24 hours of exposure (Binkley et al. 2019). Similarly, PCL nanofiber scaffolds containing AgNPs were prepared by *in situ* reduction using N,N-dimethylformamide in tetrahydrofuran solution and the addition of PCL in the solution for electrospinning, demonstrating good antibacterial effect against six strains of Gram-positive and Gram-negative bacteria despite using a low concentration of AgNPs for the nanofibers (Lopez-Esparza et al. 2016). In a different approach, a complexation-reduction method was used to synthesise the AgNPs within a chitosan-aniline nanogel, the AgNPs are afterwards released when the nanogel is irradiated by light at 405 nm, and electrospun PCL nanofibers are immersed in a dispersion of AgNPs-nanogels to immobilize them onto the surface of the nanofibers (Ballesteros, Correa, and Zucolotto 2020). AgNPs biosynthesised by *Bacillus* sp. were incorporated into PCL membranes prepared by electrospinning, demonstrating inhibitory activity against coagulase-negative *Staphylococcus epidermis* and *Staphylococcus haemolyticus* strains (Thomas et al. 2015).

#### 2.5.4 Polylactic acid

Poly(lactic acid) or polylactide (PLA) is a polymer derived from lactic acid (2-hydroxypropionic acid) which has been extensively researched for use in medical applications due to its bioresorbable properties, allowing biocompatibility in the human body (Auras, Harte, and Selke 2004). PLA has also a high potential to substitute commodity plastics for several industrial applications, because it is a thermoplastic with high strength and high modulus that is biosynthesised by fermentation of sugars obtained from renewable sources such as sugarcane

or corn starch (Farah, Anderson, and Langer 2016). Currently, PLA is already being used for the fabrication of food and beverage packing products with short shelf life, including containers, drinking cups, lamination films, blister packages, salad cups and thermoformed containers used in retail markets for fresh fruit and vegetables (Auras et al. 2004). PLA structure is shown in Figure 11. PLA structure can be synthesised as different stereoisomers, such as poly(L-lactide) (PLLA), poly(D-lactide) (PDLA) and poly(DL-lactide) (PDLLA), because lactic acid, its precursor molecule, exists as two different enantiomers L- and D-lactic acid (Farah et al. 2016). By controlling the stereochemical architecture of PLA, different properties can also be modified, including speed and degree of crystallization, mechanical properties and processing temperatures of the polymer (Auras et al. 2004). Despite the advantages of PLA, the material also has some drawbacks, such as poor toughness, slow degradation rate, relative hydrophobicity, and lack of reactive side-chain groups, which limits its relevance to some the applications and brings the necessity to develop blends and composites to improve its properties for suitability and broaden its candidacy for a more extensive range of applications (Farah et al. 2016).

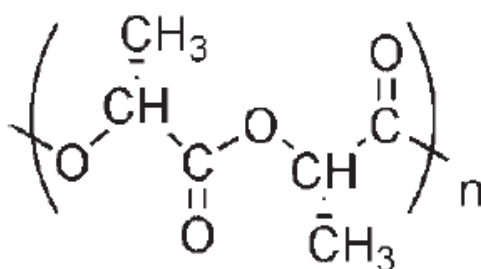


Figure 11. Structure of PLA (Auras et al. 2004).

The potential of PLA for medical applications makes this polymer a great candidate for incorporation of antibacterial properties, including the preparation of AgNP nanocomposites. For example, PLA was dissolved in a mix of dichloromethane and dimethylformamide solvents, where AgNO<sub>3</sub> was added, followed by the addition of sodium NaBH<sub>4</sub> as reducing agent to allow the formation of AgNPs. The composite films were formed through solvent-casting and demonstrated strong antibacterial activity against Gram-negative *E. coli* and *Vibrio parahaemolyticus*, and Gram-positive *S. aureus* (Shameli et al. 2010). In a different approach, AgNPs were synthesised using chitosan as a reducing and stabilizing agent. PLA, oligomeric lactic acid and the chitosan-AgNPs were mixed in a micro-extruder with two twin conical co-

rotating screws. The dual mechanism of action of the AgNPs and the cationic effect of chitosan demonstrated enhanced antimicrobial action against *E. coli* and *S aureus*, while also increasing the toughness and elongation and break of the films (Sonseca et al. 2020). A different nanocomposite was formulated by modifying carrot cellulose nanofibrils with AgNPs and then the modified nanofibrils were used as a filler for PLA, for improving mechanical properties and provide antibacterial action to the composite. The films were fabricated through solvent casting, by mixing the PLA and the AgNP-modified nanofibrils in dichloromethane. Antibacterial activity against *E. coli* and *Bacillus cereus* was observed only at contact surface with the material, which suggested the inability of NPs and ions to migrate from the composite (Szymańska-Chargot et al. 2020).

### 2.5.5 Bacterial Cellulose

Bacterial cellulose (BC) is a biopolymer that has attracted a lot of interest in research and industrial sectors, given that it is highly pure compared to plant-produced cellulose. BC has several exclusive properties, such as high liquid holding capacity, flexibility, mouldability, and high mechanical strength in the wet state (Gorgieva and Trček 2019). Furthermore, BC's biocompatibility renders it as a suitable material for a broad range of applications, particularly in the biomedical field, such as wound healing systems, tissue regeneration, scaffolds, and transdermal applications (Sharma and Bhardwaj 2019; Silva et al. 2017). The structure of BC (Figure 12), as well as the cellulose found in plants, is composed of a linear array of glucose molecules linked by  $\beta$ -1,4-glycosidic bonds. The cellulose chains aggregate through hydrogen bonds and Van der Waals forces, forming a long thread of glucan chains in a crystalline structure, called microfibrils (Rongpipi et al. 2019).

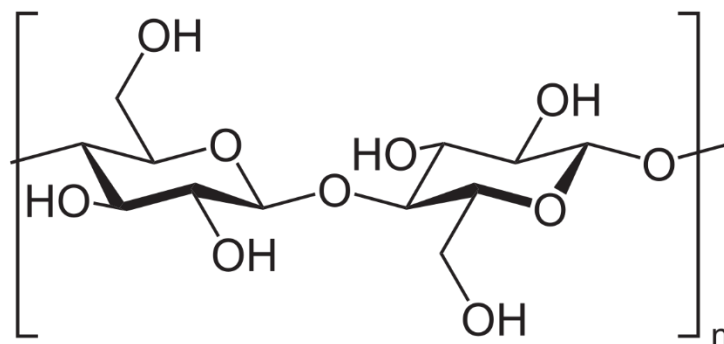


Figure 12. Structure of BC, consisting of linear chains of glucose units linked by  $\beta$ -1,4-glycosidic bonds (Manoukian et al. 2019).



The production process for BC is regarded as one of the crucial steps that controls the properties of the resulting material. Various species of bacteria, including Gram-negative and Gram-positive, and different substrates can be used for BC production. Such variety results in different morphologies, structures, properties and applications of the produced BC (Wang, Tavakoli, and Tang 2019). Between Gram-positive bacteria only few species have been reported to produce BC, such as: *Bacillus* sp. (Bagewadi et al. 2020), *Leifsonia* sp. (Velmurugan et al. 2015), *Lactobacillus* sp. (Khan, Kadam, and Dutt 2020), and *Rhodococcus* sp (Tanskul, Amornthatree, and Jaturonlak 2013). In contrast, the number of Gram-negative BC producers is significantly higher. Species belonging to *Pseudomonas* (Arrebola et al. 2015), *Escherichia* (Monteiro et al. 2009), *Alcaligenes* (Cannon and Anderson 1991), *Enterobacter* (Hungund and Gupta 2010), *Salmonella* (Römling and Lünsdorf 2004), *Acetobacter* (Aswini, Gopal, and Uthandi 2020), and *Komagataeibacter* genera, among others, have been reported as BC producers in the literature. On the other hand, bio-cellulose can be synthesised in a cell-free system in the presence of appropriate enzymatic machinery after disrupting bacterial cell walls (Ullah et al. 2015).

Recently, one of the most attractive genera that has been studied for BC production is *Komagataeibacter*. Several species from this genus have been identified as strong cellulose producers, including *Komagataeibacter xylinus*, *Komagataeibacter medellinensis*, *Komagataeibacter oboediens*, *Komagataeibacter pomaceti*, *Komagataeibacter nataicola*, *Komagataeibacter rhaeticus* (Gorgieva and Trček 2019).

The utilization of other materials as substrates for BC production, together with glucose has been recently evaluated as an approach for improving the properties of resulting BC (Żywicka et al. 2018). Such approaches can also be extended to the enhancement of antimicrobial activity of BC given its wide range of applications in the biomedical field. Improvement of polymers' antimicrobial properties is a popular research topic (Comini et al. 2022). Different techniques have been proposed to produce BC with enhanced antimicrobial properties. These include the addition of antibiotics (Lemnaru et al. 2020), inorganic antimicrobials such as metallic nanoparticles (Pal et al. 2017), carbon nanomaterials (Miyashiro, Hamano, and Umemura 2020) and organic antimicrobials such as natural polymers, bioactive substances (Bodea et al. 2022) or synthetic compounds (Zheng et al. 2020). Moreover, based on reported literature it has been demonstrated that associating two antimicrobial agents into a single composite can

have significant benefits due to the combined action of both compounds to overcome microbial resistance (Bush 2017; Guo et al. 2022).

## CHAPTER 3 – MATERIALS AND METHODS

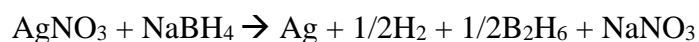
### 3.1 TSNP

#### 3.1.1 Materials

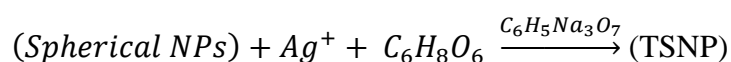
HPLC grade water (34877-2.5L), Sodium citrate tribasic (C8532-100G) [TSC], Poly(sodium 4-styrenesulfate) (434574-5G) [PSSS], Sodium borohydride (213462-25G) [NaBH<sub>4</sub>], Silver nitrate (204390-10G) [AgNO<sub>3</sub>], L-Ascorbic acid (A92902-25G) [AA], chloroform ( ) and O-[2-(3-mercaptopropionylamino)ethyl]-O'-methylpolyethylene glycol (11124-1G-F) [SH-PEG] were obtained from Sigma-Aldrich. FRX Pump from Syrris was used for the addition of AgNO<sub>3</sub> in the small-scale synthesis. LP-BT100-1F Peristaltic Dispensing Pump with YZIII5 pump head and Tygon LMT-55 Tubing (SC0375T), provided by Drifton, were used for the addition of AgNO<sub>3</sub> in the Scaled-up process. Gold (III) chloride trihydrate (520918-1G) [HAuCl<sub>4</sub>] was obtained from Sigma-Aldrich. Biotek Synergy HT Microplate Reader, provided by Biotek Instruments GmbH, was used for the readings of spectra and monitoring of LSPR changes in the TSNP.

#### 3.1.2 Synthesis of TSNP

The TSNP synthesis was done using a seed-mediated approach, adapted from Aherne et al (2008). This method involved two steps; seed production and TSNP growth. For the seed production, 5 mL of TSC (2.5 mM), 0.25 mL of PSSS (500 mg/L) and 0.3 mL of NaBH<sub>4</sub> (10mM) were mixed, followed by the addition of 5 mL of AgNO<sub>3</sub> (0.5 mM) at a rate of 2 mL/min on constant stirring. For the TSNP growth, 5 mL of distilled water, 0.075 mL of AA (10mM) and various quantities of seed solution were mixed, followed by the addition of 3 mL of AgNO<sub>3</sub> (0.5 mM) at a rate of 1 mL/min and finally, the addition of 0.5 mL of TSC (25 mM). The solution can be diluted as desired with distilled water. The method described was performed using distilled water for all synthesis steps and for preparation of all the solutions. NaBH<sub>4</sub> was used for the reduction of AgNO<sub>3</sub> and seed formation. The chemical reaction occurs as follows (Solomon et al. 2007):



TSC and PSSS were used as stabilizers for the seed production, and both have been reported to aid the formation of the nanoplates. It is postulated that citrate ions and PSSS (being a charged polymer), bind to the surface of the {111} face of the particles, promoting growth of the NPs in triangular plate shape (Aherne et al. 2008; Kelly et al. 2012). Afterwards, in the growth step, the spherical Ag seeds can react with new Ag<sup>+</sup> ions in the presence of ascorbic acid and citrate ions, forming the TSNP. The chemical reaction can be explained as follows (Etacheri et al. 2010):



TSC was added at the end of the synthesis to stabilize the nanoplates. By adjusting the final volume of the solution to 10 mL with water, this method resulted in a concentration of 16.62 ppm of atomic Ag.

### 3.1.2.1 Optimised Method for TSNP Synthesis

Increased concentration of NPs is desired to aid treatment for the intended TSNP-polymer processing. A reduction of 20% of water for the synthesis was successfully achieved without negatively affecting the results. Therefore, the standard protocol for the TSNP used in this project is as follows:

All glassware used in the procedure was previously rinsed with a small amount of nitric acid (HNO<sub>3</sub>). Then, glassware was rinsed with tap water at least 7 times to eliminate all traces of HNO<sub>3</sub>, and finally, rinsed with distilled water. Performing this cleaning procedure helps eliminate possible traces of undesired chemicals from other experiments where the glassware is used, preventing interference on the synthesis reaction. In addition, the use of ultrapure water is preferred to avoid contaminations or interference in the reaction. Ultrapure water was used in all reaction steps and solutions prepared. NaBH<sub>4</sub> and AA solutions were prepared fresh each time the synthesis reaction is carried out. Constant stirring of the solution was also an important factor for consistency of results and to reduce the formation of spherical NPs in the solution.

Seed preparation was not modified from the method reported by Aherne et al (2008). After preparation, seed solution was left on the bench, covered by parafilm for at least four hours, to ensure reaction is fully completed. The seed solution turned into a dark yellow colour a few minutes after finishing its preparation, as shown in Figure 13. For the TSNP synthesis, a smaller

amount of water was used to increase the concentration of the formed NPs in solution. As for the seed volume used, it can be changed depending on the size desired for the nanoplates, increasing it to obtain smaller nanoplates or reducing it for bigger ones. Different volumes ranging between 0.2-0.7 mL were used, until eventually; 0.35 mL became the standard. Consequently, the adapted method consists in mixing 4 mL of water, 0.075 mL of AA (10 mM) and 0.35 mL of seed solution (25.56 ppm of Ag), followed by the addition of 3 mL of  $\text{AgNO}_3$  (0.5 mM) at a rate 1 mL/min. Finally, 0.5 mL of TSC (25 mM) are added when the reaction is finished, resulting in a final Ag concentration of 21.34 ppm and a volume of 8 mL. Noticeably, upon adding  $\text{AgNO}_3$ , the colour starts changing from yellow to shades of orange, then shades of red, then purple and finally takes a dark blue colour, as demonstrated in Figure 13.

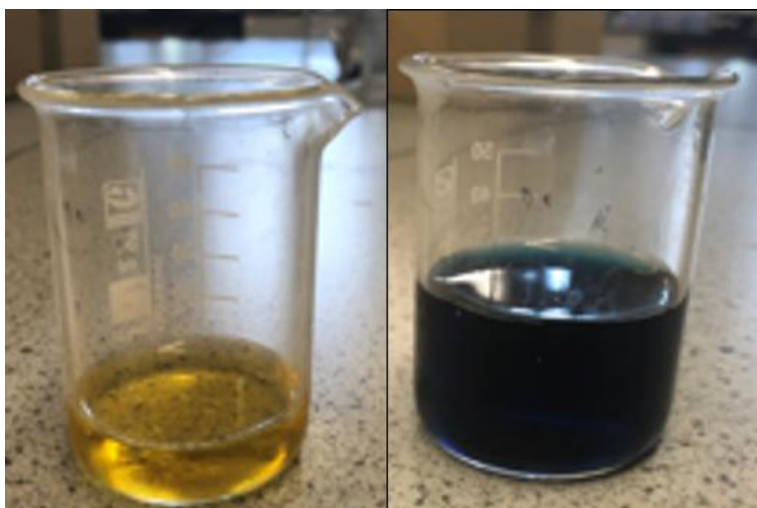


*Figure 13. Seed solution (left) and TSNP solution (right).*

### **3.1.2.2 Scale-Up of TSNP Production**

LP-BT100-1F Peristaltic Dispensing Pump with YZII15 pump head and Tygon LMT-55 Tubing (SC0375T), provided by Drifton, were used for the addition of  $\text{AgNO}_3$ .

Scaling up the TSNP volume can be achieved by increasing all the volumes from the adapted method proportionally to the desired increase in final volume. For instance, to increase the final volume from 8 mL to 80 mL, 30 mL of  $\text{AgNO}_3$  would be used in the TSNP growth, instead of 3 mL. The method for the preparation of 300 mL of solution is outlined here, as it became the recurrent volume prepared for the experiments carried out.

Seed volume required to be increased as well, since the 10.55 mL obtained with the standard procedure are not enough for this reaction. Thus, to prepare 20 mL of seeds, 8.53 mL of water, 0.95 mL of TSC (25 mM), 0.47 mL of PSSS (500 mg/mL) and 0.57 mL of NaHB<sub>4</sub> (10 mM) are mixed, followed by the addition of 9.48 mL of AgNO<sub>3</sub> (0.5 mM) at a rate of 3.79 mL/min. After 4 hours, the seeds can be used in the second step of the reaction, mixing 150 mL of water, 2.81 mL of AA (10 mM) and 13.12 mL of seed solution (25.56 ppm), followed by the addition of 112.5 mL of AgNO<sub>3</sub> (0.5 mM) at a rate of 37.5 mL/min, then 18.75 mL of TSC (25 mM) were added after reaction was finished.

### **3.1.2.3 UV-Vis Spectroscopy for Monitoring of the Optical Properties of TSNP**

The optical properties of metallic nanoparticles like AgNPs and AuNPs are traditionally monitored through UV-Vis spectroscopy because it is an excellent technique for the characterisation of a sample's response to light in a wide wavelength range, by performing a spectral reading, and the LSPR appears on the absorption spectrum of the NPs as a distinctive peak (Berry 2023). Therefore, readings of the spectrum in the UV-Vis range can be helpful to detect LSPR shifts as a function of changes in particle size, particle geometry and even functionalisation of the NPs with diverse analytes. Spectral readings in the UV-Vis range were performed in a Biotek Synergy HT Microplate Reader, in the range between 350-900 nm, with a reading step for 1 nm.

### **3.1.3 TSNP Gold Coating**

TSNP gold coating was done based on the method reported by Zhang et al. (2014), consisting on the use of a small amount of HAuCl<sub>4</sub> salt and a high concentration of AA for the reduction of AuCl<sub>4</sub> and the inhibition of Ag oxidation at the surface of the TSNP. Deposition of a thin layer of gold in the edges of the TSNP occurs due to galvanic replacement. TSNP solution was prepared as indicated in section 3.1.2. Afterwards, 18.9 µl of AA (10 mM) were added per each ml of TSNP solution to be coated, while solution was stirred. A ratio of 1:0.05 (Ag: Au) was considered upon adding HAuCl<sub>4</sub> (0.5 mM). Considering the TSNP solution contains 378 µl of AgNO<sub>3</sub> per each millilitre of solution, this results in 18.9 µl of HAuCl<sub>4</sub> per each ml of TSNP solution. To verify the efficacy of the gold layer on protecting the nanoplates from etching, the AuTSNP were exposed to NaCl 10 mM and 20 mM, in a 50:50 volumetric ratio.

### **3.1.3.1 AuTSNP Sucrose Sensitivity Test**

Briefly, small amounts of AuTSNP were dispersed in sucrose solutions of different concentrations (10%, 20%, 30%, 40% and 50% sucrose (w/w) in ultrapure water), increasing the refractive index as the sucrose concentration rises. Afterwards, 20  $\mu$ l of AuTSNP (prepared as described in section 3.1.3) were dispersed in 780  $\mu$ l of each sucrose solution. UV-Vis spectrum of each sample was then recorded.

### **3.1.3.2 AuTSNP for Fibronectin (Fn) Detection**

AuTSNP were used to monitor Fn conformational changes induced under different pH conditions. As described by Brennan-Fournet et al (2015), Fn has a compact, folded conformation under physiological buffer conditions (pH 7.4) but is extended at a more acidic pH. In the same study, AuTSNP were used to monitor these conformational changes in real time and the same method was followed for this experiment. Disodium phosphate buffer (pH 4) and phosphate buffer (pH 7) were prepared to induce Fn conformational transition. To prepare 0.2 M disodium phosphate ( $\text{Na}_2\text{HPO}_4$ ) buffer, 2.84 g of  $\text{Na}_2\text{HPO}_4$  was dissolved in 100 ml of 0.2 M NaCl solution, pH was measured to be 4. Phosphate buffer 0.1 M was prepared by mixing 40.5 ml of  $\text{Na}_2\text{HPO}_4$  buffer (0.2 M) with 9.5 ml of  $\text{NaH}_2\text{PO}_4$  (0.2 M), and the pH was measured to be 7. AuTSNP solution was mixed in a 1:1 ratio with a 0.01% PEG (MW 10,000) solution, which served to minimise the influence of Fn direct contact with the nanoplate surface on the conformational behaviour of the protein. A small volume of both buffers was diluted to 0.01 M before use. 350  $\mu$ l of buffer was mixed with 50  $\mu$ l of AuTSNP-PEG solution and 25  $\mu$ l of Fn (1 mg/ml), for each buffer. UV-Vis spectra of the solutions were recorded.

### **3.1.4 TSNP Thermal Evaluation**

TSNP solution, prepared as described in section 3.1.2.2 was exposed to different temperatures to evaluate the possible effect of the high temperatures during polymer processing. This was done using an oven to control the temperature, and the experiment was carried out using two different designs. For the first test, the temperatures tested were 80°, 100° and 120° C. Before using the TSNP solution, it was concentrated from 21.34 ppm to approximately 128 ppm using a centrifuge (16,162 x g, 45 min) to eliminate water and reduce the volume six times. A tube containing 2 ml of the concentrated TSNP solution was placed an oven at 80 °C for 5 minutes, then at 100 °C for 5 minutes and finally at 120 °C for 5 minutes. UV-Vis spectra were recorded before the temperature test and after testing each temperature. For the second test, separate

tubes were exposed to 120° C and 150 °C for five minutes respectively and a tube of non-centrifuged TSNP solution was also tested to compare between concentrated (128 ppm) and non-concentrated (21.34 ppm) TSNP solutions. UV-Vis spectra were recorded before and after the temperature test.

#### **3.1.4.1 TSNP Concentration by Water Evaporation**

After evaluating the results from temperature tests, a method was designed to concentrate the TSNP solution without using a centrifuge, but evaporating water from the solution instead. The first attempt consisted on exposing 150 ml of the TSNP solution (21.34 ppm) to short heat cycles of 150 °C for 10 minutes, then cooling down the solution for 10 minutes on the bench and another 10 minutes inside the fridge. After 4 cycles, TSNP solution colour started changing from dark blue to purple, so the cycle times were reduced to 5 minutes for oven, bench and fridge cooling steps (Sample A). The cycles were repeated several times over a period of 5 days until approximately 70 ml of solution was evaporated. Additionally, 80 ml of TSNP solution (21.34 ppm) were subjected to the initial 10 minutes cycle until the volume was reduced to 18 ml (Sample B), on order to evaluate the impact of heating time on this procedure. UV-Vis of TSNP solutions prior to evaporation and from both samples was recorded.

On evaluating the results, it was decided to significantly reduce the temperature, while at the same time increasing the time of exposure to heat. 200 ml of TSNP solution, prepared as described in section 3.1.2.2 were kept inside the oven at 40 °C for 8 days, until approximately 50% of the water volume was evaporated. UV-Vis spectra of the solution was recorded before and after heat treatment. Estimated concentration of the solution after evaporation is 42.64 ppm of atomic silver.

#### **3.1.5 TSNP protection using halloysite nanotubes**

TSNP solution was mixed with halloysite nanotubes (HNT) as a mean of encapsulation for protection of the TSNP from polymer processing conditions. HNTs are a type of kaolinite clay with a hollow tubular structure, which possess positive and negative charge on the inner and outer surface respectively (Jana et al. 2017), The objective was to potentially take advantage of the TSNP charge to bind them to the HNT. 200 mg of HNT powder were mixed with 2 ml of TSNP solution (40 ppm after evaporation, sample A from section 3.1.4.1), until the powder was completely dissolved. The solution was the left overnight inside the oven at 40° C to dry,



and the dried material was recovered and milled down to make a powder. The procedure was repeated trying an alternative way to dry the mixed material, by drying inside the oven at 40° only for 3 hours and then centrifuging the remaining liquid (12,400 x g for 40 minutes).

### 3.1.6 Transfer of TSNP to Chloroform

Transfer of the TSNP to chloroform was carried out as a strategy to achieve a mix of TSNP and dissolved polymers in the same solution. Chloroform is a hydrophobic solvent, therefore immiscible with water and it is not possible to mix it with the TSNP in their aqueous solution format. TSNP solutions prepared as described in section 3.1.2.2 was concentrated with thermal evaporation at 40 °C as described in section 3.1.4.1, and having an estimated concentration of 42.64 ppm. The transfer was done by coating the NPs with thiol terminated polyethylene glycol (SH-PEG) and centrifuging, based on a previously reported method (Park et al. 2016). 3.33 mg of SH-PEG were added per milliliter of TSNP solution (43 ppm) and stirred for a couple of minutes. Then chloroform and treated TSNP were put in a tube in a 50:50 proportion and centrifuged at 16,162 x g for at least 45 minutes, and the aqueous phase was removed using a pipette. The process of the solution before and after centrifugation is illustrated in Figure 14.

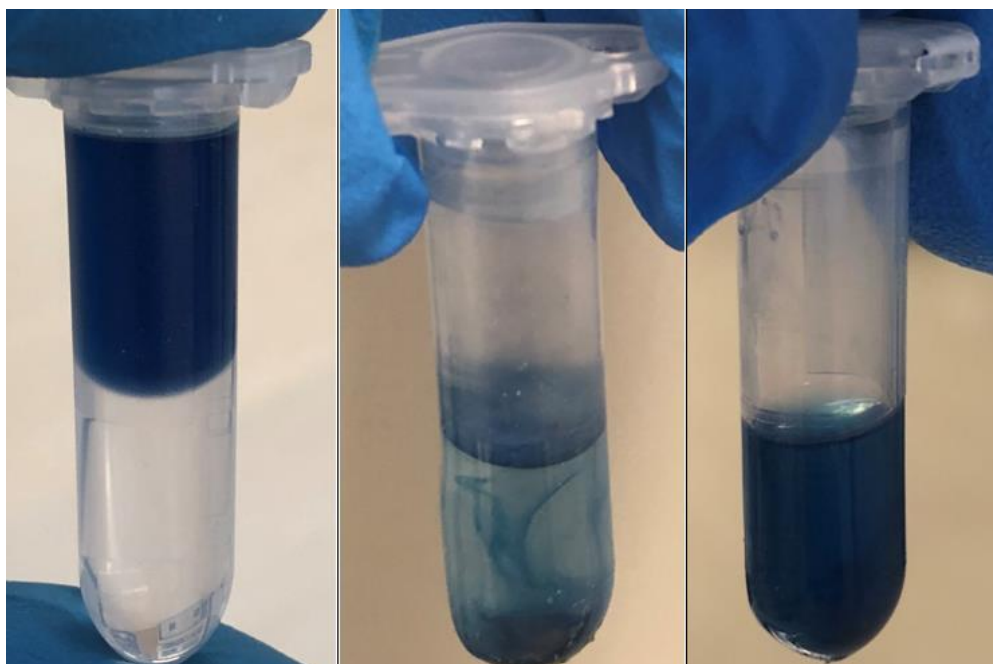


*Figure 14. Transfer of TSNP from water to chloroform. From left to right: tube before centrifugation, after centrifugation and after removing the aqueous phase and re-suspending the TSNP.*

### 3.2 Integration of TSNP in Polymers

Different methods were used to introduce TSNP in tested polymers: Extrusion was evaluated as a method to introduce the NPs into PP, Solvent casting was performed in PEG, PCL, PC and PLA, and Ex-situ incorporation methods were used on BC, PCL and PLA. Stability assays were performed on some of the resulting solvent casted and ex-situ treated films in order to determine if the incorporated TSNP were protected from etching and would be stable during exposure to a solution containing saline. The resulting solvent casted materials were characterised and their biological activity was examined by performing cytotoxicity and antimicrobial evaluations.

#### 3.2.1 Materials

Lab M Glucose (Dextrose) (MC013A), Neogen Balanced Peptone No. 1 (NCM0257A), and Neogen Yeast Extract (Pure Autolyzate) without salt (NCM0218A), and Lab M Luria-Bertani (LB) Broth (Lennox) (LAB173-A) were obtained from Cruinn Diagnostics Limited. Citric acid (C2404-500G) were obtained from Sigma Aldrich. Sodium phosphate dibasic dodecahydrate (71650) [ $\text{Na}_2\text{HPO}_4$ ] was obtained from Fluka Analytical Potassium Chloride (7447-40-7) was obtained from Fisher Scientific.

Polymers: Polyethylene glycol 20000 (8.17018) [PEG] was obtained from Merck. Polycaprolactone (PCL) CAPA 6250 [MW 25,000] was obtained from Perstorp. Ingeo™ Polylactic acid Biopolymer PLA 4044D and PLA 4043D were obtained from NatureWorks LLC. Exxon Mobil PP 7011 Polypropylene was obtained from Exxonmobil. Makrolon 2858 Polycarbonate was obtained from Bayer Material Science.

BC was produced in our lab by the bacterial strain *Komagataeibacter medellinensis* ID13488, as described in section 3.2.2.

#### 3.2.2 Bacterial Cellulose (BC) production method

The BC was produced using *Komagataeibacter medellinensis* ID13488. Pre-culture of the bacteria was prepared in Hestrin and Schramm (HS) liquid medium (2% glucose, 0.5% yeast extract, 0.5% peptone, 0.27%  $\text{Na}_2\text{HPO}_4$  and 0.15% citric acid), and the incubation was carried out for 2 days at 30°C on a rotary shaker with an agitation rate of 180 rpm. All the different media batches were inoculated with 100  $\mu\text{L}/\text{mL}$  from pre-culture (10% v/v inoculum), and

incubated statically at 30°C for 14 days. After incubation, BC hydrogels were removed from liquid media. Bare BC films were washed in a 0.5 M potassium hydroxide (KOH) solution in the water bath (1h, 100°C) and neutralised with distilled water. After the washing process, films were dried overnight at 60°C.

### **3.2.3 Extrusion**

A method was designed to perform extrusion of polypropylene (PP) and TSNP solution through liquid-assisted extrusion, which consists in liquid feeding the extruder and letting the generated vapour be evacuated through atmospheric venting ports (Herrera, Mathew, and Oksman 2015). A co-rotating 27mm Leistritz Twin-Screw Extrusion Line was used. Two vents were opened in the extrusion barrel, one at the beginning next to the feeding hopper and the other one near the end of the screws. PP pellets were fed into the hopper and drops of TSNP solution were fed into the first vent. The second vent was intended to let the vapour out of the barrel. The temperature profile set for the extruder, from hopper to dye, was: 160° → 180° → 190° → 200° → 210°. Before feeding TSNP drops into the vent, samples of extruded pure PP were collected for comparison.

#### **3.2.3.1 Post-Extrusion Incorporation on PCL**

Post-extrusion incorporation was evaluated as a method to allow integration of the TSNP into the polymer, in a way that the TSNP can be close to the surface of the film, and allow for Ag<sup>+</sup> ions and the peptides to interact with the bacteria and lead to inhibition of their growth. While at the same time, avoiding the exposure of the TSNP to high processing temperatures. PCL pellets were processed in a small prism twin screw extruder at 52 °C and 70 rpm. Rolls were used at the exit of the extruder dye and TSNP solution was sprayed as shown in Figure 15, after the polymer exited the dye, but before it went through the rolls. Technically, the rolls can squeeze the polymer to form a thin film and at the same time push the solution in the surface of the polymer to allow for integration of the TSNP, as the polymer is still hot and soft. The spraying was performed first using TSNP in water solution and it was afterwards changed to TSNP in chloroform solution.



*Figure 15. Spraying TSNP solution as the PCL exits the extrusion die and goes through the rolls.*

### **3.2.4 Solvent casting**

Solvent casting was applied as a strategy to integrate the TSNP within polymer by using a solvent to dissolve the polymer and mix it with the TSNP solution, to let the solvent evaporate afterwards. The purpose was to allow the TSNP to get encapsulated within the polymeric matrix without exposing them directly to air, which would lead to fast oxidation. Therefore, a small-scale adaptation of the solvent casting method was implemented to enable the formation of TSNP-incorporated films. The polymers that were used to evaluate this method were PEG, PCL, PC and PLA. The methodology for each one is described below.

Poly-(ethylene glycol) (PEG) solvent casting was performed because it is a hydrophilic polymer that can be easily mixed with the aqueous TSNP solution. 600 mg of PEG (MW 20,000) were dissolved with agitation in 20 ml of ethanol 70% at room temperature, to prepare a solution containing 3% PEG. This step was repeated four times to prepare 4 different samples to be solvent casted. The first sample was poured in a glass petri dish without adding any other agent. The second sample was mixed with 2 ml of TSNP solution (40 ppm after evaporation, sample A from section 3.1.4.1) before pouring in a petri dish. The third sample was mixed with

200 mg of HNT powder and then poured into a petri dish. Fourth sample was mixed with 200 mg of HNT powder and 2 ml of TSNP solution and poured in another petri dish. All samples were left to dry overnight inside a fume hood. After drying the PEG was removed from the petri dish using a spatula. Another sample was made increasing the PEG concentration to 5% and mixing with 2 ml of TSNP solution (43 ppm, evaporated at 40 °C as described in section 3.1.4.1).

PCL, PC and PLA (grades 4043 and 4044) solvent castings were performed. The solvent used to dissolve these polymers was chloroform, which is immiscible with water, therefore it was necessary to transfer the TSNP from water to chloroform as described in section 3.1.6.

The procedure to solvent cast either PCL or PC was the same. 600 mg of polymer pellets were dissolved with agitation at room temperature, in 20 ml of chloroform to prepare a 3% solution (w/v). 2 ml of TSNP in chloroform solution were added and mixed, then it was poured in a petri dish and left inside the fume hood to evaporate the chloroform. When drying, the lid of the petri dish was not used, but the dish was covered with a small cardboard box inside the fume hood, as it acted to protect from air currents and let the chloroform evaporate evenly from the surface.

In the case of PLA, both grades (4043 and 4044) were used to determine if any difference was observed. The procedure followed was the same for both grades, and also similar to that applied for PCL and PC. 600 mg of the PLA pellets were weighted for each sample and dissolved in 15 ml of chloroform, forming a solution containing 4% (w/v) polymer. Afterwards, 2 ml of TSNP in chloroform solution were added and the solution was mixed, and poured into glass petri dishes and left inside waste fume hood to dry overnight.

### **3.2.5 Ex-situ incorporation of TSNP**

#### **3.2.5.1 Incorporation into BC**

Cut pieces of approximately 20 mg of each examined BC films were immersed into 5 ml of TSNP solution (21.34 ppm) as illustrated in Figure 16, and incubated overnight at 30°C with shaking on horizontal platform (100 rpm). Afterwards, films were removed from the solution and dried overnight at 60°C.



*Figure 16. BC materials immersed in TSNP solution for overnight incubation. Bare BC films and Curcumin-BC films are included. Top row: Bare BC, middle row: BC-Cur2%, bottom row: BC-Cur10%.*

### **3.2.5.2 Incorporation into PCL and PLA**

Previously extruded films of PCL and PLA of approximately 2 x 2.25 cm, 1.55 mm thickness for PLA, and 1 mm thickness for PCL (Figure 17) were used.



*Figure 17. Films of PCL (top) and PLA (bottom), before adding the solvent.*

Inside the fume hood, three drops of TSNP in chloroform solution were added to the surface of each film, as shown in Figure 18. The films were left inside the fume hood for approximately one hour to allow the chloroform to evaporate.

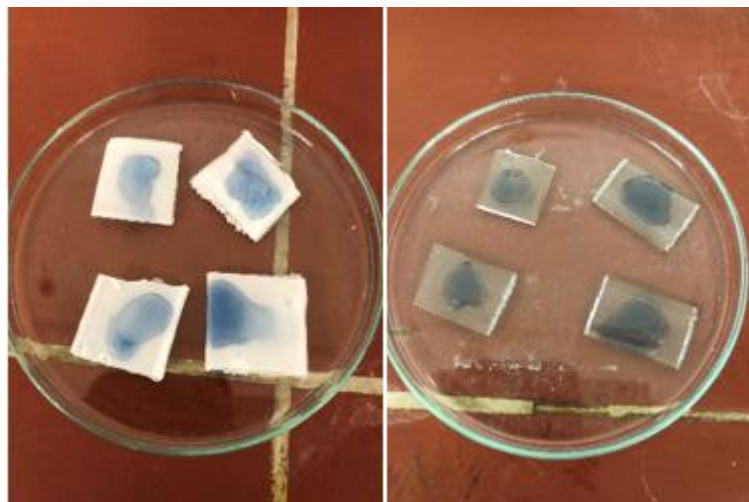


*Figure 18. Drops of TSNP in chloroform solution placed on the surface of extruded PCL films (left) and PLA films (right).*

### **3.2.6 Stability Assay**

#### **3.2.6.1 Stability on Water and NaCl**

The stability of TSNP integrated in the polymer films through the methods described in section 3.2.4, was evaluated. The purpose was to determine if the TSNP would remain attached to the polymer after washing with water and if they would be protected from etching during exposure to a saline solution. For this, the films were washed separately with distilled water and 20 mM NaCl solution for 1 minute and then left inside the same solutions for 2 hours.

#### **3.2.6.2 Stability in Potassium Chloride**

To evaluate the stability of the film treatment in potassium chloride (KCl), the stability of the TSNP solution prepared as indicated on section 3.1.2.1 was also evaluated for comparison purposes. Solutions of KCl in concentrations of 1 M, 0.1 M, 0.01 M, 1 mM and 0.1 mM were prepared. In Eppendorf tubes, 500  $\mu$ l of KCl solution and 500  $\mu$ l of TSNP solution were mixed, using a different tube for every concentration of KCl. UV-Vis spectrum of each treated solution and the non-treated TSNP were then read in the plate-reader spectrophotometer.

Stability test was performed on films of PC and PLA, prepared as indicated on section 3.2.4, as well as PCL and PLA films treated as described in section 3.2.5.2. The films were cut on a size small enough to fit inside the Eppendorf tubes, and were submerged in the KCl solution for 15 minutes, respectively. Finally, visual comparison was made with films that were not washed in the KCl solution.

### **3.2.7 Materials characterisation**

#### **3.2.7.1 Scanning Electron Microscope (SEM) Analysis**

SEM images were obtained using Mira XMU SEM (Tescan™, Czech Republic) in back scattered electron mode for surface analysis. The accelerating voltages utilized were 10 kV for PCL and 5 kV for PLA films. Prior to analysis, test samples were placed on an aluminium stub, and the samples were sputtered with a gold using Baltec SCD 005 for 110 s at 0.1 mbar vacuum before testing.

Energy Dispersive X-ray Spectroscopy (EDS) was used to confirm presence of silver in the samples immersed in TSNP solution. Data were gathered by an X-Max EDS system (Oxford Instruments, Oxford, UK) with Inca software.

#### **3.2.7.2 Thermal properties**

##### **3.2.7.2.1 Differential Scanning Calorimetry (DSC) Analysis**

The thermal behaviour of the films was evaluated by a DSC Perkin Elmer 4000 (Perkin Elmer Washington, Ma, USA) with Pyris Software (Version 13.3.1) under an inert nitrogen stream. About 10 mg of specimen was sealed in an aluminium pan and the DSC scans were recorded while heating from 10 – 200 °C at a heating rate of 10 °C/min, and then cooled to 10 °C. Thermal properties such as the glass transition temperature (T<sub>g</sub>), melting temperature (T<sub>m</sub>) and cold crystallization temperature (T<sub>c</sub>) were obtained from the second heating scan. In addition, the percentage of crystallinity (X<sub>c</sub>) was calculated according to the following Equation (Eq 2) (W. Li et al., 2017):

$$X_c(\%) = \frac{\Delta H_m}{W\Delta H_{m_0}} \times 100 \quad (\text{Eq 2})$$



Where  $\Delta H_m$  (J/g) is the heat of fusion of the sample,  $\Delta H_{m0}$  is the heat of fusion for completely crystalline PLA (93.7 J/g) (Li et al., 2017) and PCL (136 J/g) (Simão et al., 2017) and  $W$  (g) is the weight fraction of PCL and PLA in the samples.

### 3.2.7.2.2 Thermogravimetric (TGA) Analysis

Thermal stability of the films was determined using a thermogravimetric analyser Pyris TGA 1 (Perkin Elmer Washington, Ma, USA) with software Pyris 1. The film samples were taken in a standard aluminium pan and heated from 30 to 600 °C at the rate of 10 °C/min under a nitrogen flow of 50 mL/min.

### 3.2.7.3 Mechanical Properties

Mechanical properties of the films were tested using a 20 N tensometer Lloyd TA1 (Zwick Roell, Barcelona, Spain) with software Nexygen Plus version 3.0. All the samples were cut into 5 × 70 mm pieces, and the tensile speed was 50 mm/min at room temperature according to ASTM D638. An average of six test values were taken for each sample.

### 3.2.7.4 Evaluation of Antimicrobial Activity

The antimicrobial activity of casted films was evaluated against *Escherichia coli* ATCC 11775 and *Staphylococcus aureus* ATCC 25923 in LB broth (10 g/L tryptone, 10 g/L NaCl, 5 g/L yeast extract, pH 7.2) using adapted standard broth micro-dilution assay for bacteria that grow aerobically, as recommended by the CLSI (Clinical and Laboratory Standards Institute 2012). Prepared films (1cm<sup>2</sup>) were used as samples, with bare films as a negative control and tested microorganisms as a positive control. Growth of the respective test organisms (10<sup>5</sup> CFU/mL) after 24 h at 37°C was measured as optical density (OD) at 600 nm using a Microplate Reader. Serial dilution of cultivated broth was plated and incubated (30°C, 24 h) and number of colonies (CFU/mL) developed on the bare and treated films was calculated.

Antimicrobial effect (AE) of bare and TSNP treated PCL and PLA composite films was then calculated using the following equation (Eq 3) (D'Agostino et al. 2017).

$$AE = \log NC - \log NE \quad (\text{Eq 3})$$

Where NC is the number of CFU/mL developed on the bare films, and NE is the number of CFU/mL counted after exposure to TSNP treated films.

### 3.2.7.5 Cytotoxicity of derived films

The cytotoxicity of PCL, PLA (performed by solvent casting as described in section 3.2.4) and BC films (prepared as described in section 3.2.5.1) was evaluated by testing against human fibroblasts (MRC-5) obtained from ATCC. Films were sterilized under UV light for 20 min and then immersed into RPMI (Roswell Park Memorial Institute) medium, in a concentration of 1 mg/ml for the BC films and 10 mg/ml for the PCL and PLA films. The samples were incubated at 37°C, 180 rpm for 48 h. After incubation, samples were centrifuged (5000 rpm, 15 min), and sterilized by filtering using 0.22 µm pore size filters.

Cells were plated into a flat-bottom 96-well plate at a concentration of  $1 \times 10^4$  cells per well in RPMI medium supplemented with 100 µg/mL streptomycin, 100 U/mL penicillin, and 10% (v/v) fetal bovine serum (FBS) and incubated for 24 hours at 37°C to allow the formation of a monolayer. After 24 h of cells incubation, RPMI medium was substituted with decreasing concentrations of extracts: 100%, 50%, 25% and 12.5% (v/v) while the control samples contained only RPMI medium. The incubation at 37°C, 5% CO<sub>2</sub> continued for 48 h and the cytotoxicity was determined afterwards using 3-(4,5-dimethylthiazol-2-yl)-2,5-diphenyltetrazoliumbromide (MTT) reduction assay. (Hansen et al., 1989)

The extent of MTT reduction to formazan was measured by spectrophotometer at 540 nm using a Tecan Infinite 200 Pro multiplate reader (Tecan Group Ltd., Mannedorf, Switzerland). The results were presented as percentage of the control (untreated cells) that was arbitrarily set to 100%.

## 3.3 Further enhancement of BC antimicrobial properties

### 3.3.1 Materials

Curcumin (FC09321) was obtained from Biosynth Carbosynth.

PHB (P226) was obtained from Biomer. Polycaprolactone (PCL) CAPA 6250 [MW 25,000] was obtained from Perstorp. Ingeo™ Polylactic acid Biopolymer PLA 4044D was obtained from NatureWorks LLC.

BC was produced in our lab by the bacterial strain *Komagataeibacter medellinensis* ID13488, as described in section 3.2.2.

### **3.3.2 Cultivation with curcumin**

Additionally to the incorporation of TSNP, curcumin was also incorporated to the BC materials to evaluate if the antimicrobial response could be increased by combining two different antimicrobial active compounds. Previously described (section 3.2.2) BC production was performed in HS medium supplemented with 2% and 10% curcumin (w/v). Same as in the production of bare BC films, all the batches were inoculated with 100  $\mu\text{L}/\text{mL}$  of pre-culture (10% v/v). After incubation, the films were removed from the liquid media and immersed in distilled water. Contrary to bare BC films, the curcumin-treated films were not washed with KOH to prevent degradation of the curcumin. Instead, they were autoclaved (121  $^{\circ}\text{C}$ , 15 min). After the washing process, films were dried overnight at 60 $^{\circ}\text{C}$ .

TSNP incorporation for all produced BC films was performed as described in section 3.2.5.1, by immersion of the films in TSNP solution.

### **3.3.3 Estimation of curcumin absorption from media**

The amount of curcumin absorbed from the cultivation media into the BC films was estimated through spectrophotometric readings of the media before and after culture. The UV-Visible spectral measurements were performed in a UV 1280 Shimadzu (Japan) spectrophotometer using 10 mm path length matched quartz cuvettes (Mondal et al., 2016). The measurements were taken in the wavelength range of 200-700 nm. In aqueous solution, curcumin has a peak at 427 nm and a shoulder at 360 nm. Peak area was used for estimation of curcumin incorporation via comparison between non-inoculated media and media after 14 days of incubation.

### **3.3.4 Fourier-transform infrared (FTIR) spectroscopy of BC films**

A Perkin-Elmer Spectrum One FTIR spectrometer (Perkin Elmer Inc., Washington, USA) fitted with a universal ATR sampling accessory, and Perkin Elmer software, was used to record the spectra of dried BC films. The spectral resolution was 4  $\text{cm}^{-1}$  and 20 scans were acquired for each spectrum (4000 – 650  $\text{cm}^{-1}$ ).

### **3.3.5 Evaluation of BC films stability via weathering tests**

Weather testing was carried out on the BC films to determine their stability against UV irradiation using a QUV/se accelerated weather tester from Q-Lab (Westlake, Ohio, USA) in

compliance with the ISO 4892 test standard. Fluorescent UV-A lamps with a radiant emission range of 365 nm down to 295 nm were used to simulate sunlight exposure. A set temperature of 40°C was used in the chamber and UV irradiance of 0.76 W/m<sup>2</sup>. Samples were exposed to moisture spray and UV light cyclically in 4-h increments. In total, the samples were exposed for 20 h in each condition.

To quantify the effects of weathering, spectrophotometry was used before and after exposure to measure the degree of colour change in samples. A CM-3610A bench-top spectrophotometer from Konica Minolta (Tokyo, Japan) with an 8° observant angle was used to measure the colour change in specimens. Procedures followed the ISO 11664-4 test standard and the  $\Delta E^*$  (CIEDE2000) metric was used to calculate colour difference.

### **3.3.5 Evaluation of Water Absorption and Water Retention**

To determine if the introduction of curcumin had some effect on the water absorption and the water retention of the BC films, triplicated samples of bare BC and BC-Cur2% were prepared by cutting circles of approximately 1 cm in diameter, with the help of a hole puncher. The absorption and retention of the materials was evaluated for distilled water, pH 4, pH 7.4 and pH 9 buffers. The initial weight of each sample was recorded before the samples were immersed in water or buffer for the absorption test. After each sample was immersed in 2ml of water or buffer, samples were removed and weighted after 15, 30 and 45 minutes of immersion, then after every hour until the 9<sup>th</sup> hour was reached, and finally after 24 hours passed. For the retention test, samples were removed from the liquid, weighted and left to dry at room temperature. Weight measurements were done after 15, 30 and 45 minutes, and then every hour until the weight of every sample reached the initial weight before immersion, which happened after 4 hours, then a final measurement was done after 24 hours.

### **3.3.6 Biological Evaluations**

#### **3.3.6.1 Antibacterial Evaluation of BC films**

The antimicrobial activity of all the dried BC films was evaluated against *Escherichia coli* ATCC 95922 and *Staphylococcus aureus* ATCC 25923 in Luria-Bertani (LB) broth (10 g/L tryptone, 10 g/L NaCl, 5 g/L yeast extract, pH 7.2). Overnight cultures of the bacteria were diluted to concentration of 10<sup>8</sup> CFU/mL to be used as pre-culture. Dried BC films (10 mg of each specimen) were immersed in fresh LB broth and inoculated with 1% (v/v) from pre-

culture, for a final concentration of  $10^6$  CFU/mL of bacteria. Untreated BC films were used as negative control. After incubation for 24 h at 37°C and 100 rpm, BC films were removed from the cultures and optical density (OD) of the cultivated broth was measured at 630 nm using a Biotek Synergy HT Microplate Reader (Biotek Instruments GmbH, Bad Friedrichshall, Germany). Growth percentage was calculated using the following equation (Eq 4).

$$\text{Growth Percentage} = \left( \frac{\text{Absorbance of tested sample}}{\text{Absorbance of positive control}} \right) \times 100 \quad (\text{Eq 4})$$

### 3.3.6.2 *Danio rerio* Embryotoxicity Assay

BC materials were incubated in embryo water (100mg per mL) 24h at 30°C with shaking on horizontal platform (180 rpm), and that extract was used for toxicology assessment. *In vivo* toxicity evaluation was carried out on the zebrafish (*D. rerio*) model, in compliance with general rules of the OECD Guidelines for the testing of chemicals where followed while zebrafish embryotoxicity assay was performed (OECD, 2013). Briefly, zebrafish embryos were produced by mating of adult females and males (ratio 1:2), collected, washed from detritus and distributed into 24-well plates containing 10 embryos per well in 1 mL embryo water (0.2 g/L of Instant Ocean® Salt in distilled water), and incubated at 28 °C. Experiments were performed in triplicate using 30 embryos per each tested concentration. Non-treated embryos were used as a negative control. Embryos were examined under the stereomicroscope (SMZ143-N2GG, Motic, Germany) every 24 h during five days, counting and discarding dead embryos and observing teratogenic effects. After the assay embryos were killed by freezing at -20 °C for 24 h. All experiments involving zebrafish were performed in compliance with the European directive 2010/63/EU and the ethical guidelines of the Guide for Care and Use of Laboratory Animals of the Institute of Molecular Genetics and Genetic Engineering, University of Belgrade.

### 3.3.6.3 *Caenorhabditis elegans* Survival Assay

The nematode *Caenorhabditis elegans* AU37, obtained from the *Caenorhabditis* Genetics Center (CGC), University of Minnesota, Minneapolis, Minnesota, US. *C. elegans* AU37 (*glp-4*; *sek-1*), was used to establish the toxicity of BC materials.

For this assay 25 mg of each BC films was suspended in 2,5 ml of M9 medium (45 ml of 5xM9 salt, 50 ml of glucose solution 50% (w/v), 500 µl of 1M MgSO<sub>4</sub>, 25 µl of 1M CaCl<sub>2</sub>, 250 µl

vitamins, 250 µl of trace elements solution, 125 µl of Ampicillin 50 µg/ml, and final volume adjusted to 250ml with double distilled water). Samples were incubated at 37°C, with shaking on horizontal platform at 180 rpm for 24 h. After incubation, BC films were removed from the suspension and extracts were prepared in the following concentrations: 50 µg/ml, 25 µg/ml, 12.5 µg/ml and 6.25 µg/ml.

The worm was propagated under standard conditions; synchronized by hypochlorite bleaching, and cultured on nematode growth medium using *Escherichia coli* OP50 as a food source, as described previously (Stiernagle 2006). The *C. elegans* AU37 survival assay was carried out following the standard procedure (Brackman et al. 2011) with some minor modifications. Briefly, synchronized worms (L4 stage) were suspended in a medium containing 95% M9 buffer (3.0 g of KH<sub>2</sub>PO<sub>4</sub>, 6.0 g of Na<sub>2</sub>HPO<sub>4</sub>, 5.0 g of NaCl, and 1 mL of 1 M MgSO<sub>4</sub>·7H<sub>2</sub>O in 1 L of water), 5% LB broth (Oxoid, Basingstoke, UK), and 10 µg mL<sup>-1</sup> of cholesterol (Sigma-Aldrich, Munich, Germany). The experiment was carried out in 96-well flat-bottomed microtiter plates (Sarstedt, Nümbrecht, Germany) in the final volume of 100 µL per well. The wells were filled with 50 µL of the suspension of nematodes (25–35 nematodes) and 50 µL of tested BC film suspension. Subsequently, the plates were incubated at 25 °C for 48 h. The fraction of dead worms was determined after 48 h by counting the number of dead worms and the total number of worms in each well, using a stereomicroscope (SMZ143-N2GG, Motic, Germany). All BC films suspensions were tested three times in each assay and each assay was repeated two times (n = 6). As a negative control experiment, nematodes were exposed to the medium containing 1% DMSO.

### **3.3.7 BC Blends preparation and antimicrobial activity evaluation**

Blends of BC with PHB were fabricated in order to evaluate if properties of BC could be further improved. PHB powder, PCL pellets and PLA pellets were respectively dissolved in chloroform to make solutions containing 40g/L of each polymer. Stripes of 1x10 cm of BC and BC-Cur10% were cut and each sample was immersed in 30ml of polymer solution inside 50ml Falcon Tubes. Tubes containing the samples were incubated overnight at 30 °C and 120 rpm, in a horizontal position. After incubation, the films were removed from the solution and left inside waste fume hood for at least 4 hours to allow complete evaporation of all the chloroform. The films were immersed in 20 ml of distilled water and autoclaved (121 °C, 15 min) prior to the test of antimicrobial activity. The antimicrobial evaluation was performed as described in section 3.3.6.1.

### **3.4 Statistical Analysis**

Statistical analysis for the mechanical evaluation of solvent casted films was performed with a paired T-test, with a 95% confidence interval. The analysis for the in vitro cytotoxic evaluation was performed using one-way analysis of variance (ANOVA) and grouped using the Tukey method with a 95% confidence interval. Statistical analysis for the antimicrobial evaluation was performed using ANOVA, paired with the Dunnett method and a 95% confidence interval. The software used to perform these analyses was Minitab (Version 20.2) for Windows (64-bit). All data collected for this study were expressed as mean  $\pm$  standard deviation. A sample size of six was used for the mechanical properties test of solvent casted films, a sample size of four was used for each concentration tested in the cytotoxicity evaluation, and a sample size of three was used for the antimicrobial evaluation.

## **CHAPTER 4 – TSNP FORMULATION FOR INCORPORATION WITHIN POLYMERIC MATERIALS**

### **4.1 Preface**

In this chapter, the results from synthesis of TSNP through a seed-mediated approach as previously described are evaluated using spectrophotometric readings within the UV-Vis spectrum. The characteristic optical properties of the TSNP have been demonstrated and the LSPR was used as a tool to monitor changes in the size and morphology of the nanoplates. LSPR showed no significant changes after the original protocol for synthesis of the TSNP was modified, first to increase the concentration of silver in the solution, and subsequently for scaling up of production. LSPR monitoring was also used for the verification of gold coating and its provision of protection to the TSNP from the etching effects of NaCl. The sensitivity of gold-coated TSNP was also verified through LSPR monitoring, by using different sucrose

concentrations to change the refractive index of the solution. Furthermore, the gold-coated TSNP were demonstrated as a suitable biosensor for the monitoring of the two different conformations of fibronectin.

In the TSNP formulation for integration into the polymers, the resistance of the TSNP to high temperatures was evaluated, considering the possibility of integrating the TSNP before or during processing of the polymer, where high temperatures are used. LSPR monitoring was also a useful tool to evaluate if drastic morphological changes occurred after exposure to such temperatures. Moreover, further increase in the concentration of TSNP in the solution may be desired for purposes including masterbatch preparations. Thermal evaporation was demonstrated as a suitable method to achieve this, by demonstrating that significant changes in the LSPR of the TSNP solution were not observed on going through concentration procedures. The combination of TSNP with halloysite nanotubes was also evaluated as a strategy to protect the TSNP from polymer processing conditions. Finally, successful transfer of the TSNP from aqueous phase to an organic phase (chloroform in this case) by coating them with SH-PEG and application of centrifugal force. The purpose of transferring the TSNP to an organic phase is to enable mixing with polymers in the same dissolution.

## **4.2 Synthesis of TSNP**

It has been established that different morphologies of AgNPs present different properties to one another. In the case of TSNP and other nanostructures with sharp geometries, it has been observed that the tips can provide a greater electric-field enhancement, allowing optical properties to be more easily tuned and controlled, compared to spherical AgNPs (Kelly et al. 2003). Furthermore, the same sharp edges and corners present in TSNP make them more susceptible to oxidation, resulting in a higher rate of Ag<sup>+</sup> ions released compared to spherical NPs, resulting in a higher antimicrobial activity (Lu et al. 2015). Given these interesting properties and the lack of research on TSNP for antimicrobial applications in polymeric materials, studies were performed to evaluate their suitability as antimicrobial additives polymer and biopolymers.

TSNP were synthesised following the method described in section 3.1.2. Figure 19 shows the normalized UV-Vis spectrum of the seeds and the TSNP prepared using 200 µl of seeds. LSPR peak wavelength of the seeds is 398 nm the full width at half maximum (FWHM) of the curve is 79 nm (437 – 358 nm). In case of the TSNP, the peak wavelength is at 603 nm and the



FWHM is 125 nm (662 – 537 nm). These spectra are consistent with the ones obtained by Aherne et al (2008).

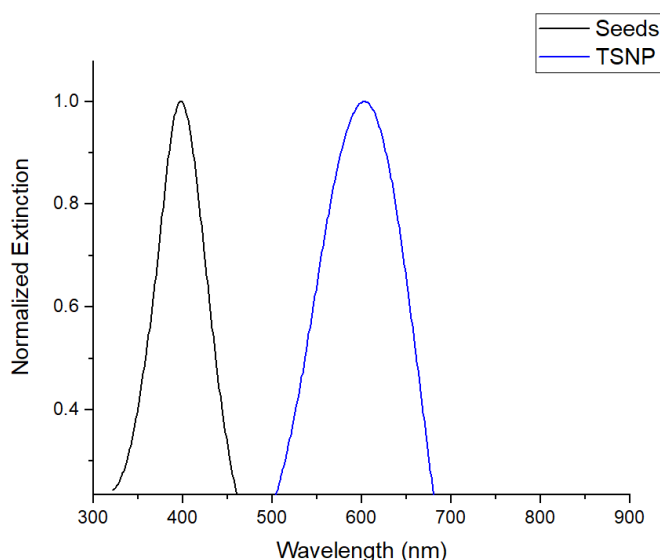


Figure 19. UV-Vis Spectrum of Ag Seeds and TSNP (200 µl seeds).

#### 4.2.1 Optimised Method for TSNP Synthesis

As described in section 3.1.2.1, the resulting concentration of Ag in the TSNP solution can be increased with slight variations in the volumes used in the synthesis method, without compromising the uniformity and structure observed in the resulting LSPR of the optimised TSNP. Figure 20 shows the resulting curves from LSPR after optimising the method to increase the concentration in the solution and adjusting the volume of seeds to 350 µl in the TSNP synthesis. LSPR of the seeds curve has a peak of 395 nm and a FWHM of 79 nm (435 – 356 nm). TSNP curve has its peak at 601 nm and a FWHM of 150 nm (663 – 513 nm). These results are similar to the ones obtained by the original method, proving to be unaffected by the reduction of 20% of water, with the concentration of atomic Ag calculated to increase from 16.62 ppm to 21.34 ppm. High concentrations are desirable to include the TSNP into polymer processing, reducing the amount of water required to be removed and increasing the number of nanoplates available for the process. Therefore, this formulation was used as the base line for scaling up the TSNP synthesis.

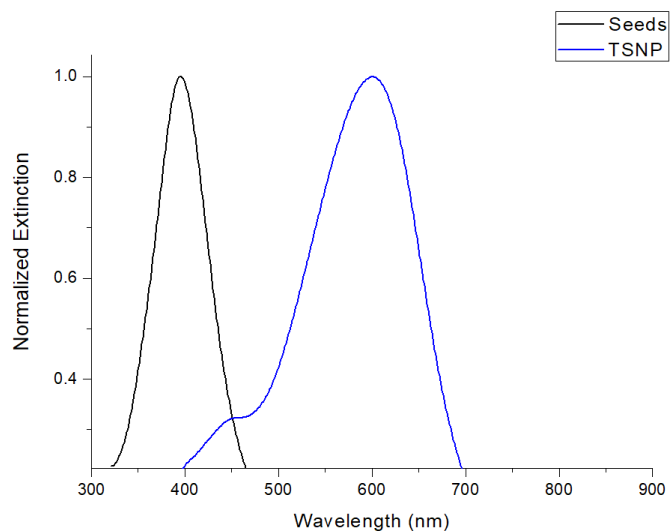


Figure 20. UV-Vis Spectrum of Ag Seeds and TSNP (Optimized method).

#### 4.2.2 TSNP Scale-Up

Following the method described in section 3.1.2.2, 300 mL of TSNP solution were prepared. Figure 21 shows the normalized UV-Vis spectrum of one of the batches prepared for this scaled up volume. LSPR peak wavelength is 584 nm and FWHM of 112 nm (635 – 523 nm). Although there is a small blue shift in the peak and a small reduction in FWHM compared to the results obtained from smaller volumes, these differences are not expected to represent a reduction in antimicrobial activity or in the stability of the nanoparticles, hence, the scale up method is considered functional.

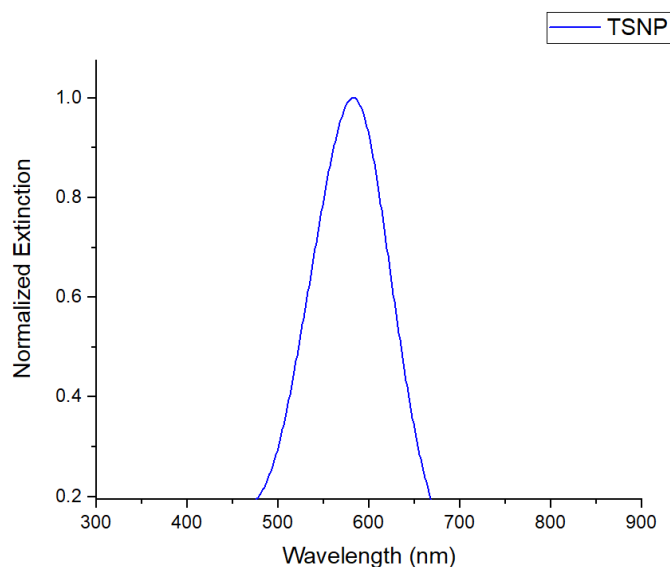


Figure 21. UV-Vis Spectrum of Scaled Up TSNP (300 mL).

### 4.3 TSNP Gold Coating & Protection Check

Unprotected TSNP can be highly susceptible to degradation or etching by catalytic oxidation in the presence of chlorine or other reactive ions. This can lead to alterations of the geometry and structure of the TSNP, normally resulting in a substantial blue shift in their spectrum and impairing their LSPR properties (Zhang et al. 2014). Different coatings can be used to protect the TSNP structure, but most coatings will also affect the plasmonic response of the nanoparticles. A method used by Zhang et al. (2014) proved to successfully coat TSNP edges with a layer of gold, providing the nanoparticles with protection from etching while allowing them to maintain their plasmonic response and refractive index sensitivity. The same method was adapted and used for coating of the TSNP as described in section 3.1.3, and the efficacy of the gold layer protection was evaluated with NaCl.

Figure 22 shows the effect of gold coating on LSPR spectrum of TSNP and also after exposing the AuTSNP to NaCl 10 mM and 20 mM. For the seeds curve, LSPR peak is found at 395 nm and the FWHM is 79 nm (435 – 356 nm). TSNP has a LSPR peak of 600 nm and a FWHM of 149 nm (663 – 514 nm). After gold coating, the LSPR red-shifted to 612 nm and the FWHM slightly increased to 153 (674 – 521 nm). After being exposed to NaCl solution, the LSPR blue-shifted to 580 nm. FWHM also changed after exposing the NPs to NaCl 10 mM showing a slight reduction to 145 nm (647 – 502 nm), and in the case of NaCl 20 mM, it was 136 nm (638

– 502 nm). In accordance to the results reported by Aherne et al (2009), red shift is attributed to an increase in size caused by the added gold. Blue shift, on the contrary is a result of etching and reduction in size. Even though the blue shift is not big in this case, the amount of gold added can still be adjusted to completely protect the TSNP from etching in these NaCl concentrations.

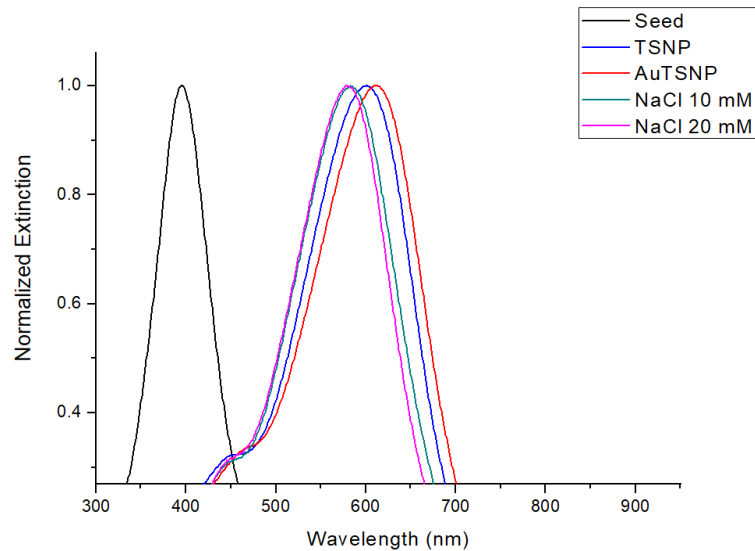


Figure 22. UV-Vis Spectrum of seeds, TSNP, AuTSNP and protection check.

#### 4.3.1 AuTSNP Sucrose Sensitivity Test

The sucrose sensitivity test, as described in section 3.1.3.1 was performed to verify the sensitivity of LSPR of the AuTSNP, by changing the refractive index of the nanoplates' local environment. As refractive index is increased by increasing sucrose concentration, LSPR exhibits red shifts (an increase in  $\lambda_{max}$  peak) that prove the sensitivity of the NPs to the surrounding environment (Figure 23). LSPR peak values of AuTSNP corresponding to each sucrose concentration are shown in Table 1, as well as the respective shift magnitude in regard to the initial AuTSNP wavelength. LSPR shows a gradual peak wavelength increase, corresponding to the increase in the refractive index of the solution. Only exception is the curve from sucrose 30%, showing an unexpected behaviour with a bigger peak wavelength than the curve from 40%.

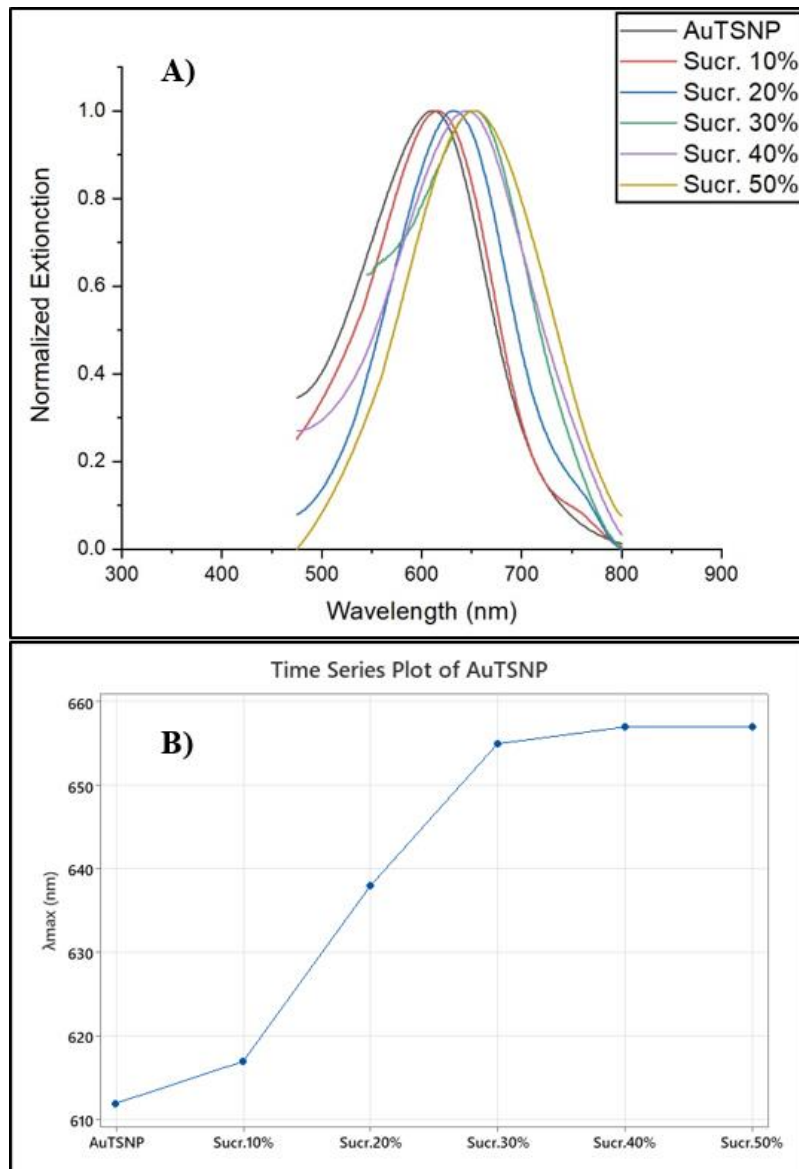


Figure 23. A) UV-Vis Spectrum of AuTSNP as a result of increasing refractive index of the solution. B)  $\lambda_{max}$  values of AuTSNP changing as a result of increasing the refractive index of the solution.

Table 1. Shift of LSPR peak wavelength of AuTSNP as a result of refractive index increase.

<i>Sample</i>	<i>LSPR Peak Wavelength</i>	<i>LSPR Shift</i>
<i>AuTSNP</i>	612 nm	-
<i>Sucr. 10%</i>	617 nm	5 nm (Red)
<i>Sucr. 20%</i>	638 nm	26 nm (Red)
<i>Sucr. 30%</i>	655 nm	43 nm (Red)
<i>Sucr. 40%</i>	647 nm	35 nm (Red)
<i>Sucr. 50%</i>	657 nm	45 nm (Red)

#### 4.3.2 AuTSNP for Fibronectin Detection

One of the main characteristics of TSNP is their high refractive index sensitivity, which is further increased by the gold-coating process. This property allows for the use of AuTSNP in a variety of biosensing applications, including the detection of protein conformational changes. Previous work by Brennan-Fournet et al. (2015) has demonstrated the ability of AuTSNP to successfully detect the conformational changes in Fibronectin that are induced by pH changes. Fibronectin presents a compact conformation around pH 7, and extended at pH 4. The highly sensitive LSPR resonance wavelength of AuTSNP can easily detect changes in the refractive index of their surrounding medium, for example, by the binding of analytes or molecules at the surface of the NPs (Haes and Duyne 2002). The same experiment, as reported by Brennan-Fournet et al. (2015) was performed simply as a test for the efficacy of the Au-coating method on the adapted TSNP synthesis.

Figure 24 shows the redshifted spectra for AuTSNP after coating with PEG and Fn and exposing them to two different pH. LSPR peak wavelength of the AuTSNP is originally 598 nm. The sample exposed to pH 7.23 shifts to 633 nm while the one exposed to pH 4.16 has a

greater red shift, with a peak on 642 nm. Results reported by Brennan-Fournet et al. (2015) have also shown a greater red shift on the sample exposed to an acidic pH, when the Fn is extended. However, the shift they report is much bigger (almost 100 nm) compared to the one at physiological pH, while in our case it was only 9 nm. This means that our developed method might need some adjustments to be more sensitive to biosensing of conformational changes in a protein, such as Fn.

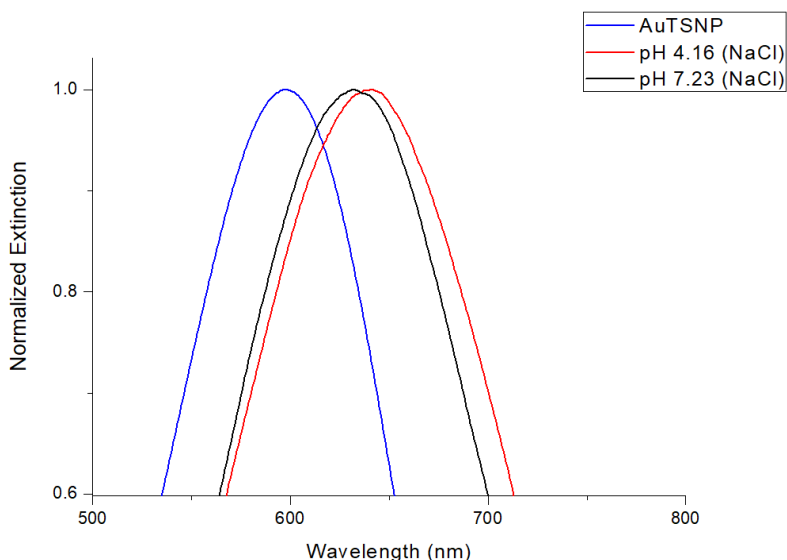


Figure 24. UV-Vis Spectra of Fn-coated AuTSNP exposed to basic and acid pH.

#### 4.4 TSNP Temperature Test

As described in section 3.1.4, two different approaches were used to test the effect of temperature on TSNP, the first one consisted on exposing the same TSNP sample to temperatures of 80, 100 and 120 °C for 5 minutes under each temperature, and the resulting spectra are shown in Figure 25. Initial peak wavelength for the TSNP sample was 519 nm. After exposing to 80 and 100 °C the LSRP blue-shifted to 504 nm and 456 nm, respectively. The peak maintained initial wavelength after exposing to 120 °C. After evaluating the results, it was not entirely clear if the observed blue shifts were caused only by the high temperature or if the time of exposure to heat was also playing a role on the observed changes. Therefore, the second test exposing different samples of TSNP to 120 °C and 150 °C for 5 minutes respectively, was performed as described in section 3.1.4.

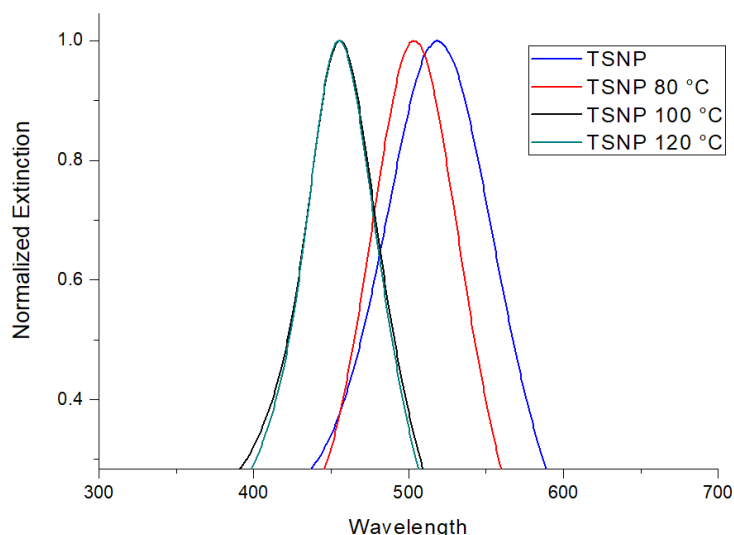


Figure 25. UV-Vis Spectrum of TSNP after exposure of a single sample to different temperatures, for 5 minute periods under each temperature.

Resulting spectra readings are shown in Figure 26, where we can see that in both cases, LSPR wavelength peak remained at 516 nm, except in the case of the sample of 21.34 ppm exposed to 120 °C, where a small red shift to 528 nm can be observed. It is unclear why this shift occurred, as high temperature was observed to cause blue shifts as oxidation is promoted. However, the results helped prove that TSNP can undergo exposure to high temperature for a short time without suffering significant damage.

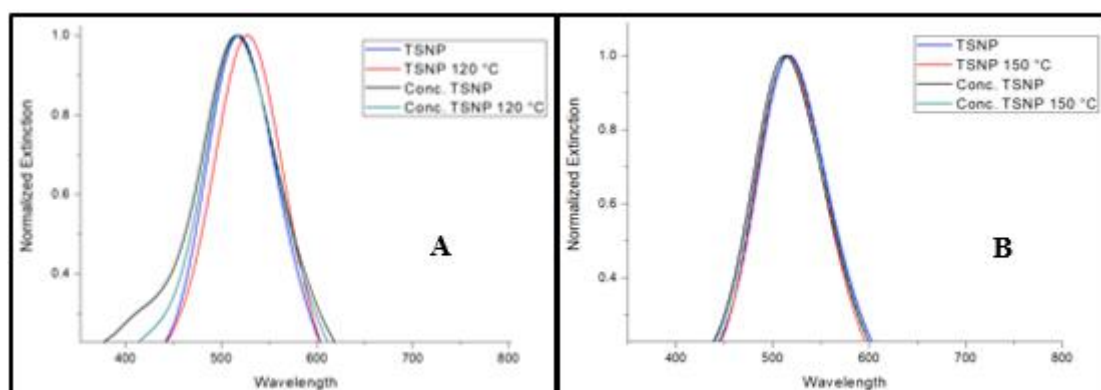


Figure 26. UV-Vis Spectra of two different sets of samples of TSNP and concentrated TSNP before and after exposure to A)120 °C and B)150 °C, showing practically no shifts in spectrum even after being exposed to higher temperatures, compared to the sample shown in Figure 25.



#### 4.4.1 TSNP Thermal Evaporation

As described in section 3.1.4.1, water evaporation from TSNP solution started on cycles of 10 minutes and then continued on cycles of 5 minutes (Sample A) and a second sample was carried further through the 10 minutes cycle (Sample B). UV-Vis Spectra of the TSNP before and after being exposed to heat through the described process, are shown in Figure 27. Initial LSPR wavelength and Ag concentration of TSNP solution is displayed in Table 2, as well as final LSPR wavelength, Ag concentration and volume for Sample A and Sample B, respectively. The spectra, LSPR wavelength and volume of water evaporated showed a great difference just by changing the time on the cycles inside of the oven.

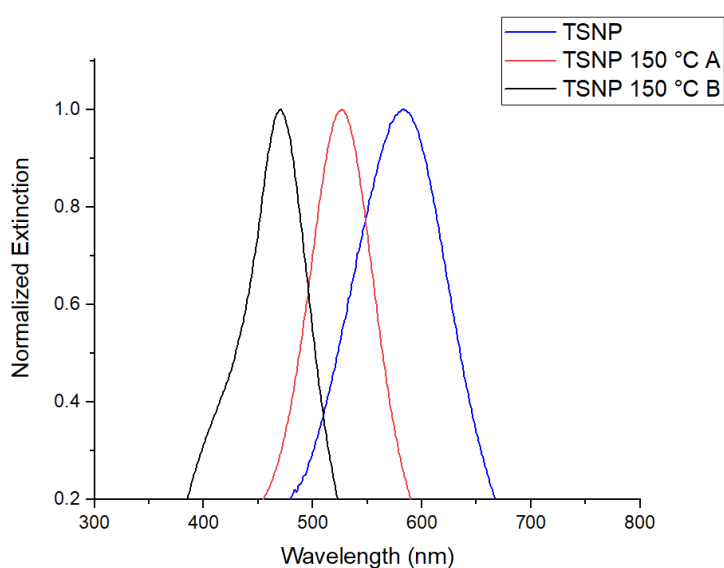


Figure 27. Effect on UV-Vis spectrum of TSNP after evaporating water at 150 °C by two different methods, where sample A was exposed to 150 °C on 5-minute cycles, and sample B was exposed to the same temperature on 10-minute cycles.

Table 2. Changes in LSPR wavelength, Ag Concentration and Volume for TSNP solution after treatments at 150 °C.

Sample	LSPR Peak Wavelength	Ag Concentration	Initial Volume	Final Volume
TSNP (Initial State)	583 nm	21.34 ppm	-	-
Sample A	525 nm	40 ppm	150 ml	80 ml
Sample B	471 nm	94.86 ppm	80 ml	18 ml

Colour of the TSNP solution before going through the evaporation process and the final colour of samples A and B can be observed in Figure 28. As it can be seen in the pictures, changes on the size or shape of the nanoplates, caused by heat or oxidation, can be readily noticeable with the naked eye and corroborated with spectrophotometry due to the optic properties they possess.



*Figure 28. Colour of TSNP solution before and after evaporation process: Left) Initial colour of TSNP solution; Centre) Final colour of sample A; Right) Final colour of sample B.*

As mentioned in section 3.1.4.1, after observing the results presented above, evaporation with a much lower temperature, under longer times was attempted. Figure 29 shows the resulting UV-Vis spectrum of TSNP (21.34 ppm) before evaporation, with a LSPR peak wavelength of 621 nm. After 8 days inside the oven at 40 °C, peak wavelength presented a small blue shift to 617 nm and the concentration was estimated to be approximately 43 ppm. FWHM also exhibited a change from 153 nm (707 – 554 nm) of the original solution to 178 nm (722 – 544 nm). Taking into account the prolonged time inside the oven, differences between both spectra were not significant and were not considered an issue, as increasing the concentration is the principal objective of this method, and it proved to be a good option to consider.

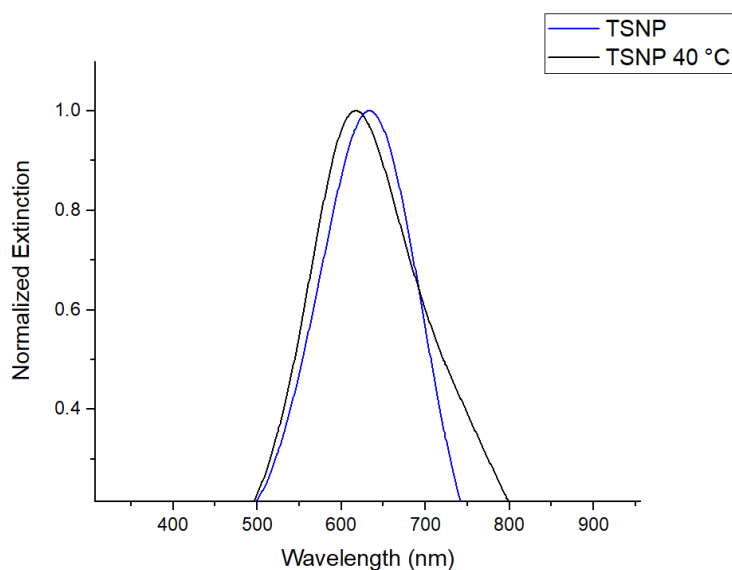


Figure 29. UV-Vis spectra of TSNP before and after evaporation at 40 °C.

#### 4.5 TSNP protection using halloysite nanotubes

As described in section 3.1.5, TSNP and HNT were mixed to evaluate the behaviour as a possible strategy to encapsulate and protect the TSNP. Results are shown in Figure 30, it can be seen that TSNP solution and HNT powder were easily mixed into a homogeneous solution and the purple colour in the solution was maintained. However, after drying, the purple colour was lost and the dried powder had a pale-yellow colour (pure HNT was originally white), indicating TSNP were probably etched. Figure 30-D shows the result after centrifuging, where it can be observed that purple colour was not maintained and different layers formed, which appears to indicate that the TSNP and the HNT separated during the centrifugation.



Figure 30. Mixed TSNP+HNT: A) Pure HNT Powder; B) TSNP+HNT solution; C) Dried and ground TSNP+HNT; D) Centrifuged TSNP+HNT.

#### 4.6 Transfer of TSNP to Chloroform

The TSNP were transferred from aqueous solution to an organic phase (chloroform). Chloroform was selected for being a suitable solvent in which selected polymers (PC, PCL and PLA) were easily dissolved. Use of chloroform allowed addition of TSNP and polymers to a single solution, their mixing and film forming through solvent casting (section 3.2.4). The transfer was performed as described in section 3.1.6. UV-Vis spectra of the TSNP before and after coating of SH-PEG, as well as after the transfer were read in the plate-reader spectrophotometer. Additionally, a fresh sample of TSNP solution that was not concentrated by thermal evaporation (concentration of 21.34 ppm) was also read, for comparison purposes. The UV-Vis spectra of the aforementioned samples are shown in Figure 31. LSPR peak wavelengths were 633 nm for fresh TSNP, 617 nm for concentrated TSNP, 596 nm for SH-PEG coated TSNP and 650 nm after transfer to chloroform. Therefore, a blue shift of 16 nm occurred after thermal concentration of TSNP, from there, another blue shift of 21 nm occurred after coating the concentrated TSNP with SH-PEG and after transferring to chloroform a red shift of 54 nm was displayed. Respectively, FWHM started at 153 nm (706 – 553 nm) for the non-concentrated, then to 179 nm (544 – 723 nm) for the concentrated TSNP, 197 nm (514 – 711 nm) for SH-PEG coated and 168 nm (565 – 733 nm) for the chloroform solution. In the

case of the peak wavelengths, the most drastic shift occurred in the last step, after transferring to chloroform, and contrary to the other shifts, a red shift occurred in that case. This could be explained by the increase in the refractive index from water, which is approximately 1.33 (Bashkatov and Genina 2003), to chloroform, which is around 1.44 (Samoc 2003). Increases in the refractive index have been observed to produce red shifts in the LSPR of TSNP (Aherne et al. 2009).

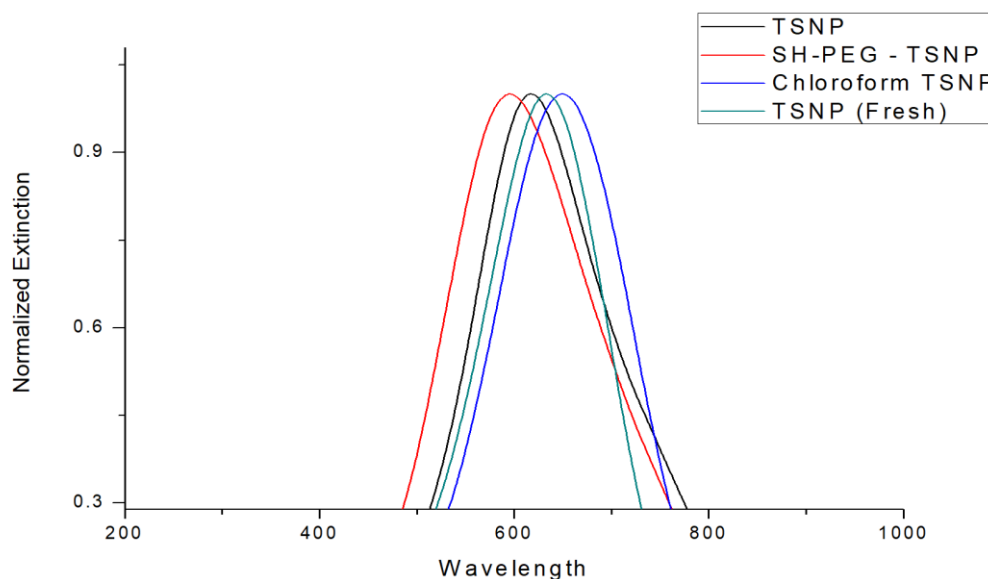


Figure 31. UV-Vis spectra of non-concentrated TSNP, concentrated TSNP, SH-PEG coated TSNP and TSNP after transfer to chloroform.

#### 4.7 Summary

In this chapter, successful synthesis of TSNP and its suitability as biosensing tools were demonstrated. Furthermore, Ag concentration was successfully increased during synthesis and post-synthesis through thermal evaporation, without drastic effects on the optical properties of the TSNP. As a strategy to incorporate TSNP in hydrophobic polymers, the nanoplates were transferred to chloroform, which is a solvent capable of dissolving several hydrophobic polymers, including PC, PCL, and PLA. UV-Vis spectra readings taken before and after the transfer of the TSNP to chloroform demonstrate that no drastic changes in the structure of the TSNP occurred. Therefore, transferring the TSNP to an organic phase was confirmed a suitable approach to allow their combination with hydrophobic polymers within a single solution, as it is demonstrated in the next chapter.

## CHAPTER 5 – TSNP INTEGRATION WITHIN POLYMERIC SYSTEMS

### 5.1 Preface

This chapter describes the results from the different approaches undertaken to integrate the TSNP into selected polymers. Integration into PP was performed through liquid-assisted extrusion. However, the high processing temperatures resulted in the fast oxidation of the TSNP. Solvent casting was evaluated as a system that does not involve high temperatures. Different concentrations of PEG were evaluated for solvent casting, considering PEG is a hydrophilic polymer that can be easily mixed with the aqueous solution of TSNP and also with the HNT. Increasing the concentration of PEG apparently resulted in better protection for the TSNP from air, as the colour was maintained in a closer tone to the original, although the blue colour was not fully maintained even by using a concentration of 5% of PEG. For the solvent casting of PC, PCL, and PLA, the solvent used to dissolve the polymers was chloroform, and they were mixed with the TSNP in a chloroform solution, which resulted in better protection for the TSNP from air after evaporation of the solvent, allowing the films to maintain the blue colour of the TSNP. Afterwards, the use of solvent casted films for extrusion was also explored. Post-extrusion incorporation was successfully used to integrate the TSNP into PCL films, although distribution of the nanoplates in the surface of the polymer was not ideal, which is why the same principle of adding the TSNP in chloroform solution to the surface of the film was evaluated but without extrusion. Finally, the stability of the TSNP integrated to PCL and PLA films through solvent absorption was evaluated in water, NaCl solution and KCl solution.

### 5.2 Extrusion

#### 5.2.1 Integration of TSNP in Polypropylene through Extrusion Process

Polypropylene (PP) is a highly versatile polymer with great chemical, physical and mechanical properties with a low cost production. A high diversity in structural designs and mechanical properties can be achievable, making it suitable for a wide range of applications (Maddah 2016). Particularly, its suitability for food packing applications and clinical instruments, render it as a great candidate to study incorporation of antimicrobially active agents, such as TSNP.

Figure 32 shows a comparison between extruded pure PP and PP+TSNP, obtained as described in section 3.2.3. The only visible difference is the colour, as pure PP films were white and

PP+TSNP were beige. This colour suggests that TSNP got oxidized, probably because water evaporated almost instantaneously when the drops were fed into the extruder, leaving the NPs vulnerable to air and high temperature, to which they are very sensitive (Gangishetty, Scott, and Kelly 2016; Trautmann et al. 2019). Although the absence of the blue colour is an indication of loss of the triangular shape of the nanoplates, it is possible that the colour presented in the treated PP film is still caused by AgNPs, but in a much smaller particle size and the triangular shape not present anymore. A method to integrate spherical AgNPs into PP through extrusion was achieved by Oliani et al. (2015), although in that case, the NPs were dispersed in a Polyvinylpyrrolidone solution. Given the more sensitive nature of the triangular geometry of TSNP, it is best to try avoiding high temperatures such as the one required to extrude PP, as the geometry is quickly compromised during this process.



*Figure 32. Extruded PP (Left) and PP+TSNP (Right).*

### **5.2.2 Post-extrusion incorporation on PCL**

Given the results in section 5.2.1, where the TSNP were rapidly etched as a result of the high temperature, it was decided to test a different approach that would not involve exposing the TSNP to such high temperatures. This consisted on processing PCL, which has a much smaller processing temperature for extrusion (60 °C), and spraying the TSNP solution on the surface of the extrusion dye, when the polymer is still soft, and before it goes through the rolls, which could help on spreading and incorporating the NPs into the polymer.

As described in section 3.2.3.1, the TSNP solution was applied at the end of PCL extrusion process to incorporate the TSNP in the soft melted polymer. TSNP water solution was used first without success, as the hydrophobicity of the polymer did not permit the integration of the solution even though the material was soft (Figure 33).



*Figure 33. Post-extrusion addition of TSNP (in water solution). The blue spots show drops of TSNP solution which could not be absorbed by the polymer even in a melted state, due to its hydrophobicity.*

Following this, the same method was performed using solution of TSNP in chloroform. Contrary to the water solution, the chloroform solution was easily absorbed in the extruded PCL film, as it can be observed in Figure 34. Easy absorption of the solution occurred, and the colour of the solution remained (the TSNP turned from blue to purple after some time in the chloroform solution) indicating stability of the TSNP structure after drying the solution. Dispersion of the TSNP could be improved by making adjustments to the method, in order to allow the solution to be applied more evenly along the surface of the polymer.



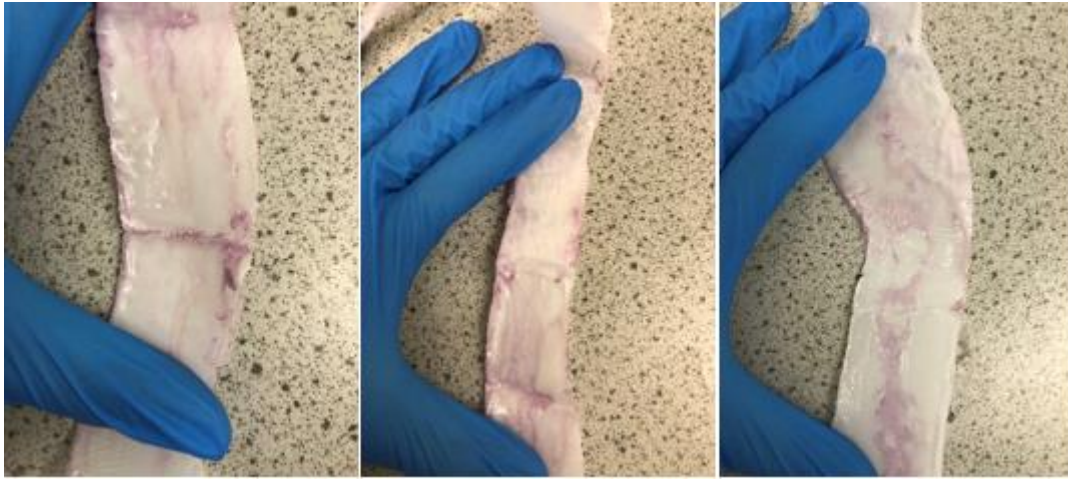


*Figure 34. PCL containing TSNP (in chloroform solution), incorporated post-extrusion, where purple spots represent the areas where the TSNP solution was absorbed into the polymer.*

### **5.3 Solvent Casting**

Solvent casting is a classic technique for film manufacturing, developed over a hundred years ago for the photographic industry, but it is still used today for the production of different engineering plastics, medical films, optical films and some electronic applications. Fundamentally, the method consists in the dissolution of a solid polymer in the form of flakes, granules, chips or powder, into a pure solvent or a mixture. Once the solution is ready, it can be poured into a flat surface to allow the formation of the film by evaporation of the solvent. This can be done in a mould-like structure for small-scale films or rolling belts with incorporated drying air systems for large-scale applications (Siemann 2005). The main point of interest about this technique, is that it provides the possibility to mix polymers and the TSNP in a liquid solution, and to form films without the requirement of high-temperature processing.

#### **5.3.1 Polyethylene Glycol Solvent Casting**

Solvent casted Polyethylene glycol (PEG) did not form a film after the ethanol was dried, on the surface of the petri dishes PEG crystals were formed as it can be observed in Figure 35. Original colours before ethanol was evaporated are shown in Figure 35-A. TSNP purple colour was not maintained in any of the two samples where it was included, indicating NPs were etched after the solvent was evaporated and they were exposed to oxygen.

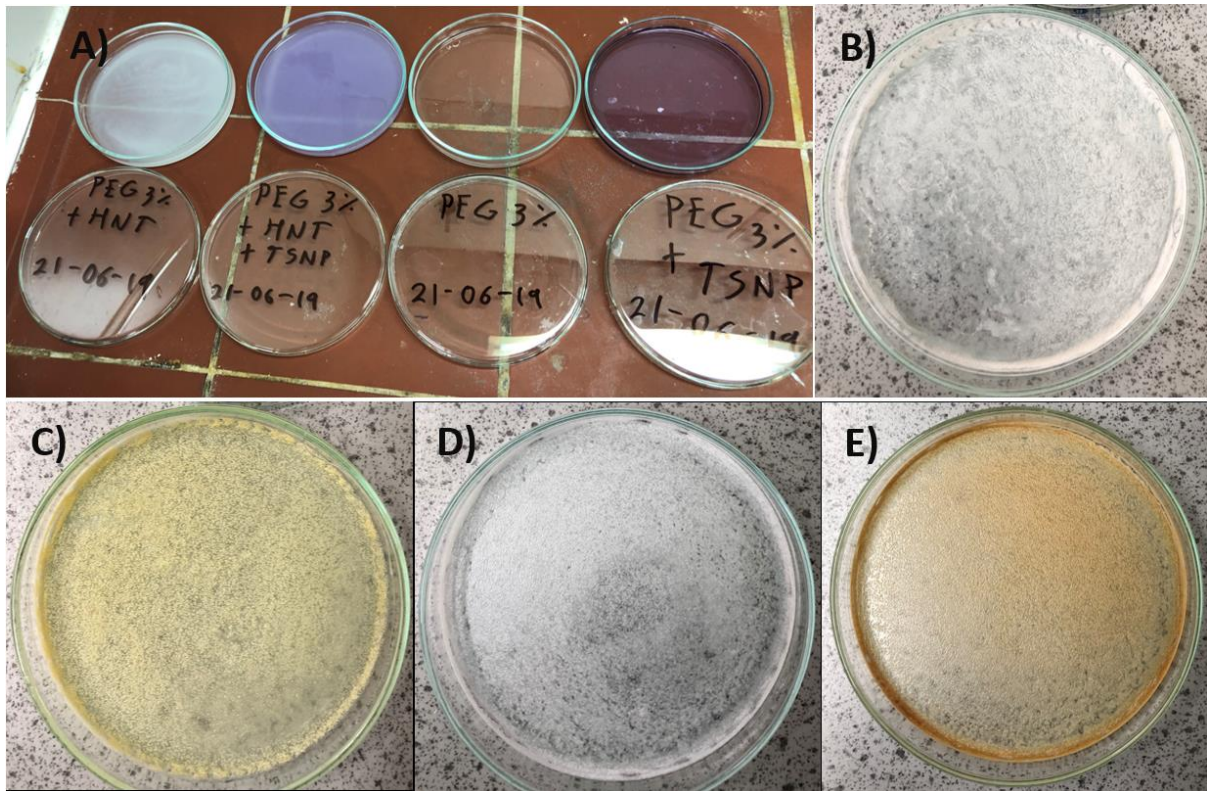
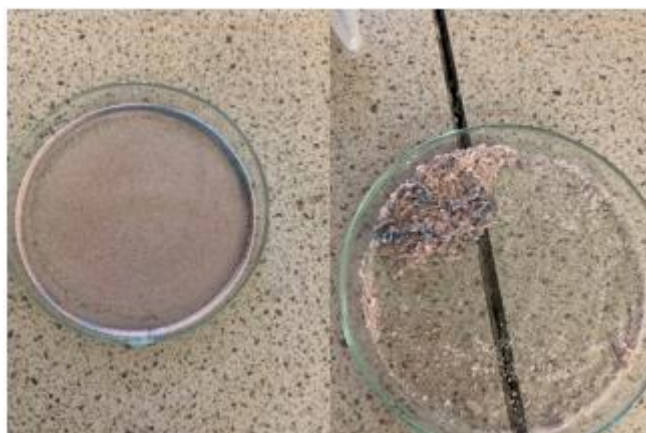


Figure 35. Solvent Casted PEG 3%: A) Solutions before ethanol evaporation; B) Solvent casted PEG+HNT; C) Solvent casted PEG+HNT+TSNP; D) Solvent casted PEG; E) Solvent casted PEG+TSNP.

In the case of solvent casted PEG with a concentration of 5%, a different sample of TSNP solution was used and this sample had a blue colour initially. In this case, it can be observed in Figure 36 that the colour did not turn to yellow, it turned to pink instead and even some parts on the edge of the petri dish maintained the blue colour. This might mean the NPs suffered less oxidation or etching compared to the sample with 3% PEG, and this could be an effect of increasing the concentration of PEG. PEG functionalization has already been used to coat and protect AgNPs for antimicrobial applications, for instance study by Fahrina et al. (2022), where they prepared a solution containing 25% PEG and formed AgNPs inside the solution by addition of  $\text{AgNO}_3$ , which was then freeze-dried to obtain a powder (Fahrina et al. 2022). However, the resulting powder obtained by this method was used as an additive for anti-fouling purposes in a membrane. Given that producing film polymers would be a more suitable option for the food and medical applications intended for the current study, it was decided to test the solvent casting method with different polymers.



*Figure 36. Solvent casted PEG 5%, after evaporating the solvent (left) and after scrapping the polymer off the petri dish (right). Showing that this method did not allow the formation of a PEG film.*

### **5.3.2 Polycarbonate (PC), Polycaprolactone (PCL) and Polylactic Acid (PLA) Solvent Casting**

Polycarbonate (PC), Polycaprolactone (PCL) and Polylactic Acid (PLA) were selected to be tested because of their versatility and different applications. PCL and PLA in particular, are biopolymers with a wide range of applications in the medical and food packaging industries due to their biocompatibility and structural properties (DeStefano, Khan, and Tabada 2020; Malikmammadov et al. 2018). PLA is one of the most promising biodegradable biomaterials, as it has already replaced several non-biodegradable petroleum-based plastics in many food packaging applications (Luyt and Malik 2018). PCL on the other hand, has mostly been used for many medical applications thanks to its high biodegradability, and it has still several potential applications in this field (Espinoza et al. 2020). Given the interest around these polymers, it is relevant to research the improvement of some of their properties that could be beneficial for the aforementioned properties, such as providing antimicrobial activity.

In the case of solvent casted PC and PCL, films were formed through the method described in section 3.2.4. As it can be observed in Figure 37, in both cases blue colour of the TSNP was maintained. This method performs as a suitable approach to incorporate TSNP within polymers without compromising the NPs at first sight, as the permanence of the blue colour is an indicative for the structure of the TSNP not going under drastic changes. The structure and viability of the TSNP when incorporated to these polymers through this method should be further evaluated in the future.

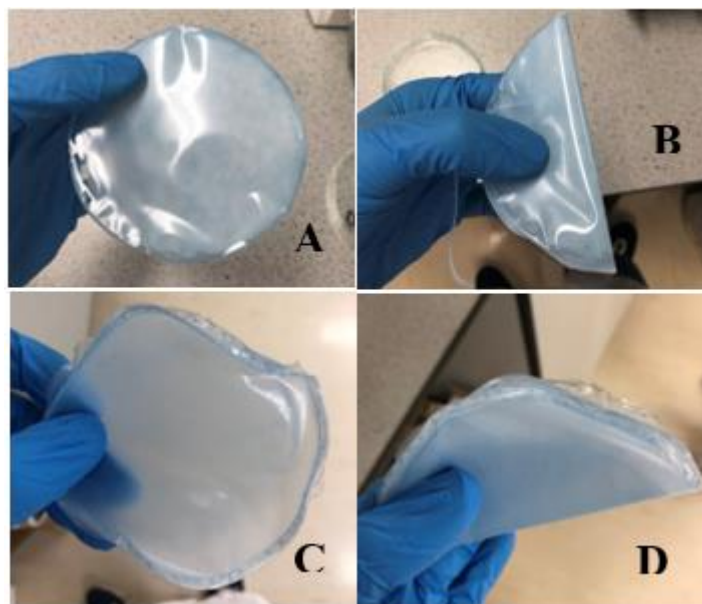


Figure 37. Solvent casted PC (A and B) and PCL (C and D). The films were folded in B and D to display the flexibility of the materials.

Similarly, films of PLA were formed through this method. However, as it can be observed in Figure 38, the colour of the TSNP is less evident in the film and it shows a more transparent appearance. This could be caused by the polymer itself and might not represent any damage in the structure of the nanoparticles, nonetheless, it would have to be further investigated to determine how stable the TSNP are when incorporated into this polymer. No visual difference was observed between the 4043 and 4044 grades of PLA.

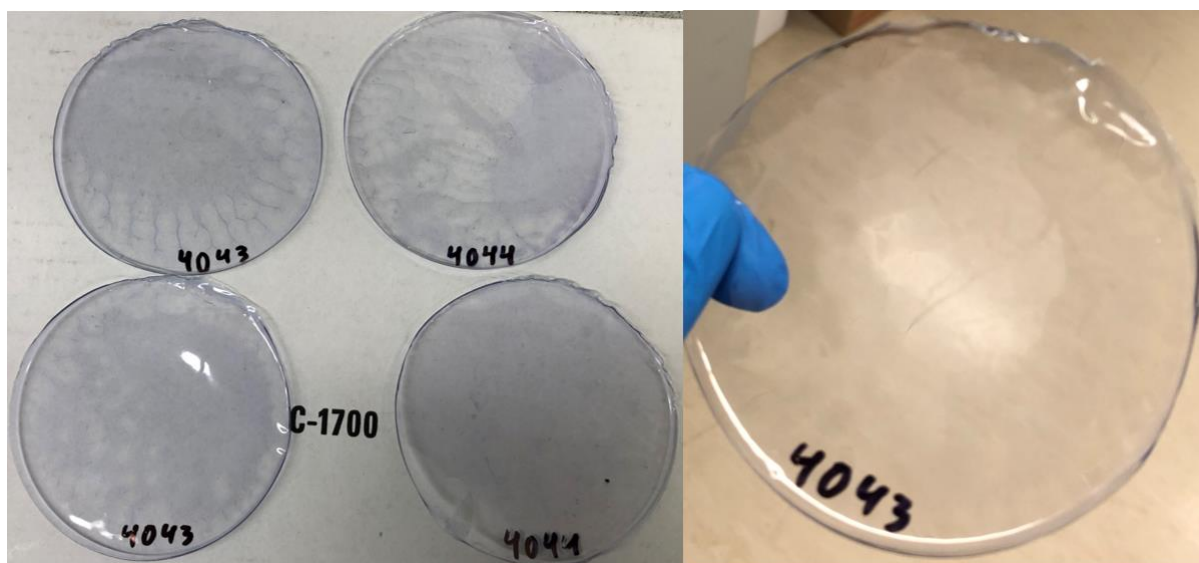


Figure 38. Solvent Casted PLA (Grades 4043 and 4044). Left picture against a white background allows to observe the blue colour present in the films, whilst right picture shows that the film presents a higher transparency, compared to films shown in Figure 37.

#### 5.4 Ex-situ incorporation on PCL and PLA

After evaluating the results shown in section 5.2.2, it was decided to test a similar method but in laboratory conditions, without making use of the extruder and the rolls, following the method described in section 3.2.5.2, where three drops of TSNP in chloroform solution were directly added to the surface of previously extruded PCL and PLA films. Figure 39 shows the results after the chloroform fully evaporated from the PCL and PLA films. It can be observed that the blue colour was maintained in both films, meaning that the TSNP are not oxidizing and therefore they are not in direct contact with air (Trautmann et al. 2019). As PCL is a softer polymer, it was slightly dissolved by the chloroform in some spots and the solution seemed to penetrate deeper into the polymer structure than in the case of PLA. In fact, PLA did not show any sign of being dissolved by the amount of chloroform added, and the TSNP formed a thin layer on top of the surface. Interestingly, the blue colour of the TSNP was maintained even though the TSNP did not seem to have incorporated within the PLA film, contrary to previous experiments of PEG solvent castings described in section 3.2.4 where TSNP readily lost colour upon contact with air. Therefore, it is hypothesised that the SH-PEG added to allow transfer of the TSNP to chloroform, also allowed the formation of a thin film layer on top of the surface of PLA, where TSNP were protected from air and were able to maintain their structure, even after drying.

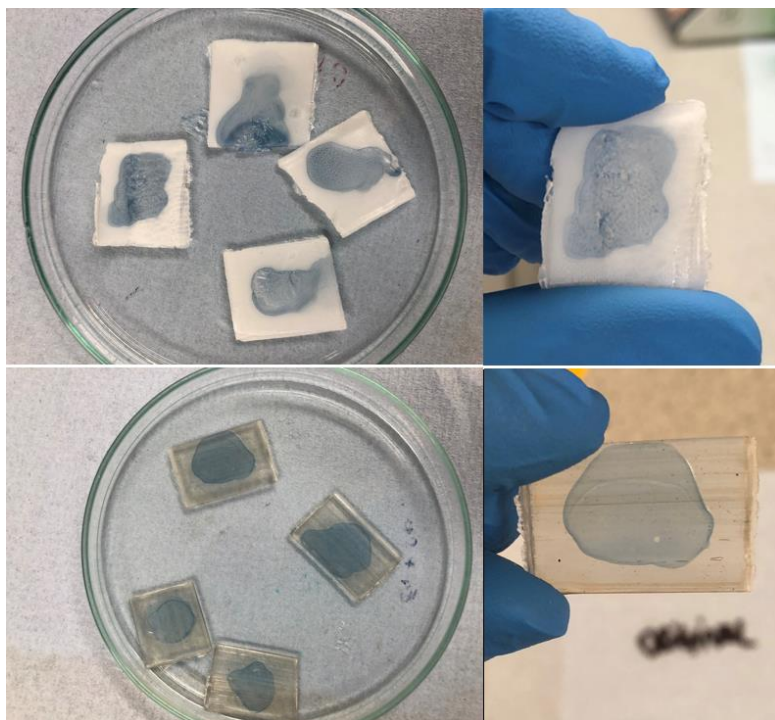


Figure 39. PCL (top) and PLA (bottom) films after incorporation of TSNP on the surface of the polymers by the ex-situ method.

## **5.5 Stability Assay**

### **5.5.1 Stability on Water and Sodium Chloride (NaCl)**

As it has been established that TSNP can be very susceptible to etching by oxidation under certain conditions, like the presence of certain ions (Y. Zhang et al. 2014), it is necessary to evaluate their stability after they have been incorporated in the surface of PCL and PLA with the methods described in section 3.2.5.2, which consisted on depositing 3 drops of TSNP solution in chloroform, and allowing the chloroform to evaporate. The first step undertaken to evaluate this was simply by washing them inside distilled water and NaCl. NaCl was used because the TSNP are highly sensitive to chlorine ions, and distilled water was used as a control, to make sure the TSNP would not be washed out easily even without the presence of a high concentration of ions.

After washing the fabricated films with distilled water and 20 mM NaCl solution as described in section 3.2.6.1, visual evaluation of the specimens was performed to determine if evident changes occurred as a result of the washing. Figure 40 illustrates the results of 1-minute and 20-minute washing in distilled water for TSNP-incorporated PCL and PLA films, respectively. Only a slight decrease in the intensity of the colour was observed in both films, but more noticeably in the PCL films. However, even with the intensity of the colour slightly fading in some cases, the colour did not completely disappear from the polymer surface in any of the tested samples. The colour of the nanoparticles has previously been used as an indicator of their stability. A study by Velgosova et al. (2022) performed a method for the synthesis of AgNps in different shapes, and colour change was used to evaluate the over-time stability of the colloid solutions, to evaluate the effect of etching by exposure to light (Velgosova et al. 2022). These results indicate that the TSNP integrated into these PCL and PLA polymers do not get washed or etched immediately when coming in contact with water, and even have the capability to remain in the polymer after a couple of hours immersed in water.

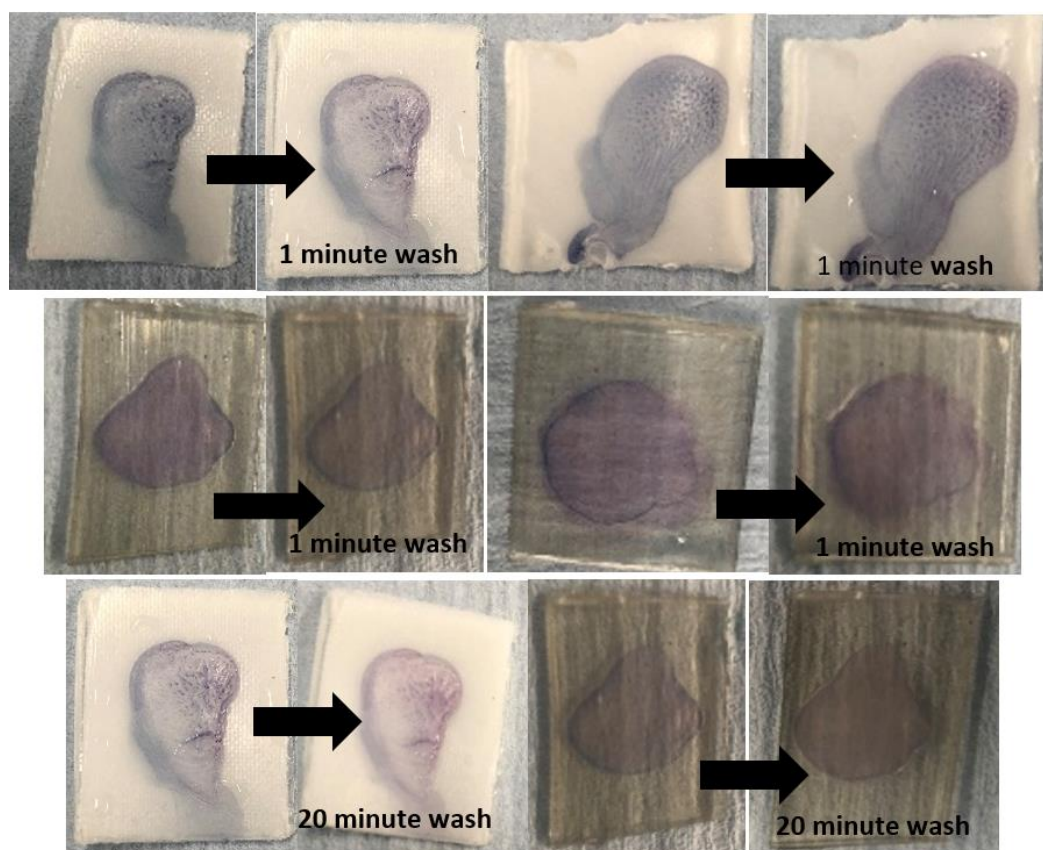


Figure 40. Photographs of TSNP-Incorporated PCL and PLA films for stability test in distilled water. Top row shows PCL films before and after 1 minute in distilled water. Middle row shows PLA films before and after 1 minute in distilled water. Bottom row shows, on the left side, a PCL film before and after 2 hours in distilled water, and on the right side, a PLA film before and after 2 hours in distilled water.

Washing of the studied films in 20 mM NaCl solution for 1 minute and 2 hours is shown in Figure 41. The reduction in the colour intensity was minimal for both samples, even with the presence of NaCl in the solution, which can cause etching of the TSNP if they are unprotected. Similarly to the washings in distilled water, the reduction in the intensity of the colour of the TSNP is very slight, but it can be noticeable on both polymers. Given the susceptibility of the TSNP to oxidation when exposed to air or to saline solutions, it is clear that TSNP integration in the polymers through the *ex-situ* method (section 3.2.5.2) allows them to obtain some degree of protection. However, the slight reductions in the colour suggest that TSNP are not deeply encapsulated within the polymer, as in the case of the films prepared through the solvent casting method (section 3.2.4). This could be advantageous for the antimicrobial activity, as there is a greater possibility for the  $\text{Ag}^+$  ions being released to reach the surface of the polymer and interacting with the bacteria (Martínez-Abad 2011; Tylkowski et al. 2019). However, this will be further evaluated in the following sections.

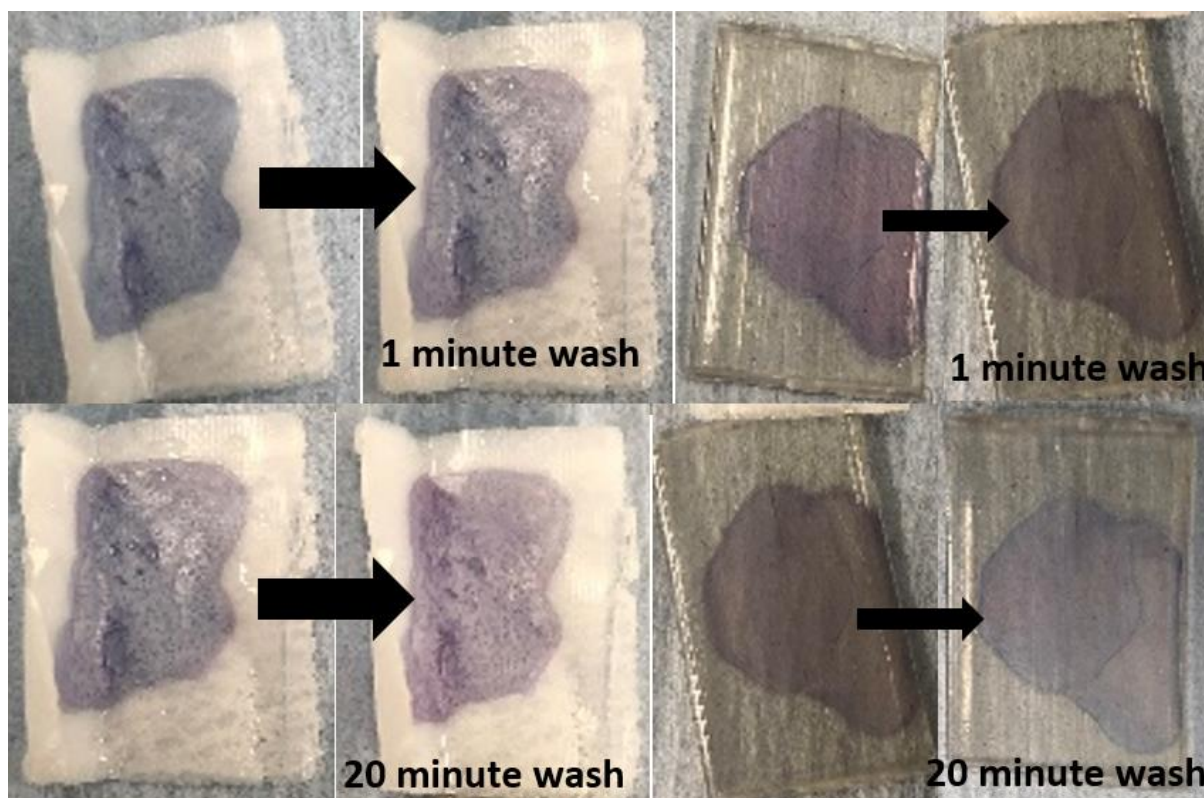


Figure 41. Photographs of TSNP-Incorporated PCL and PLA films after being washed in NaCl for 1 minute and 2 hours. Pictures on the top row show the films before and after the 1-minute wash in NaCl, PCL on the left and PLA on the right. Pictures on the bottom row show the films before and after the 2-hour wash in NaCl, PCL on the left and PLA on the right.

### 5.5.2 Stability on Potassium Chloride (KCl)

Given the results obtained in section 5.5.1, it was decided to expand the stability test to solvent casted PLA and PCL, fabricated as described in section 3.2.4. To do this, it was also decided to test several concentrations of a chloride salt (KCl), which were also added to the TSNP aqueous solution to compare their etching effect with the one of the polymer-incorporated, if any. It has previously been established that the TSNP's sharp corners can make them extremely susceptible to etching by adverse conditions, such as heat or induced oxidation by the presence of other ions. Chloride ions can etch the corners and side faces of the TSNP, changing their geometry into disk-like nanoplates and therefore altering the characteristic colour of the solution. KCl has previously been used in studies where the shape transformation of TSNP as a result of etching by chloride was examined (An et al. 2008).

Stability of the TSNP solution, prepared as described in section 3.1.2.1 was evaluated using several concentrations of KCl. Such method would be used as a reference to determine the



level of protection provided by the polymeric matrix on which the TSNP have been incorporated. Figure 42 shows the colour change of the TSNP solution (concentration of 42.68 ppm) after being exposed to the KCl solution in the concentrations of 1 M, 0.1 M, 0.01 M, 1 mM and 0.1 mM respectively. As it can be observed, in 1 M and 0.1 M, the colour of the NPs got completely lost and became a transparent solution. In the case of 0.01 M and 1 mM concentrations, the blue colour changed to a yellow tone, very similar to the one of the seeds during the synthesis of the TSNP (section 3.1.2). As for the lowest concentration, the blue colour remained practically unchanged. This result indicates that the TSNP are indeed very sensitive to saline solutions, and are able to tolerate only very low concentrations of KCl without losing their triangular shape (concentrations 0.01 M and 1 mM) or even breaking down their nanostructure completely (concentrations 1 M and 0.1 M) as a result of oxidation.



*Figure 42. Colour of the TSNP solution before adding the KCl solution (left picture) and after adding the KCl solutions (right picture) in the concentrations of 1 M, 0.1 M, 0.01 M, 1 mM and 0.1 mM, shown in the same order from left to right.*

The structural changes in the TSNP by the etching effect of the KCl solutions were also observed in their UV-Vis spectra, shown in Figure 43. In this case, contrary to other spectra plots shown in other sections, the spectral curves were not normalized to show the reduction in the absorbance of the peak, as a result of the reduction in the concentration of NPs. LSPR max of the TSNP before the addition of KCl was 658 nm. For the 1 M and 0.1 M concentrations there are no peaks, indicating the absence of detectable AgNPs. For 0.01 M, the LSPR max peak was at 410 nm, indicating a blue shift of 248 nm with respect to the initial TSNP solution. For the 1 mM concentration the blue shift was slightly shorter, 234 nm with respect to the initial solution, having a LSPR max at 424 nm. In the case of 0.1 mM, the lowest concentration, the

LSPR max was 657 nm, which means practically no shift with regard to the initial solution. The samples that became transparent reflect this in the UV-Vis spectrum by showing no peak. On the other hand, samples with yellow colour show a similar LSPR peak to the one exhibited by the seeds in the TSNP synthesis (~400 nm), indicating that the TSNP structure could be reduced back to a small spherical NPs, similar to the seeds. Additionally, exposure to the lowest concentration did not show any significant change to the LSPR peak wavelength, only a reduction in the absorbance caused by the addition of the KCL solution and reduction in the TSNP concentration.

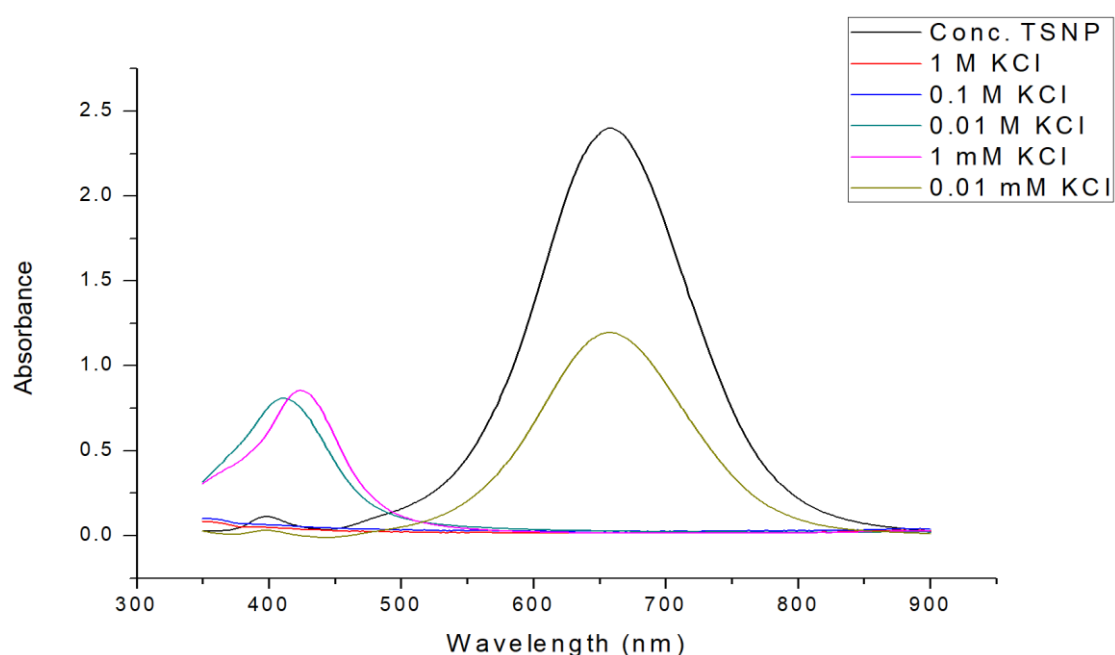


Figure 43. UV-Vis Spectra of TSNP solution before and after adding KCl solution in the respective concentrations.

After evaluating how the different concentrations of KCl affected the aqueous solution of TSNP, the stability of the TSNP-incorporated polymers was evaluated to determine the level of protection they were providing to the TSNP. Figure 44 shows pieces of the solvent casted films of PCL and PLA, obtained as described in section 3.2.4, before and after being submerged for 15 minutes in the different concentrations of KCL. As it can be observed, there are no visual differences on the colours of the submerged and non-submerged films, indicating that the TSNP are protected from etching and will maintain their morphology within the polymer film (Li et al. 2018; Yoon et al. 2019; Zhang et al. 2021).

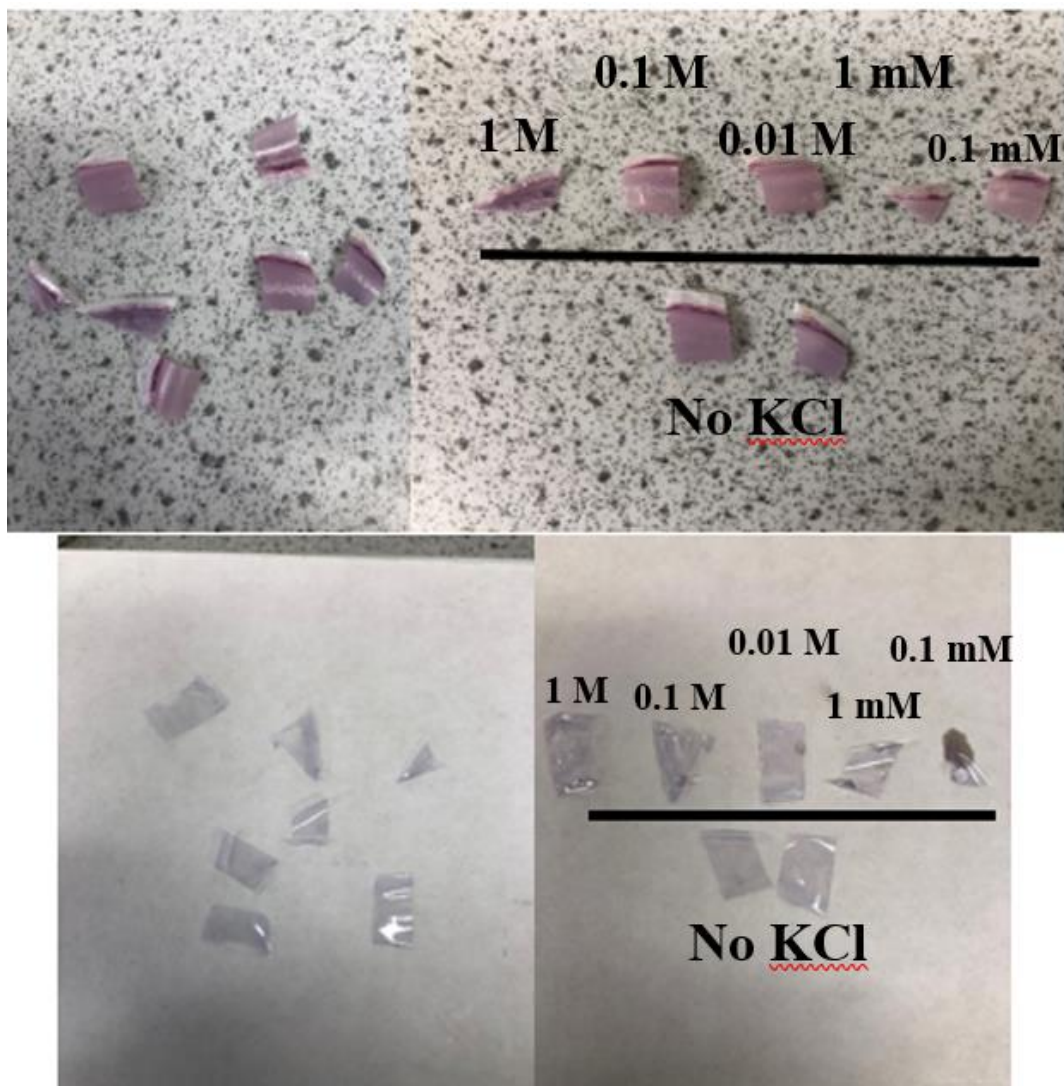


Figure 44. Photographs of PCL (top) and PLA (bottom) solvent casted films before and after being submerged in KCl solution.

Figure 45 illustrates the PCL and PLA films prepared as described in section 3.2.5.2, before and after submerging in the different concentrations of KCl solution. As it can be observed, there are no visual differences in the colours of the submerged and non-submerged films, except for a slight reduction in the intensity of the colour for the PCL film submerged in 1 M solution (circled sample), indicating that the TSNP are protected from etching and will maintain their morphology within the polymer film.

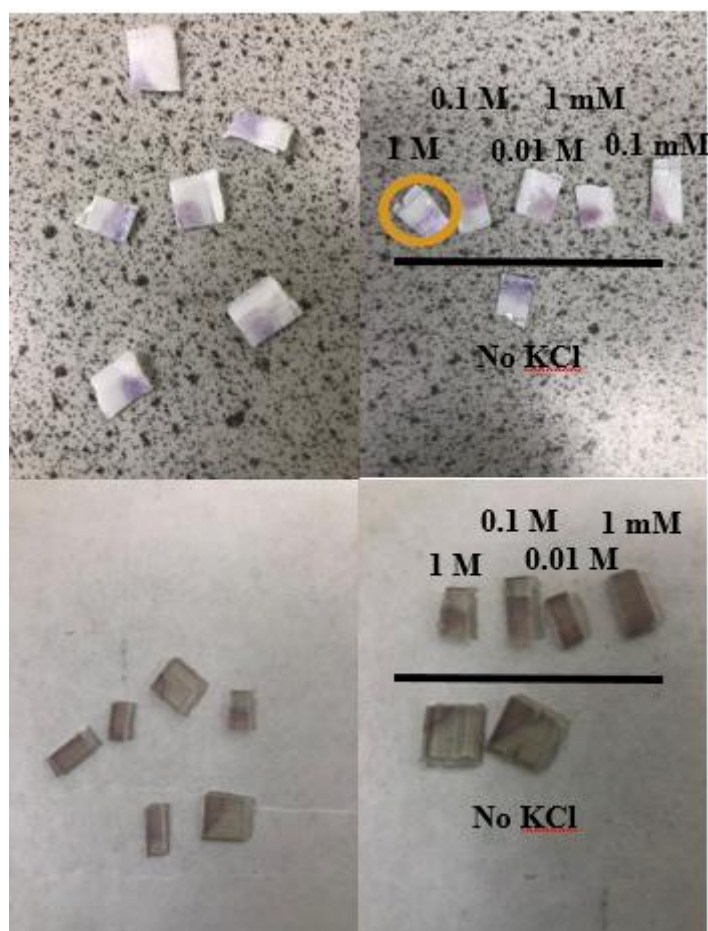


Figure 45. Photographs of PCL (top) and PLA (bottom) TSNP treated films before and after being submerged in KCl solution.

The results presented in section 5.5 show the stability of the TSNP upon integration to some polymers through solvent casting and the ex-situ method. A concentration of 20 mM of NaCl, and increasing concentrations from 1mM to 1M of KCl were used. This would result in a  $\text{Cl}^-$  ions concentration approximately 10x higher than the one present in human blood, which normally ranges between 96 and 106 mM. (Morrison 1990). Potassium concentration in blood ranges between 3.5 and 5.5 mM (Rastegar 1990), while sodium concentration normally ranges between 137 and 142 mM (Ackerman 1990). Although further studies would be required, this results indicate that this integration methods would potentially be stable enough to be used in medical applications.

## 5.6 Summary

In this chapter, integration of TSNP through extrusion, solvent casting and calendaring/solvent absorption was evaluated. Solvent casting, post-extrusion incorporation and ex-situ incorporation proved to be suitable approaches to achieve the integration of TSNP without

compromising the shape and structure of the NPs. In the case of post-extrusion incorporation, the polymers that resulted in the successful formation of a film including the characteristic colour of the TSNP, were PC, PCL and PLA. On the other hand, addition of TSNP in chloroform solution to the surface of the polymer was successfully evaluated for PCL and PLA. Stability assays demonstrated that TSNP were protected from oxidation by air and salts, and they could not be easily washed off by water or saline solution. After demonstrating the suitability of these methods for integration of TSNP, the next step is to evaluate the antimicrobial activity on the materials and characterisation of the solvent casted films, which were considered the most satisfactory result, regarding the homogeneity of the blue TSNP colour and the potential versatility of the produced films.

## **CHAPTER 6 – CHARACTERISATION AND ANTIMICROBIAL EVALUATION OF SOLVENT CASTED FILMS**

### **6.1 Preface**

In this chapter, the best performing method for integration of TSNP into polymeric materials was further studied by evaluating the resulting films. Films formed through the solvent casting method described in section 3.2.4 visually demonstrated a good integration of the TSNP into the material. This is indicated by the presence of the blue colour, characteristic of the TSNP when their structure and shape is maintained. Results presented in the previous chapter, in section 5.5 indicated that TSNP are stable within the materials after integration through solvent casting. Following these results, the films were characterised and the antimicrobial activity was evaluated.

Morphological characterisation of the films was performed by SEM, where it was observed that TSNP have some tendency for aggregation within the polymeric matrixes of PCL and PLA. Thermal characteristics of the films were evaluated through DSC, where it was demonstrated that the glass transition ( $T_g$ ), cold crystallization peak ( $T_c$ ), the melting process ( $T_m$ ) and degree of crystallinity ( $X_c$ ) were not significantly affected by the addition of TSNP to PCL and PLA films. Thermal stability of the films was evaluated through TGA analysis, where it was shown that the incorporation of TSNP did not have a significant effect on the thermal degradation profile of PCL and PLA films. The evaluation of mechanical properties included the determination of Tensile Strength (TS), Elastic Modulus (EM) and elongation at break ( $\epsilon$ ) for the produced films, where the most significant changes observed were a reduction in the  $\epsilon$  for PCL and an increase in EM for PLA after the addition of TSNP to the films. Finally, the antimicrobial activity of the films was evaluated. All the TSNP-treated films demonstrated inhibitory effect against the tested Gram-positive and Gram-negative bacterial strains. However, PLA treated films demonstrated a higher inhibition effect than PCL films, especially against the Gram-negative strain.

### **6.2 Scanning Electron Microscope (SEM) Analysis**

SEM analysis was performed for the investigation of TSNP's dispersion in PCL and PLA films. The cross-section morphology of all the films is shown in Figure 46. The illustrative SEM

images of the pure PCL and PLA films presented a good compact structure, with a smooth appearance. The cross-section of TSNP treated PCL (Figure 46, b) and TSNP treated PLA (Figure 46, d) films showed rougher surfaces. On the whole, the TSNP had some tendency of aggregation in PCL and PLA films. Such behaviour can be attributed to the high surface energy that TSNP possess which is affected by changes in size of the NPs and environmental factors such as pH and ionic strength (Shuaib et al. 2020).

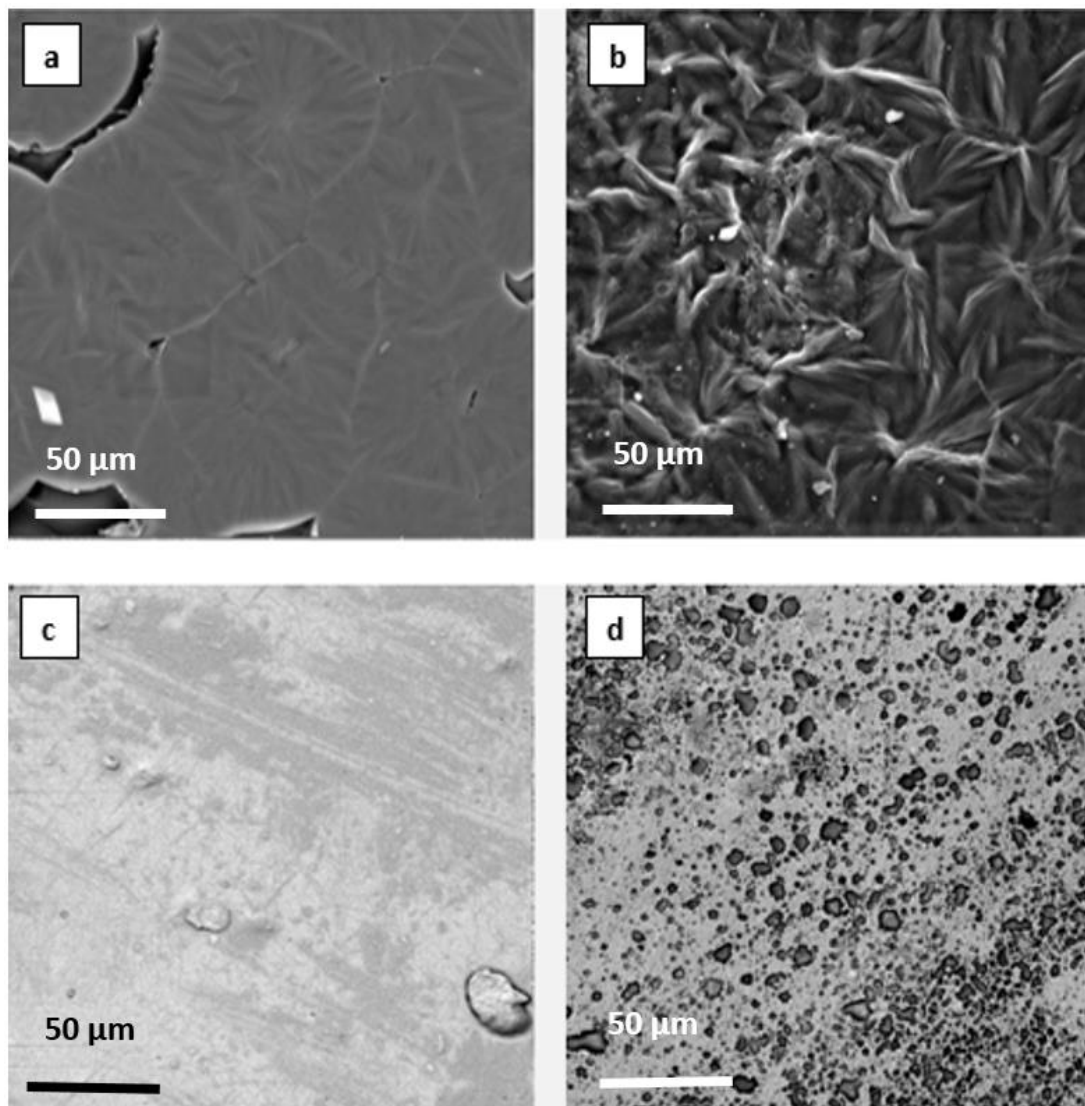


Figure 46. SEM images of: [a] PCL, [b] TSNP/PCL, [c] PLA and [d] TSNP/PLA films

### 6.3 Differential Scanning Calorimetry (DSC) analysis

The typical DSC curves of bare and TSNP treated PCL and PLA films are shown in Figure 47, A and B, respectively. The glass transition ( $T_g$ ), cold crystallization peak ( $T_c$ ), the melting process ( $T_m$ ) and degree of crystallinity ( $X_c$ ) data are summarized in Table 3. Noticeably, TSNP had a limited effect on the thermal transitions of the treated polymers. For instance, compared to the bare PCL film, the addition of TSNP did not affect the  $T_g$  (56 °C) and  $T_c$  (27 °C) of the PCL. Additionally, in PLA treated films, the values of  $T_g$  and  $T_m$  did not vary significantly from the bare PLA film. This can be attributed to the non-significant effect of the TSNP on the mobility of the PCL and PLA macromolecular chains (Li et al. 2017). These results come in accordance with previous reports where the addition of Ag NPs did not result in obvious changes in the  $T_m$  values of PCL films (Benhacine, Hadj-Hamou, and Habi 2016). Another study by Mróz et al., also found out that nanosilver did not significantly affect the thermal transitions of PLA treated films (Mróz et al. 2013).

Moreover, as listed in Table 3, the addition of the TSNP led to the increase in the degree of crystallinity in PLA up to 27%, but no significant effect was observed on PCL films ( $X_c = 47\%$ ). In case of PLA treated films, the resultant increase in the percentage of  $X_c$  can be explained by the phenomenon of heterogeneous nucleation. A similar result has been obtained by Chu et al., where the  $X_c$  of PLA was increased as a result of addition of Ag NPs (Chu et al. 2017).

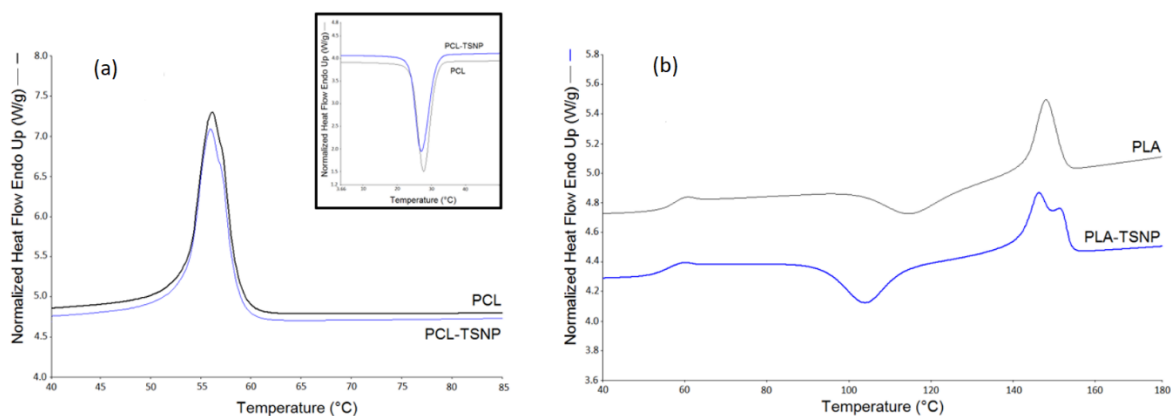


Figure 47. DSC curves for second heating of a) bare and treated PCL films and b) bare and treated PLA films.

Table 3. Thermal Characteristics of pure and TSNP treated films.

Sample	$T_g$ (°C)	$T_m$ (°C)	$T_c$ (°C)	$X_c$ (%)
PCL	-	56.06	27.75	47.9



TSNP/PCL	-	55.92	27.36	47.6
PLA	56.7	148.1	52.94	21.5
TSNP/PLA	55.1	146.25	50.73	27.4

#### 6.4 Thermogravimetric (TGA) Analysis

TGA analysis was carried out to study the thermal stability of the prepared films. The TGA curves of bare and TSNP treated PCL films are shown in Figure 48, A while Figure 48, B demonstrates the TGA curves of bare and TSNP treated PLA films. From the thermogravimetric curves, it can be observed that the bare and TSNP treated films have a relatively good thermal stability, since all the maximum mass losses occurred between 400 to 500 °C. As shown in Figure 48, A, the onset degradation temperature ( $T_{\text{onset}}$ ) of pure PCL was approximately 439 °C and the degradation was complete at about 550 °C. In PLA films the  $T_{\text{onset}}$  was 380 °C and complete degradation was observed at 475 °C. Both,  $T_{\text{onset}}$  and completed degradation temperature of the TSNP treated PLA and PCL films were not significantly different when compared with their pure films. Therefore, we can conclude that the addition of TSNP obviously maintained the thermal stability of the PCL and PLA films. These results come in accordance with previously published studies where no significant difference in thermal stability was observed upon the addition of nanosilver coated chitosan to PLA films (Gorrasi, Sorrentino, and Pantani 2015; Nootsuwan et al. 2018). Similarly, the addition of different silver concentrations did not change the thermogravimetric behaviour of PLA samples after 7 days in composting conditions as reported by (Gorrasi et al. 2015). On the other hand, Cerkez et al. (2017) and Leonés et al. (2020) concluded that PCL films and PCL electrospun fibers did not show a significant difference in thermal decomposition when treated with Ag NPs (Cerkez, Sezer, and Bhullar 2017; Leonés et al. 2020).

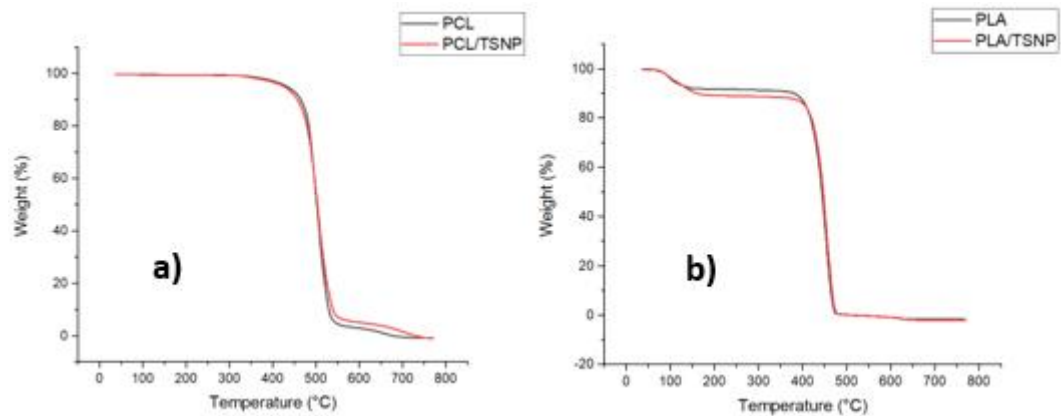


Figure 48. TGA curves of a) bare and TSNP treated PCL films, and b) bare and TSNP treated PLA.

## 6.5 Evaluation of Mechanical Properties

Tensile strength (TS), elastic modulus (EM) and elongation at break ( $\epsilon$ ) of the fabricated films were obtained through tensile testing, as described in section 3.2.7.3. The Stress-Strain graphs of each of the tested samples are shown in Appendix 1, Figure 74 to Figure 77. The pure films of PCL and PLA exhibited a lower tensile strength (13.97 MPa for PCL and 21.99 MPa for PLA), and a higher percentage of elongation at break (11.07% for PCL and 4.84% for PLA) values compared to TSNP treated films (Figure 49). According to the statistical analysis, performed through a paired t-test in Minitab, as described in section 3.4, the P-values for TS and  $\epsilon$  of PLA samples are 0.089 and 0.489 respectively. Therefore, with a confidence interval of 95%, the null hypothesis (both means are not significantly different) failed to be rejected because both P-values are higher than  $\alpha=0.05$ , and the incorporation of TSNP did not have a significant effect on TS and  $\epsilon$  for the PLA samples. On the other hand, for the PCL samples the P-value for TS (0.022) and for  $\epsilon$  (0.002) are both lower than  $\alpha=0.05$ , meaning the null hypothesis is rejected in both cases, and the integration of TSNP did have a significant effect on the TS and  $\epsilon$  of PCL samples. EM values are presented in Figure 50, where an increase in the obtained value for PLA-TSNP is observed and a very slight decrease in the value for PCL-TSNP, compared to their respective bare film samples. The statistical analysis shows that with a confidence interval of 95%, the EM of PLA and PLA-TSNP means are significantly different ( $0.011 < 0.05$ ) and the EM of PCL and PCL-TSNP are not significantly different ( $0.369 > 0.05$ ).

These results come in accordance with Augustine et al. (2016), who reported that electrospun PCL membranes either maintained TS and EM values or exhibited an increase in those parameters at higher percentage of added Ag NPs (Augustine, Kalarikkal, and Thomas 2016). For PLA films similar results were obtained by Ali et al. (2014), as they observed an increase in TS after the addition of Ag NPs to PLA (Ali, Tariq, and Noori 2014). Similarly, an increase in TS was also reported by Szymanska-Chargot et al. (2020) after fabricating a PLA composite containing Ag NPs and nanocellulose from Carrot Pomace (Szymańska-Chargot et al. 2020). In the current study, the increase of TS for PCL and PLA films after being mixed with the TSNP can be attributed to the high compatibility between TSNP and the model polymers. However, the TSNP treated PCL films suffered a significant decrease in the elongation at break percentage resulting in the formation of a very brittle film. Such result might be due to the TSNP stacking (as observed in SEM images) which reduced the mobility of the polymer chains. A similar outcome was also reported by Abdelaziz et al. (2020) as a result of adding hydroxyapatite nanoparticles to PCL composites (Abdelaziz et al. 2020).

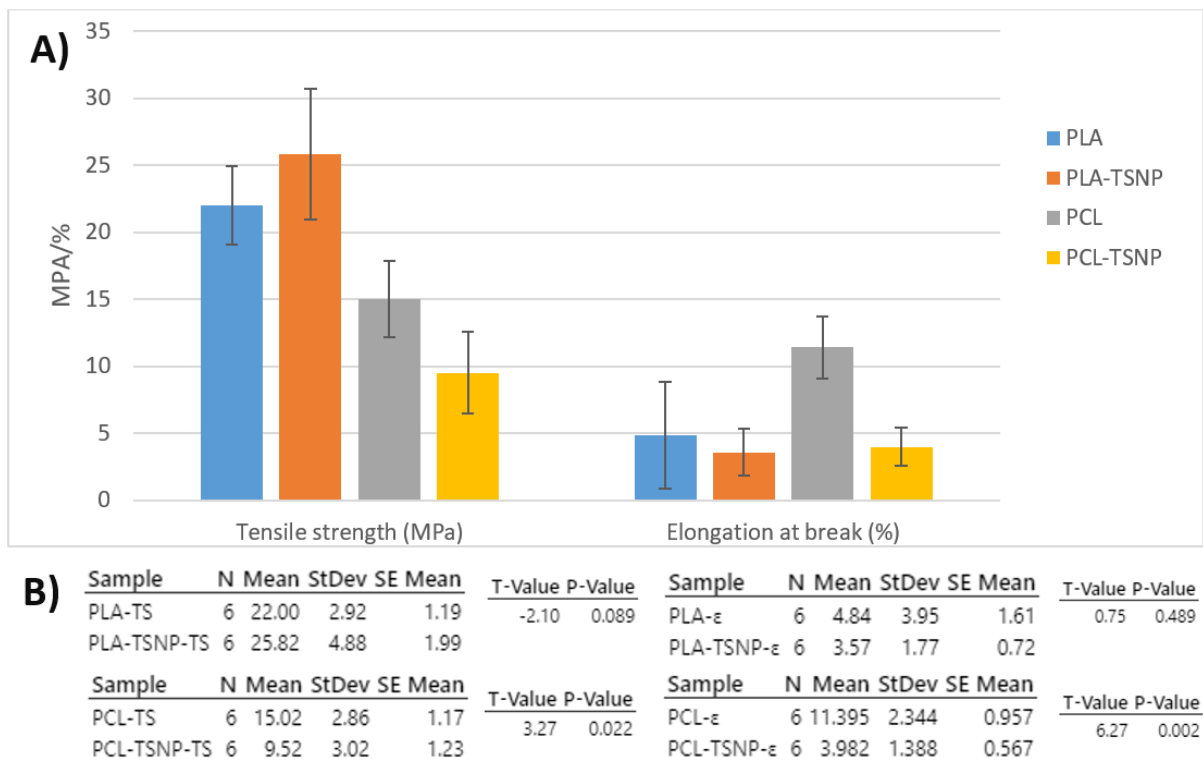


Figure 49. A) Tensile strength (TS) and elongation at break ( $\epsilon$ ) of bare and TSNP-integrated solvent casted PLA and PCL films. B) Results from paired t-test statistical analysis for TS and  $\epsilon$  of the PLA and PCL films (N=6).

Concerning the EM of the fabricated films, it was found that the incorporation of TSNP led to an increase in the EM of PLA film due to the high stiffness of the TSNP as fillers compared to pure PLA. Alternatively, there was no significant difference between the bare and TSNP treated PCL films. A similar trend was also observed by Augustine et al. (2016), where nanocomposites containing a small concentration of Ag NPs did not show a significant change in the elastic modulus of PCL composites (Figure 50) (Augustine et al. 2016).

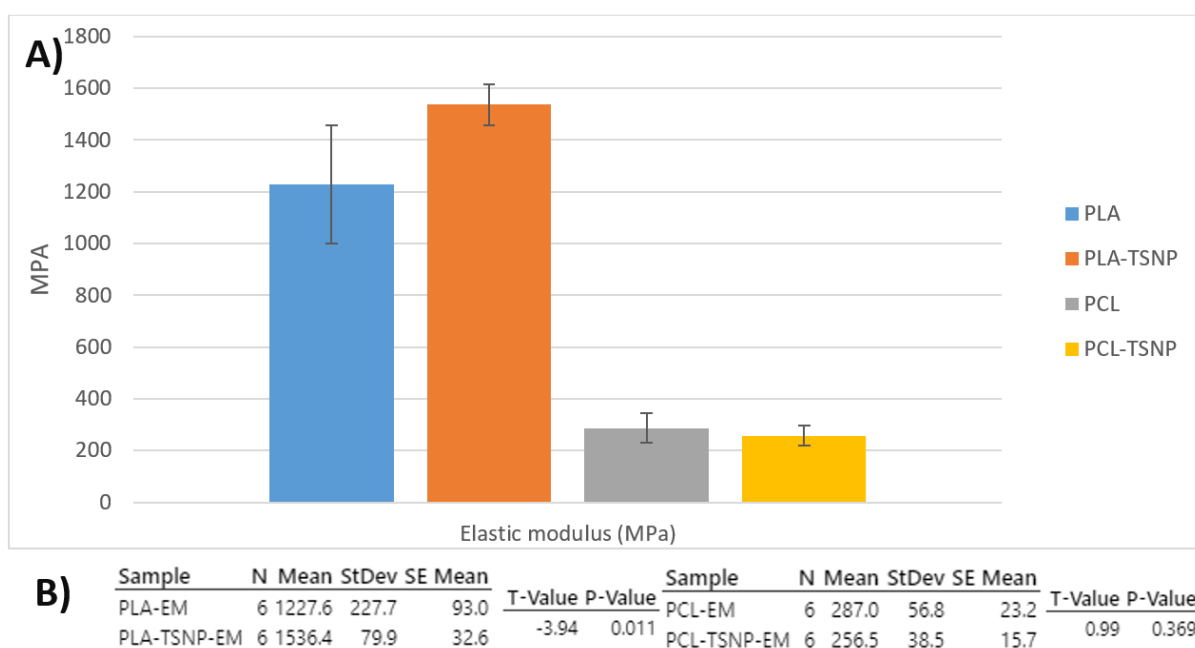


Figure 50. A) Elastic modulus (EM) of bare and TSNP-integrated solvent casted PLA and PCL films. B) Results from paired *t*-test statistical analysis for EM of the PLA and PCL films (N=6).

## 6.6 Antimicrobial Evaluation of Solvent Casted Films

Dispersion of nanoparticles inside polymer matrix can influence the mechanical and barrier properties, but also it can change its biological nature. As previously mentioned, TSNP are proven to possess considerable antimicrobial activities and as such the incorporation of TSNP in PCL and PLA films can improve the composites antibacterial characteristics. In our present study, both Gram-positive (*S. aureus* ATCC 25923) and Gram-negative (*E. coli* ATCC 11775) bacteria were used to assess the antimicrobial properties of TSNP treated PCL and PLA composite films with respect to bare films. These bacterial species were chosen as representatives of common harmful microorganisms occurring in various biomedical related products (González-Fandos et al. 2000; H. Lu et al. 2015). The particular chosen strains are not

of high medical concern, as they are both listed with a biosafety level 2, meaning they present only a moderate health hazard when they are not manipulated with proper precautions. Figure 51 shows the results of antimicrobial activity obtained from OD readings (630 nm) after 24h incubation of the films in liquid LB media. The respective bacterial controls of *E. coli* and *S. aureus* incubated without materials were considered as the 100% for survivability. The survivability of the bacteria was decreased in the presence of both materials, for both *E. coli* and *S. aureus*. PCL showed a reduction of approximately 20% for *S. aureus* and 30% for *E. coli*, while PLA showed a higher reduction on both cases; approximately 50% for *S. aureus* and 45% for *E. coli*.

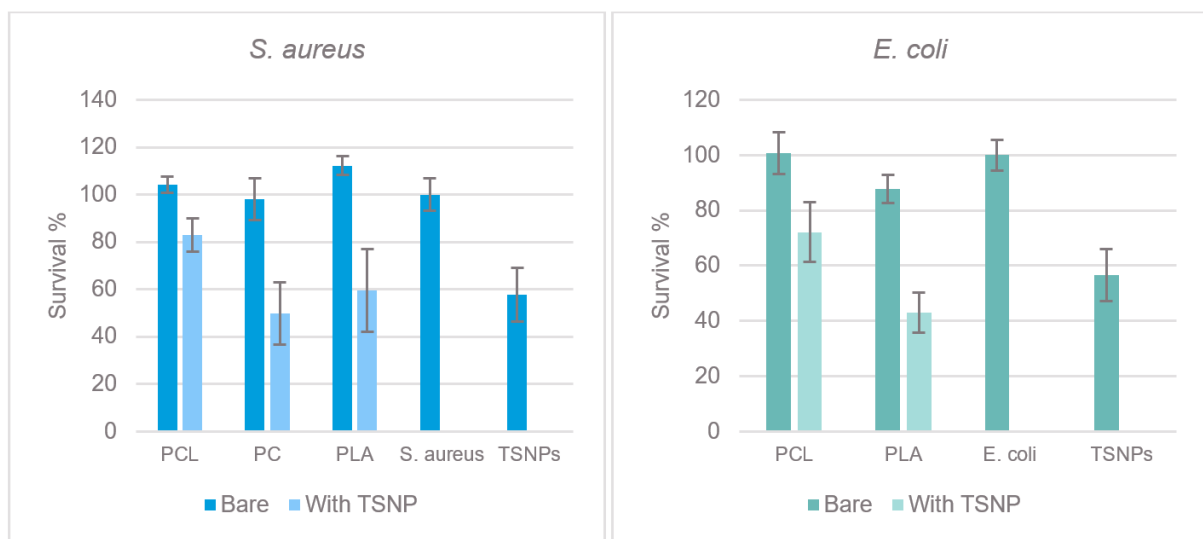


Figure 51. Antimicrobial Activity of Solvent Casted PCL and PLA films, bare and with TSNP, for both tested strains. Survival % obtained with OD measurements at 630 nm, considering the OD of the bacterial control as the 100%.

Antimicrobial effect (AE) of bare and TSNP treated PCL and PLA composite films was calculated as described in section 3.2.7.4. Briefly PCL and PLA films were immersed in the broth during the cultivation of the *S. aureus* and *E. coli* strains. After 24 hours of incubation, the films were removed and the OD of the broth was measured. AE was calculated by plating and incubating serial dilutions from cultivation broth after incubation with the films, and number of CFU was counted, to obtain a logarithmic difference between the CFU/mL of bare films and TSNP-treated films. With the use of this equation, the higher the value obtained, it represents a higher antimicrobial activity since there is a higher difference in the obtained number of CFU between treated and non-treated materials. If the obtained result was 0, it would

represent no difference between the developed CFU on the materials, and a negative number would imply that the treated material is promoting a higher bacterial growth.

As shown in Table 4, all TSNP treated films exerted an acceptable inhibitory effect against the tested Gram-positive and Gram-negative bacterial strains. Such antimicrobial activity is attributed to the TSNP incorporated in the composite films where the bare PCL and PLA films showed no antibacterial activity. Additionally, solvent casted TSNP/PLA films demonstrated higher AE values than TSNP/PCL films against both *S. aureus* and *E. coli* which can be attributed to the easiness of Ag<sup>+</sup> ions release from the surface of PLA than PCL matrix. Such results come in accordance with Ahi et al. (2019) who demonstrated that PLA films treated with a microbicidal compound, such as propolis had higher antimicrobial activity that PCL ones against *S. aureus* (Ahi et al. 2019).

It is also worth mentioning that TSNP treated films showed increased antibacterial activity against Gram-negative bacteria than towards Gram-positive ones. This is due to the scarce thickness of the cell wall in the Gram-negative bacteria, making them more susceptible to the action of Ag<sup>+</sup> ions released by the TSNP from the treated films (Abbaszadegan et al. 2015; Pazos-Ortiz et al. 2017).

Table 4. Antimicrobial effect (AE) values\* for TSNP treated films

Bacterial strain	TSNP/PCL films	TSNP/PLA films
<i>E. coli</i> ATCC 11775	0.10	0.35
<i>S. aureus</i> ATCC 25923	0.11	0.28

\* Values are obtained as the average of three measurements. AE = log N<sub>C</sub> – log N<sub>E</sub>.

## 6.7 Cytotoxicity of Solvent Casted Films

The cytotoxicity of the solvent casted PLA and PCL was evaluated by using a human fibroblasts cell line (MRC5) exposed to PCL and PLA film extracts of different concentrations, previously prepared in RPMI medium under dynamic conditions. The viability of MRC5 cells

was assessed using a standard MTT assay as described in section 3.2.7.5, where non-treated MRC5 cells were used as the positive control and their mean growth considered as the 100% to compare with the other samples. The results presented in Figure 52 show a survival rate above 50% for all tested samples, compared to untreated cell controls. Bare PCL showed no toxicity towards the tested cell line, maintaining a survival rate even higher than the one of the MRC5 control. On the other hand, the sample of PCL containing TSNP showed a decrease in the cell survival rate, up to 68.9% cell survival with the highest concentration used, and 81.5% with the lowest one. A similar tendency was observed in a study for Ag-coated electrospun PCL scaffolds, performed by Lim & Sultana (2016), where the scaffolds coated with Ag showed a reduced percentage of survivability compared to the control, which was presented in terms of absorbance in their case. However, in the case of their experiment, this reduction in the survival rate was smaller and was not considered significant (Lim and Sultana 2016). Nonetheless, in our experiment, only the highest concentration used resulted in a cell viability below 70%, which is the minimum to consider the materials as biocompatible (Andreani et al. 2017). This percentage is used only as a reference, and a more accurate value can be chosen upon development of the materials for more specific applications.

A similar tendency was observed in the case of PLA materials (also shown in Figure 52), with the bare PLA showing a higher cell viability than the control group, and the PLA-TSNP samples showing a reduced viability. In this case, the viability of the bare PLC decreased up to 61% with the maximum concentration and to 84.5% with the smaller concentration used. This is in accordance to some other published studies, for example, the one published by Wang et al. (2020), where they evaluate the cytotoxicity of Ag-coated PLA membranes, and they obtain a good cell viability for the bare PLA membranes, even higher than their control, and the viability is reduced as they increase the concentration of Ag that is incorporated to the membranes (Wang et al. 2020).

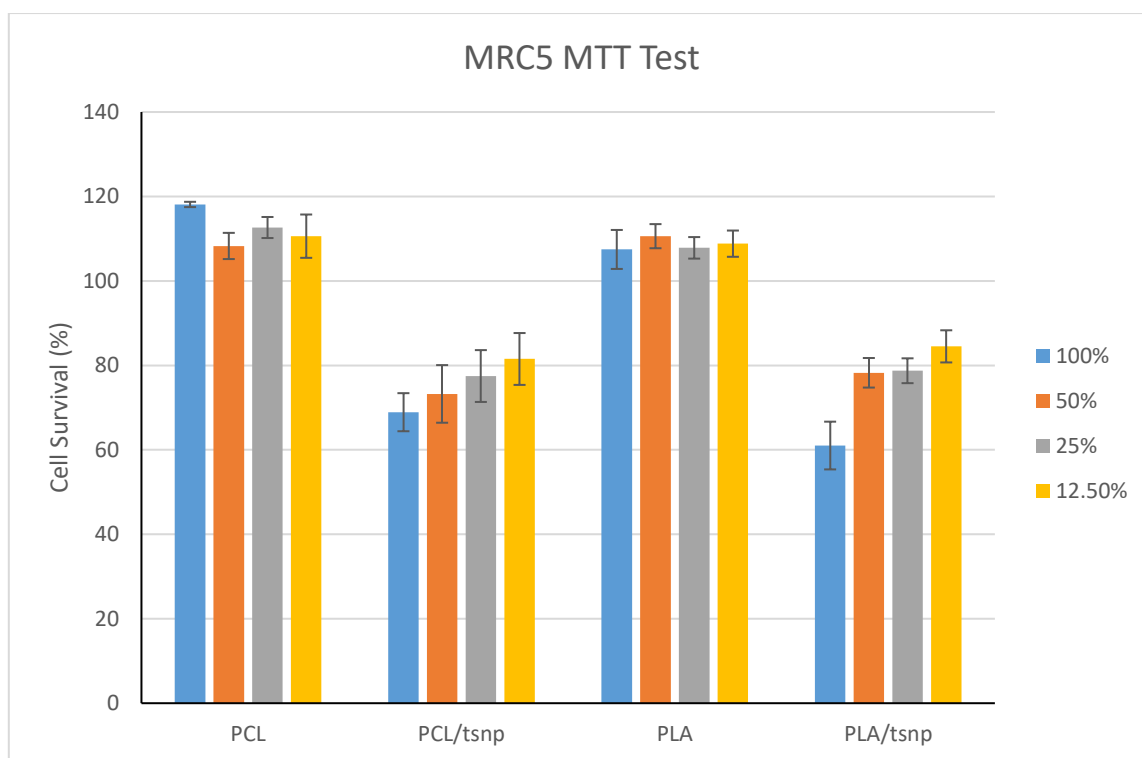


Figure 52. Survival percentage of MRC5 Lung Fibroblasts upon exposure to different concentrations of PLA and PCL extracts, with and without TSNP. The extract with the maximum concentration 100%, was prepared by incubating 10mg/mL of the corresponding PCL and PLA materials, which were then diluted up to 12.5%.

## 6.8 Summary

In this chapter, solvent casted PLA and PCL films with integrated TSNP were evaluated for morphological, thermal and mechanical characterisation, as well as antimicrobial performance. Results demonstrated that the integration of the TSNP through this method is suitable and it provides the films with inhibitory activity against *E. coli* and *S. aureus* strains growth. Furthermore, it was observed that thermal properties of the films were not affected after the incorporation of the nanoplates. However, aggregation of the nanoplates in the matrix of both evaluated polymers was also observed, and changes in some of the mechanical properties such as a reduction in the observed  $\epsilon$  of PCL and an increase in the EM of PLA. Further research would be required in order to attempt to improve the distribution of nanoplates in the films and prevent aggregation, as well as improving the mechanical properties and enhancing the antimicrobial activity of the produced films.



## CHAPTER 7 – BACTERIAL CELLULOSE/CURCUMIN + TSNP FILMS; CHARACTERISATION AND ANTIMICROBIAL EVALUATION

### 7.1 Preface

Bacterial cellulose (BC) is a biopolymer that has attracted a lot of interest in research and industrial sectors, given that it is highly pure compared to plant-produced cellulose. As well as several exclusive properties, such as high liquid holding capacity, flexibility, mouldability, and high mechanical strength in the wet state (Gorgieva and Trček 2019). Furthermore, BC's biocompatibility renders it as a suitable material for a broad range of applications, particularly in the biomedical field, such as wound healing systems, tissue regeneration, scaffolds, and transdermal applications (Sharma and Bhardwaj 2019; Silva et al. 2017).

Given its wide range of applications, exploring the improvement of BC properties, such as antimicrobial activity through the incorporation of active compounds can result highly beneficial. Therefore, in this chapter, supplementation of curcumin during BC production and posterior incorporation of TSNP for antimicrobial purposes was explored. During production of BC by *Komagataeibacter medellinensis* bacterial strain, 2% and 10% (w/v) of curcumin were supplemented. Resulting films demonstrated clear colour differences as a result of curcumin supplementation, as well as an increase in the yield production, over 2x in the dry weight of the BC-Cur10% films, compared to bare BC films.

After the incorporation of TSNP through immersion and incubation in the aqueous TSNP solution, BC films acquired a blue colour. Through the morphological characterisation of the films, done by SEM-EDS, it was possible to observe adhered curcumin particles, as well as silver clusters on the surface of the treated films. TGA analysis demonstrated that BC films containing curcumin and TSNP did not significantly change their thermal degradation behaviour compared to bare BC films. FTIR was used to identify the changes in the functional groups after the supplementation with curcumin and TSNP incorporation. Weathering test was used to address the stability of the films under exposition to UV light over a period of time. An antimicrobial evaluation was performed to assess the efficiency of the films in the inhibition of Gram-positive and Gram-negative strains growth. The presence of curcumin enhanced the antimicrobial action of the films, compared to bare BC material, and the combination of curcumin and TSNP showed an even greater antibacterial effect, especially against the Gram-

positive strain evaluated, *S. aureus*. Biological evaluations were also performed, evaluating the *in-vitro* cytotoxic effect against a human lung fibroblast cell line (MRC5), and *in-vivo* toxicity against *D. rerio* and *C. elegans* model organisms. Overall, the materials demonstrated acceptable biocompatibility, by showing a toxic response only on the highest concentrations used. In the case of the cell line, a high toxic response was observed in the highest concentrations of the films containing only curcumin, but high survivability was observed with the films containing 10% curcumin and TSNP. A similar tendency was observed in the evaluation with *D. rerio*, where curcumin-only films produced heart and liver toxicity, while films with both curcumin and TSNP produced no observable toxic or teratogen effects. Finally, it was confirmed that films did only produce a maximum of 10% death rate in the highest concentrations of treated BC films against *C. elegans*, demonstrating their biosafety.

## **7.2 Curcumin-supplemented Production of Bacterial Cellulose (BC) and integration of TSNP**

As previously mentioned, curcumin has become a natural compound of high interest for the research community, thanks to its anti-inflammatory, anti-oxidant and anti-infective properties giving it great potential for a great diversity of applications, especially in the medical sector (Raduly et al. 2021). However, the biomedical applications of curcumin have been partially limited by its poor water solubility and bioavailability. One potential strategy to overcome these limitations is to introduce curcumin into polymer-based materials that would work as a delivery system, allowing to direct its bioactive properties (Alven et al. 2020). On the other hand, BC has also gained a lot of interest due to its biocompatibility and exclusive properties. These include a high liquid holding capacity, flexibility, mouldability and high mechanical strength in the wet state (Gorgieva and Trček 2019). As a result, it is suitable for a wide range of applications, especially in the biomedical field, including wound healing systems, tissue regeneration, scaffolds, and transdermal applications (Sharma and Bhardwaj 2019; Silva et al. 2017). Considering these overlapping applications, it is clear that there is room to explore the manufacture of BC-based composites with incorporated curcumin and TSNP, to provide a higher antimicrobial activity and potentially expand even more the applications of this biopolymer.

Trial experiments performed with TSNP-incorporated BC, prepared as described in section 3.2.5.1, showed excellent antimicrobial performance against *S. aureus* and *E. coli*, as it is

presented in the following sections. In order to further improve the antimicrobial performance of these materials, it was decided to test the incorporation of a secondary antibacterial agent. As it has been stated, curcumin also exhibits a broad-spectrum antimicrobial activity, which makes it a suitable candidate for combined use with TSNP, looking for an additive effect that would further improve the antimicrobial activity of the BC materials, as shown in the following sections.

### 7.2.1 BC Production using curcumin as a supplement

*Komagataeibacter medellinensis* (ID13488) bacterial strain was used for the production of BC in HS medium and HS medium supplemented with 2% and 10% of curcumin (w/v) (Figure 53), as described in section 3.3.2. Using visual inspection, the BC films exhibited clear colour differences as a result of curcumin supplementation. The intensity of the acquired orange colour is notably greater for the sample supplemented with 10% curcumin (BC-Cur10%), compared to the one with 2% (BC-Cur2%). Although curcumin exhibits a broad-spectrum antimicrobial activity, it did not affect the production of BC under the conditions used for this cultivation. Several factors could be involved on this, such as the concentration of curcumin, the concentration of bacteria used for inoculation, the poor solubility of curcumin in water, etc. Furthermore, it has been proposed that one of the reasons why BC producers produce BC on the first place, is to use it as a defense mechanism to resist environmental stressors, so it is possible that the production is accelerated and/or enhanced under certain stress conditions (Anguluri et al. 2022).

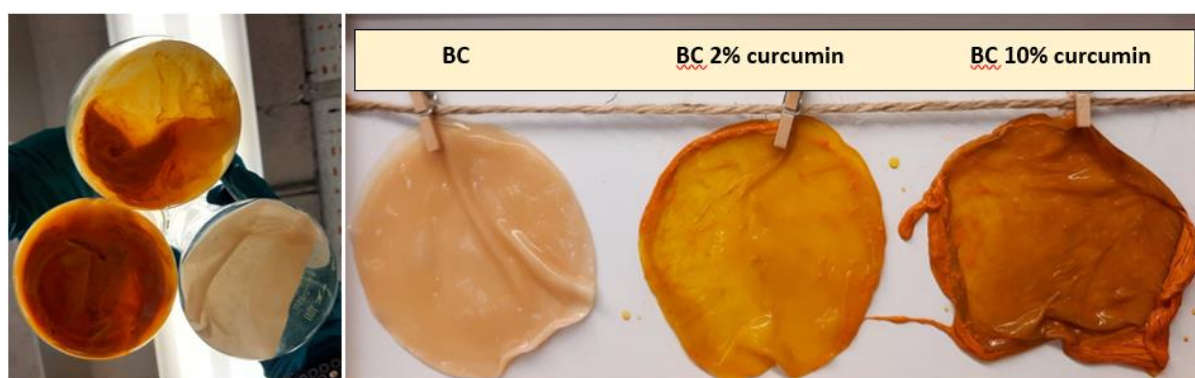


Figure 53. Left: Difference between BC pellicles in HS and curcumin-modified HS media after 14 days of incubation. Right: BC produced in HS medium (Left), in 2% curcumin supplemented (Center) and in 10% curcumin supplemented HS medium (Right).

### 7.2.1.1 Estimation of curcumin absorption from media

After 14 days of incubation, the produced BC was dried and weighed. Due to the presence of curcumin in the medium, BC pellicles resulted with higher mass in comparison to non-supplemented medium (Figure 54), which occurred because the curcumin was absorbed in between the BC pellicles. During the incubation, it was also observed that BC production would start faster in the samples with curcumin than in the regular HS medium. This could happen as a defense mechanism of the bacteria, which would accelerate the production of BC to try to protect themselves from the harmful effects of curcumin. BC has been postulated to be produced to provide mechanical, chemical and biological protection to the bacterial cells trapped in the polymeric network. This allows to keep the bacteria at the air-liquid interface and allows it to gain easier access to oxygen from the air (Urbina et al. 2021). UV-Visible spectral measurements showed that 27.8% and 41% of curcumin was absorbed by BC films, respectively, during an incubation period of two weeks.

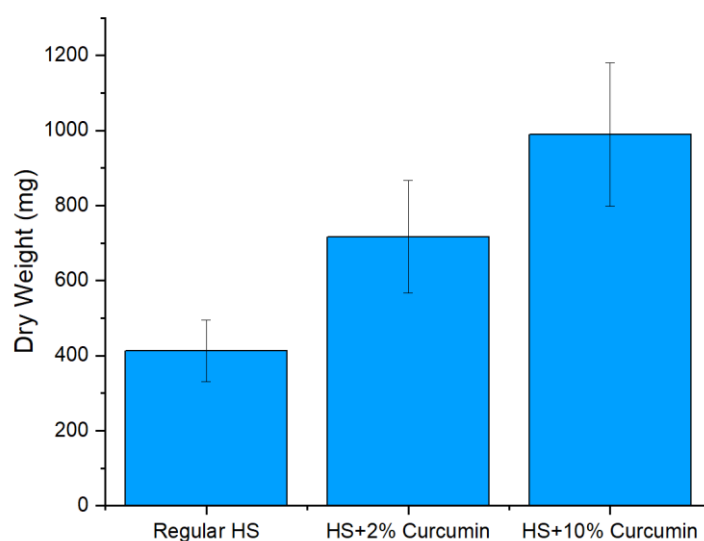


Figure 54. Dry weight of BC and curcumin-supplemented BC with 2% and 10%.

### 7.2.2 Preparation of TSNP incorporated BC films

Introduction of TSNP into the produced BC and Cur-BC films was performed as described in section 3.2.5.1. Upon completion of the procedure, visual differences were shown in the films that were treated with TSNP, as the films turned into a dark blue/purple colour, as shown in Figure 55.



*Figure 55. Top) BC produced in regular HS medium (Left), in 2% curcumin supplemented (Center) and in 10% curcumin supplemented (Right). (Bottom) Regular BC (Left), BC with 2% supplemented curcumin (Center) and BC with 10% supplemented curcumin (Right) after TSNP*

## **7.2.3 Characterisation of produced BC films**

### **7.2.3.1 Morphological characterisation and estimation of TSNP absorption**

Morphological characterisation of the produced BC films was performed by SEM analysis, while the estimation of TSNP absorption into the TSNP treated BC films was performed through EDS, as described in section 3.2.7.1. SEM micrographs of the dried BC films grown in the presence of curcumin are shown in Figure 56. Smooth surface was observed in bare BC films (Figure 56, A), while samples with incorporated curcumin showed crystal particles on the surface of the material (Figure 56, C, E). Presence of curcumin crystals indicates their strong interaction with the nanofibril matrix of BC (Akrami-Hasan-Kohal, Tayebi, and Ghorbani 2020).

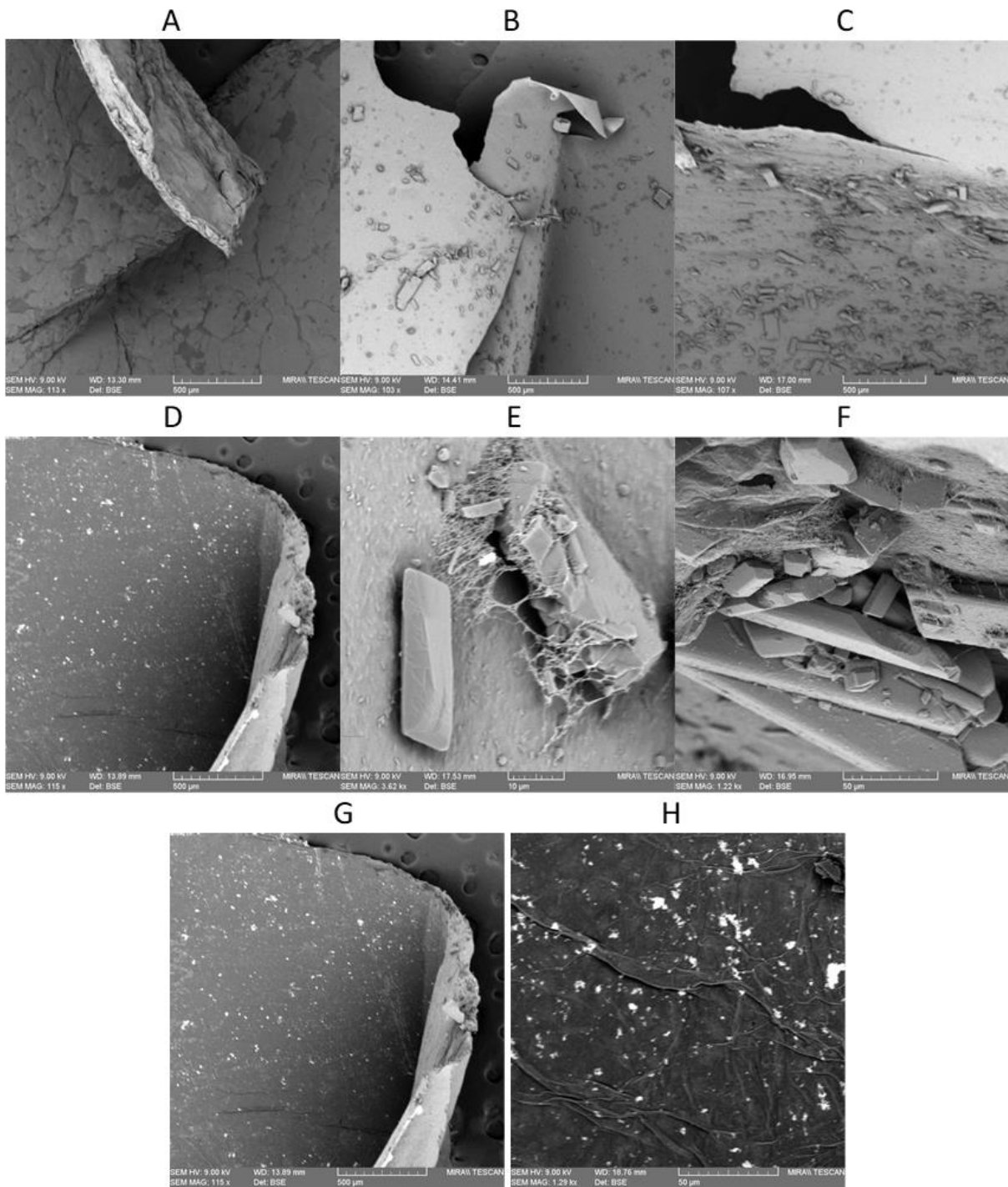


Figure 56. SEM micrographs of BC film 100x (A) and 10kx (B); BC-Cur2% 100x (C) and 3.5kx (D); BC-Cur10% 100x (E) and 1.2kx (F); BC-TSNP 115x (G) and 1.29kx (H).

The distribution of TSNP appearing as white bright dots on the surface of BC films is illustrated in Figure 57. The percentage of TSNP within the BC films was determined with the help of EDS analysis, 5 different white dots were randomly selected and analysed. The presence of silver (Ag) was confirmed for all the selected spots in tested samples (BC-TSNP-Cur2%, BC-

TSNP-Cur10%). EDS analysis revealed strong signal in the silver region with the average percentages of 80.56 and 63.9% for examined materials, respectively, as shown in Table 5.

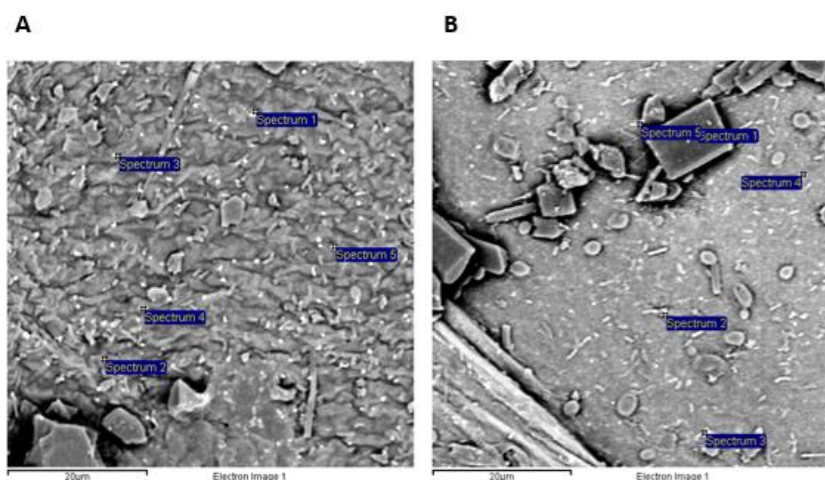


Figure 57. SEM micrographs of examined materials with spots selected for EDS analysis: BC-TSNP-Cur2% (A) and BC-TSNP-Cur10% (B)

Table 5. Result of EDS Analysis performed on 5 different points of BC-TSNP-Cur10% film.

Spectrum	O	Na	Cl	K	Ag	Total
Spectrum 1	57.2				42.8	100.0
Spectrum 2	32.4	3.8	5.4	2.7	55.8	100.0
Spectrum 3	15.9	2.4	4.1	1.7	76.0	100.0
Spectrum 4	22.1	4.0	5.3	2.2	66.3	100.0
Spectrum 5	17.5	2.0	4.2		76.3	100.0
Max.	57.2	4.0	5.4	2.7	76.3	
Min.	15.9	2.0	4.1	1.7	42.8	

### 7.2.3.2 Thermogravimetric Analysis

The TGA analysis was carried out to study the thermal stability of the fabricated BC films. The TGA curves of bare BC and BC-Cur and BC-Cur-TSNP films are shown in Figure 58. All the films started gradually losing mass below 100°C which could be attributed to the moisture content in the BC films. Maximum mass loss occurred between 200°C and 600°C. For most samples, the onset degradation temperature (Tonset) was around 213°C and the degradation rate was stabilized at 600°C. Furthermore, it can be indicated that the incorporation of curcumin and TSNP did not significantly affect the thermal stability of the BC films and this come in accordance with reported literature (Miñano, Puiggalí, and Franco 2020; Pal et al. 2017).

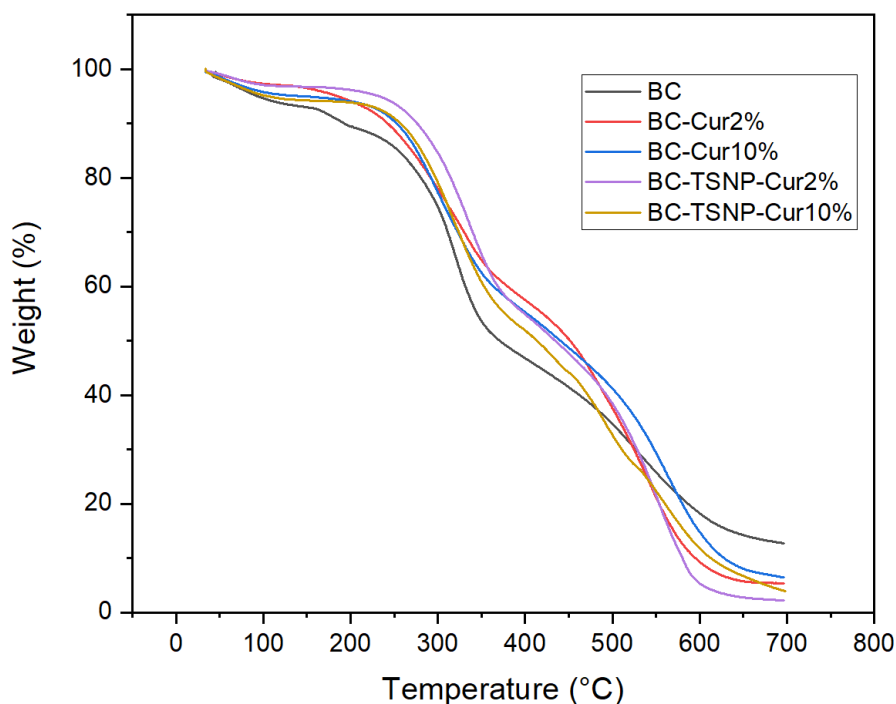


Figure 58. TGA curves of BC, Cur treated BC and Cur-TSNP treated BC films.

### 7.2.3.3 Fourier-transform infrared spectroscopy

FTIR analysis was performed to obtain a comparative view on the functional groups in BC and their changes after addition of curcumin and TSNP. The resulting FTIR spectra for the BC specimens are shown in Figure 59 and functional group assignments for the identified peaks are illustrated in Table 6 and Table 7. The spectrum of bare BC showed characteristic peaks at  $3277\text{ cm}^{-1}$  (O-H stretching vibration),  $2918\text{ cm}^{-1}$  (C-H stretching),  $1626\text{ cm}^{-1}$ ,  $1535\text{ cm}^{-1}$  (protein amide II absorption),  $1156\text{ cm}^{-1}$  (C-O-C asymmetric bending/stretching),  $1055 - 1033\text{ cm}^{-1}$  (bending of C-O-H bond of carbohydrates) and  $665\text{ cm}^{-1}$  (C-OH out of plane bending) (Gea et al., 2011; S. S. Wang et al., 2018). The spectrum for curcumin allowed to identify characteristic peaks at  $3504\text{ cm}^{-1}$  (O-H stretching vibration),  $1600\text{ cm}^{-1}$  (benzene ring stretching vibration),  $1503\text{ cm}^{-1}$  (C=O and C=C vibrations),  $1426\text{ cm}^{-1}$  (olefinic C-H bending vibrations),  $1272\text{ cm}^{-1}$  (aromatic C-O stretching vibrations) and  $1026\text{ cm}^{-1}$  (Chen et al. 2015; Gunasekaran et al. 2008; Ismail et al. 2014; Nandiyanto et al. 2017).

Spectrum of BC-Cur10% shows characteristic peaks from both, BC and curcumin. As shown in Figure 59 and Table S1, the peak assigned to OH stretching vibration of BC exhibited a shift from  $3340\text{ cm}^{-1}$  to  $3346\text{ cm}^{-1}$ , and the peak assigned to C=O and C=C vibrations of curcumin, shifted from  $1503\text{ cm}^{-1}$  to  $1507\text{ cm}^{-1}$ . A weak peak at  $1279\text{ cm}^{-1}$  was attributed to C-H bending



in the spectrum of BC (Wang et al. 2017), while it was much stronger in the same wavelength for BC-Cur10%. The small peaks that showed from 1550  $\text{cm}^{-1}$  to 1100  $\text{cm}^{-1}$  in the BC spectrum were masked by larger curcumin peaks in the spectrum of BC-Cur10%. The rest of the peaks either remained in the same wavelength or had a small shift of 1 – 2  $\text{cm}^{-1}$  only, when compared to BC or curcumin spectra. Thus, the obtained results confirm the incorporation of curcumin into the BC matrix and suggest a chemical interaction with the cellulose fibrils. A similar tendency was observed by Sajjad et al. after incorporating curcumin into BC sheets, where additional peaks appeared and the characteristic peaks of BC suffered small shifts (Sajjad et al. 2020) .

In the spectrum obtained for BC-TSNP-Cur10%, a shift from 3340 to 3277  $\text{cm}^{-1}$  was observed in the OH peak. The peak related to C=O and C=C vibrations was also shifted from 1503 to 1512  $\text{cm}^{-1}$  with respect to the curcumin spectrum. Additionally, when compared to the spectrum of BC-Cur10%, several peaks showed reduced intensities between 1500 and 1000  $\text{cm}^{-1}$  which are estimated to occur due to the impregnation of TSNP within the matrix of BC-Cur films.

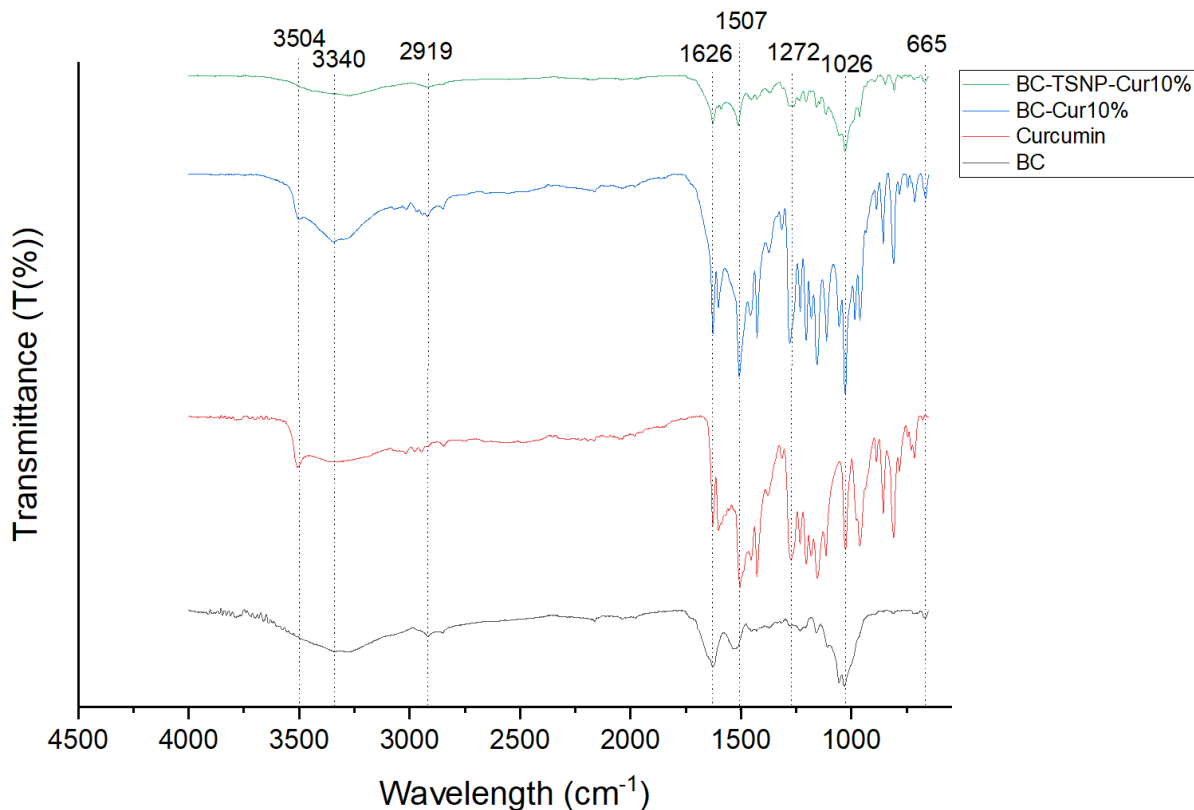


Figure 59. FTIR Spectra for BC, Curcumin, BC-Cur10%, BC-TSNP and BC-TSNP-Cur10%.

Table 6. FTIR peak assignments for BC, Curcumin, BC-Cur10%, BC-TSNP, BC-TSNP-Cur10%. Part 1, from 4000 cm<sup>-1</sup> to 1425 cm<sup>-1</sup>.

Wavelength (cm <sup>-1</sup> )	BC			3340			2918	2850	1626				1535		
	Cur	3504	3018		2975	2947		2846		1626	1600	1503		1453	1426
	BC-Cur10%			3346			2919	2848		1627	1602	1507		1457	1427
	BC-TSNP			3344			2916	2850		1650			1580		
	BC-TSNP-Cur10%			3277			2920			1626		1512			
Functional groups	OH stretching vibration	Aromatic ring	OH stretching vibration	Asymmetric C-CH <sub>3</sub> stretching	Asymmetric C-CH <sub>3</sub> stretching	C-H stretching of CH <sub>2</sub> and CH <sub>3</sub>	CH <sub>2</sub> asymmetric stretching	H-O-H bending of absorbed water.	Aromatic C=C stretching	C-N and C-C stretching (Proteins)	Benzene ring stretching vibrations	C=O and C=C vibrations	Protein amide II absorption	Aromatic C-C stretching	Olefinic C-H bending vibrations
References	(Chen et al., 2015; Ismail et al., 2014; Nandiyanto et al., 2017)	(Nandiyanto et al., 2017)	(Gea et al., 2011; S. S. Wang et al., 2017)	(Rohman et al., 2015)	(Rohman et al., 2015)	(Gea et al., 2011; S. S. Wang et al., 2017)	(Gea et al., 2011; S. S. Wang et al., 2017)	(Gea et al., 2011; S. S. Wang et al., 2017)	(Chen et al., 2015; Jyoti et al., 2016)	(Chen et al., 2015)	(Chen et al., 2015)	(Gea et al., 2011)	(Gunasekaran et al., 2008)	(Chen et al., 2015)	(Chen et al., 2015)

Table 7. FTIR peak assignments for BC, Curcumin, BC-Cur10%, BC-TSNP, BC-TSNP-Cur10%. Part 2, from 1425 cm<sup>-1</sup> to 650 cm<sup>-1</sup>.

Wavelength (cm <sup>-1</sup> )	BC		1371	1279			1156		1055	1033					665	
	Cur				1272	1231		1154			1026	961	855	745	730	
	BC-Cur10%		1374		1279	1232	1154		1055		1028	961	856	744		664
	BC-TSNP	1422	1371	1280			1161		1055	1031						664
	BC-TSNP-Cur10%			1280		1233	1158				1028					664
	<b>Functional groups</b>	Symmetric and asymmetric stretching vibration of CH <sub>2</sub>	N=O symmetry stretching	C-H bending	Aromatic C-O stretching vibrations	C-O stretching	C-O-C asymmetric bending/stretching	Aromatic C-H in plane deformation	Bending of C-O-H bond of carbohydrates	Bending of C-O-H bond of carbohydrates	C-O-C stretching vibrations. Aromatic C-H out of plane deformation	Alkene CH <sub>2</sub> out of plane bending	CH in-plane bending	CH out of plane bending	CH out of plane bending	C-OH out of plane bending
	<b>References</b>	(Zhong et al., 2018)	(Jyoti et al., 2016)	(S. S. Wang et al., 2017)	(Chen et al., 2015; Gunasekaran et al., 2008; Ismail et al., 2014; Nandiyanto et al., 2017)	(Gunasekaran et al., 2008)	(Gea et al., 2011; S. S. Wang et al., 2017)	(Gunasekaran et al., 2008)	(S. S. Wang et al., 2017)	(S. S. Wang et al., 2018)	(Chen et al., 2015; Gunasekaran et al., 2008; Nandiyanto et al., 2017)	(Gunasekaran et al., 2008)	(Gunasekaran et al., 2008)	(Gunasekaran et al., 2008)	(Gunasekaran et al., 2008)	(Gea et al., 2011)

#### 7.2.3.4 Evaluation of BC films stability via weathering tests

When combined with humidity, the colour of an organic pigment can fade much more quickly than due to light alone. For this reason, weather testing is often carried out to measure irradiation effects with humidity. Curcumin is not a very light-fast material and its colour fades quickly when exposed to such conditions. Even with the addition of UV absorbers and hindered amine light stabilisers, curcumin remains relatively unstable.

As shown in Figure 60, warping occurred in all 5 samples after weather testing. This indicates that the combination of UV and moisture caused structural changes to the BC film, presumably due to reduced chain length from photo-oxidative degradation on the exposed surface, which was more than that on the rear of samples. The weathering cycles caused embrittlement of samples containing curcumin, without TSNP. Large deposits of curcumin were present on the surface of samples, indicating that perhaps much of the curcumin is rejected from the wafer as the solution dries. The degree of incompatibility between the BC and curcumin was less pronounced in the samples containing TSNP. While it is not clear from the Figure 60, spectrophotometry measurements showed colour fading in all samples. The values for colour changes due to weathering exposure are presented in Table 8 as  $\Delta E^*$  to calculate colour difference. Due to the initial colour differences between samples, it is not fair to directly compare  $\Delta E^*$  values between cases; however, it is clear that none of the materials are UV stable. Not only is there a significant colour change for each case, but the embrittlement and disintegration of the material indicates a likely deterioration in mechanical properties due to UV light exposure. Such behaviour will be addressed and resolved in future work.

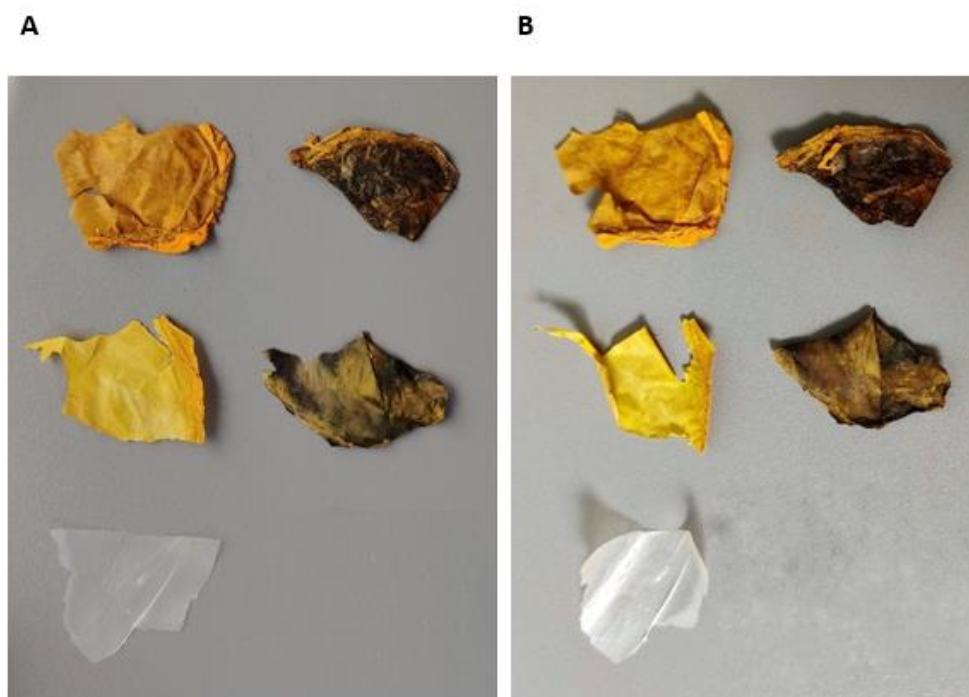


Figure 60. Samples before (A) and after (B) weather testing. From left-to-right, top-to-bottom: BC-Cur10%, BC-TSNP-Cur10%, BC-Cur2%, BC-TSNP-Cur2% and BC.

Table 8. Colour change,  $\Delta E^*$  for each sample case due to weather testing.

Samples	$\Delta E^*$
BC	2.83
BC-Cur2%	12.74
BC-Cur10%	6.40
BC-TSNP-Cur2%	4.69
BC-TSNP-Cur10%	6.87

### 7.2.3.5 Evaluation of Water Absorption and Water Retention

Swelling and water retention tests were performed to compare the absorption capacity of BC before and after the addition of curcumin. The experiments were performed as described in section 3.3.5, using distilled water, and buffers of pH 4, pH 7.4 and pH 9. The results for swelling and water retention of distilled water over a 24 hour period are presented in Figure 61. As it can be observed in the graphs, the amount of water absorbed by the bare BC samples was significantly higher than the amount absorbed by the samples with curcumin. The bare BC samples increased their weight from 3 mg to 60 mg in 24 hours, while the BC/Cur samples increased their weight only to 37 mg. For the water retention test, both materials follow a very similar rate for the release of the absorbed water.

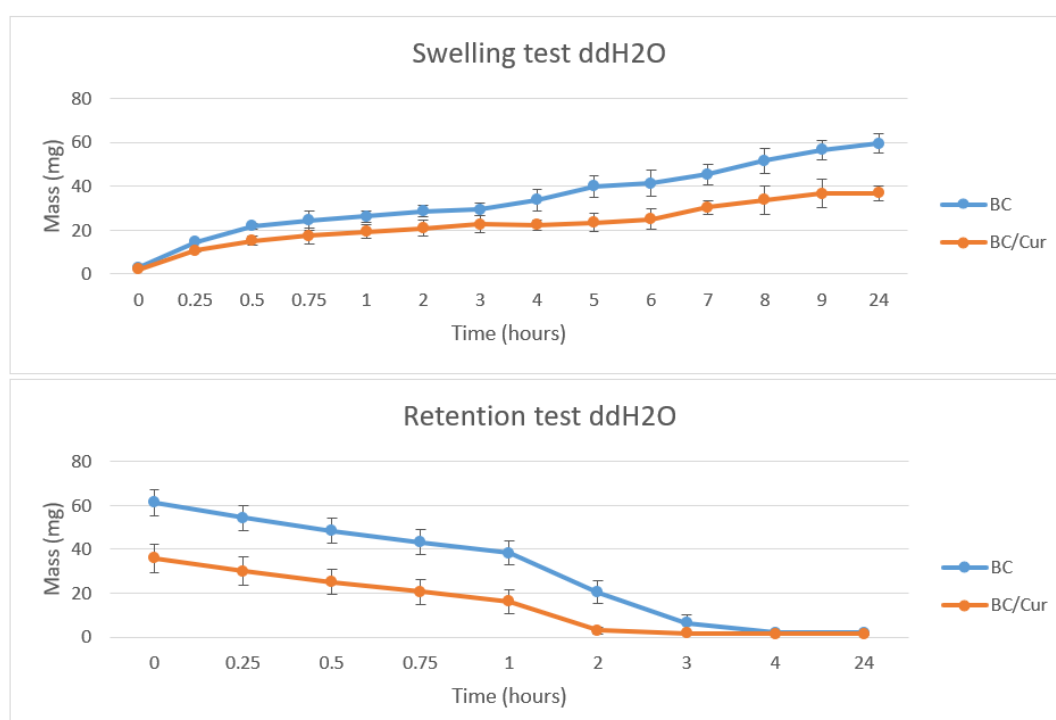


Figure 61. Water absorption (Top) & Water retention (bottom) of BC and BC-Cur samples in distilled water.

On the other hand, during the test performed in pH 4 buffer, presented in Figure 62, the behaviour of both specimens was not so different from one another. Both materials showed a weight increase from 3 mg to 31 mg on average after 24 hours. The tendency was also maintained during the retention test, as both materials dried up at very similar rates.

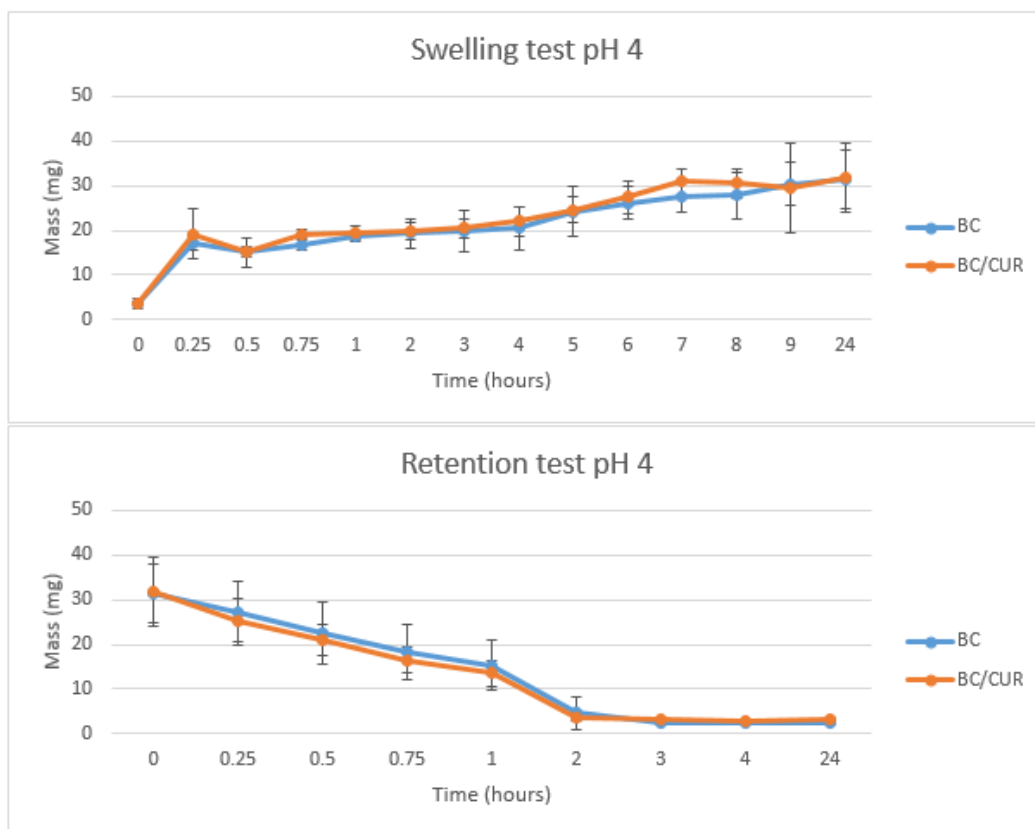


Figure 62. Water absorption (Top) & Water retention (bottom) of BC and BC-Cur samples in buffer pH 4.

In the case of the tests performed with buffers pH 7.4 and 9, presented in Figure 63 and Figure 64 respectively, the materials presented a more similar tendency to that of distilled water. In both cases, the samples of bare BC absorbed a bigger volume of buffer than the BC/Cur samples. For the pH 7.4 swelling test, the BC samples increased their weight from 3mg to 40 mg, while the BC/Cur samples increased only to 31 mg after 24 hours. Similarly, for the pH 9 swelling test, the increase BC samples reached 46 mg and the BC/Cur samples final weight was 33 mg after 24 hours. Similarly to the aforementioned tests, the water retention had similar behaviour among both specimens, for both the pH 7.4 tests and the pH 9 tests.

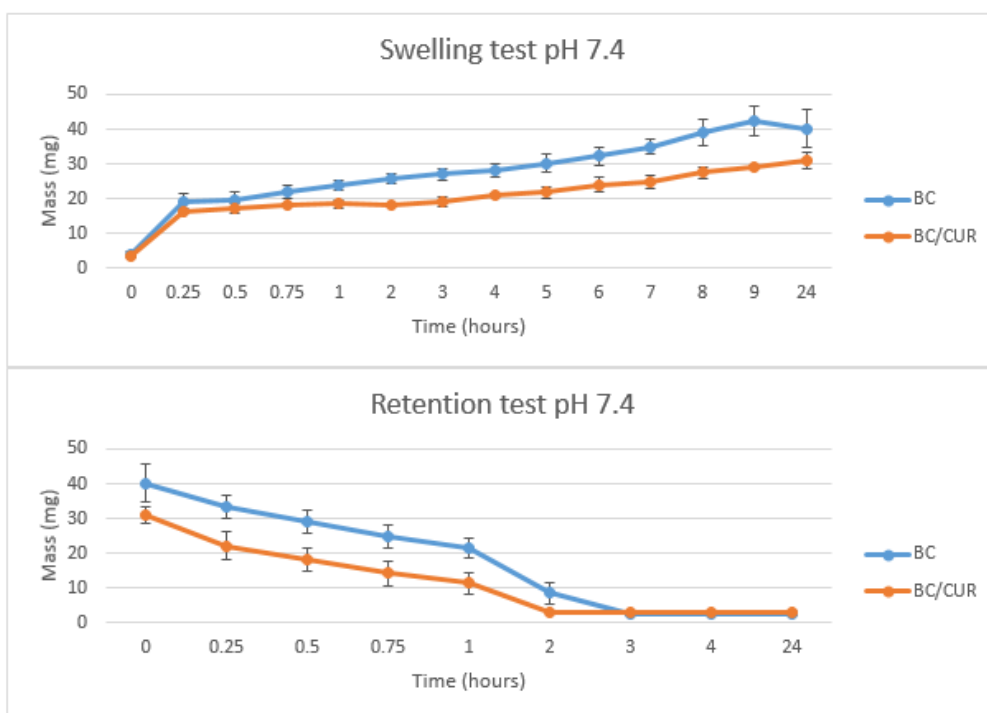


Figure 63. Water absorption (Top) & Water retention (bottom) of BC and BC-Cur samples in buffer pH 7.4.

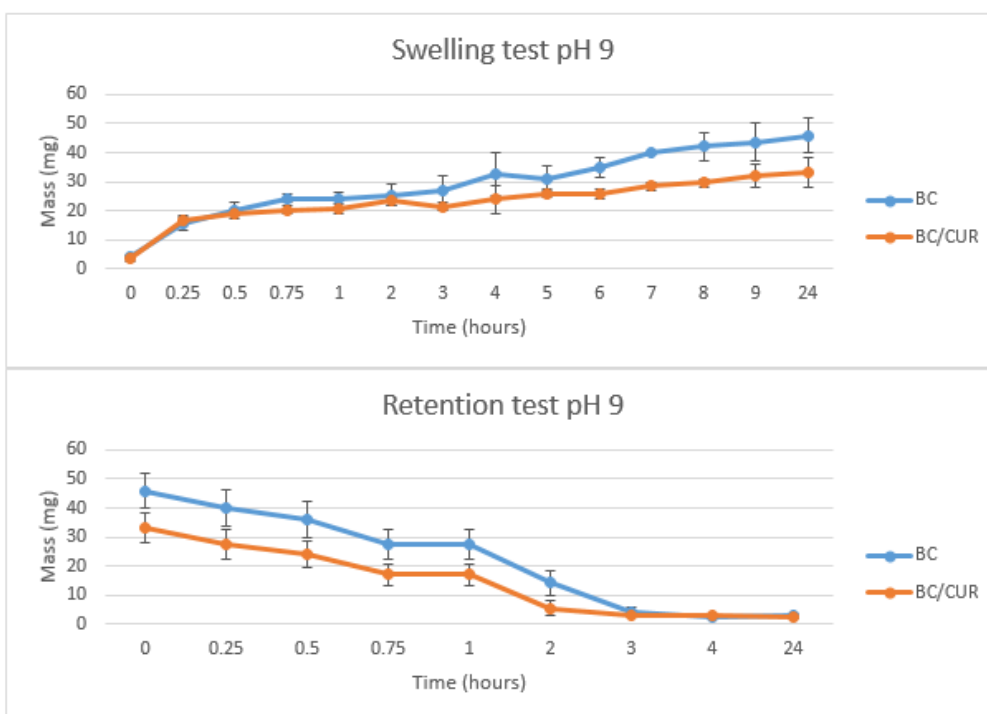


Figure 64. Water absorption (Top) & Water retention (bottom) of BC and BC-Cur samples in buffer pH 9.

Overall, the bare BC samples showed a higher capacity for absorption than the BC/Cur samples after 24 hours of immersion. With the exception of the samples tested in pH 4, where the



swelling of both specimens was very similar. These results come in accordance with those presented by Chiaoprakobkij et al. (2020), where swelling tests were performed on curcumin-loaded BC/alginate/gelatin composites, using pH 7.4 PBS and pH 6.4 artificial saliva. They observed a decrease in the fluid uptake capacity for the samples containing curcumin, and the uptake capacity would decrease even further upon the increase of curcumin incorporated in the composites (Chiaoprakobkij, Suwanmajo, and Sanchavanakit 2020).

## **7.2.4 Biological Evaluations**

The produced BC-CUR and BC-TSNP-CUR materials were evaluated for antimicrobial activity against *E. coli* (ATCC 11775) and *S. aureus* (ATCC 25923). And their toxicological effect was assessed against a human lung fibroblast cell line (MRC5), *C. elegans* and *D. rerio* organisms. The results for each evaluation are detailed in the following sections.

### **7.2.4.1 Antibacterial Evaluation of BC films**

Antimicrobial activity of derived BC films was evaluated against *S. aureus* and *E. coli*, as representatives of Gram-positive and Gram-negative bacteria, respectively. Results are displayed in Figure 65-A as bacterial growth percentage. This evaluation was performed in direct contact of the materials with the bacteria, by immersing the materials in the inoculated cultures. Pure BC film did not affect the growth of the tested strains in the desired fashion, on the contrary, the growth was enhanced by approximately 10% in both bacterial strains. Nevertheless, the antimicrobial performance of the BC films was significantly enhanced in the presence of curcumin, reducing the growth by approximately 15% in BC-Cur2% film, and up to 33% with BC-Cur10% films. Such results could be attributed to the antimicrobial activity of curcumin itself, which boosted the overall antimicrobial activity of the BC-Cur films. The antimicrobial activity was also concentration dependant since it increased with the increase of curcumin amount added during the cultivation of BC. These observations come in coordination with previously published results by Sajjad et al. (2020) (Sajjad et al. 2020).

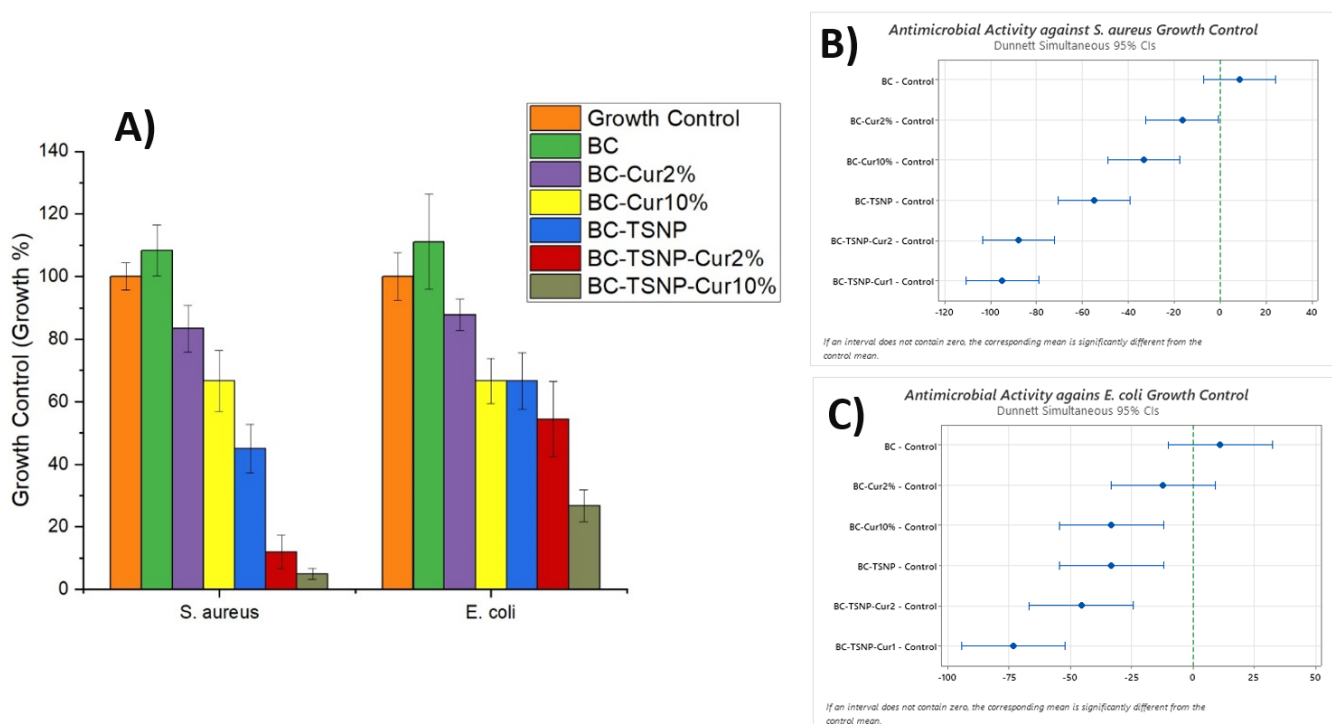


Figure 65. A) Antimicrobial activity of derived BC films measured as absorbance rate at 630 nm, considering the bacterial growth control as the 100%. B) Dunnett statistical analysis ( $\alpha=0.05$ ) for bacterial growth in presences of BC specimens compared against *S. aureus* growth control. C) Dunnett statistical analysis ( $\alpha=0.05$ ) for bacterial growth in presences of BC specimens compared against *E. coli* control ( $n=3$ ).

Moreover, incorporation of TSNP in BC-Cur films resulted in further inhibition of *E. coli* growth (up to 67% of reduction) and even greater inhibition against *S. aureus* (up to 95% of growth reduction). Contrary to our results, Gupta et al. (2020) observed higher growth inhibition against the Gram-negative strain than the Gram-positive, when testing the antimicrobial activity for *ex situ* curcumin loaded BC (Gupta et al. 2020). Nonetheless, curcumin has previously demonstrated to exhibit a higher antimicrobial effect towards Gram-positive strains than Gram-negative (Adamczak et al. 2020; Tyagi et al. 2015; Zorofchian Moghadamtousi et al. 2014), which suggests that the activity of curcumin is predominant in the case of these Cur-TSNP-loaded BC films against Gram-positive strains.

The statistical analysis to compare the bacterial growth in the presence of each BC specimen against the bacterial positive control was performed as described in section 3.3.6.1, with a one-way ANOVA paired with a Dunnett test and a significance level of  $\alpha=0.05$ . On the samples tested with *E. coli*, we can observe that the mean of all the groups, with the exception of BC

and BC-Cur2%, are significantly different to the mean of the positive control, with a confidence interval of 95% (Figure 65-C). In the case of the samples tested against *S. aureus*, only the bare BC specimens did not show a significant difference to the mean of the positive control, with a confidence interval of 95% (Figure 65-B).

#### **7.2.4.2 Cytotoxicity Assay**

Cytotoxicity was evaluated by using a human fibroblasts cell line (MRC5) exposed to BC film extracts of different concentrations, previously prepared in RPMI medium under dynamic conditions. The viability of MRC5 cells was assessed using a standard MTT assay as described in section 3.2.7.5. The results presented in Figure 66 indicate that more than 80% cells survived after being in contact with 100% concentrations of BC film extracts indicating their low toxicity. It was also shown that only 100% concentrations of BC-Cur2% and BC-Cur10% film extracts induce significant decrease in MRC5 cells viability after 48 h treatments. Significant toxicity was related to 100% and 50% concentrations of both BC-TSNP and BC-TSNP-Cur2%. Interestingly, the increased amounts of curcumin in BC-TSNP-Cur10% film extract resulted in considerably reduced toxicity since more than 80% cells survived after being in contact with the highest concentration of this extract. This unexpected results might suggest that the possibility of an antagonistic interaction being present when there is a high concentration of curcumin being used in combination with the TSNP. A proposed hypothesis involves an interaction between TSNP and curcumin, which might have reduced the amount of both compounds being released during the incubation of the materials for the preparation of the extracts used in the cytotoxicity assay. However, further studies are required to determine the exact causes for the observed results.

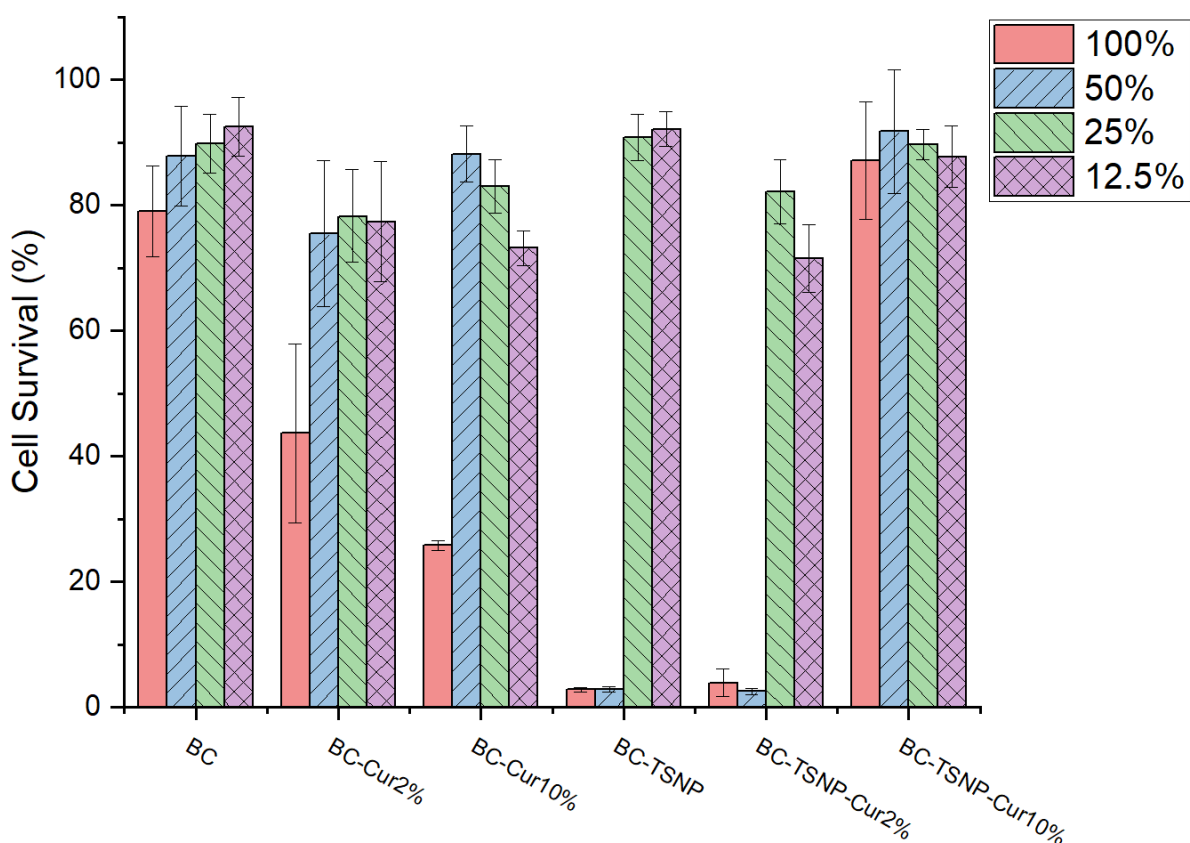


Figure 66. Survival rate of cell line (MRC5) after exposure to BC film extracts of different concentrations (n=4).

Statistical analysis, performed as described in section 3.4, was used to compare the mean cell survivability of MRC5 fibroblasts when incubated with 100% and 50% concentration extracts of the BC specimens. As it can be observed in Figure 67, when the fibroblasts were incubated in the presence of 100% extracts, only the mean survivability of BC-TSNP-Cur10% is statistically non-significant, with a confidence interval of 95%. However, when the fibroblasts were incubated in with 50% extracts, only mean survivability of BC-TSNP and BC-TSNP-Cur2% were statistically significant, with a confidence interval of 95% (Figure 68).

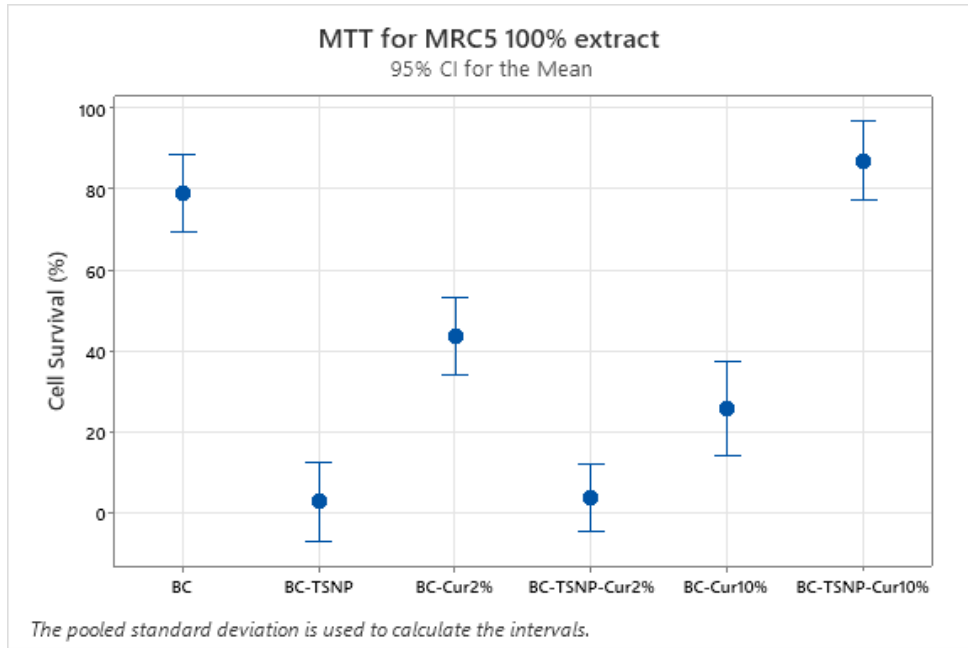


Figure 67. One-way ANOVA comparison of means from cell survivability of MRC5 fibroblasts, in the presence of 100% extract of each BC specimen (n=4).

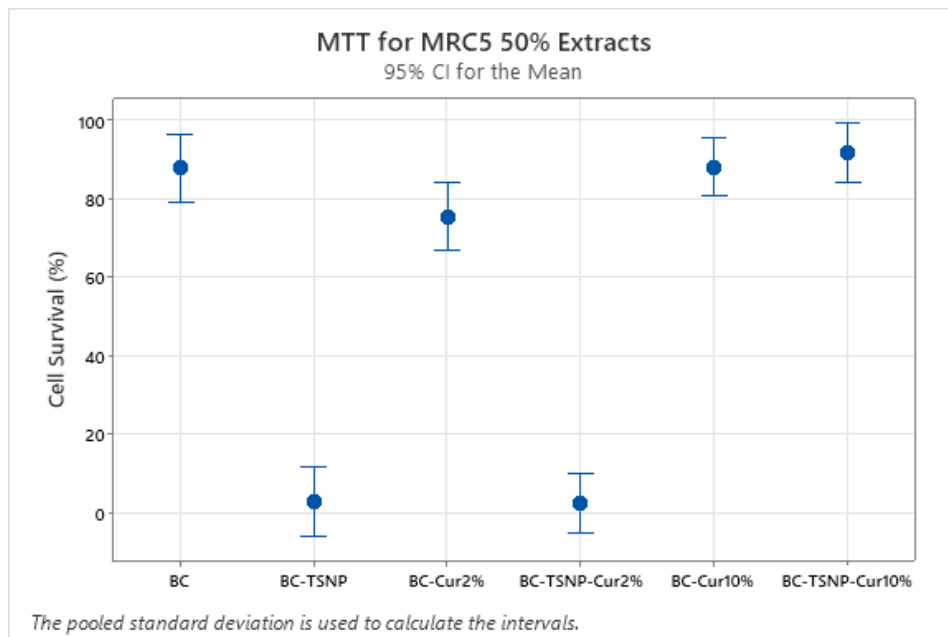


Figure 68. One-way ANOVA comparison of means from cell survivability of MRC5 fibroblasts, in the presence of 50% extract of each BC specimen (n=4).

#### **7.2.4.3 *Danio rerio* Embryotoxicity Assay**

Effects of BC materials were examined on zebrafish embryos in four different concentrations: 12.5, 10, 5 and 2.5%. Percentages for alive, dead and teratogenic embryos exposed to each concentration of the materials are shown in Figure 69, and visual effects on the development of the embryos are displayed in Figure 70. Control material BC was not significantly toxic, while BC TSNP in the highest tested concentration (50%) was toxic, with the teratogenic effects as microcephaly and hepatotoxicity. Supplementation of BC with curcumin in two concentrations causes toxic effects on zebrafish, mostly heart and liver toxicity, while BC-TSNP-CUR2% and BC-TSNP-CUR10% did not have any toxic or teratogen effects on zebrafish embryos. Previously published study, where curcumin was tested separately on zebrafish embryos, showed the severe toxicity of this compound, with some of the teratogenic effects including bent or hook-like tails, spinal column curving, edema in pericardial sac, retarded yolk sac resorption, and shorter body length (Wu et al. 2007). While in a different study, tested in lower dosages, curcumin had a moderate acute toxicity effect on zebrafishes with no obvious morphological abnormalities (Gao et al. 2014). Additionally, silver nanoparticles are toxic for zebrafish development, one study revealed that nanoparticle treatments resulted in concentration-dependent toxicity, typified by phenotypes that had abnormal body axes, twisted notochord, slow blood flow, pericardial edema and cardiac arrhythmia (Asharani et al. 2008). However, in the case of these materials, the extracts obtained from the materials containing both TSNP and curcumin did not show a toxic effect towards the zebrafish embryos under the examined conditions. Further studies are required to investigate on the reason for this to happen, as there could be different possible explanations for these results. For instance, it could be due to interactions occurring between the TSNP and curcumin where the mechanism that produce their toxicity individually is cancelled when they are combined. One of the possible interactions could be related to a higher difficulty for the release of these compounds from the BC during the incubation for the preparation of extracts. This is one of the main differences between the experiments for evaluation of antimicrobial activity and for toxicity, as the materials were only in direct contact with the organisms in the antimicrobial assay, but for the toxicity assay extracts from the materials were prepared. This is currently a limitation to compare the results, but it would need to be considered for future experiments if these materials are further developed for more specific applications.

\***Acknowledgment:** Scoring and evaluation of physiological changes on zebrafish were not performed by myself. This experiment was performed in the Institute of Molecular Genetics and Genetic Engineering, in Belgrade, Serbia. I was assisted by Dr. Ivana Aleksic, and the evaluation of the obtained results were mainly performed by her.

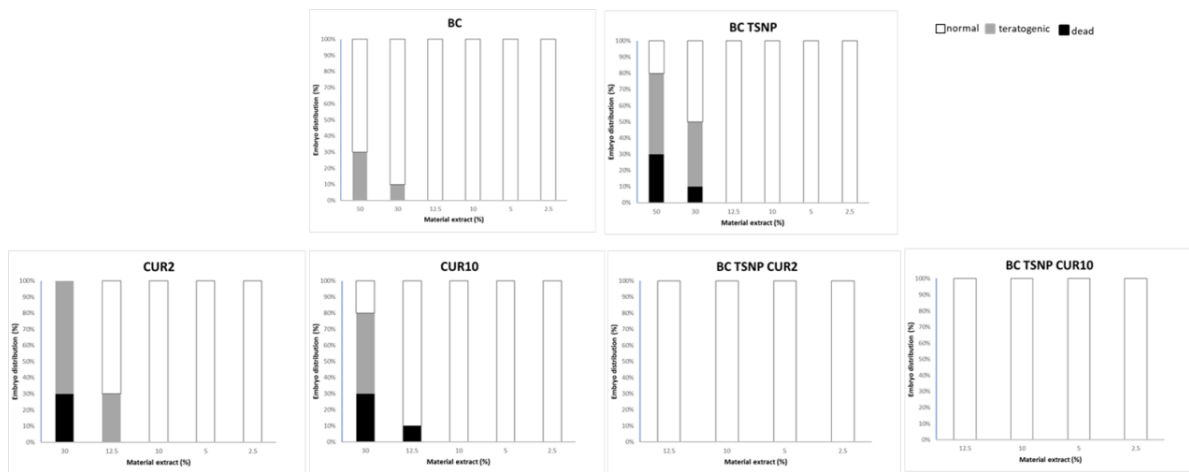


Figure 69. Diagrams for each tested material extract with the percentages of alive, dead and teratogenic embryos.

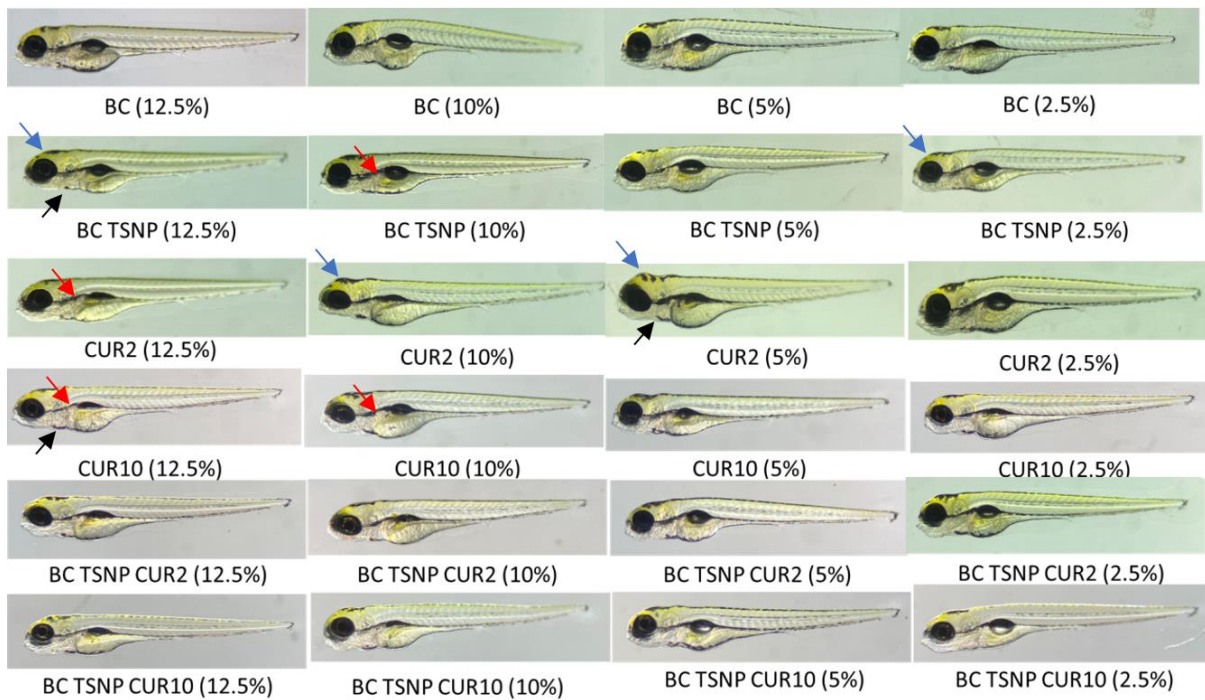


Figure 70. Effect of BC materials on development of zebrafish embryos, images of zebrafish embryos at 120 hpf treated with different extracts concentrations and untreated as a control. Blue arrows point to head abnormalities, red arrows point to liver abnormalities and black arrows point to heart abnormalities.

#### 7.2.4.4 *Caenorhabditis elegans* Survival Assay

In order to confirm previous results, effects of BC materials were examined on *C. elegans* model system in four different concentrations: 50, 25, 12.5, and 6.25  $\mu\text{g/ml}$ , as described in section 3.3.6.3 and results are presented in Figure 71. The model organism *C. elegans* has been widely used to evaluate biological activity and interactions of nanoparticles and natural products with different targets in organisms (Ha et al. 2022; Li et al. 2021).

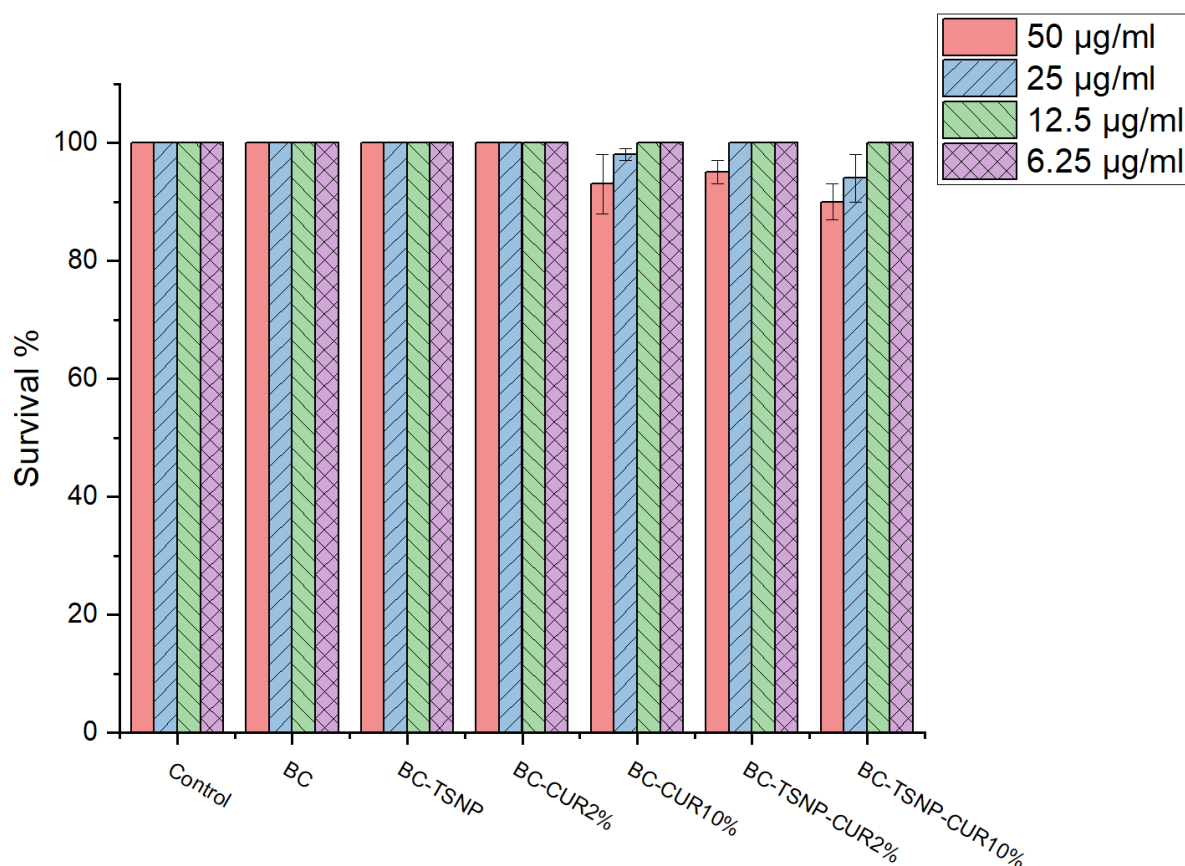


Figure 71. *C. elegans* survival rate (24h).

Overall BC materials showed little to no toxicity with only around 10% dead at highest concentration for BC-TSNP-CUR2%, BC-TSNP and BC-CUR10%. Previous studies on curcumin itself reported that this compound can prolong lifespan and influence age-related biomarkers in *C. elegans* (Liao et al. 2011). In the other hand, nanoparticles, especially silver, have shown significant toxic effect with this model organism (Yang et al. 2012). Our results are implying that used concentration of TSNP incorporated in BC films was not sufficient in order to significantly affect *C. elegans* under examined conditions.



#### **7.2.4.5 Discussion of Results of Biological Evaluation**

The incorporation of curcumin into BC, as well as the incorporation of TSNP lead to growth inhibition of *E. coli* and *S. aureus* strains. This inhibitory effect was further enhanced by the combined incorporation of both compounds. On the other hand, the materials showed practically no toxicity towards *C. elegans* and a moderated toxic effect towards zebrafish, but some of the concentrations used show toxicity towards the MRC5 lung fibroblast cell line. It is important to emphasize that only the tests for antimicrobial activity were performed with the materials in direct contact with the microorganisms, while the toxicity tests were performed using different concentrations of extracts prepared from the materials, as described in section 3.3.6. Therefore, comparison between the antimicrobial results and the toxicity results would be inaccurate. In the future, when these materials are further developed to fulfil a more specific application, it is necessary to adapt the methods accordingly, and use the same method for both the antimicrobial and the toxicology evaluations, which should be chosen according to the type of application that would be intended for the material and whether or not it would be in direct contact with the microorganisms and/or the user. However, in practical terms and due to the technical conditions in which the experiments are performed (such as concentration of the organisms and the volumes required to work with them), it would be easier to implement the use of extracts for antimicrobial evaluation, than to implement direct contact evaluation for the toxicological evaluation. Additionally, the extracts concentration can be adjusted according to the volumes required for each individual test.

One interesting aspect to point out is the reduced toxicity when curcumin and TSNP were combined, compared to the samples containing these compounds individually. This effect was more clearly observed in the tests with the MRC5 fibroblasts (the material with 10% curcumin and TSNP showed no significant toxicity) and with zebrafish (both materials with curcumin and TSNP had no significant toxic effect). There are a few hypotheses that could explain this; 1) an interaction that might be occurring between the TSNP and as the concentration of curcumin is increased, this limits the release of both of them from the materials during the preparation of the extracts. 2) The antioxidant effect of curcumin could be reducing the oxidation rate of the TSNP, therefore reducing the amount of Ag<sup>+</sup> ions released and preventing the generation of toxic ROS. It is also important to highlight that whatever the mechanism is that is cancelling both compounds it was only observed after the preparation of extracts, and it was not noticeable when the materials were in direct contact for the antimicrobial activity test.

Therefore, it would be relevant to expand the studies with contact and no-contact evaluation, to make the effects more comparable across the different organisms. But further tests would also be required to fully determine the mechanisms involved in both the antimicrobial activity and the toxicity effects that are observed upon combined integration of curcumin with TSNP.

If the mechanical properties are improved in future work, the developed BC materials have the potential to be used in the medical or food packaging sectors, thanks to its antimicrobial properties and the low toxicity exhibited. The requirements that a material needs to meet in order to be suitable for medical applications can be very specific according to regulations and standards regarding any particular application. However, in general terms, the material requires to comply with health and safety principles, suitability for its purpose, long-term safety, and transport and storage stability. Furthermore, the material should allow for the fabrication of a device that is compatible with biological tissues, has a reduced risk of infection and microbial contamination, and with an extensive risk assessment (Altayyar 2020). Similarly, regulation for packaging materials that are intended for food contact (Regulation (EC) No 1935/2004), indicates that they are required to be manufactured under good quality practices, ensuring that under normal conditions of use the materials will not transfer their constituents to food in amounts which could: Endanger human health, bring unacceptable changes in food composition or deteriorate the organoleptic characteristics of the product (European Parliament 2004).

### **7.3 Fabrication of BC Blends and incorporation of Curcumin and TSNP**

BC blends were fabricated with PLA, PCL and PHB, followed by incorporation of curcumin and TSNP, as described in section 3.3.7. Resulting films are displayed in Figure 72. As it can be observed, the incorporation of curcumin resulted in the films showing a yellow colour, and incorporation of TSNP resulted in the films turning to blue colour, even for the specimens that already contained curcumin.

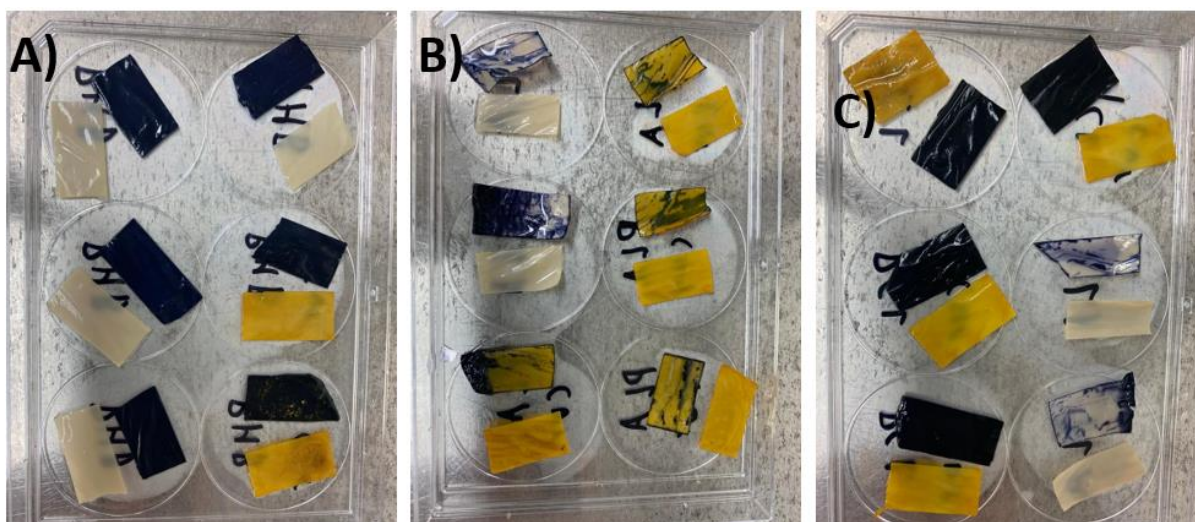


Figure 72. BC-blends without curcumin (white films), with curcumin (yellow films) and with incorporated TSNP (Blue films) made with A) PHB, B) PLA and C) PCL.

### 7.3.1 Antibacterial Evaluation of BC Blends

The antimicrobial evaluation of the prepared BC blends was performed as described in section 3.3.6.1, and the results for PCL, PLA and PHB blends incorporated with curcumin and TSNP can be observed in Figure 73. As it can be observed, the PCL and PLA blends showed no significant antimicrobial activity, even with the incorporation of curcumin and TSNP. Contrary to the results exhibited by the PLA and PCL blends, the blend made with PHB showed significant antimicrobial activity against both *E. coli* and *S. aureus* strains after the incorporation of curcumin and TSNP.

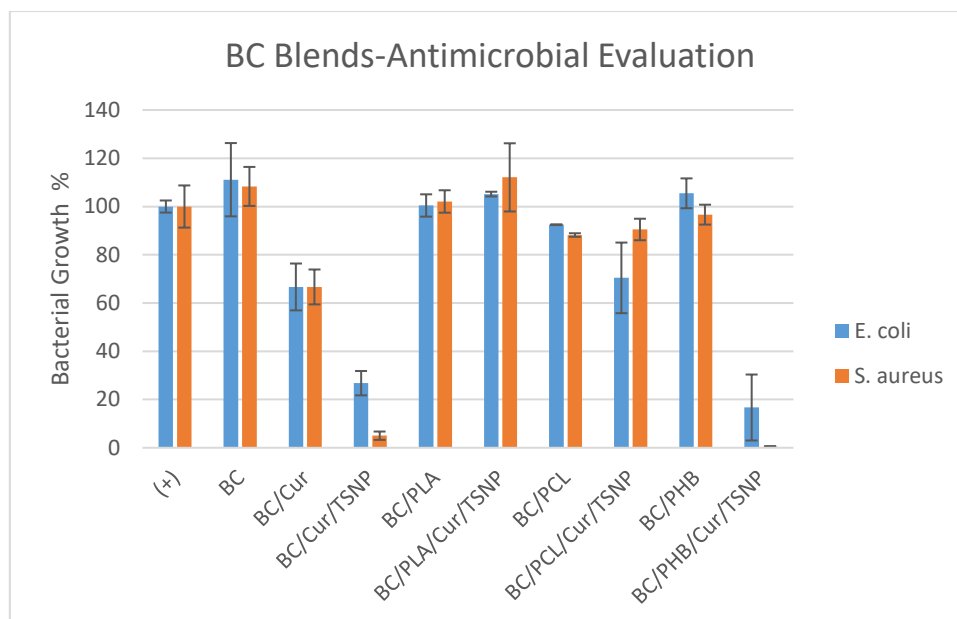


Figure 73. Results of Antimicrobial evaluations for blends of BC with PLA, PCL and PHB, incorporated with Curcumin and TSNP, as well as bare materials used as control.

## 7.4 Summary

In this chapter, the improvement of antimicrobial properties of BC through culture supplementation of curcumin and post-culture incorporation of TSNP was explored. The supplementation of curcumin resulted in an increase of produced dry weight of BC, up to 2 times in the film containing 10% curcumin. Adhesion of curcumin and TSNP on the surface of the BC films was confirmed through SEM-EDS. The treatment showed no significant changes on the thermal degradation profile of the films, evaluated by TGA. FTIR analysis allowed to identify the changes on functional groups upon the treatment of the films. Weathering tests revealed some colour changes and increase of brittleness after exposition to UV, which should be addressed in future research. The addition of curcumin and TSNP demonstrated on their own to increase the antimicrobial activity of the BC films, and even more so when they were combined, especially against the Gram-positive strain, *S. aureus*. *In-vitro* and *in-vivo* toxicological evaluations demonstrated a low toxicity of the materials, especially for the materials containing the combination of both added compounds. Fabrication of treated BC films through this method resulted in a successful increase of bacterial inhibition activity while at the same time maintaining an acceptable biosafety in the materials, which would allow to research the use of this method in potential applications of the biomedical and food packing sectors.

## CHAPTER 8 – CONCLUSION

In this research, the synthesis, optimisation, scale-up, formulation and integration of TSNP within different polymers and biopolymers was explored. The characterisation of the best performing films and the evaluation of their antimicrobial activity is reported. Additionally, incorporation of curcumin to further improve the antimicrobial action of TSNP in the best performing materials was examined. The characterisation and biological evaluation of these materials with combined antimicrobial activity was also reported. More specifically:

- TSNP were successfully synthesised through a previously reported seed-mediated chemical method. Optimisation of this method was performed to increase the resulting concentration of TSNP in the final solution (up to 28.4%), and the produced volume was scaled-up. The LSPR sensitivity of the TSNP was demonstrated through a sucrose test and a fibronectin monitoring assay. Thermal induced evaporation was demonstrated to be a suitable method for further increasing in the concentration of the TSNP solution (up to 400%), showing no significant damage to the structure of TSNP upon examination through UV-Vis spectra readings. Additionally, the use of this method represents an alternative to the use of a centrifuge, which is not a suitable method when high volumes are required. Furthermore, transfer of TSNP from an aqueous phase to an organic phase was confirmed as a suitable approach to facilitate their combination with hydrophobic polymers.
- Susceptibility of the TSNP to oxidation is reported to increase the antimicrobial effect of TSNP; however, it also represented a challenge, as the NPs would rapidly lose triangular shape or reduce in size under certain conditions, making processing for polymer integration a complex task. Special conditions are required to avoid the TSNP from making direct contact with air when they are not in solution, as they oxidize immediately. Solvent casting and the *ex situ* addition of solvent solution to the polymer surface proved to be effective approaches to integrate the TSNP within polymers while avoiding their sudden oxidation. This was achieved using a solvent casting method for PC, PCL and PLA, and an *ex situ* incorporation method for PCL, PLA and BC. PCL and PLA exhibited the best performance for the resulting solvent casted films while BC exhibited the best overall performance.

- The solvent casted PCL and PLA films were characterised for morphological, thermal and mechanical properties. SEM analysis showed limited (or a degree of) aggregation of the TSNP in the matrix of both polymers. Some of the mechanical properties were also affected, as PCL-TSNP showed a significant reduction in its elongation % at break (up to 66%). On the other hand, PLA showed a significant increase in the elastic modulus after incorporation of TSNP (25%). In terms of the thermal properties of the films, significant changes were not observed as a result of the TSNP incorporation. Antimicrobial evaluation demonstrated that the integration of the TSNP using this method provides the films with inhibitory activity against *E. coli* and *S. aureus* strains growth. Further research is required in order to further improve the antimicrobial activity, as well as improve the distribution of nanoplates in the films, preventing aggregation and improving the mechanical properties of the films.
- Given the notable results obtained for antimicrobial activity of TSNP-incorporated BC, an additional antimicrobial agent was included to further improve these antimicrobial properties through an additive effect. Curcumin was incorporated during the culture step in the production of BC. The supplementation of curcumin resulted in an increased yield for the dry mass of produced BC. The presence of curcumin and TSNP in the matrix of BC films was confirmed through SEM-EDS. TGA evaluation showed no significant changes in the thermal degradation profile of treated BC films. The functional groups of curcumin and TSNP were identified in the BC-TSNP-Cur films through FTIR. The films demonstrated high antimicrobial activity, especially for the films that included the combination of curcumin and TSNP. The highest activity of these films was observed against the Gram-positive strain *S. aureus* (95% growth inhibition). In an apparently antagonistic interaction, BC films with 10% curcumin and incorporated TSNP have shown reduced toxicity with 80% cells survival rate in toxicity *in vitro* assay. Achievement of this feature is important considering the fact that material can be characterised as biocompatible once cells viability is over 70%, and therefore this formulation has the potential to be considered for further research into more specific biomedical applications. However, this is just the initial evaluation after developing these materials for the first time. A more detailed study for toxicity and biocompatibility would be necessary if the materials are further developed for specific applications. This study suggests that curcumin and TSNP incorporated in bacterial

cellulose together does not show high toxicity on *C. elegans* and zebrafish development in examined conditions.

- The additive effect of these natural compounds leading to improved biological activity of the BC films obtained in this study will be further addressed in the future. Given this, further research to improve additional properties of the produced BC films, such as mechanical properties, has the potential to enable the suitability of these materials for biomedical and food packaging applications.

In summary, the antimicrobial efficacy of TSNP-integrated polymers and biopolymers was demonstrated. Additionally, the combined system of TSNP-Curcumin exhibited an even higher efficacy after integration into a BC matrix, while maintaining a low toxicity. Further research is required to explore the mechanism of curcumin-TSNP action and to fine-tune the mechanical properties of these materials, in order to increase the range of potential applications.

More specifically, future research should cover the following points:

- Improvement of the mechanical properties of BC in order to turn it into a suitable material to be used in medical and/or food packaging applications. This could be achieved through blending of BC with other biopolymers and/or plasticizers.
- Reduce the costs involved in the production of BC, particularly related to the high amount of glucose required. This could be achieved by testing additives that could boost the produced yield of BC, in a similar way to how curcumin did it, allowing to reduce the amount of glucose required during the production stage.
- Further tests on the antimicrobial activity and toxicity of the curcumin-TSNP combined system, to get deeper insight on the mechanism and the factors that influence the observed activity.

## **CHAPTER 9 – COMPLETED TRAINING AND WORK DISSEMINATION**

### **9.1 Completed Training**

- Health & Safety Induction for laboratory work (October 2018).
- Research Integrity Module – Engineering and Technology (11 April 2019). \*Certificate available in Appendix 10
- Course on Medical Polymers and Processing Technology, provided by First Polymer Training Skillnet (17 October 2019). \*Certificate available in Appendix 11
- Represented AIT on meeting with partners to discuss Interreg application of Curcol Project. Interreg application was successful, and the meeting took place at Avans University of Applied Sciences in Breda, Netherlands (Dec 2019).
- Postgraduate Pathways Module (July 2020)
- Research Integrity Module (August 2020)

### **Technical and Instrumentation Training**

- Spectrophotometry
- Microbiology techniques
- Dynamic Mechanical Analysis (DMA)
- Tensometer
- Fourier-Transform Infrared Spectroscopy (FTIR)
- Extruder



## 9.2 Work Dissemination

- **Garcia EL**, Mojicevic M, Milivojevic D, Aleksic I, Vojnovic S, Stevanovic M, Murray J, Attallah OA, Devine D, Fournet MB. Enhanced Antimicrobial Activity of Biocompatible Bacterial Cellulose Films via Dual Synergistic Action of Curcumin and Triangular Silver Nanoplates. *International Journal of Molecular Sciences*. 2022; 23(20):12198. <https://doi.org/10.3390/ijms232012198> \*Available in Appendix 16
- Buckley, J., Adams, L., Aribilola, I., Arshad, I., Azeem, M., Bracken, L., Breheny, C., Buckley, C., Chimello, I., Fagan, A., Fitzpatrick, D. P., Garza Herrera, D., Gomes, G. D., Grassick, S., Halligan, E., Hirway, A., Hyland, T., Imtiaz, M. B., Khan, M. B., **Lanzagorta Garcia, E.**, ... Zhang, L. (2021). An assessment of the transparency of contemporary technology education research employing interview-based methodologies. *International Journal of Technology and Design Education*, 0123456789. <https://doi.org/10.1007/s10798-021-09695-1>
- Attallah, O. A., Mojicevic, M., **Garcia, E. L.**, Azeem, M., Chen, Y., Asmawi, S., & Fournet, M. B. (2021). Macro and Micro Routes to High Performance Bioplastics : Properties. <https://doi.org/10.3390/polym13132155> \*Available in Appendix 15
- **Garcia, E. L.**, Attallah, O. A., Mojicevic, M., Devine, D. M., & Fournet, M. B. (2021). Antimicrobial active bioplastics using triangular silver nanoplate integrated polycaprolactone and polylactic acid films. *Materials*, 14(5), 1–15. <https://doi.org/10.3390/ma14051132> \*Available in Appendix 14
- Venkatesh, C., Laurenti, M., Bandeira, M., **Lanzagorta, E.**, Lucherini, L., Cauda, V., & Devine, D. M. (2020). Biodegradation and antimicrobial properties of zinc oxide–polymer composite materials for urinary stent applications. *Coatings*, 10(10), 1–22. <https://doi.org/10.3390/coatings10101002> \*Available in Appendix 13
- Rodriguez Barroso, L., **Lanzagorta Garcia, E.**, Azaman, F. A., Devine, D. M., Lynch, M., Huerta, M., & Fournet, M. B. (2020). Monitoring of extracellular matrix protein conformations in the presence of biomimetic bone tissue regeneration scaffolds. *Key Engineering Materials*, 865 KEM, 43–47. <https://doi.org/10.4028/www.scientific.net/KEM.865.43> \*Available in Appendix 12

## 9.5 Conferences and Presentations

- Poster presentation at AIT Research Seminar (April 2019). \*Available in Appendix 1
- Speaker at Bioengineering in Ireland (BiNI) 2020, abstract titled “Sustainable Antimicrobial Polymeric Biomedical Film Engineering Using Ag<sup>+</sup> Nanoreservoir Formulations”. \*Abstract available in Appendix 2
- Poster presentation at AIT Research Seminar (June 2020). \*Available in Appendix 3
- Poster presented for BioICEP Poster Event, October 2020, titled “Sustainable Antimicrobial Polymeric Food Packing and Anti-Infection Medical Plastics Preparation Using Antimicrobial Peptide and Ag<sup>+</sup> Nanoreservoir Formulations”. \*Poster available in Appendix 4
- Speaker at FEMS 2020 Online Conference on Microbiology, abstract titled “Sustainable Antimicrobial Biopolymeric Food & Biomedical Film Engineering Using Bioactive AMP-Ag<sup>+</sup> Formulations”. \*Abstract available in Appendix 5
- Poster presenter at EFB Virtual Conference 2021, abstract titled “Enhancement of Bacterial Cellulose Antimicrobial Performance via Curcumin Supplementation and Silver Nanoparticle Incorporation”. \*Poster available in Appendix 6
- Poster presenter at FEMS Conference on Microbiology 2022, in Belgrade, Serbia. Abstract titled “Preparation and Antimicrobial Evaluation of Bacterial Cellulose/Poly(3-Hydroxybutyrate) Blends Activated with Curcumin for Biomedical and Food Packing Purposes”. \*Poster available in Appendix 7

## REFERENCES

- Abbas, Mudassar, Nida Naeem, Hina Iftikhar, and Usman Latif. 2018. "Synthesis, Characterization and Antimicrobial Properties of Silver Nanocomposites." *IntechOpen* i(tourism):13. doi: <http://dx.doi.org/10.5772/57353>.
- Abbaszadegan, Abbas, Yasamin Ghahramani, Ahmad Gholami, Bahram Hemmateenejad, Samira Dorostkar, Mohammadreza Nabavizadeh, and Hashem Sharghi. 2015. "The Effect of Charge at the Surface of Silver Nanoparticles on Antimicrobial Activity against Gram-Positive and Gram-Negative Bacteria: A Preliminary Study." *Journal of Nanomaterials*. doi: <http://dx.doi.org/10.1155/2015/720654>.
- Abdelaziz, Dina, Amr Hefnawy, Essam Al-Wakeel, Abeer El-Fallal, and Ibrahim M. El-Sherbiny. 2020. "New Biodegradable Nanoparticles-in-Nanofibers Based Membranes for Guided Periodontal Tissue and Bone Regeneration with Enhanced Antibacterial Activity." *Journal of Advanced Research* (xxxx). doi: 10.1016/j.jare.2020.06.014.
- Abou El-Nour, Kholoud M. M., Ala'a Eftaiha, Abdulrhman Al-Warthan, and Reda A. A. Ammar. 2010. "Synthesis and Applications of Silver Nanoparticles." *Arabian Journal of Chemistry* 3(3):135–40. doi: 10.1016/j.arabjc.2010.04.008.
- Ackerman, George L. 1990. "Chapter 194 Serum Sodium." in *Clinical Methods: The History, Physical, and Laboratory Examinations*. 3rd edition.
- Adamczak, Artur, Marcin Ożarowski, and Tomasz M. Karpiński. 2020. "Curcumin, a Natural Antimicrobial Agent with Strain-Specific Activity." *Pharmaceuticals* 13(7):1–12. doi: 10.3390/ph13070153.
- Adedeji, W. A. 2016. "The Treasure Called Antibiotics." *Annals of Ibadan Postgraduate Medicine* 14(2):56–57.
- Aherne, Damian, Denise E. Charles, Margaret E. Brennan-Fournet, John M. Kelly, and Yurii K. Gun'ko. 2009. "Etching-Resistant Silver Nanoprisms by Epitaxial Deposition of a Protecting Layer of Gold at the Edges." *Langmuir* 25(17):10165–73. doi: 10.1021/la9009493.
- Aherne, Damian, Deirdre M. Ledwith, Matthew Gara, and John M. Kelly. 2008. "Optical Properties and Growth Aspects of Silver Nanoprisms Produced by a Highly Reproducible and Rapid Synthesis at Room Temperature." *Advanced Functional Materials* 18(14):2005–16. doi: 10.1002/adfm.200800233.
- Ahi, Zehra Betul, Nergis Zeynep Renkler, Mine Gul Seker, and Kadriye Tuzlakoglu. 2019. "Biodegradable Polymer Films with a Natural Antibacterial Extract as Novel Periodontal Barrier Membranes." *International Journal of Biomaterials* 2019. doi: 10.1155/2019/7932470.
- Ahmad, Jabran, Xianghua Wen, Fengjuan Li, and Bo Wang. 2019. "Novel Triangular Silver Nanoparticle Modified Membranes for Enhanced Antifouling Performance." *RSC Advances* 9(12):6733–44. doi: 10.1039/c8ra10540e.
- Akrami-Hasan-Kohal, Mohammad, Lobat Tayebi, and Marjan Ghorbani. 2020. "Curcumin-Loaded Naturally-Based Nanofibers as Active Wound Dressing Mats: Morphology, Drug Release, Cell Proliferation, and Cell Adhesion Studies." *New Journal of Chemistry* 44(25):10343–51. doi: 10.1039/d0nj01594f.
- Akter, Mahmuda, Md Tajuddin Sikder, Md Mostafizur Rahman, A. K. M. Atiqu. Ullah, Kaniz Fatima Binte Hossain, Subrata Banik, Toshiyuki Hosokawa, Takeshi Saito, and Masaaki Kurasaki. 2018. "A Systematic Review on Silver Nanoparticles-Induced Cytotoxicity: Physicochemical Properties and Perspectives." *Journal of Advanced Research* 9:1–16. doi: 10.1016/j.jare.2017.10.008.
- Ali, Nadia Abbas, Farah Tariq, and Mohammed Noori. 2014. "Crystallinity, Mechanical, and Antimicrobial

Properties of Polylactic Acid / Microcrystalline Cellulose / Silver Nanocomposites.” *International Journal of Application or Innovation in Engineering & Management* 3(1):77–81.

- Alibolandi, Mona, Marzieh Mohammadi, Seyed Mohammad Taghdisi, Khalil Abnous, and Mohammad Ramezani. 2017. “Synthesis and Preparation of Biodegradable Hybrid Dextran Hydrogel Incorporated with Biodegradable Curcumin Nanomicelles for Full Thickness Wound Healing.” *International Journal of Pharmaceutics* 532(1):466–77. doi: 10.1016/j.ijpharm.2017.09.042.
- Altayyar, Saleh S. 2020. “The Essential Principles of Safety and Effectiveness for Medical Devices and the Role of Standards.” *Medical Devices: Evidence and Research* 13:49–55. doi: 10.2147/MDER.S235467.
- Alven, Sibusiso, Xhamla Nqoro, and Blessing Aderibigbe. 2020. “Polymer-Based Materials Loaded with Curcumin For.” *Polymers* 12(10):2286.
- Alves, Thais Francine, Marco V. Chaud, Denise Grotto, Angela Faustino Jozala, Raksha Pandit, Mahendra Rai, and Carolina Alves dos Santos. 2018. “Association of Silver Nanoparticles and Curcumin Solid Dispersion: Antimicrobial and Antioxidant Properties.” *AAPS PharmSciTech* 19(1):225–31. doi: 10.1208/s12249-017-0832-z.
- An, Jing, Bin Tang, Xianliang Zheng, Ji Zhou, Fengxia Dong, Shuping Xu, Ye Wang, Bing Zhao, and Weiqing Xu. 2008. “Sculpturing Effect of Chloride Ions in Shape Transformation from Triangular to Discal Silver Nanoplates.” *Journal of Physical Chemistry C* 112(39):15176–82. doi: 10.1021/jp802694p.
- Andreani, Tatiana, Verónica Nogueira, Vera V. Pinto, Maria José Ferreira, Maria Graça Rasteiro, Amélia M. Silva, Ruth Pereira, and Carlos M. Pereira. 2017. “Influence of the Stabilizers on the Toxicity of Metallic Nanomaterials in Aquatic Organisms and Human Cell Lines.” *Science of the Total Environment* 607–608:1264–77. doi: 10.1016/j.scitotenv.2017.07.098.
- Anees Ahmad, Syed, Sabya Sachi Das, Ayesha Khatoon, Mohammed Tahir Ansari, Mohd Afzal, Md Saquib Hasnain, and Amit Kumar Nayak. 2020. “Bactericidal Activity of Silver Nanoparticles: A Mechanistic Review.” *Materials Science for Energy Technologies* 3:756–69. doi: 10.1016/j.mset.2020.09.002.
- Anguluri, Kavitha, Salvatore La China, Marcello Brugnoli, Stefano Cassanelli, and Maria Gullo. 2022. “Better under Stress: Improving Bacterial Cellulose Production by *Komagataeibacter Xylinus* K2G30 (UMCC 2756) Using Adaptive Laboratory Evolution.” *Frontiers in Microbiology* 13(October):1–13. doi: 10.3389/fmicb.2022.994097.
- Anjum, Sadiya, Amlan Gupta, Deepika Sharma, Deepti Gautam, Surya Bhan, Anupama Sharma, Arti Kapil, and Bhuvanesh Gupta. 2016. “Development of Novel Wound Care Systems Based on Nanosilver Nanohydrogels of Polymethacrylic Acid with Aloe Vera and Curcumin.” *Materials Science and Engineering C* 64:157–66. doi: 10.1016/j.msec.2016.03.069.
- Arrebola, Eva, Víctor J. Carrión, José Antonio Gutiérrez-Barranquero, Alejandro Pérez-García, Pablo Rodríguez-Palenzuela, Francisco M. Cazorla, and Antonio de Vicente. 2015. “Cellulose Production in *Pseudomonas Syringae* Pv. *Syringae*: A Compromise between Epiphytic and Pathogenic Lifestyles.” *FEMS Microbiology Ecology* 91(7):1–12. doi: 10.1093/femsec/fiv071.
- Asharani, P. V., Yi Lian Wu, Zhiyuan Gong, and Suresh Valiyaveetil. 2008. “Toxicity of Silver Nanoparticles in Zebrafish Models.” *Nanotechnology* 19(25). doi: 10.1088/0957-4484/19/25/255102.
- Aswini, K., N. O. Gopal, and Sivakumar Uthandi. 2020. “Optimized Culture Conditions for Bacterial Cellulose Production by *Acetobacter Senegalensis* MA1.” *BMC Biotechnology* 20(1):1–16. doi: 10.1186/s12896-020-00639-6.
- Audoit, Jérémie, Lydia Laffont-dantras, Antoine Lonjon, Eric Dantras, Jérémie Audoit, Lydia Laffont-dantras, Antoine Lonjon, Eric Dantras, and Colette Lacabanne Percolative. 2016. “Percolative Silver Nanoplates / PVDF Nanocomposites : Bulk and Surface Electrical Conduction.” 78:104–10.

- Augustine, Robin, Nandakumar Kalarikkal, and Sabu Thomas. 2016. "Electrospun PCL Membranes Incorporated with Biosynthesized Silver Nanoparticles as Antibacterial Wound Dressings." *Applied Nanoscience (Switzerland)* 6(3):337–44. doi: 10.1007/s13204-015-0439-1.
- Auras, Rafael, Bruce Harte, and Susan Selke. 2004. "An Overview of Polylactides as Packaging Materials." *Macromolecular Bioscience* 4(9):835–64.
- Bagewadi, Zabin K., Jayateerth S. Bhavikatti, Uday M. Muddapur, Deepak A. Yaraguppi, and Sikandar I. Mulla. 2020. "Statistical Optimization and Characterization of Bacterial Cellulose Produced by Isolated Thermophilic *Bacillus Licheniformis* Strain ZBT2." *Carbohydrate Research* 491(February):107979. doi: 10.1016/j.carres.2020.107979.
- Ballesteros, Camilo A. S., Daniel S. Correa, and Valtencir Zucolotto. 2020. "Polycaprolactone Nanofiber Mats Decorated with Photoresponsive Nanogels and Silver Nanoparticles: Slow Release for Antibacterial Control." *Materials Science and Engineering C* 107(September 2019):110334. doi: 10.1016/j.msec.2019.110334.
- Baptista, Pedro V., Matthew P. McCusker, Andreia Carvalho, Daniela A. Ferreira, Niamh M. Mohan, Marta Martins, and Alexandra R. Fernandes. 2018. "Nano-Strategies to Fight Multidrug Resistant Bacteria-"A Battle of the Titans"." *Frontiers in Microbiology* 9(JUL):1–26. doi: 10.3389/fmicb.2018.01441.
- Bashkatov, Alexey N., and Elina A. Genina. 2003. "Water Refractive Index in Dependence on Temperature and Wavelength: A Simple Approximation." Pp. 393–95 in *Proceedings of SPIE - The International Society for Optical Engineering*.
- Beer, Christiane, Rasmus Foldbjerg, Yuya Hayashi, Duncan S. Sutherland, and Herman Autrup. 2012. "Toxicity of Silver Nanoparticles-Nanoparticle or Silver Ion?" *Toxicology Letters* 208(3):286–92. doi: 10.1016/j.toxlet.2011.11.002.
- Belete, Tafere Mulaw. 2019. "Novel Targets to Develop New Antibacterial Agents and Novel Alternatives to Antibacterial Agents." *Human Microbiome Journal* 11(January):100052. doi: 10.1016/j.humic.2019.01.001.
- Benakashani, F., A. R. Allafchian, and S. A. H. Jalali. 2016. "Biosynthesis of Silver Nanoparticles Using Capparis Spinosa L. Leaf Extract and Their Antibacterial Activity." *Karbala International Journal of Modern Science* 2(4):251–58. doi: 10.1016/j.kijoms.2016.08.004.
- Benhacine, Fayçal, Assia siham Hadj-Hamou, and Abderrahmane Habi. 2016. "Development of Long-Term Antimicrobial Poly ( $\epsilon$ -Caprolactone)/Silver Exchanged Montmorillonite Nanocomposite Films with Silver Ion Release Property for Active Packaging Use." *Polymer Bulletin* 73(5):1207–27. doi: 10.1007/s00289-015-1543-9.
- Bernatová, Silvie, Ota Samek, Zdenek Pilát, Mojmír Šerý, Jan Ježek, Petr Ják, Martin Šiler, Vladislav Krzyžánek, Pavel Zemánek, Veronika Holá, Milada Dvoráková, and Filip Ružicka. 2013. "Following the Mechanisms of Bacteriostatic versus Bactericidal Action Using Raman Spectroscopy." *Molecules* 18(11):13188–99. doi: 10.3390/molecules181113188.
- Berry, Matthew. 2023. "UV-Vis Spectroscopy for Characterising the Optical Properties of Gold Nanoparticles." *Edinburgh Instruments*. Retrieved (<https://www.edinst.com/uv-vis-spectroscopy-for-characterising-the-optical-properties-of-gold-nanoparticles/>).
- Binkley, Dakota M., Bryan E. J. Lee, Sokunthearath Saem, Jose Moran-Mirabal, and Kathryn Grandfield. 2019. "Fabrication of Polycaprolactone Electrospun Nanofibers Doped with Silver Nanoparticles Formed by Air Plasma Treatment." *Nanotechnology* 30(21):215101. doi: 10.1088/1361-6528/ab0444.
- Bodea, Ioana M., Giorgiana M. Cătunescu, Carmen R. Pop, Nicodim I. Fiț, Adriana P. David, Mircea C. Dudescu, Andreea Stănilă, Anuța M. Rotar, and Florin I. Beteg. 2022. "Antimicrobial Properties of Bacterial

Cellulose Films Enriched with Bioactive Herbal Extracts Obtained by Microwave-Assisted Extraction.” *Polymers* 14(7). doi: 10.3390/polym14071435.

- Brackman, Gilles, Paul Cos, Louis Maes, Hans J. Nelis, and Tom Coenye. 2011. “Quorum Sensing Inhibitors Increase the Susceptibility of Bacterial Biofilms to Antibiotics in Vitro and in Vivo.” *Antimicrobial Agents and Chemotherapy* 55(6):2655–61.
- Brennan-Fournet, Margaret E., Miriam Huerta, Yi Zhang, George Malliaras, and Roisin M. Owens. 2015. “Detection of Fibronectin Conformational Changes in the Extracellular Matrix of Live Cells Using Plasmonic Nanoplates.” *Journal of Materials Chemistry B* 3(47):9140–47. doi: 10.1039/c5tb02060c.
- Bruinsma, N., J. M. Hutchinson, A. E. van den Bogaard, H. Giamarellou, J. Degener, and E. E. Stobberingh. 2003. “Influence of Population Density on Antibiotic Resistance.” *Journal of Antimicrobial Chemotherapy* 51(2):385–90. doi: 10.1093/jac/dkg072.
- Bush, Karen. 2017. “Synergistic Antibiotic Combinations.” *Topic in Medicinal Chemistry* 25:169–244. doi: [https://doi.org/10.1007/7355\\_2017\\_23](https://doi.org/10.1007/7355_2017_23).
- Cai, Tuanjie, Yan Gao, Jilin Yan, Ying Wu, and Junwei Di. 2017. “Visual Detection of Glucose Using Triangular Silver Nanoplates and Gold Nanoparticles.” *RSC Advances* 7(46):29122–28. doi: 10.1039/c7ra00593h.
- Cannon, Robert E., and Steven M. Anderson. 1991. “Biogenesis of Bacterial Cellulose.” *Critical Reviews in Microbiology* 17(6):435–47. doi: 10.3109/10408419109115207.
- Carlson, C., S. M. Hussein, A. M. Schrand, L. K. Braydich-Stolle, K. L. Hess, R. L. Jones, and J. J. Schlager. 2008. “Unique Cellular Interaction of Silver Nanoparticles: Size-Dependent Generation of Reactive Oxygen Species.” *Journal of Physical Chemistry B* 112(43):13608–19. doi: 10.1021/jp712087m.
- Cerkez, Idris, Ayse Sezer, and Sukhwinder K. Bhullar. 2017. “Fabrication and Characterization of Electrospun Poly(e-Caprolactone) Fibrous Membrane with Antibacterial Functionality.” *Royal Society Open Science* 4(2). doi: 10.1098/rsos.160911.
- Chang, Chiao Yun, Hsiang Ting Lin, Ming Sheng Lai, Teng Yi Shieh, Chien Chung Peng, Min Hsiung Shih, and Yi Chung Tung. 2018. “Flexible Localized Surface Plasmon Resonance Sensor with Metal–Insulator–Metal Nanodisks on PDMS Substrate.” *Scientific Reports* 8(1):1–8. doi: 10.1038/s41598-018-30180-8.
- Charles, Denise E., Damian Aherne, Matthew Gara, Deirdre M. Ledwith, Yurii K. Gun, John M. Kelly, Werner J. Blau, and Margaret E. Brennan-fournet. 2010. “Versatile Solution Phase Triangular Silver Nanoplates for Highly Sensitive Plasmon Resonance Sensing.” *ACS Nano* 4(1):55–64.
- Chen, Xing, Li Qiang Zou, Jing Niu, Wei Liu, Sheng Feng Peng, and Cheng Mei Liu. 2015. “The Stability, Sustained Release and Cellular Antioxidant Activity of Curcumin Nanoliposomes.” *Molecules* 20(8):14293–311. doi: 10.3390/molecules200814293.
- Chen, Yu Hung, and Chen Sheng Yeh. 2002. “Laser Ablation Method: Use of Surfactants to Form the Dispersed Ag Nanoparticles.” *Colloids and Surfaces A: Physicochemical and Engineering Aspects* 197(1–3):133–39. doi: 10.1016/S0927-7757(01)00854-8.
- Cheon, Ja Young, Su Jun Kim, Young Ha Rhee, Oh Hyeong Kwon, and Won Ho Park. 2019. “Shape-Dependent Antimicrobial Activities of Silver Nanoparticles.” *International Journal of Nanomedicine* 14:2773–80. doi: 10.2147/IJN.S196472.
- Chiaoprakobkij, Nadda, Thapanar Suwanmajo, and Neeracha Sanchavanakit. 2020. “Curcumin-Loaded Bacterial Cellulose / Alginate / Gelatin.” *Molecules* 25(3800):1–18. doi: 10.3390/molecules25173800.
- Chouhan, Neelu. 2018. “Silver Nanoparticles - Fabrication, Characterization and Applications.” *Intech*. doi: 10.5772/intechopen.71247.

- Chu, Zhuangzhuang, Tianrui Zhao, Lin Li, Jian Fan, and Yuyue Qin. 2017. "Characterization of Antimicrobial Poly (Lactic Acid)/Nano-Composite Films with Silver and Zinc Oxide Nanoparticles." *Materials* 10(6). doi: 10.3390/ma10060659.
- Chugh, Heerak, Damini Sood, Ishita Chandra, Vartika Tomar, Gagan Dhawan, and Ramesh Chandra. 2018. "Role of Gold and Silver Nanoparticles in Cancer Nano-Medicine." *Artificial Cells, Nanomedicine and Biotechnology* 46(sup1):1210–20. doi: 10.1080/21691401.2018.1449118.
- Cirillo, Giuseppe, Manuela Curcio, Umile Gianfranco Spizzirri, Orazio Vittorio, Paola Tucci, Nevio Picci, Francesca Iemma, Silke Hampel, and Fiore Pasquale Nicoletta. 2017. "Carbon Nanotubes Hybrid Hydrogels for Electrically Tunable Release of Curcumin." *European Polymer Journal* 90(March):1–12. doi: 10.1016/j.eurpolymj.2017.03.011.
- Clinical and Laboratory Standards Institute. 2012. "Methods for Antimicrobial Susceptibility Testing of Anaerobic Bacteria; Approved Standard-Eighth Edition." *CLSI Document M11-A8* 32(5):11–19.
- Comini, Sara, Sara Scutera, Rosaria Sparti, Giuliana Banche, Bartolomeo Coppola, Cinzia Margherita Berteau, Gabriele Bianco, Noemi Gatti, Anna Maria Cuffini, Paola Palmero, and Valeria Allizond. 2022. "Combination of Poly (  $\epsilon$ -Caprolactone ) Biomaterials and Essential Oils to Achieve Anti-Bacterial and Osteo-Proliferative Properties for 3D-Scaffolds in Regenerative Medicine." *Pharmaceutics*.
- Conly, J. M., and B. L. Johnston. 2005. "Where Are All the New Antibiotic." *Canadian Journal of Infectious Diseases and Medical Microbiology* 16(3):159–60.
- D'Agostino, Agnese, Angelo Taglietti, Roberto Desando, Marcella Bini, Maddalena Patrini, Giacomo Dacarro, Lucia Cucca, Piersandro Pallavicini, and Pietro Grisoli. 2017. "Bulk Surfaces Coated with Triangular Silver Nanoplates: Antibacterial Action Based on Silver Release and Photo-Thermal Effect." *Nanomaterials* 7(1). doi: 10.3390/nano7010007.
- Dakal, Tikam Chand, Anu Kumar, Rita S. Majumdar, and Vinod Yadav. 2016. "Mechanistic Basis of Antimicrobial Actions of Silver Nanoparticles." *Frontiers in Microbiology* 7(NOV):1–17. doi: 10.3389/fmicb.2016.01831.
- DeStefano, Vincent, Salaar Khan, and Alonzo Tabada. 2020. "Applications of PLA in Modern Medicine." *Engineered Regeneration* 1(April):76–87. doi: 10.1016/j.engreg.2020.08.002.
- Djafari, Jamila, Carlos Fernández-Lodeiro, Adrián Fernández-Lodeiro, Vanessa Silva, Patrícia Poeta, Gilberto Igrejas, Carlos Lodeiro, José Luis Capelo, and Javier Fernández-Lodeiro. 2019. "Exploring the Control in Antibacterial Activity of Silver Triangular Nanoplates by Surface Coating Modulation." *Frontiers in Chemistry* 7(FEB):1–11. doi: 10.3389/fchem.2018.00677.
- Doern, Christopher D. 2014. "When Does 2 plus 2 Equal 5? A Review of Antimicrobial Synergy Testing." *Journal of Clinical Microbiology* 52(12):4124–28. doi: 10.1128/JCM.01121-14.
- Van Dong, Pham, Chu Hoang Ha, Le Tran Binh, and Jörn Kasbohm. 2012. "Chemical Synthesis and Antibacterial Activity of Novel-Shaped Silver Nanoparticles." *International Nano Letters* 2(1):1–9. doi: 10.1186/2228-5326-2-9.
- Encyclopaedia Britannica. 2016. "Polypropylene | Properties, Definition, & Uses | Britannica." Retrieved September 17, 2020 (<https://www.britannica.com/science/polypropylene>).
- Espinoza, Sergio Miguel, Harshal Indrabhan Patil, Eduardo San Martin Martinez, Rocio Casañas Pimentel, and Pradum Pundlikrao Ige. 2020. "Poly- $\epsilon$ -Caprolactone (PCL), a Promising Polymer for Pharmaceutical and Biomedical Applications: Focus on Nanomedicine in Cancer." *International Journal of Polymeric Materials and Polymeric Biomaterials* 69(2):85–126. doi: 10.1080/00914037.2018.1539990.
- Etacheri, Vinodkumar, Reenamole Georgekutty, Michael K. Seery, and Suresh C. Pillai. 2010. "Single Step

- Morphology-Controlled Synthesis of Silver Nanoparticles.” *Materials Research Society Symposium Proceedings* 1217:7–13. doi: 10.1557/PROC-1217-YO8-40.
- European Commission. 2000. “Toxicological Data on Colouring Agents for Medicinal Products: E 174 Silver.” Retrieved ([https://ec.europa.eu/health/ph\\_risk/committees/scmp/documents/out30\\_en.pdf](https://ec.europa.eu/health/ph_risk/committees/scmp/documents/out30_en.pdf)).
- European Parliament. 2004. “Consolidated Text: Regulation (EC) No 1935/2004 of the European Parliament and of the Council of 27 October 2004 on Materials and Articles Intended to Come into Contact with Food and Repealing Directives 80/590/EEC and 89/109/EEC.” Retrieved (<https://eur-lex.europa.eu/legal-content/EN/TXT/?uri=CELEX%3A02004R1935-20210327&qid=1690214288466>).
- Fahrina, Afrillia, Nasrul Arahman, Sri Aprilia, Muhammad Roil Bilad, Silmina Silmina, Widia Puspita Sari, Indah Maulana Sari, Poernomo Gunawan, Mehmet Emin Pasaoglu, Vahid Vatanpour, Ismail Koyuncu, and Saeid Rajabzadeh. 2022. “Functionalization of PEG-AgNPs Hybrid Material to Alleviate Biofouling Tendency of Polyethersulfone Membrane.” *Polymers* 14(9):1–15. doi: 10.3390/polym14091908.
- Fang, Xian, Hongxuan Ren, Hong Zhao, and Zengxi Li. 2017. “Ultrasensitive Visual and Colorimetric Determination of Dopamine Based on the Prevention of Etching of Silver Nanoprisms by Chloride.” *Microchimica Acta* 184(2):415–21. doi: 10.1007/s00604-016-2024-z.
- Farah, Shady, Daniel G. Anderson, and Robert Langer. 2016. “Physical and Mechanical Properties of PLA, and Their Functions in Widespread Applications — A Comprehensive Review.” *Advanced Drug Delivery Reviews* 107:367–92.
- Flasche, Stefan, and Katherine E. Atkins. 2018. “Balancing Benefits and Risks of Antibiotic Use.” *Journal of Infectious Diseases* 218(9):1351–53. doi: 10.1093/infdis/jiy344.
- Fortune Business Insights. 2022. *The Global Curcumin Market Is Projected to Grow from \$79.94 Million in 2022 to \$155.24 Million by 2029, at a CAGR of 9.95% in Forecast Period, 2022-2029*.
- Freestone, Ian, Nigel Meeks, Margaret Sax, and Catherine Higgitt. 2007. “The Lycurgus Cup - A Roman Nanotechnology.” *Gold Bulletin* 40(4):270–77. doi: <https://doi.org/10.1007/BF03215599>.
- Furletov, A. A., V. V. Apyari, A. V. Garshev, S. G. Dmitrienko, and Yu A. Zolotov. 2017. “Triangular Silver Nanoplates as a Spectrophotometric Reagent for the Determination of Mercury(II).” *Journal of Analytical Chemistry* 72(12):1203–7. doi: 10.1134/S1061934817120061.
- Gangishetty, Mahesh K., Robert W. J. Scott, and Timothy L. Kelly. 2016. “Thermal Degradation Mechanism of Triangular Ag@SiO<sub>2</sub> Nanoparticles.” *Dalton Transactions* 45(24):9827–34. doi: 10.1039/c6dt00169f.
- Gao, Xiao Ping, Feng Feng, Xiao Qi Zhang, Xiao Xin Liu, Yu Bin Wang, Jin Xiong She, Zhi Heng He, and Ming Fang He. 2014. “Toxicity Assessment of 7 Anticancer Compounds in Zebrafish.” *International Journal of Toxicology* 33(2):98–105. doi: 10.1177/1091581814523142.
- Gawish, S. M., and S. Mosleh. 2020. “Antimicrobial Polypropylene Loaded by Silver Nano Particles.” *Fibers and Polymers* 21(1):19–23. doi: 10.1007/s12221-020-9519-2.
- Ghorbani, H. Reza, A. Akbar Safekordi, H. Attar, and S. M. Rezaya. Sorkhabadi. 2011. “Biological and Non-Biological Methods for Silver Nanoparticles Synthesis.” *Chemical and Biochemical Engineering Quarterly* 25(3):317–26.
- Ghosh, Sougata, Sumersing Patil, Mehul Ahire, Rohini Kitture, Sangeeta Kale, Karishma Pardesi, Swaranjit Cameotra, Jayesh Bellare, Dilip D. Dhavale, Amit Jabgunde, and Balu A. Chopade. 2012. “Synthesis of Silver Nanoparticles Using Dioscorea Bulbifera Tuber Extract and Evaluation of Its Synergistic Potential in Combination with Antimicrobial Agents.” *International Journal of Nanomedicine* 7:483–96.
- Gong, Chang Yang, Qin Jie Wu, Yu Jun Wang, Dou Dou Zhang, Feng Luo, Xia Zhao, Yu Quan Wei, and Zhi



- Yong Qian. 2013. "A Biodegradable Hydrogel System Containing Curcumin Encapsulated in Micelles for Cutaneous Wound Healing." *Biomaterials* 34(27):6377–87. doi: 10.1016/j.biomaterials.2013.05.005.
- González-Fandos, E., M. Giménez, C. Olarte, S. Sanz, and A. Simón. 2000. "Effect of Packaging Conditions on the Growth of Micro-Organisms and the Quality Characteristics of Fresh Mushrooms (*Agaricus Bisporus*) Stored at Inadequate Temperatures." *Journal of Applied Microbiology* 89(4):624–32. doi: 10.1046/j.1365-2672.2000.01159.x.
- Gorgieva, Selestina, and Janja Trček. 2019. "Bacterial Cellulose: Production, Modification and Perspectives in Biomedical Applications." *Nanomaterials* 9(10):1–20. doi: 10.3390/nano9101352.
- Gorrasi, Giuliana, Andrea Sorrentino, and Roberto Pantani. 2015. "Modulation of Biodegradation Rate of Poly(Lactic Acid) by Silver Nanoparticles." *Journal of Polymers and the Environment* 23(3):316–20. doi: 10.1007/s10924-015-0720-0.
- Greulich, Christina, Dieter Braun, Alexander Peetsch, Jörg Diendorf, Bettina Siebers, Matthias Epple, and Manfred Köller. 2012. "The Toxic Effect of Silver Ions and Silver Nanoparticles towards Bacteria and Human Cells Occurs in the Same Concentration Range." *RSC Advances* 2(17):6981–87. doi: 10.1039/c2ra20684f.
- Guarino, Vincenzo, Gennaro Gentile, Luigi Sorrentino, and Luigi Ambrosio. 2017. *Polycaprolactone: Synthesis, Properties, and Applications*.
- Gunasekaran, S., R. K. Natarajan, S. Natarajan, and R. Rathikha. 2008. "Structural Investigation on Curcumin." *Asian Journal of Chemistry* 20(4):2903–13.
- Guo, Chuanpan, Fang Cheng, Gaolei Liang, Shuai Zhang, Shuxia Duan, Yingkun Fu, Fabio Marchetti, Zhihong Zhang, and Miao Du. 2022. "Multimodal Antibacterial Platform Constructed by the Schottky Junction of Curcumin-Based Bio Metal – Organic Frameworks and Ti<sub>3</sub>C<sub>2</sub>T<sub>x</sub> MXene Nanosheets for Efficient Wound Healing." *2200064*:1–14. doi: 10.1002/anbr.202200064.
- Gupta, Abhishek, Sophie M. Briffa, Sam Swingler, Hazel Gibson, Vinodh Kannappan, Grazyna Adamus, Marek Kowalczyk, Claire Martin, and Iza Radecka. 2020. "Synthesis of Silver Nanoparticles Using Curcumin-Cyclodextrins Loaded into Bacterial Cellulose-Based Hydrogels for Wound Dressing Applications." *Biomacromolecules* 21(5):1802–11. doi: 10.1021/acs.biomac.9b01724.
- Ha, Ngoc Minh, Son Hung Tran, Yhong Hee Shim, and Kyungsu Kang. 2022. "Caenorhabditis Elegans as a Powerful Tool in Natural Product Bioactivity Research." *Applied Biological Chemistry* 65(1). doi: 10.1186/s13765-022-00685-y.
- Hackenberg, Stephan, Agmal Scherzed, Michael Kessler, Silke Hummel, Antje Technau, Katrin Froelich, Christian Ginzkey, Christian Koehler, Rudolf Hagen, and Norbert Kleinsasser. 2011. "Silver Nanoparticles: Evaluation of DNA Damage, Toxicity and Functional Impairment in Human Mesenchymal Stem Cells." *Toxicology Letters* 201(1):27–33. doi: 10.1016/j.toxlet.2010.12.001.
- Hadrup, Niels, Anoop K. Sharma, and Katrin Loeschner. 2018. "Toxicity of Silver Ions, Metallic Silver, and Silver Nanoparticle Materials after in Vivo Dermal and Mucosal Surface Exposure: A Review." *Regulatory Toxicology and Pharmacology* 98:257–67.
- Haes, Amanda J., and Richard P. Van Duyne. 2002. "A Nanoscale Optical Biosensor: Sensitivity and Selectivity of an Approach Based on the Localized Surface Plasmon Resonance Spectroscopy of Triangular Silver Nanoparticles." (7):10596–604. doi: 10.1021/JA020393X.
- Hatcher, H., R. Planalp, J. Cho, F. M. Torti, and S. V. Torti. 2008. "Curcumin: From Ancient Medicine to Current Clinical Trials." *Cellular and Molecular Life Sciences* 65(11):1631–52. doi: 10.1007/s00018-008-7452-4.
- Herrera, Natalia, Aji P. Mathew, and Kristiina Oksman. 2015. "Plasticized Poly(lactic Acid)/Cellulose

- Nanocomposites Prepared Using Melt-Extrusion and Liquid Feeding: Mechanical, Thermal and Optical Properties.” *Composites Science and Technology* 106:149–55. doi: 10.1016/j.compscitech.2014.11.012.
- Hewlings, Susan J., and Douglas S. Kalman. 2017. “Curcumin: A Review of Its Effects on Human Health.” *Foods* 6(10):1–11. doi: 10.3390/foods6100092.
- Huang, Biao, Mingxian Liu, and Changren Zhou. 2017. “Cellulose–Halloysite Nanotube Composite Hydrogels for Curcumin Delivery.” *Cellulose* 24(7):2861–75. doi: 10.1007/s10570-017-1316-8.
- Hungund, Basavaraj S., and S. G. Gupta. 2010. “Production of Bacterial Cellulose from *Enterobacter Amnigenus* GH-1 Isolated from Rotten Apple.” *World Journal of Microbiology and Biotechnology* 26(10):1823–28. doi: 10.1007/s11274-010-0363-1.
- Iravani, S., H. Korbekandi, S. V. Mirmohammadi, and B. Zolfaghari. 2014. “Synthesis of Silver Nanoparticles: Chemical, Physical and Biological Methods.” *Research in Pharmaceutical Sciences*.
- Ismail, E. H., D. Y. Sabry, H. Mahdy, and M. M. H. Khalil. 2014. “Synthesis and Characterization of Some Ternary Metal Complexes of Curcumin with 1,10-Phenanthroline and Their Anticancer Applications.” *Journal of Scientific Research* 6(3):509–19. doi: 10.3329/jsr.v6i3.18750.
- Jahanmardi, Yasaman, Mohammad A. Tavanaie, and Ali R. Tehrani-Bagha. 2021. “Curcumin Release from Blended Polycaprolactone/Poly(lactic Acid) Electrospun Nanofibrous Meshes.” *Journal of Industrial Textiles* 50(7):1065–78. doi: 10.1177/1528083719851845.
- Jaiswal, Swati, and Prashant Mishra. 2017. “Antimicrobial and Antibiofilm Activity of Curcumin-Silver Nanoparticles with Improved Stability and Selective Toxicity to Bacteria over Mammalian Cells.” *Medical Microbiology and Immunology* 207(1):39–53. doi: 10.1007/s00430-017-0525-y.
- Jana, Subhra, Anastasiya V. Kondakova, Svetlana N. Shevchenko, Eugene V. Sheval, Kirill A. Gonchar, Victor Yu Timoshenko, and Alexander N. Vasiliev. 2017. “Halloysite Nanotubes with Immobilized Silver Nanoparticles for Anti-Bacterial Application.” *Colloids and Surfaces B: Biointerfaces* 151:249–54. doi: 10.1016/j.colsurfb.2016.12.017.
- Jeevanandam, Jaison, Ahmed Barhoum, Yen S. Chan, Alain Dufresne, and Michael K. Danquah. 2018. “Review on Nanoparticles and Nanostructured Materials: History, Sources, Toxicity and Regulations.” *Beilstein Journal of Nanotechnology* 9(1):1050–74. doi: 10.3762/bjnano.9.98.
- Jin, R., Y. Cao, C. A. Mirkin, K. L. Kelly, G. C. Schatz, and J. G. Zheng. 2001. “Photoinduced Conversion of Silver Nanospheres to Nanoprisms.” *Science* 294(5548):1901–3. doi: 10.1126/science.1066541.
- Kamar, Samaa Samir, Dina Helmy Abdel-Kader, and Laila Ahmed Rashed. 2019. “Beneficial Effect of Curcumin Nanoparticles-Hydrogel on Excisional Skin Wound Healing in Type-I Diabetic Rat: Histological and Immunohistochemical Studies.” *Annals of Anatomy* 222:94–102. doi: 10.1016/j.aanat.2018.11.005.
- Kawata, Koji, Masato Osawa, and Satoshi Okabe. 2009. “In Vitro Toxicity of Silver Nanoparticles at Noncytotoxic Doses to HepG2 Human Hepatoma Cells.” *Environmental Science and Technology* 43(15):6046–51. doi: 10.1021/es900754q.
- Kędziora, Anna, Mateusz Speruda, Eva Krzyżewska, Jacek Rybka, Anna Łukowiak, and Gabriela Bugła-Płoskońska. 2018. “Similarities and Differences between Silver Ions and Silver in Nanoforms as Antibacterial Agents.” *International Journal of Molecular Sciences* 19(2). doi: 10.3390/ijms19020444.
- Kelly, J. M., G. Keegan, and M. E. Brennan-Fournet. 2012. “Triangular Silver Nanoparticles: Their Preparation, Functionalisation and Properties.” *Acta Physica Polonica A* 122(2):337–45. doi: 10.12693/APhysPolA.122.337.
- Kelly, K. Lance, Eduardo Coronado, Lin Lin Zhao, and George C. Schatz. 2003. “The Optical Properties of Metal

- Nanoparticles\_ The Influence of Size, Shape, and Dielectric Environment.” *Journal of Physical Chemistry B* 107:668–77.
- Khan, Hina, Ashish Kadam, and Dharm Dutt. 2020. “Studies on Bacterial Cellulose Produced by a Novel Strain of Lactobacillus Genus.” *Carbohydrate Polymers* 229(October 2019):115513. doi: 10.1016/j.carbpol.2019.115513.
- Khodashenas, Bahareh, and Hamid Reza Ghorbani. 2015. “Synthesis of Silver Nanoparticles with Different Shapes.” *Arabian Journal of Chemistry*. doi: 10.1016/j.arabjc.2014.12.014.
- Kim, Soo Hwan, Hyeong Seon Lee, Deok Seon Ryu, Soo Jae Choi, and Dong Seok Lee. 2011. “Antibacterial Activity of Silver-Nanoparticles against Staphylococcus Aureus and Escherichia Coli.” *Korean Journal of Microbiology and Biotechnology* 39(1):77–85.
- Kirkland, A. I., D. A. Jefferson, D. G. Duff, P. P. Edwards, and I. Gameson. 1993. “Structural Studies of Trigonal Lamellar Particles of Gold and Silver.” *Proceedings of the Royal Society of London. Series A: Mathematical and Physical Sciences* 440(1910):589–609. doi: 10.1098/rspa.1993.0035.
- Kittler, S., C. Greulich, J. Diendorf, M. Köller, and M. Epple. 2010. “Toxicity of Silver Nanoparticles Increases during Storage Because of Slow Dissolution under Release of Silver Ions.” *Chemistry of Materials* 22(16):4548–54. doi: 10.1021/cm100023p.
- Klaus, Tanja, Ralph Joerger, Eva Olsson, and Claes Göran Granqvist. 1999. “Silver-Based Crystalline Nanoparticles, Microbially Fabricated.” *Proceedings of the National Academy of Sciences of the United States of America* 96(24):13611–14. doi: 10.1073/pnas.96.24.13611.
- Knauer, Andrea, Andrea Csáki, Wolfgang Fritzsche, Christophe A. Serra, Nicolas Leclerc, and J. Michael Köhler. 2013. “Micro Continuous Flow-through Synthesis of Triangular Silver Nanoprisms and Their Incorporation in Complexly Composed Polymer Microparticles.” *Chemical Engineering Journal* 227:191–97. doi: 10.1016/j.cej.2012.07.041.
- Kohanski, Michael A., Daniel J. Dwyer, and James J. Collins. 2010. “How Antibiotics Kill Bacteria: From Targets to Networks.” *Nature Reviews Microbiology* 8(6):423–35. doi: 10.1038/nrmicro2333.
- Kramer, Axel, and Ojan Assadian. 2014. “Survival of Microorganisms on Inanimate Surfaces.” Pp. 7–26 in *Use of Biocidal Surfaces for Reduction of Healthcare Acquired Infections*. Vol. 9783319080.
- Kudryashov, Mikhail, Alexander Logunov, Daniela Gogova, Aleksandr Mashin, and Giovanni De Filpo. 2020. “Ag/PVP/PAN Nanocomposites with Triangular Nanoprisms of Silver Synthesized by UV-Induced Polymerization: Morphology Manipulation and Optical Properties Tuning.” *Optical Materials* 101(November 2019):109746. doi: 10.1016/j.optmat.2020.109746.
- Lackner, Maximilian. 2015. *Chapter: Bioplastics - Biobased Plastics as Renewable and/or Biodegradable Alternatives to Petroplastics*.
- Lee, Sang Hun, and Bong Hyun Jun. 2019. “Silver Nanoparticles: Synthesis and Application for Nanomedicine.” *International Journal of Molecular Sciences* 20(4). doi: 10.3390/ijms20040865.
- Lee, Sang Hyun, Kiwhan Sung, Taek-Mo Chung, Sung-Goo Lee, Kyung Dae Min, Sangman Koo, and Chang Gyoun Kim. 2008. “Preparation of Silver Nanoparticles and Antibiotic Test of Its Polycarbonate Films Composite.” *Journal of Nanoscience and Nanotechnology* 8(10):1–4. doi: 10.1166/jnn.2008.055.
- Lemnar, Georgiana Mădălina, Roxana Doina Truşcă, Cornelia Ioana Ilie, Roxana Elena Țiplea, Denisa Ficai, Ovidiu Oprea, Anicuța Stoica-Guzun, Anton Ficai, and Lia Mara Dițu. 2020. “Antibacterial Activity of Bacterial Cellulose Loaded with Bacitracin and Amoxicillin: In Vitro Studies.” *Molecules* 25(18). doi: 10.3390/molecules25184069.

- Leonés, Adrián, Alicia Mujica-Garcia, Marina Patricia Arrieta, Valentina Salaris, Daniel Lopez, José Maria Kenny, and Laura Peponi. 2020. "Organic and Inorganic PCL-Based Electrospun Fibers." *Polymers* 12(6):1–15. doi: 10.3390/polym12061325.
- Li, Kai, Xiaotong Jia, Aiwei Tang, Xibin Zhu, Huan Meng, and Yingfeng Wang. 2012. "Preparation of Spherical and Triangular Silver Nanoparticles by a Convenient Method." *Integrated Ferroelectrics* 136(1):9–14. doi: 10.1080/10584587.2012.686405.
- Li, Li, Laiping Zhang, Yan Zhao, and Zhengbo Chen. 2018. "Colorimetric Detection of Hg(II) by Measurement the Color Alterations from the 'before' and 'after' RGB Images of Etched Triangular Silver Nanoplates." *Microchimica Acta* 185(4):1–6. doi: 10.1007/s00604-018-2759-9.
- Li, Wenhui, Cheng Zhang, Hai Chi, Lin Li, Tianqing Lan, Peng Han, Haiyan Chen, and Yuyue Qin. 2017. "Development of Antimicrobial Packaging Film Made from Poly(Lactic Acid) Incorporating Titanium Dioxide and Silver Nanoparticles." *Molecules* 22(7). doi: 10.3390/molecules22071170.
- Li, Xingyi, Shuo Chen, Binjun Zhang, Mei Li, Kai Diao, Zhaoliang Zhang, Jie Li, Yu Xu, Xianhuo Wang, and Hao Chen. 2012. "In Situ Injectable Nano-Composite Hydrogel Composed of Curcumin, N,O-Carboxymethyl Chitosan and Oxidized Alginate for Wound Healing Application." *International Journal of Pharmaceutics* 437(1–2):110–19. doi: 10.1016/j.ijpharm.2012.08.001.
- Li, Yimeng, Lishi Zhong, Lili Zhang, Xiaobing Shen, Lu Kong, and Tianshu Wu. 2021. "Research Advances on the Adverse Effects of Nanomaterials in a Model Organism, *Caenorhabditis Elegans*." *Environmental Toxicology and Chemistry* 40(9):2406–24. doi: 10.1002/etc.5133.
- Liao, Vivian Hsiu Chuan, Chan Wei Yu, Yu Ju Chu, Wen Hsuan Li, Yi Chen Hsieh, and Teng Ting Wang. 2011. "Curcumin-Mediated Lifespan Extension in *Caenorhabditis Elegans*." *Mechanisms of Ageing and Development* 132(10):480–87. doi: 10.1016/j.mad.2011.07.008.
- Lim, Mim Mim, and Naznin Sultana. 2016. "In Vitro Cytotoxicity and Antibacterial Activity of Silver-Coated Electrospun Polycaprolactone/Gelatine Nanofibrous Scaffolds." *3 Biotech* 6(2):1–10. doi: 10.1007/s13205-016-0531-6.
- Liu, Wei, Yuan Wu, Chang Wang, Hong C. Li, Thanh Wang, Chun Y. Liao, Lin Cui, Qun F. Zhou, Bing Yan, and Gui B. Jiang. 2010. "Impact of Silver Nanoparticles on Human Cells: Effect of Particle Size." *Nanotoxicology* 4(3):319–30. doi: 10.3109/17435390.2010.483745.
- Liu, Xiaxia, Linglong Li, Yaodong Yang, Yadong Yin, and Chuanbo Gao. 2014. "One-Step Growth of Triangular Silver Nanoplates with Predictable Sizes on a Large Scale." *Nanoscale* 6(9):4513–16. doi: 10.1039/c4nr00254g.
- Lopez-Esparza, Juan, Leon Francisco Espinosa-Cristobal, Alejandro Donohue-Cornejo, and Simon Yobanny Reyes-Lopez. 2016. "Antimicrobial Activity of Silver Nanoparticles in Polycaprolactone Nanofibers against Gram-Positive and Gram-Negative Bacteria." *Industrial and Engineering Chemistry Research* 55(49):12532–38. doi: 10.1021/acs.iecr.6b02300.
- Loree, John, and Sarah L. Lappin. 2022. "Bacteriostatic Antibiotics." *StatPearls*. Retrieved (<https://www.ncbi.nlm.nih.gov/books/NBK547678/>).
- Lu, Haixia, Junli Zhu, Jianrong Li, and Jinru Chen. 2015. "Effectiveness of Active Packaging on Control of *Escherichia Coli* O157:H7 and Total Aerobic Bacteria on Iceberg Lettuce." *Journal of Food Science* 80(6):M1325–29. doi: 10.1111/1750-3841.12878.
- Lu, Weiwei, Kaisheng Yao, Jianji Wang, and Jiongliang Yuan. 2015. "Ionic Liquids-Water Interfacial Preparation of Triangular Ag Nanoplates and Their Shape-Dependent Antibacterial Activity." *Journal of Colloid and Interface Science* 437:35–41. doi: 10.1016/j.jcis.2014.09.001.

- Luyt, Adriaan S., and Sarah S. Malik. 2018. *Can Biodegradable Plastics Solve Plastic Solid Waste Accumulation?* Elsevier Inc.
- Maddah, Hisham A. 2016. "Polypropylene as a Promising Plastic: A Review." 6(1):1–11. doi: 10.5923/j.ajps.20160601.01.
- Mahira, Shaheen, Anjali Jain, Wahid Khan, and Abraham J. Domb. 2019. "Antimicrobial Materials — An Overview." Pp. 1–37 in *Antimicrobial Materials for Biomedical Applications*.
- Malikmammadov, Elbay, Tugba Endogan Tanir, Aysel Kiziltay, Vasif Hasirci, and Nesrin Hasirci. 2018. *PCL and PCL-Based Materials in Biomedical Applications*. Vol. 29. Taylor & Francis.
- Manoukian, Ohan S., Naseem Sardashti, Teagen Stedman, Katie Gailiunas, Anurag Ojha, Aura Penalosa, Christopher Mancuso, Michelle Hobert, and Sangamesh G. Kumbar. 2019. *Biomaterials for Tissue Engineering and Regenerative Medicine*. Vols. 1–3. Elsevier Inc.
- Mantravadi, Pavan K., Karunakaran A. Kalesh, Renwick C. J. Dobson, and Andr O. Hudson. 2019. "The Quest for Novel Antimicrobial Compounds: Emerging Trends in Research , Development ,." 1–34. doi: 10.3390/antibiotics8010008.
- Manzano, Marisa, Priya Vizzini, Kun Jia, Pierre Michel Adam, and Rodica Elena Ionescu. 2016. "Development of Localized Surface Plasmon Resonance Biosensors for the Detection of *Brettanomyces Bruxellensis* in Wine." *Sensors and Actuators, B: Chemical* 223:295–300. doi: 10.1016/j.snb.2015.09.099.
- Martínez-Abad, A. 2011. "Silver-Based Antimicrobial Polymers for Food Packaging." *Multifunctional and Nanoreinforced Polymers for Food Packaging* 347–67. doi: 10.1533/9780857092786.3.347.
- McKeen, Laurence W. 2012. "Environmentally Friendly Polymers." *Permeability Properties of Plastics and Elastomers* 287–304. doi: 10.1016/b978-1-4377-3469-0.10013-x.
- Michael, Carolyn Anne, Dale Dominey-Howes, and Maurizio Labbate. 2014. "The Antimicrobial Resistance Crisis: Causes, Consequences, and Management." *Frontiers in Public Health* 2(SEP):1–8. doi: 10.3389/fpubh.2014.00145.
- Michael Kotlarchyk. 1999. "Scattering Theory." Pp. 2074–84 in *Encyclopedia of Spectroscopy and Spectrometry*.
- Miller, Melissa B., and Bonnie L. Bassler. 2001. "QUORUM SENSING IN BACTERIA." *Annual Review of Microbiology* 55(4):165–99. doi: <https://doi.org/10.1146/annurev.micro.55.1.165>.
- Miñano, Joan, Jordi Puiggali, and Lourdes Franco. 2020. "Effect of Curcumin on Thermal Degradation of Poly(Glycolic Acid) and Poly(ε-Caprolactone) Blends." *Thermochimica Acta* 693(September). doi: 10.1016/j.tca.2020.178764.
- Miyashiro, Daisuke, Ryo Hamano, and Kazuo Umemura. 2020. "A Review of Applications Using Mixed Materials of Cellulose, Nanocellulose and Carbon Nanotubes." *Nanomaterials* 10(2). doi: 10.3390/nano10020186.
- Mohammadi, Elham, Seyed Meysam Amini, Seyed Hossein Mostafavi, and Seyed Mohammad Amini. 2021. "An Overview of Antimicrobial Efficacy of Curcumin-Silver Nanoparticles." *Nanomedicine Research Journal* 6(2):105–11. doi: 10.22034/nmrj.2021.02.002.
- Monteiro, Cláudia, Inder Saxena, Xiaoda Wang, Abdul Kader, Werner Bokranz, Roger Simm, David Nobles, Milan Chromek, Annelie Brauner, R. Malcolm Brown, and Ute Römling. 2009. "Characterization of Cellulose Production in *Escherichia Coli* Nissle 1917 and Its Biological Consequences." *Environmental Microbiology* 11(5):1105–16. doi: 10.1111/j.1462-2920.2008.01840.x.

- Morones, Jose Ruben, Jose Luis Elechiguerra, Alejandra Camacho, Katherine Holt, Juan B. Kouri, Jose Tapia Ramirez, and Miguel Jose Yacaman. 2005. "The Bactericidal Effect of Silver Nanoparticles." *Nanotechnology* 16(10):2346–53. doi: 10.1088/0957-4484/16/10/059.
- Morrison, Gail. 1990. "Chapter 197 Serum Chloride." in *Clinical Methods: The History, Physical, and Laboratory Examinations. 3rd edition.*
- Mosconi, Giuliana, María Fernanda Stragliotto, Walter Slenk, Laura E. Valenti, Carla E. Giacomelli, Miriam C. Strumia, and Cesar G. Gomez. 2020. "Original Antifouling Strategy: Polypropylene Films Modified with Chitosan-coated Silver Nanoparticles." *Journal of Applied Polymer Science* 137(10):48448. doi: 10.1002/app.48448.
- Mróz, Patrycja, Sylwia Białas, Maria Mucha, and Halina Kaczmarek. 2013. "Thermogravimetric and DSC Testing of Poly(Lactic Acid) Nanocomposites." *Thermochimica Acta* 573:186–92. doi: 10.1016/j.tca.2013.09.012.
- Nair, Rajesh Sreedharan, Andrew Morris, Nashiru Billa, and Chee Onn Leong. 2019. "An Evaluation of Curcumin-Encapsulated Chitosan Nanoparticles for Transdermal Delivery." *AAPS PharmSciTech* 20(2):1–13. doi: 10.1208/s12249-018-1279-6.
- Nandiyanto, A. B. D., A. S. Wiryani, A. Rusli, A. Purnamasari, A. G. Abdullah, Ana, I. Widiaty, and R. Hurriyati. 2017. "Extraction of Curcumin Pigment from Indonesian Local Turmeric with Its Infrared Spectra and Thermal Decomposition Properties." *Materials Science and Engineering* 755(1). doi: 10.1088/1757-899X/180/1/012136.
- Nguyen, K. C., V. L. Seligy, A. Massarsky, T. W. Moon, P. Rippstein, J. Tan, and A. F. Tayabali. 2013. "Comparison of Toxicity of Uncoated and Coated Silver Nanoparticles." *Journal of Physics: Conference Series* 429(1). doi: 10.1088/1742-6596/429/1/012025.
- Nootsuwan, Nollapan, Kankavee Sukthavorn, Worawat Wattanathana, Suchada Jongrungruangchok, Chatchai Veranitisagul, Nattamon Koonsaeng, and Apirat Laobuthee. 2018. "Development of Antimicrobi Al Hybrid Materials from Polylactic Acid and Nano-Silver Coated Chitosan." *Oriental Journal of Chemistry* 34(2):683–92. doi: 10.13005/ojc/340210.
- Occupational Safety and Health Administration (OSHA). 2021. "SILVER, METAL & SOLUBLE COMPOUNDS (as Ag)<sup>†</sup>." Retrieved (<https://www.osha.gov/chemicaldata/519>).
- Oliani, Washington Luiz, Duclerc Fernandes Parra, Luis Filipe Carvalho Pedroso Lima, Nilton Lincopan, and Ademar Benevolo Lugao. 2015. "Development of a Nanocomposite of Polypropylene with Biocide Action from Silver Nanoparticles." *Journal of Applied Polymer Science* 132(29):n/a-n/a. doi: 10.1002/app.42218.
- Omnexus. n.d. "Polycarbonate (PC) Plastic: Properties, Uses, & Structure - Guide." Retrieved September 17, 2020 (<https://omnexus.specialchem.com/selection-guide/polycarbonate-pc-plastic#content>).
- Packiavathy, Issac Abraham Sybiya Vasantha, Selvam Priya, Shunmugiah Karutha Pandian, and Arumugam Veera Ravi. 2014. "Inhibition of Biofilm Development of Uropathogens by Curcumin - An Anti-Quorum Sensing Agent from Curcuma Longa." *Food Chemistry* 148:453–60. doi: 10.1016/j.foodchem.2012.08.002.
- Pal, Sudipto, Rossella Nisi, Mariangela Stoppa, and Antonio Licciulli. 2017. "Silver-Functionalized Bacterial Cellulose as Antibacterial Membrane for Wound-Healing Applications." *ACS Omega* 2(7):3632–39. doi: 10.1021/acsomega.7b00442.
- Pal, Sukdeb, Yu Kyung Tak, and Joon Myong Song. 2007. "Does the Antibacterial Activity of Silver Nanoparticles Depend on the Shape of the Nanoparticle? A Study of the Gram-Negative Bacterium Escherichia Coli." *Applied and Environmental Microbiology* 73(6):1712–20. doi: 10.1128/AEM.02218-06.
- Paridah, M. ..., Amin Moradbak, A. .. Mohamed, Folahan Abdulwahab taiwo Owolabi, Mustapha Asniza, and Shawkataly H. .. Abdul Khalid. 2016. "Localized Surface Plasmon Resonances: Noble Metal Nanoparticle

- Interaction with Rare-Earth Ions.” *Intech*. doi: <http://dx.doi.org/10.5772/57353>.
- Park, Hee Jin, Jee Yeon Kim, Jaeun Kim, Joon Hee Lee, Ji Sook Hahn, Man Bock Gu, and Jeyong Yoon. 2009. “Silver-Ion-Mediated Reactive Oxygen Species Generation Affecting Bactericidal Activity.” *Water Research* 43(4):1027–32. doi: 10.1016/j.watres.2008.12.002.
- Park, Jin Ock, So Hye Cho, Jae Seung Lee, Wonjoo Lee, and Seung Yong Lee. 2016. “A Foolproof Method for Phase Transfer of Metal Nanoparticles via Centrifugation.” *Chemical Communications* 52(8):1625–28. doi: 10.1039/c5cc09344a.
- Pazos-Ortiz, Erick, Jose Hafid Roque-Ruiz, Efrén Amador Hinojos-Márquez, Juan López-Esparza, Alejandro Donohué-Cornejo, Juan Carlos Cuevas-González, León Francisco Espinosa-Cristóbal, and Simón Yobanny Reyes-López. 2017. “Dose-Dependent Antimicrobial Activity of Silver Nanoparticles on Polycaprolactone Fibers against Gram-Positive and Gram-Negative Bacteria.” *Journal of Nanomaterials* 2017. doi: 10.1155/2017/4752314.
- Petryayeva, Eleonora, and Ulrich J. Krull. 2011. “Localized Surface Plasmon Resonance: Nanostructures, Bioassays and Biosensing-A Review.” *Analytica Chimica Acta* 706(1):8–24. doi: 10.1016/j.aca.2011.08.020.
- Pham, Lyna, Le Hang Dang, Minh Dung Truong, Thi Hiep Nguyen, Ly Le, Van Thu Le, Nguyen Dang Nam, Long Giang Bach, Van Toan Nguyen, and Ngoc Quyen Tran. 2019. “A Dual Synergistic of Curcumin and Gelatin on Thermal-Responsive Hydrogel Based on Chitosan-P123 in Wound Healing Application.” *Biomedicine and Pharmacotherapy* 117(June):0–11. doi: 10.1016/j.biopha.2019.109183.
- Praditya, Dimas, Lisa Kirchhoff, Janina Brüning, Heni Rachmawati, Joerg Steinmann, and Eike Steinmann. 2019. “Anti-Infective Properties of the Golden Spice Curcumin.” *Frontiers in Microbiology* 10(MAY):1–16. doi: 10.3389/fmicb.2019.00912.
- Prestinaci, Francesca, Patrizio Pezzotti, and Annalisa Pantosti. 2015. “Antimicrobial Resistance: A Global Multifaceted Phenomenon.” *Pathogens and Global Health* 109(7):309–18. doi: 10.1179/2047773215Y.0000000030.
- Qing, Yun’an, Lin Cheng, Ruiyan Li, Guancong Liu, Yanbo Zhang, Xiongfeng Tang, Jincheng Wang, He Liu, and Yanguo Qin. 2018. “Potential Antibacterial Mechanism of Silver Nanoparticles and the Optimization of Orthopedic Implants by Advanced Modification Technologies.” *International Journal of Nanomedicine* 13:3311–27. doi: 10.2147/IJN.S165125.
- Raduly, Florentina Monica, Valentin Raditoiu, Alina Raditoiu, and Violeta Purcar. 2021. “Curcumin: Modern Applications for a Versatile Additive.” *Coatings* 11(5). doi: 10.3390/coatings11050519.
- Rai, Mahendra, Kateryna Kon, Avinash Ingle, Nelson Duran, Stefania Galdiero, and Massimiliano Galdiero. 2014. “Broad-Spectrum Bioactivities of Silver Nanoparticles: The Emerging Trends and Future Prospects.” *Applied Microbiology and Biotechnology* 98(5):1951–61. doi: 10.1007/s00253-013-5473-x.
- Rastegar, Asghar. 1990. “Chapter 195 Serum Potassium.” in *Clinical Methods: The History, Physical, and Laboratory Examinations*. 3rd edition.
- Ravindra, Sakey, Antoine F. Mulaba-Bafubiandi, V. Rajinikanth, K. Varaprasad, N. Narayana Reddy, and K. Mohana Raju. 2012. “Development and Characterization of Curcumin Loaded Silver Nanoparticle Hydrogels for Antibacterial and Drug Delivery Applications.” *Journal of Inorganic and Organometallic Polymers and Materials* 22(6):1254–62. doi: 10.1007/s10904-012-9734-4.
- Raza, Muhammad Akram, Zakia Kanwal, Anum Rauf, Anjum Nasim Sabri, Saira Riaz, and Shahzad Naseem. 2016. “Size and Shape-Dependent Antibacterial Studies of Silver Nanoparticles Synthesized by Wet Chemical Routes.” *Nanomaterials* 6(4). doi: 10.3390/nano6040074.

- Remziye Güzel, and Gülbahar Erdal. 2016. "Synthesis of Silver Nanoparticles." *Intech* 13. doi: 10.5772/INTECHOPEN.75363.
- Reynoso-García, Paris Jonathan, Marisol Güizado-Rodríguez, Victor Barba, Gabriel Ramos-Ortiz, and Hugo Martínez-Gutiérrez. 2018. "Stabilization of Silver Nanoparticles with a Dithiocarbamate Ligand and Formation of Nanocomposites by Combination with Polythiophene Derivative Nanoparticles." *Advances in Condensed Matter Physics* 2018. doi: 10.1155/2018/4376051.
- Rezvan, Gelareh, Gholamreza Pircheraghi, and Reza Bagheri. 2018. "Curcumin Incorporated PVA-Borax Dual Delivery Hydrogels as Potential Wound Dressing Materials—Correlation between Viscoelastic Properties and Curcumin Release Rate." *Journal of Applied Polymer Science* 135(45):1–11. doi: 10.1002/app.46734.
- Römling, Ute, and Heinrich Lünsdorf. 2004. "Characterization of Cellulose Produced by Salmonella Enterica Serovar Typhimurium." *Cellulose* 11(3/4):413–18. doi: 10.1023/b:cell.0000046411.74345.8f.
- Rongpipi, Sintu, Dan Ye, Enrique D. Gomez, and Esther W. Gomez. 2019. "Progress and Opportunities in the Characterization of Cellulose – an Important Regulator of Cell Wall Growth and Mechanics." *Frontiers in Plant Science* 9(March):1–28. doi: 10.3389/fpls.2018.01894.
- Sackey, J., A. Fell, J. B. Ngilrabanga, L. C. Razanamahandry, S. K. O. Ntwampe, and M. Nkosi. 2020. "Antibacterial Effect of Silver Nanoparticles Synthesised on a Polycarbonate Membrane." *Materials Today: Proceedings* (xxxx). doi: 10.1016/j.matpr.2020.04.121.
- Sajjad, Wasim, Feng He, Muhammad Wajid Ullah, Muhammad Ikram, Shahid Masood Shah, Romana Khan, Taous Khan, Ayesha Khalid, Guang Yang, and Fazli Wahid. 2020. "Fabrication of Bacterial Cellulose-Curcumin Nanocomposite as a Novel Dressing for Partial Thickness Skin Burn." *Frontiers in Bioengineering and Biotechnology* 8(September):1–12. doi: 10.3389/fbioe.2020.553037.
- Salle, Anna Di, Gianluca Viscusi, Francesca Di Cristo, Anna Valentino, Giuliana Gorrasi, Elena Lamberti, Vittoria Vittoria, Anna Calarco, and Gianfranco Peluso. 2021. "Antimicrobial and Antibiofilm Activity of Curcumin-Loaded." *Associated Infections. Molecules* 26:4866.
- Di Salle, Anna, Gianluca Viscusi, Francesca Di Cristo, Anna Valentino, Giuliana Gorrasi, Elena Lamberti, Vittoria Vittoria, Anna Calarco, and Gianfranco Peluso. 2021. "Antimicrobial and Antibiofilm Activity of Curcumin-Loaded Electrospun Nanofibers for the Prevention of the Biofilm-Associated Infections." *Molecules* 26(16). doi: 10.3390/molecules26164866.
- Samoc, Anna. 2003. "Dispersion of Refractive Properties of Solvents: Chloroform, Toluene, Benzene, and Carbon Disulfide in Ultraviolet, Visible, and near-Infrared." *Journal of Applied Physics* 94(9):6167–74. doi: 10.1063/1.1615294.
- Dos Santos, Carolina Alves, Marcelo Martins Seckler, Avinash P. Ingle, Indarchand Gupta, Stefania Galdiero, Massimiliano Galdiero, Aniket Gade, and Mahendra Rai. 2014. "Silver Nanoparticles: Therapeutical Uses, Toxicity, and Safety Issues." *Journal of Pharmaceutical Sciences* 103(7):1931–44. doi: 10.1002/jps.24001.
- Shameli, Kamyar, Mansor Bin Ahmad, Wan Md Zin Wan Yunus, Nor Azowa Ibrahim, russly Abdul rahman, Maryam Jokar, and Majid Darroudi. 2010. "International Journal of Nanomedicine Dovepress Silver/Poly (Lactic Acid) Nanocomposites: Preparation, Characterization, and Antibacterial Activity." *International Journal of Nanomedicine* 5–573.
- Sharma, Chhavi, and Nishi K. Bhardwaj. 2019. "Bacterial Nanocellulose: Present Status, Biomedical Applications and Future Perspectives." *Materials Science and Engineering C* 104(September 2018):109963. doi: 10.1016/j.msec.2019.109963.
- Shefa, Anha Afrin, Tamanna Sultana, Myeong Ki Park, Sun Young Lee, Jae Gyoung Gwon, and Byong Taek Lee. 2020. "Curcumin Incorporation into an Oxidized Cellulose Nanofiber-Polyvinyl Alcohol Hydrogel System Promotes Wound Healing." *Materials and Design* 186:108313. doi: 10.1016/j.matdes.2019.108313.



- Shoults-Wilson, William A., Brian C. Reinsch, Olga V. Tsyusko, Paul M. Bertsch, Gregory V. Lowry, and Jason M. Unrine. 2011. "Effect of Silver Nanoparticle Surface Coating on Bioaccumulation and Reproductive Toxicity in Earthworms (*Eisenia Fetida*)." *Nanotoxicology* 5(3):432–44. doi: 10.3109/17435390.2010.537382.
- Shrivastava, Siddhartha, Tanmay Bera, Arnab Roy, Gajendra Singh, P. Ramachandrarao, and Debabrata Dash. 2007. "Characterization of Enhanced Antibacterial Effects of Novel Silver Nanoparticles." *Nanotechnology* 18(22). doi: 10.1088/0957-4484/18/22/225103.
- Shuaib, Urooj, Tousif Hussain, Riaz Ahmad, Muhammad Zakaullah, Farrukh Ehtesham Mubarak, Sidra Tul Muntaha, and Sana Ashraf. 2020. "Plasma-Liquid Synthesis of Silver Nanoparticles and Their Antibacterial and Antifungal Applications." *Materials Research Express* 7(3). doi: 10.1088/2053-1591/ab7cb6.
- Siddiqi, Khwaja Salahuddin, Azamal Husen, and Rifaqat A. K. Rao. 2018. "A Review on Biosynthesis of Silver Nanoparticles and Their Biocidal Properties." *Journal of Nanobiotechnology* 16(1). doi: 10.1186/s12951-018-0334-5.
- Siemann, Ulrich. 2005. "Solvent Cast Technology - A Versatile Tool for Thin Film Production." *Progress in Colloid and Polymer Science* 130(June):1–14. doi: 10.1007/b107336.
- Silva, S. S., E. M. Fernandes, S. Pina, J. Silva-Correia, S. Vieira, J. M. Oliveira, and R. L. Reis. 2017. "2.11 Polymers of Biological Origin." *Comprehensive Biomaterials II* 2(June 2016):228–52. doi: 10.1016/B978-0-12-803581-8.10134-1.
- Singh, Anant Kumar, Dulal Senapati, Adria Neely, Gabriel Kolawole, Craig Hawker, and Paresh Chandra Ray. 2009. "Nonlinear Optical Properties of Triangular Silver Nanomaterials." *Chemical Physics Letters* 481(1–3):94–98. doi: 10.1016/j.cplett.2009.09.045.
- Slavin, Yael N., Jason Asnis, Urs O. Häfeli, and Horacio Bach. 2017. "Metal Nanoparticles: Understanding the Mechanisms behind Antibacterial Activity." *Journal of Nanobiotechnology* 15(1):1–20. doi: 10.1186/s12951-017-0308-z.
- Solomon, Sally D., Mozghan Bahadory, Aravindan V. Jeyarajasingam, Susan A. Rutkowsky, Charles Boritz, and Lorraine Mulfinger. 2007. "Synthesis and Study of Silver Nanoparticles." *Journal of Chemical Education* 84(2):322–25.
- Song, Zhiyong, Yang Wu, Huajuan Wang, and Heyou Han. 2019. "Synergistic Antibacterial Effects of Curcumin Modified Silver Nanoparticles through ROS-Mediated Pathways." *Materials Science and Engineering C* 99(June 2018):255–63. doi: 10.1016/j.msec.2018.12.053.
- Sonseca, Agueda, Salim Madani, Gema Rodríguez, Víctor Hevilla, Coro Echeverría, Marta Fernández-García, Alexandra Muñoz-Bonilla, Noureddine Charef, and Daniel López. 2020. "Multifunctional PLA Blends Containing Chitosan Mediated Silver Nanoparticles: Thermal, Mechanical, Antibacterial, and Degradation Properties." *Nanomaterials* 10(1). doi: 10.3390/nano10010022.
- Sotiriou, Georgios A., and Sotiris E. Pratsinis. 2010. "Antibacterial Activity of Nanosilver Ions and Particles." *Environmental Science and Technology* 44(14):5649–54. doi: 10.1021/es101072s.
- Stiernagle, Theresa. 2006. "Maintenance of *C. Elegans*." *WormBook: The Online Review of C. Elegans Biology* (1999):1–11. doi: 10.1895/wormbook.1.101.1.
- Stoehr, Linda C., Edgar Gonzalez, Andreas Stampfl, Eudald Casals, Albert Duschl, Victor Puentes, and Gertie J. Oostingh. 2011. "Shape Matters: Effects of Silver Nanospheres and Wires on Human Alveolar Epithelial Cells." *Particle and Fibre Toxicology* 8:1–15. doi: 10.1186/1743-8977-8-36.
- Szymańska-Chargot, Monika, Monika Chylińska, Piotr M. Pieczywek, Anna Walkiewicz, Giorgia Pertile, Magdalena Frac, Krystian J. Cieślak, and Artur Zdunek. 2020. "Evaluation of Nanocomposite Made of

- Polylactic Acid and Nanocellulose from Carrot Pomace Modified with Silver Nanoparticles.” *Polymers* 12(4). doi: 10.3390/POLYM12040812.
- Takeda, Emi, Wei Xu, Mitsuhiro Terakawa, and Takuro Niidome. 2022. “Tailored Structure and Antibacterial Properties of Silica-Coated Silver Nanoplates by Pulsed Laser Irradiation.” *ACS Omega* 7(8):7251–56. doi: 10.1021/acsomega.1c07058.
- Takeuchi, K. 2012. “Polycarbonates.” *Polymer Science: A Comprehensive Reference, 10 Volume Set* 5:363–76. doi: 10.1016/B978-0-444-53349-4.00148-5.
- Tanskul, Somporn, Korntip Amorntatree, and Nathakan Jaturonlak. 2013. “A New Cellulose-Producing Bacterium, *Rhodococcus* Sp. MI 2: Screening and Optimization of Culture Conditions.” *Carbohydrate Polymers* 92(1):421–28. doi: 10.1016/j.carbpol.2012.09.017.
- Teeguarden, Justin G., Paul M. Hinderliter, Galya Orr, Brian D. Thrall, and Joel G. Pounds. 2007. “Particokinetics in Vitro: Dosimetry Considerations for in Vitro Nanoparticle Toxicity Assessments.” *Toxicological Sciences* 95(2):300–312. doi: 10.1093/toxsci/kfl165.
- Thomas, Roshmi, K. R. Soumya, Jyothis Mathew, and E. K. Radhakrishnan. 2015. “Electrospun Polycaprolactone Membrane Incorporated with Biosynthesized Silver Nanoparticles as Effective Wound Dressing Material.” *Applied Biochemistry and Biotechnology* 176(8):2213–24. doi: 10.1007/s12010-015-1709-9.
- Torres, Víctor, Mónica Popa, Daniel Crespo, and José M. Calderón Moreno. 2007. “Silver Nanoprism Coatings on Optical Glass Substrates.” *Microelectronic Engineering* 84(5–8):1665–68. doi: 10.1016/j.mee.2007.01.262.
- Trautmann, Steffen, André Dathe, Andrea Csáki, Matthias Thiele, Robert Müller, Wolfgang Fritzsche, and Ondrej Stranik. 2019. “Time-Resolved Study of Site-Specific Corrosion in a Single Crystalline Silver Nanoparticle.” *Nanoscale Research Letters* 14(1). doi: 10.1186/s11671-019-3077-9.
- Travan, Andrea, Chiara Pelillo, Ivan Donati, Eleonora Marsich, Monica Benincasa, Tommaso Scarpa, Sabrina Semeraro, Gianluca Turco, and Renato Gennaro. 2009. “Nanocomposites with Antimicrobial Activity.” *Biomacromolecules* 10:1429–35. doi: Doi 10.1021/Bm900039x.
- Tyagi, Poonam, Madhuri Singh, Himani Kumari, Anita Kumari, and Kasturi Mukhopadhyay. 2015. “Bactericidal Activity of Curcumin I Is Associated with Damaging of Bacterial Membrane.” *PLoS ONE* 10(3):1–15. doi: 10.1371/journal.pone.0121313.
- Tylkowski, Bartosz, Anna Trojanowska, Martyna Nowak, Lukasz Marciniak, and Renata Jastrzab. 2019. “Applications of Silver Nanoparticles Stabilized and/or Immobilized by Polymer Matrixes.” *Physical Sciences Reviews* 2(7):1–16. doi: 10.1515/psr-2017-0024.
- Ullah, Muhammad Wajid, Mazhar Ul-Islam, Shaukat Khan, Yeji Kim, and Joong Kon Park. 2015. “Innovative Production of Bio-Cellulose Using a Cell-Free System Derived from a Single Cell Line.” *Carbohydrate Polymers* 132:286–94. doi: 10.1016/j.carbpol.2015.06.037.
- Unser, Sarah, Ian Bruzas, Jie He, and Laura Sagle. 2015. “Localized Surface Plasmon Resonance Biosensing: Current Challenges and Approaches.” *Sensors (Switzerland)* 15(7):15684–716. doi: 10.3390/s150715684.
- Urbina, Leire, María Ángeles Corcuera, Nagore Gabilondo, Arantxa Eceiza, and Aloña Retegi. 2021. “A Review of Bacterial Cellulose: Sustainable Production from Agricultural Waste and Applications in Various Fields.” *Cellulose* 28(13):8229–53. doi: 10.1007/s10570-021-04020-4.
- Vazquez-Muñoz, Roberto, Belen Borrego, Karla Juárez-Moreno, Maritza García-García, Josué D. Mota Morales, Nina Bogdanchikova, and Alejandro Huerta-Saquero. 2017. “Toxicity of Silver Nanoparticles in Biological Systems: Does the Complexity of Biological Systems Matter?” *Toxicology Letters* 276:11–20. doi: 10.1016/j.toxlet.2017.05.007.

- Velgosova, Oksana, Livia Mačák, Maksym Lisnichuk, and Marek Vojtko. 2022. "Synthesis and Analysis of Polymorphic Silver Nanoparticles and Their Incorporation into the Polymer Matrix." *Polymers* 14(13):1–12. doi: 10.3390/polym14132666.
- Velmurugan, Palanivel, Hyun Myung, Muthusamy Govarathanan, Young Joo Yi, Sang Ki Seo, Kwang Min Cho, Nanh Lovanh, and Byung Taek Oh. 2015. "Production and Characterization of Bacterial Cellulose by *Leifsonia* Sp. CBNU-EW3 Isolated from the Earthworm, *Eisenia Fetida*." *Biotechnology and Bioprocess Engineering* 20(3):410–16. doi: 10.1007/s12257-014-0793-y.
- Vinayagam, Saranya, Paramasivan Rajaiah, Amitava Mukherjee, and Chandrasekaran Natarajan. 2018. "DNA-Triangular Silver Nanoparticles Nanoprobe for the Detection of Dengue Virus Distinguishing Serotype." *Spectrochimica Acta - Part A: Molecular and Biomolecular Spectroscopy* 202:346–51. doi: 10.1016/j.saa.2018.05.047.
- Vippola, M., G. C. M. Falck, H. K. Lindberg, S. Suhonen, E. Vanhala, H. Norppa, K. Savolainen, A. Tossavainen, and T. Tuomi. 2009. "Preparation of Nanoparticle Dispersions for In-Vitro Toxicity Testing." *Human and Experimental Toxicology* 28(6–7):377–85. doi: 10.1177/0960327109105158.
- Vo, Quoc Khuong, Duc Duy Phung, Quynh Nhu Vo Nguyen, Hong Hoang Thi, Nhat Hang Nguyen Thi, Phuong Phong Nguyen Thi, Long Giang Bach, and Lam Van Tan. 2019. "Controlled Synthesis of Triangular Silver Nanoplates by Gelatin-Chitosan Mixture and the Influence of Their Shape on Antibacterial Activity." *Processes* 7(12). doi: 10.3390/PR7120873.
- Vodop'yanov, A. V., D. A. Mansfeld, A. V. Samokhin, N. V. Alekseev, and Yu V. Tsvetkov. 2017. "Production of Nanopowders by the Evaporation–Condensation Method Using a Focused Microwave Radiation." *Radiophysics and Quantum Electronics* 59(8–9):698–705. doi: 10.1007/s11141-017-9737-7.
- Wang, Jiaolong, Lilin Zhan, Xianhua Zhang, Runfa Wu, and Lan Liao. 2020. "Silver Nanoparticles Coated Poly ( L-Lactide ) Electrospun Membrane for Implant Associated Infections Prevention." 11(April):1–8. doi: 10.3389/fphar.2020.00431.
- Wang, Jing, Javad Tavakoli, and Youhong Tang. 2019. "Bacterial Cellulose Production, Properties and Applications with Different Culture Methods – A Review." *Carbohydrate Polymers* 219(May):63–76. doi: 10.1016/j.carbpol.2019.05.008.
- Wang, Shan Shan, Yong He Han, Yu Xuan Ye, Xiao Xia Shi, Ping Xiang, Deng Long Chen, and Min Li. 2017. "Physicochemical Characterization of High-Quality Bacterial Cellulose Produced by *Komagataeibacter* Sp. Strain W1 and Identification of the Associated Genes in Bacterial Cellulose Production." *RSC Advances* 7(71):45145–55. doi: 10.1039/c7ra08391b.
- Willets, Katherine A., and Richard P. Van Duyne. 2007. "Localized Surface Plasmon Resonance Spectroscopy and Sensing." *Annual Review of Physical Chemistry* 58(1):267–97. doi: 10.1146/annurev.physchem.58.032806.104607.
- Williams, David. 2008. "The Relationship between Biomaterials and Nanotechnology." *Biomaterials* 29(12):1737–38. doi: 10.1016/j.biomaterials.2008.01.003.
- Wouters, Olivier J., Martin McKee, and Jeroen Luyten. 2020. "Estimated Research and Development Investment Needed to Bring a New Medicine to Market, 2009-2018." *JAMA - Journal of the American Medical Association* 323(9):844–53.
- Wu, Chunfang, Xue Zhou, and Jie Wei. 2015. "Localized Surface Plasmon Resonance of Silver Nanotriangles Synthesized by a Versatile Solution Reaction." *Nanoscale Research Letters* 10(1):1–6. doi: 10.1186/s11671-015-1058-1.
- Wu, J. J., G. J. Lee, Y. S. Chen, and T. L. Hu. 2012. "The Synthesis of Nano-Silver/Polypropylene Plastics for Antibacterial Application." *Current Applied Physics* 12(SUPPL. 2). doi: 10.1016/j.cap.2012.02.026.

- Wu, Jheng Yu, Chin Yi Lin, Tien Wei Lin, Chuian Fu Ken, and Yu Der Wen. 2007. "Curcumin Affects Development of Zebrafish Embryo." *Biological and Pharmaceutical Bulletin* 30(7):1336–39. doi: 10.1248/bpb.30.1336.
- Xiu, Zong Ming, Qing Bo Zhang, Hema L. Puppala, Vicki L. Colvin, and Pedro J. J. Alvarez. 2012. "Negligible Particle-Specific Antibacterial Activity of Silver Nanoparticles." *Nano Letters* 12(8):4271–75. doi: 10.1021/nl301934w.
- Xu, Xuejie, Li Xu, Ganjun Yuan, Yimin Wang, Yunqiu Qu, and Meijing Zhou. 2018. "Synergistic Combination of Two Antimicrobial Agents Closing Each Other's Mutant Selection Windows to Prevent Antimicrobial Resistance." *Scientific Reports* 8(1):1–7. doi: 10.1038/s41598-018-25714-z.
- Yang, Xinyu, Andreas P. Gondikas, Stella M. Marinakos, Melanie Auffan, Jie Liu, Heileen Hsu-kim, and Joel N. Meyer. 2012. "Mechanism of Silver Nanoparticle Toxicity Is Dependent on Dissolved Silver and Surface Coating in *Caenorhabditis Elegans*." *Environmental Science & Technology* 46(2):1119–1127. doi: 10.1021/es202417t.
- Yoon, Su Jin, Yun Sik Nam, Ho Jin Lee, Yeonhee Lee, and Kang Bong Lee. 2019. "Colorimetric Probe for Ni<sup>2+</sup> Based on Shape Transformation of Triangular Silver Nanoprisms upon H<sub>2</sub>O<sub>2</sub> Etching." *Sensors and Actuators, B: Chemical* 300(June):127045. doi: 10.1016/j.snb.2019.127045.
- Zhang, Chunhong, Xiangkui Jiang, Fuhua Yu, Yang Liu, Qi Yue, Peng Yang, and Yongchun Liu. 2021. "Antagonistic Action Regulated Anti-Etching Colorimetric Detection of Thiram Residue in Soil Based on Triangular Silver Nanoplates." *Sensors and Actuators, B: Chemical* 344(May):130304. doi: 10.1016/j.snb.2021.130304.
- Zhang, Jia, Ying Sun, Hua Zhang, Bo Xu, Hanqi Zhang, and Daqian Song. 2013. "Preparation and Application of Triangular Silver Nanoplates/Chitosan Composite in Surface Plasmon Resonance Biosensing." *Analytica Chimica Acta* 769:114–20. doi: 10.1016/j.aca.2013.01.034.
- Zhang, Li, Lingli Wu, Youbin Si, and Kunhui Shu. 2018. "Size-Dependent Cytotoxicity of Silver Nanoparticles to *Azotobacter Vinelandii*: Growth Inhibition, Cell Injury, Oxidative Stress and Internalization." *PLoS ONE* 13(12):1–18. doi: 10.1371/journal.pone.0209020.
- Zhang, Qiao, Na Li, James Goebel, Zhenda Lu, and Yadong Yin. 2011. "A Systematic Study of the Synthesis of Silver Nanoplates: Is Citrate a 'Magic' Reagent?" *Journal of the American Chemical Society* 133(46):18931–39. doi: 10.1021/ja2080345.
- Zhang, Tianlu, Liming Wang, Qiang Chen, and Chunying Chen. 2014. "Cytotoxic Potential of Silver Nanoparticles." *Yonsei Medical Journal* 55(2):283–91. doi: 10.3349/ymj.2014.55.2.283.
- Zhang, Xifeng, Zhi Guo Liu, Wei Shen, and Sangiliyandi Gurunathan. 2016. "Silver Nanoparticles: Synthesis, Characterization, Properties, Applications, and Therapeutic Approaches." *International Journal of Molecular Sciences* 17(9). doi: 10.3390/ijms17091534.
- Zhang, Yi, Denise E. Charles, Deirdre M. Ledwith, Damian Aherne, Stephen Cunningham, Muriel Voisin, Werner J. Blau, Yurii K. Gun'ko, John M. Kelly, and Margaret E. Brennan-Fournet. 2014. "Wash-Free Highly Sensitive Detection of C-Reactive Protein Using Gold Derivatized Triangular Silver Nanoplates." *RSC Advances* 4(55):29022–31. doi: 10.1039/c4ra04958f.
- Zhao, Yong, Jia Guo Liu, Wei Min Chen, and Ai Xi Yu. 2018. "Efficacy of Thermosensitive Chitosan/ $\beta$ -Glycerophosphate Hydrogel Loaded with  $\beta$ -Cyclodextrin-Curcumin for the Treatment of Cutaneous Wound Infection in Rats." *Experimental and Therapeutic Medicine* 15(2):1304–13. doi: 10.3892/etm.2017.5552.
- Zheng, Dantong, Chongxing Huang, Haohe Huang, Yuan Zhao, Muhammad Rafi Ullah Khan, Hui Zhao, and Lijie Huang. 2020. "Antibacterial Mechanism of Curcumin: A Review." *Chemistry and Biodiversity* 17(8). doi: 10.1002/cbdv.202000171.

- Zheng, Lu, Shanshan Li, Jiwen Luo, and Xiaoying Wang. 2020. "Latest Advances on Bacterial Cellulose-Based Antibacterial Materials as Wound Dressings." *Frontiers in Bioengineering and Biotechnology* 8.
- Zorofchian Moghadamtousi, Soheil, Habsah Abdul Kadir, Pouya Hassandarvish, Hassan Tajik, Sazaly Abubakar, and Keivan Zandi. 2014. "A Review on Antibacterial, Antiviral, and Antifungal Activity of Curcumin." *BioMed Research International* 2014. doi: 10.1155/2014/186864.
- Żywicka, Anna, Adam F. Junka, Patrycja Szymczyk, Grzegorz Chodaczek, Jakub Grzesiak, Parish Paymon Sedghizadeh, and Karol Fijałkowski. 2018. "Bacterial Cellulose Yield Increased over 500% by Supplementation of Medium with Vegetable Oil." *Carbohydrate Polymers* 199(March):294–303. doi: 10.1016/j.carbpol.2018.06.126.

## APPENDICES

### Appendix 1. Stress-strain Graphs from Tensile Tests of Solvent Casted PCL, PLA, PCL-TSNP and PLA-TSNP films

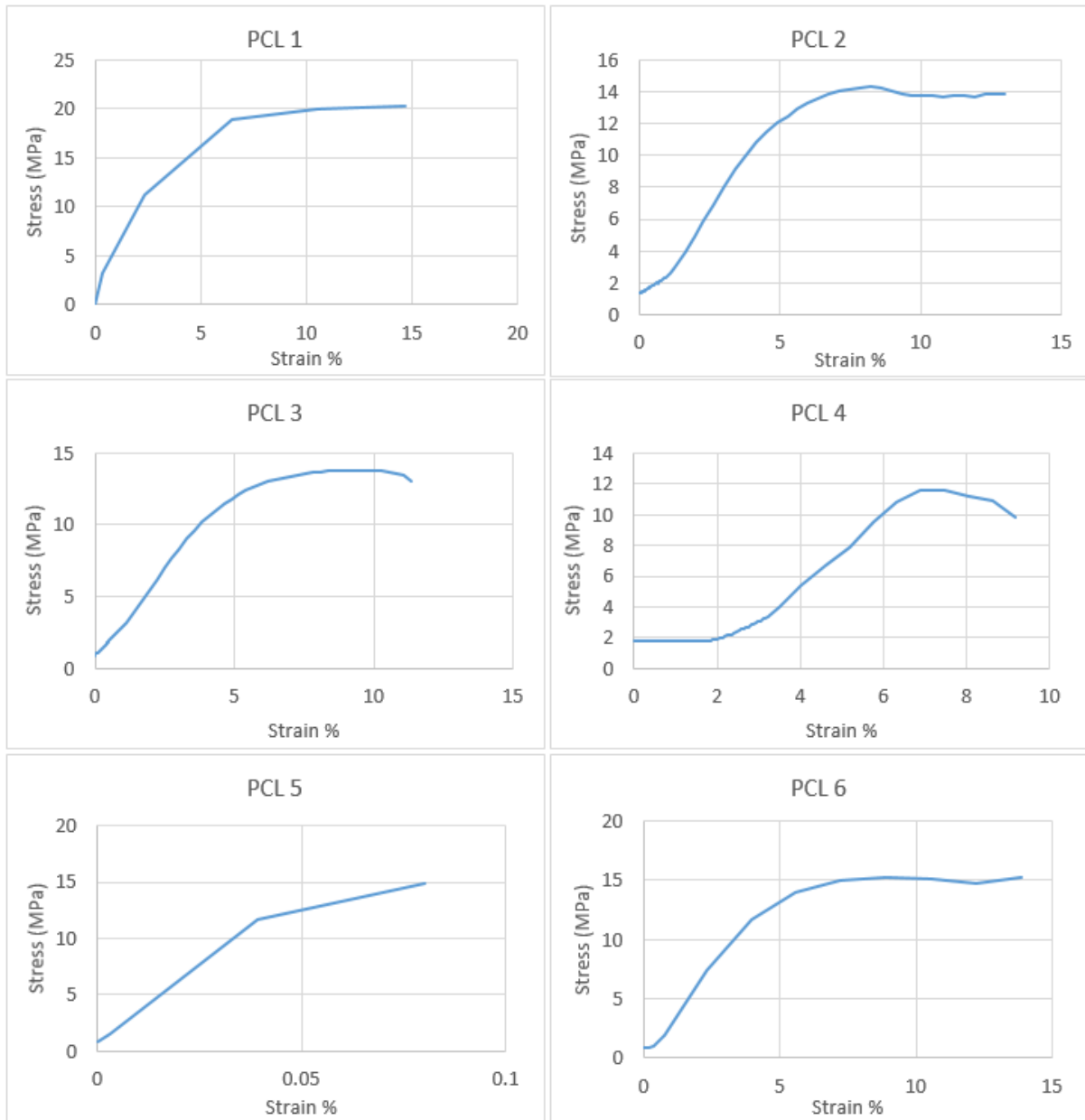


Figure 74. Stress-Strain graphs from tensile testing of bare PCL samples. Testing was performed with 6 replicates.

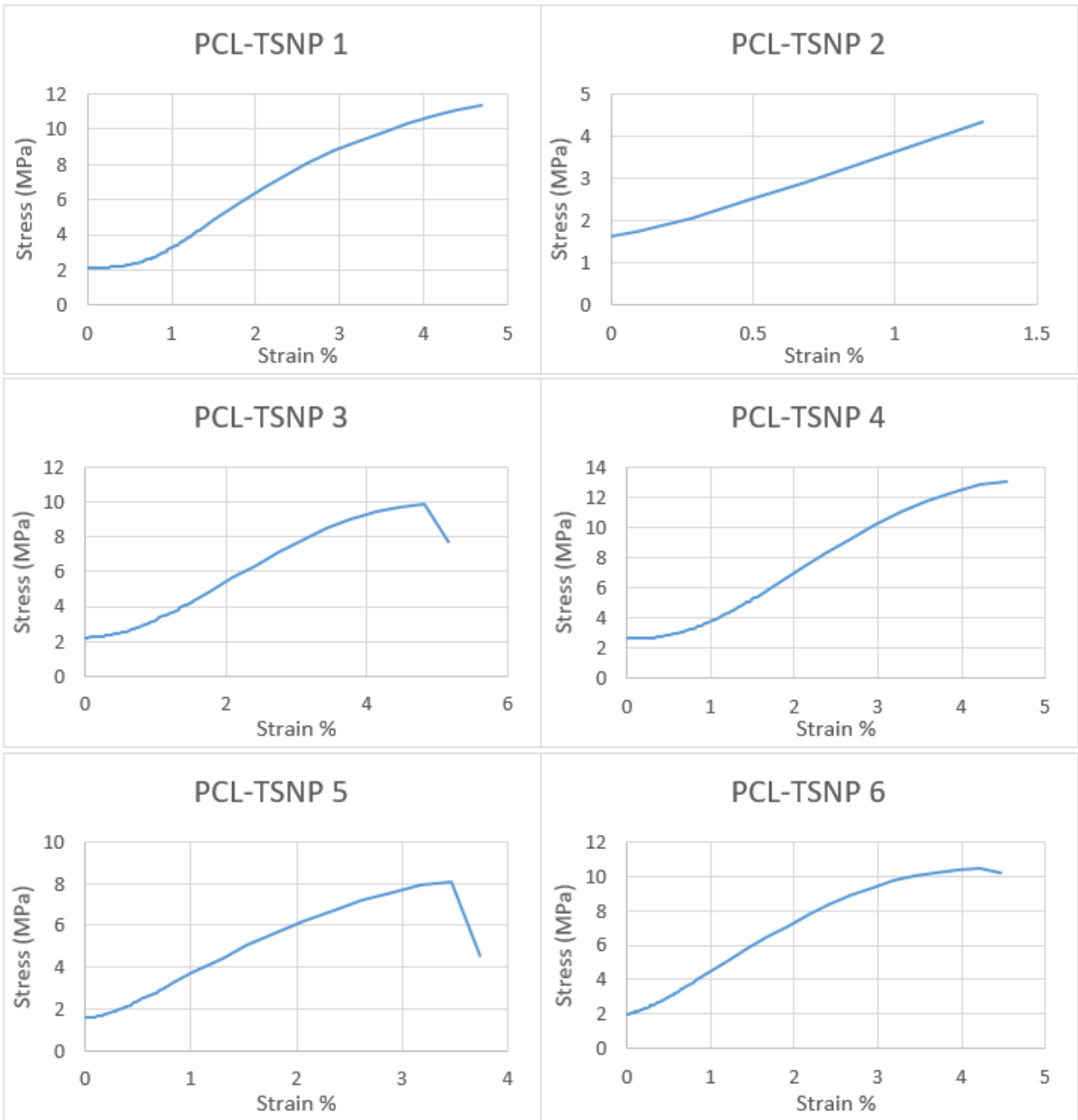


Figure 75. Stress-Strain graphs from tensile testing of PCL-TSNP samples. Testing was performed with 6 replicates.

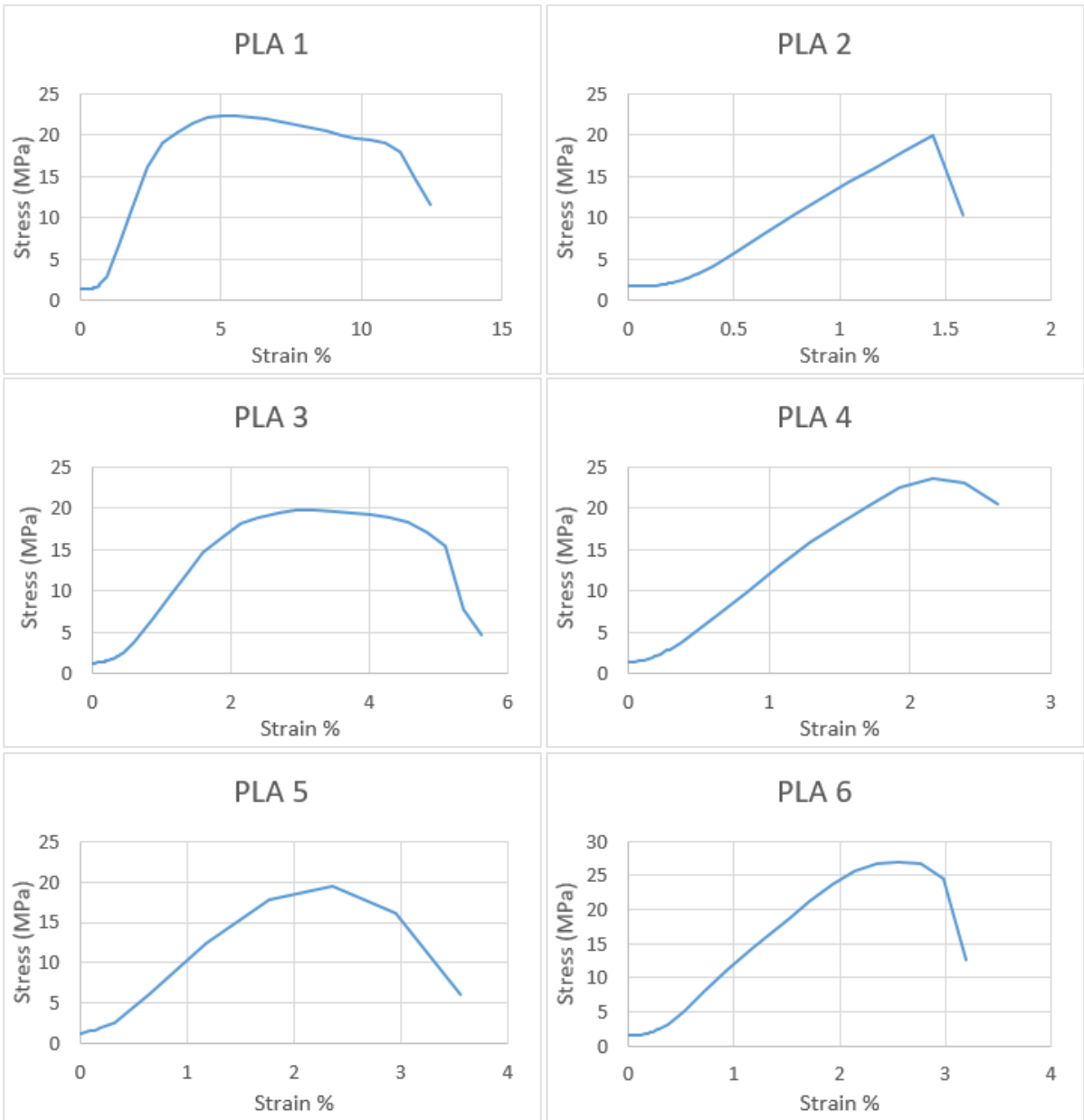


Figure 76. Stress-Strain graphs from tensile testing of bare PLA samples. Testing was performed with 6 replicates.



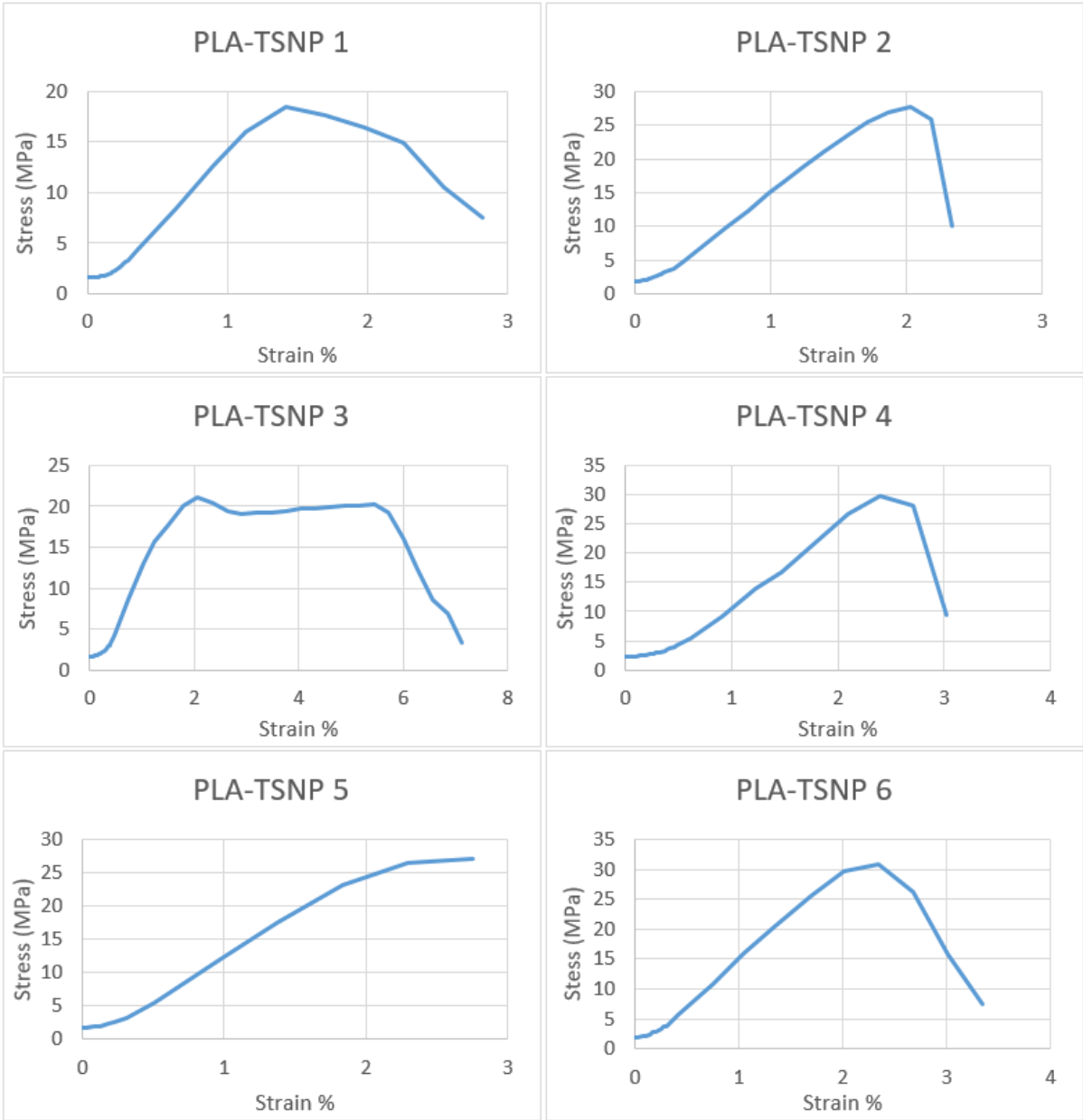



Figure 77. Stress-Strain graphs from tensile testing of PLA-TSNP samples. Testing was performed with 6 replicates.

## Appendix 2. Poster for AIT Research Seminar, April 2019

THE SUNDAY TIMES  
GOOD UNIVERSITY GUIDE  
2018  
INSTITUTE OF TECHNOLOGY OF THE YEAR

# AIT Research



## DEVELOPMENT OF UNIVERSAL PROCESSABLE ANTIMICROBIAL POLYMERS WITH EFFECTIVE MICROORGANISM CONTROL

Eduardo Lanzagorta Garcia<sup>a</sup>, Romina Pezzoli<sup>a</sup>, Laura G. Rodriguez Barroso<sup>a</sup>, Chaitra Venkatesh<sup>a</sup>, Declan M. Devine<sup>a</sup>, Margaret E. Brennan Fournet<sup>a</sup>

<sup>a</sup>Materials Research Institute, Athlone Institute of Technology, Athlone, Ireland

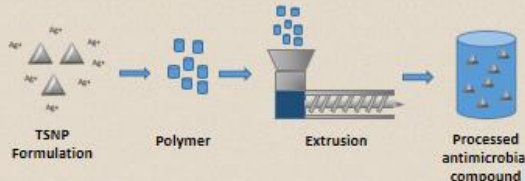
### INTRODUCTION

Environmental surfaces are common avenues for microbial contamination and transmission. Here we present proprietary formulated Triangular Silver Nanoplates (TSNPs) for the addition of vital antimicrobial properties to plastics. These ultra-high-surface-area, triangular shaped, nano-discs have powerful antimicrobial silver ion releasing action which render microbes inactive and prevent microbial colonisation and biofilm formation.


### OBJECTIVES

Development of a Polymer processing technology incorporating antimicrobial properties.

- i) Formulation of antimicrobial TSNPs for enabling polymer composite extrusion.
- ii) Evaluation of antimicrobial and physical properties of resulting polymer compound.




### RESULTS



**Extruded Polypropylene (PP)**  
Pure PP (Left) and PP-TSNP nanocomposite (Right).

### METHODS



### CONCLUSIONS

- Polymers extruded with unformulated TSNP result in degraded TSNPs and compromised antimicrobial performance.
- Formulation methods are used to design and promote resistance to extrusion conditions.

### CONTACT

- Eduardo Lanzagorta Garcia, [e.lgarcia@research.ait.ie](mailto:e.lgarcia@research.ait.ie) Materials Research Institute Athlone Insitute of Technology, Dublin Rd., Athlone, Co. Westmeath, Ireland
- Dr. Margaret E. Brennan Fournet, [mfournet@ait.ie](mailto:mfournet@ait.ie) Materials Research Insitute Athlone Insitute of Technology, Dublin Rd., Athlone, Co. Westmeath, Ireland

### REFERENCES


Kelly J. M., Keegan G. and Brennan Fournet M. E. *Acta Physica Polonica A*, (2011). DOI: 10.12693/APhysPolA.122.337  
 Abbas M., Naeem N., Iftikhar H. and Latif U. *IntechOpen*, (2018). DOI: 10.5772/intechopen.74623  
 2. Weiwei L., Kaisheng Y., Jianji W. & Jionglang Y. (2015). DOI: 10.1016/j.jcon.2014.09.001

### ACKNOWLEDGEMENT

Funding for this project was provided by AIT President Seed Fund

THE SUNDAY TIMES  
GOOD UNIVERSITY GUIDE  
2018  
INSTITUTE OF TECHNOLOGY OF THE YEAR

# AIT Research



## Appendix 3. Abstract for Bioengineering in Ireland (BiNI), January 2020

Early Stage Researcher (PhD Year 1)

Post-Doctoral Researcher/Senior Researcher/PI

Entry for the Engineers Ireland Biomedical Research Medal

Corresponding author has completed PhD and would like to review BiNI abstract submissions

Please place an X in any appropriate categories

### SUSTAINABLE ANTIMICROBIAL POLYMERIC BIOMEDICAL FILM ENGINEERING USING AG+ NANORESERVOIR FORMULATIONS

**Lanzagorta, E.<sup>1</sup>, Rodriguez, L.<sup>1</sup>, Pezzoli, R.<sup>1</sup>, Venkatesh, C.<sup>1</sup>, Bandeira, M.<sup>1</sup>, Devine, D.<sup>1</sup>, Brennan-Fournet, M.E.<sup>1</sup>**

<sup>1</sup> Athlone Institute of Technology  
email: e.lanzagorta@research.ait.ie

#### INTRODUCTION

New antimicrobial interventions are urgently required to combat rising global health and medical infection challenges. Here, an innovative antimicrobial technology, providing price competitive alternatives to antibiotics and readily integratable with currently technological systems is presented.

Triangular silver nanoplates (TSNPs) are highly discrete, homogenous and readily functionalisable Ag<sup>+</sup> nanoreservoirs<sup>1</sup> that have a proven amenability for operation within a wide range of bio-based settings<sup>2,3,4</sup>. In a design for advanced antimicrobial sustainable food packaging, antimicrobial TSNPs are formulated for processing within biodegradable biopolymers. A synergy between the propensity of biopolymers for degradation and Ag<sup>+</sup> release provides a novel mechanism for the sustained antimicrobial action of biopolymeric thin films. The aqueous TSNP synthesis is scaled up for litre scale batch production and subsequently concentrated to 43 ppm using thermally controlled H<sub>2</sub>O removal. Using polymer solvation<sup>5</sup> the TSNPs are encapsulated within Polycarbonate (PC) and Polycaprolactone (PCL). Antimicrobial test was performed on TSNP-integrated PC film.

#### MATERIALS AND METHODS

Chemicals for TSNP synthesis were obtained from Sigma Aldrich. TSNP were synthesized adapting a method from a previously described seed mediated approach<sup>6</sup>. TSNP solution Ag concentration was increased from 21.34 ppm to 42.68 ppm evaporating water at 40°C for several consecutive days. TSNP were functionalised with thiol terminated polyethylene glycol and transferred to chloroform using a previously described methodology<sup>7</sup>. PC and PCL solutions of 3% in chloroform were prepared respectively, then mixed together with chloroform transferred TSNP and finally solvent was left to evaporate and films were formed. Antimicrobial activity from PC-TSNP film was evaluated against gram-positive (*S. aureus*) and gram-negative (*E. coli*) strains, by incubating the bacteria in tryptone soy broth in the presence of the film. Bacterial growth was measured using resazurin as an indicator<sup>8</sup>.

#### RESULTS

Resulting films successfully incorporated TSNP while maintaining the integrity of the nanoplates, as indicated by the consistent optical properties and the presence of

the characteristic blue colour of the TSNP within the films. Figure 1 shows the measured bacterial growth percentage of *E. coli* and *S. aureus* incubated in the presence of PC-TSNP films and PC films compared with the controls.

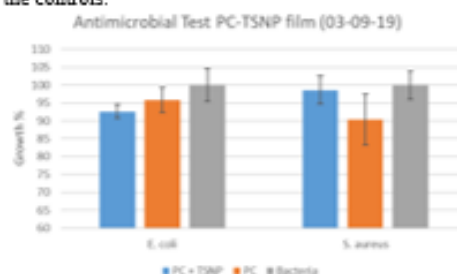



**Figure 1** Growth percentage for *E. coli* and *S. aureus* in the presence of PC-TSNP film, PC film and the control without film.

#### DISCUSSION

Overall results demonstrate TSNP can be successfully integrated into polymers using solvent casting method. In order to increase bacterial growth reduction, in particular against gram-positive strains, further processing developments are planned. Bacterial growth reduction can be improved by the formulation and application of new embedding methods to further facilitate Ag<sup>+</sup> ion release. The ability of this technology to impede bacterial attachment to medical surfaces will forge new confidence in the battle against antibiotic resistant bacteria, serving to greatly inhibiting infections and facilitating patient recovery.


#### REFERENCES

1. Dakal (et al.), *Frontiers in Microbiology* 7: 1-17, 2016.
2. Zhang (et al.), *RSC Advances* 4(55): 29022-29031, 2014.
3. Brennan-Fournet (et al.), *Journal of Materials Chemistry B* 3(47): 9140-9147, 2015.
4. Vinayagam (et al.), *Spectrochimica Acta – Part A: Molecular and Biomolecular Spectroscopy* 202: 346-351, 2018.
5. Siemann, *Progress in Colloid and Polymer Science* 130: 1-14, 2005.
6. Aherne (et al.), *Advanced Functional Materials* 18(14): 2005-2016, 2008.
7. Park (et al.), *Chemical Communications* 52(8): 1625-1628, 2016.
8. Sarker (et al.), *Methods* 42(4): 321-324, 2007.



**GOOD UNIVERSITY GUIDE 2020**  
INSTITUTE OF TECHNOLOGY OF THE YEAR

# AIT Research



## SUSTAINABLE ANTIMICROBIAL POLYMERIC FOOD PACKING AND ANTI-INFECTION MEDICAL CATHETERS PREPARATION USING ANTIMICROBIAL PEPTIDE AND Ag<sup>+</sup> NANORESERVOIR FORMULATIONS.

Eduardo Lanzagorta Garcia<sup>a</sup>, Romina Pezzoli<sup>a</sup>, Laura G. Rodriguez Barroso<sup>a</sup>, Chaitra Venkatesh<sup>a</sup>, Declan M. Devine<sup>a</sup>, Margaret E. Brennan Fournet<sup>a</sup>

<sup>a</sup>Materials Research Institute, Athlone Institute of Technology, Athlone, Ireland

### INTRODUCTION

New antimicrobial interventions are urgently required to combat rising global health and medical infection challenges. Here, an innovative antimicrobial technology, providing price competitive alternatives to antibiotics and readily integratable with currently technological systems is presented. Two cutting edge antimicrobial materials; antimicrobial peptides (AMPs) and triangular silver nanoplate (TSNPs) reservoirs for sustained Ag<sup>+</sup> action, are incorporated with plastic and bioplastics for the provision of versatile effective antimicrobial action where current approaches fail. TSNP's are highly discrete, homogenous and readily functionisable Ag<sup>+</sup> nanoresevoirs that have a proven amenability for operation within in a wide range of bio-based settings.

TSNP Synthesis

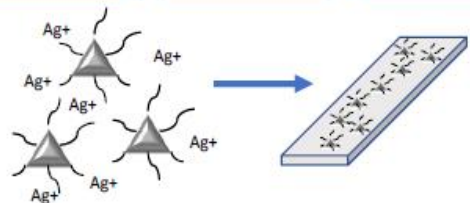
TSNP Formulation

TSNP-AMP Functionalization

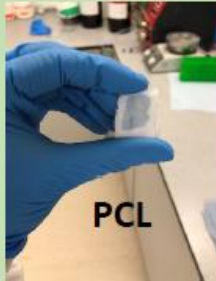

Polymer integration treatment

Evaluation of Antimicrobial activity

Evaluation of mechanical properties




### RESULTS


### CONTACT

- Eduardo Lanzagorta Garcia, [elanzag@research.ait.ie](mailto:elanzag@research.ait.ie), Materials Research Institute, Athlone Institute of Technology, Dublin Rd., Athlone, Co. Westmeath, Ireland
- Dr. Margaret E. Brennan Fournet, [mfournet@ait.ie](mailto:mefournet@ait.ie), Materials Research Institute, Athlone Institute of Technology, Dublin Rd., Athlone, Co. Westmeath, Ireland



**GOOD UNIVERSITY GUIDE 2020**  
INSTITUTE OF TECHNOLOGY OF THE YEAR

# AIT Research



Acknowledgement: Funding for this project was provided by AIT President Seed Fund

## SUSTAINABLE ANTIMICROBIAL POLYMERIC FOOD PACKING AND ANTI-INFECTION MEDICAL PLASTICS PREPARATION USING ANTIMICROBIAL PEPTIDE AND Ag<sup>+</sup> NANORESERVOIR FORMULATIONS

Eduardo Lanzagorta Garcia<sup>a</sup>, Romina Pezzoli<sup>a</sup>, Laura G. Rodriguez Barroso<sup>a</sup>, Marija Mojicevic<sup>a</sup>, Olivia Adly<sup>a</sup>, Declan M. Devine<sup>a</sup>, Margaret E. Brennan Fournet<sup>a</sup>

<sup>a</sup>Materials Research Institute, Athlone Institute of Technology, Athlone, Ireland

### INTRODUCTION

Due to overuse and misuse of antibiotics causing evolutionary stress in bacteria, resistance regeneration has been accelerated, threatening the ability of health systems to treat infectious diseases. Additionally, development of new antibiotic drugs has decreased significantly in the last decades, due to high investment costs and long times required for research, making it a risky and unattractive investment for pharmaceutical companies. Therefore, new antimicrobial interventions are urgently required to combat rising global health and medical infection challenges. Here, an innovative antimicrobial technology, providing price competitive alternatives to antibiotics and readily integratable with currently technological systems is presented. Two cutting edge antimicrobial materials; antimicrobial peptides (AMPs) and triangular silver nanoplate (TSNPs) reservoirs for sustained Ag<sup>+</sup> action, are incorporated within bioplastics, such as PCL and PLA, for the provision of versatile effective antimicrobial action where current approaches fail.

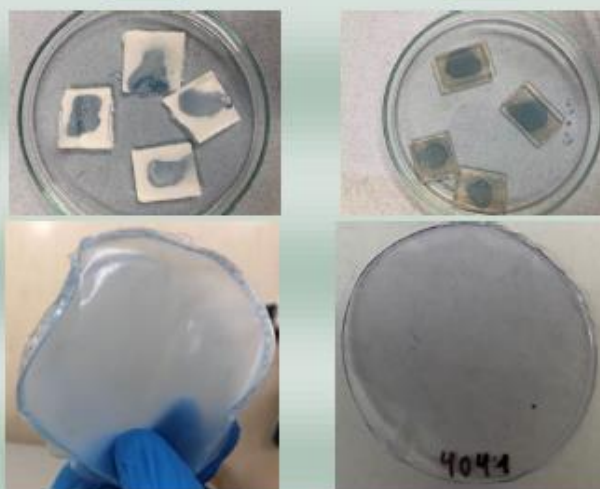


- Seed mediated approach
- Increase of concentration
- Transfer to organic phase
- For synergistic antimicrobial activity
- Solvent casting
- Calendaring
- Antimicrobial evaluation
- Characterization
- Evaluation of mechanical properties

### RESULTS

PCL

PLA



### CONCLUSIONS

- Solvent casting and calendaring are suitable approaches for incorporation of antimicrobial TSNP into biopolymers.
- Incorporation through solvent casting appears to occur deeper into polymer matrix, limiting release of Ag<sup>+</sup> for antimicrobial activity.

### REFERENCES

- Kelly J. M., Keegan C. and Brennan-Fournet M. E. *Acta Physica Polonica A*. (2011). DOI: 10.12693/APhysPolA.122.537  
 Weiwei L., Kaibing Y., Jianji W. & Jiongfang Y. (2015). DOI: 10.1016/j.jch.2014.05.001  
 Michael, C. A., Dominey-Howes, D., & Lobbata, M. *Frontiers in Public Health* (2014). DOI: <https://doi.org/10.3389/fpubh.2014.00145>

### CONTACT

Eduardo Lanzagorta Garcia: [e.lanzagorta@research.ait.ie](mailto:e.lanzagorta@research.ait.ie)  
 Margaret Brennan Fournet: [mfournet@ait.ie](mailto:mfournet@ait.ie)

Acknowledgement: Funding for this project was provided by AIT President Seed Fund



This project has received funding from the European Union's Horizon 2020 research and innovation programme under grant agreement number 870282.



## Appendix 6. Abstract presented in FEMS 2020 Online Conference, and Certificate of Participation

### Sustainable Antimicrobial Biopolymeric Food & Biomedical Film Engineering Using Bioactive AMP-Ag+ Formulations

**Background:** New antimicrobial interventions are urgently required to combat rising global health and medical infection challenges. Here, an innovative antimicrobial technology, providing price competitive alternatives to antibiotics and readily integratable with currently technological systems is presented. The potential of this technology to impede bacterial activity for food industry and medical surface applications will forge new confidence in the battle against antibiotic resistant bacteria, serving to greatly inhibit infections and facilitate patient recovery.

**Objectives:** Antimicrobial peptides (AMPs) and uncompromised sustained Ag+ action from triangular silver nanoplates (TSNPs) reservoirs, are merged for versatile effective antimicrobial action.

**Methods:** TSNP synthesis was scaled up and subsequently concentrated. Nanoplates were transferred to an organic solvent in order to facilitate integration within hydrophobic polymers. Polymer films are processed using extrusion in combination with calendaring. Polycaprolactone and Polylactic acid were initially individually processed by extrusion, TSNP solution was sprayed immediately after exiting the dye. Calendaring rolls were used to disperse and incorporate TSNP onto the surface of the extruded films. Antimicrobial tests were performed by incubating bacterial strains with the antimicrobial agents, to evaluate the reduction of bacterial growth due to the presence of the TSNP and AMP.

**Results:** The resulting films successfully incorporated TSNP and AMP-TSNP. Reduced bacterial growth was observed for both Gram positive and negative strains. The largest growth reduction was observed for AMP-TSNP treated films. The resultant antibacterial functional films are suitable to be adapted for food packing and biomedical applications.

**FEMS Online Conference on Microbiology**  
28 – 31 October 2020  
in association with the Serbian Society of Microbiology

**CERTIFICATE**

**Eduardo Lanzagorta Garcia**

**Participant – author with presentation**

Prof. dr Vaso Taleski  
Chair of the Organizing committee

Prof. dr Hilary Lappin Scott  
FEMS President

Prof. dr Bauke Oudega  
Chair of the Scientific Committee

# Appendix 7. Poster presented in EFB 2021 Virtual conference



## ENHANCEMENT OF BACTERIAL CELLULOSE ANTIMICROBIAL PERFORMANCE VIA CURCUMIN SUPPLEMENTATION AND SILVER NANOPARTICLES INCORPORATION

Eduardo Lanzagorta Garcia, Marija Mojicevic, Olivia A. Attallah, Declan Devine, Margaret Brennan Fournet  
Athlone Institute of Technology, Dublin Road, Athlone, Co. Westmeath, Ireland



### INTRODUCTION

Bacterial Nanocellulose (BC)-based materials have attracted a great deal of attention due to their unique mechanical and biodegradable properties<sup>1,2</sup>. Despite the vast applications of BC which include wound dressings, drug carriers and packaging materials, they still require a boost in their antimicrobial properties. This study is focused on the enhancement of BC antimicrobial performance during BC production in curcumin/Cur-based medium, followed by incorporation of antimicrobial triangular silver nanoparticles (TSNP) in the produced BC.

### METHODS

BC was prepared using *Komagataibacter medellinensis* strain. Cultivation was conducted in the presence and absence of curcumin. TSNP were incorporated in the produced BC, using ex situ method<sup>3</sup>. Successful incorporation of TSNP in BC was verified via energy-dispersive X-ray spectroscopy. Antimicrobial activity was tested in liquid culture against *Escherichia coli* and *Staphylococcus aureus* strains (Figure 1).



Figure 2. Wet (top) and dried (bottom) BC after cultivation in regular HS medium and medium supplemented with 2% and 10% of curcumin, respectively.



Figure 3. Optical abstract of methods used for this study: BC production with curcumin supplementation (2 and 10%), followed by TSNP incorporation and antimicrobial activity evaluation.

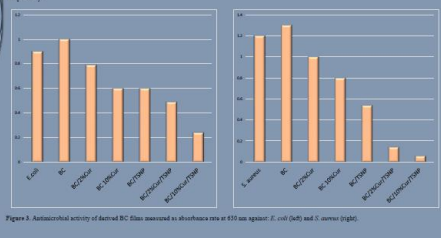


Figure 3. Antimicrobial activity of dried BC films measured as absorbance rate at 630 nm against *E. coli* (left) and *S. aureus* (right).

### RESULTS

Supplemented medium resulted in visual changes of bacterial cellulose colour and production yield (Figure 2, Table 1). It was observed that bacterial cellulose grew faster in the presence of curcumin powder.

Table 1. Bacterial cellulose yields obtained from curcumin-supplemented media

Medium	BC yield [mg]
Regular HS	127
+ 2% Cur	189.4
+ 10% Cur	306.8

Results suggested that antimicrobial performance of BC cultivated in the presence of curcumin was significantly enhanced against both tested strains in comparison to the plain BC (Figure 3). Incorporation of TSNP in the BC produced in the presence of curcumin, resulted with material that inhibits growth of *E. coli*, and an even higher inhibition against *S. aureus* (Figure 3).

### CONCLUSIONS

- Supplemented curcumin was easily absorbed by BC during its production.
- Supplementation of curcumin increased the yield of produced BC.
- Effective antimicrobial activity was observed as a result of curcumin supplementation against Gram-positive and Gram-negative evaluated strains.
- Addition of TSNP provided further increase to antimicrobial activity against both evaluated strains.
- Further analysis will be performed for optimization of supplemented production and evaluation against a wider variety of bacterial strains.

### CONTACT

Eduardo Lanzagorta Garcia:  
+349872783@student.aist.it  
e.lanzagorta@ait.ie  
@E.Lanzagorta  
www.linkedin.com/in/ed-lanz  
Marija Mojicevic:  
mmojicevic@ait.ie  
Margaret Brennan Fournet:  
mfournet@ait.ie  
BioCEP:  
@biocep

- REFERENCES
1. S.Q. Chen et al. (2018) Food Hydrocolloids, 10.1016/j.foodhyd.2018.02.031
  2. S.P. Liu et al. (2013) Cellulose, 10.1007/s10570-013-0994-3
  3. Sajedi et al. (2020) Front. Bioeng. Biotechnol., 10.3389/fbioe.2020.553037

### ACKNOWLEDGEMENT

Funding for this project was provided by AIT President Seed Fund, by European Union's Horizon 2020 research and innovation programme under grant agreement number 870202 (BioCEP) and was supported by the National Natural Science Foundation of China (grant numbers: Institute of Microbiology, Chinese Academy of Sciences, 3196113014; Beijing Institute of Technology, 3196113015; Shandong University, 3196113014). This project also received funding from a part of the funding VB NWE Programme, project number NWE1018 (CLUBCOL).

# Appendix 8. Poster presented in FEMS 2022 Microbiology Conference, and Certificate of Attendance



TUS Research



## PREPARATION AND ANTIMICROBIAL EVALUATION OF BACTERIAL CELLULOSE/POLY(3-HYDROXYBUTYRATE) BLENDS ACTIVATED WITH CURCUMIN AND SILVER FOR BIOMEDICAL AND FOOD PACKING PURPOSES

Eduardo Lanzagorta Garcia, Everton Henrique Da Silva Pereira, Marija Mojicevic, Margaret Brennan-Fournet  
Materials Research Institute, Technological University of The Shannon: Midlands Midwest

### INTRODUCTION

As the whole world is currently facing issues related to the excessive use of non-degradable single-use materials, a lot of effort has been recently directed towards the use of biodegradable polymers derived from renewable sources. However, these biopolymers still present some limitations to substitute commodity plastics, such as low thermal stability and poor mechanical properties, and they need to be improved by the development of new blends and composites. Blends of bacterial cellulose (BC) with poly(3-hydroxybutyrate) (PHB) show a promising alternative thanks to the unique mechanical properties of BC1,2 and the thermoplastic properties of PHB3. Furthermore, the addition of active compounds to provide antimicrobial properties is desirable to provide greater benefits in the use of these materials for medical and food packing applications. In our previous research it was shown that synergy of Curcumin and Triangular Silver nanoplates (TSNPs) showed a remarkable antimicrobial effect when incorporated into BC materials. In this study that effect was examined on BC/PHB blends produced by a method of interpenetrating polymer networks.

### METHODS

- BC was synthesized by *Komagataibacter medellinensis* (ID13488), cultivated in HS liquid medium (2% glucose, 0.5% yeast extract, 0.27% Na<sub>2</sub>HPO<sub>4</sub>, 0.15% citric acid and 0.5% peptone) at 30 °C, for 3 weeks in static conditions.
- BC/PHB blends incorporating active curcumin were produced by an interpenetrating polymer networks method. Briefly, a solution of 40g/L of PHB in chloroform was prepared, and 2% (w/v) of curcumin powder was added. BC films were immersed in the solution and incubated with agitation for 24 hours, at 30 °C and 120 rpm.
- Antimicrobial activity was tested in liquid culture against *Escherichia coli* (ATCC 25922) and *Staphylococcus aureus* (ATCC 25923) strains.



Figure 1. Method for production of BC films, BC/PHB blends, BC/Cur blends and incorporation of TSNP.



Figure 2. SEM micrographs of BC/Cur 100x (Left), BC/Cur 1.2kx (Center) and BC/TSNP 115x (Right).

### RESULTS

- Resulting BC materials showed successful incorporation of curcumin and TSNP (Figure 2).
- BC materials including curcumin alone showed a slight reduction of bacterial growth against *E. coli* (Figure 3).
- Incorporation of TSNP showed a significantly higher reduction of bacterial growth against both evaluated strains (Figure 3).

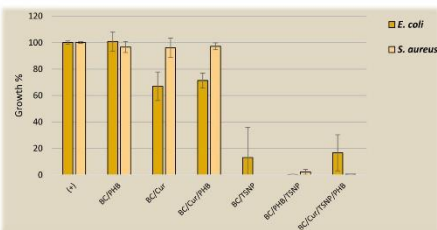


Figure 3. Antimicrobial activity of derived BC films and BC/PHB blends measured as absorbance rate at 630 nm.

### CONCLUSION

Incorporation of TSNP showed a powerful antimicrobial effect on the BC materials. Synergy of Curcumin and TSNP needs to be further investigated to determine their potential application for biomedical and food packaging purposes. This includes toxicological evaluations, as well as mechanical and morphological characterizations.

### REFERENCES

1. S.Q. Chen et al. (2018) Food Hydrocolloids, 10.1016/j.foodhyd.2018.02.031
2. S.P. Liu et al. (2013) Cellulose, 10.1007/978-94-007-9994-3
3. M. B. R. Albuquerque et al. (2020) Polymers and Polymer Composites, 10.1177/0967391120912098

### ACKNOWLEDGEMENTS

Funding for this project was provided by: TUS President Seed Fund, H3020 BioCEP project (870292) and Curcol project funded by Interreg VB NWE (NWE1058).



The Federation of European Microbiological Societies

## CERTIFICATE OF PRESENTATION

This is to certify that

Mr Eduardo Lanzagorta Garcia, Ireland

presented their abstract

PREPARATION AND ANTIMICROBIAL EVALUATION OF BACTERIAL CELLULOSE/POLY(3-HYDROXYBUTYRATE) BLENDS ACTIVATED WITH CURCUMIN FOR BIOME

as a(n) On-Demand Poster at  
the FEMS Conference on Microbiology 2022  
held from 30 June to 2 July in Belgrade, Serbia and online.





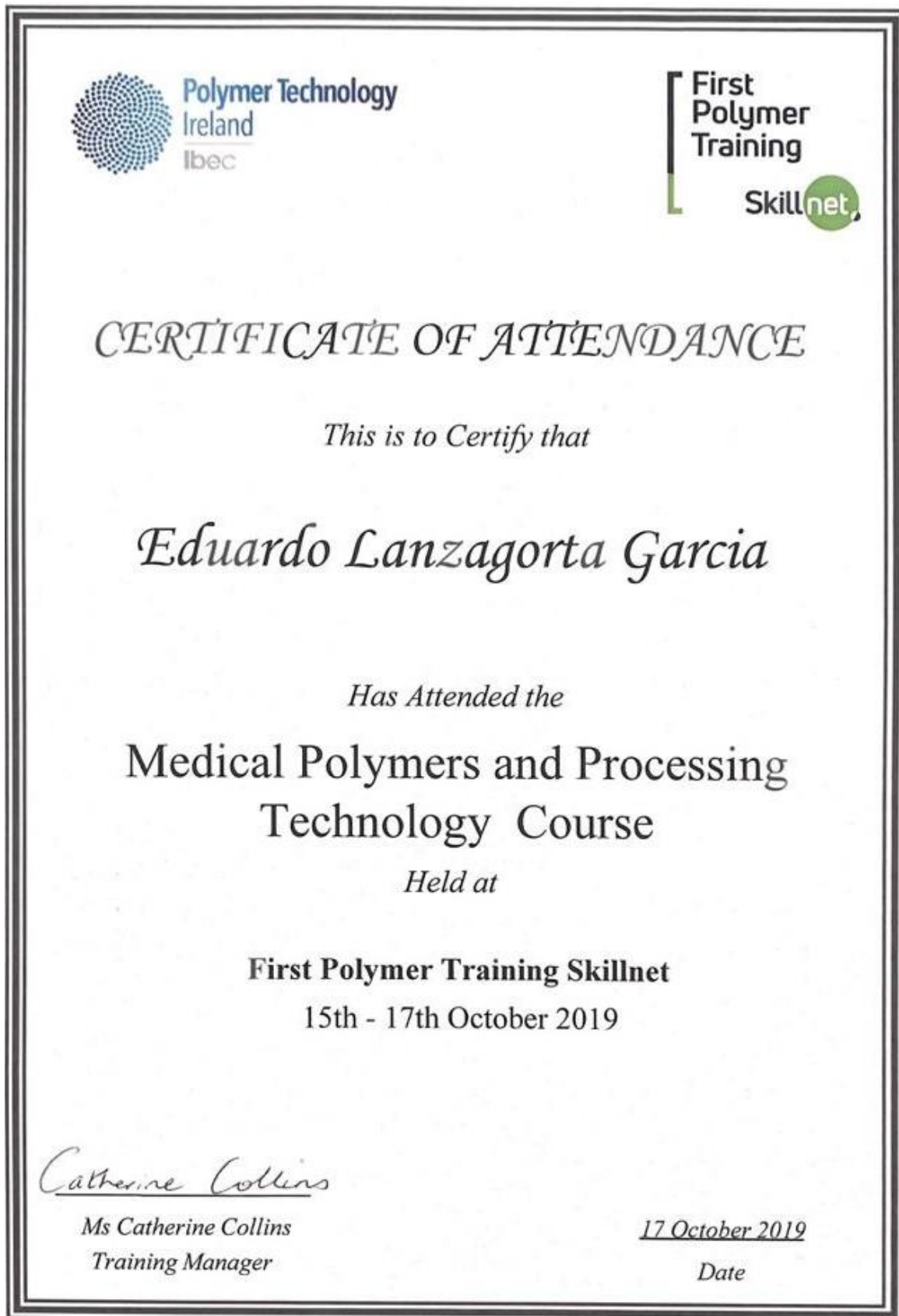
**Appendix 9. Participation certificate for AIT Poster and Research Seminar, June 2020**



## Appendix 10. Completion certificate of Research Integrity Module for Engineering and Technology



Appendix 11. Attendance certificate of “Medical Polymers and Processing Technology” course, at First Polymer Training Skillnet, October 2019.



## Monitoring of Extracellular Matrix Protein Conformations in the Presence of Biomimetic Bone Tissue Regeneration Scaffolds

Rodriguez Barroso, L.<sup>1a</sup>, Lanzagorta Garcia, E.<sup>1b</sup>, Azaman, F.A.<sup>1c</sup>,  
Devine, D.M.<sup>1d</sup>, Lynch M.<sup>1e</sup>, Huerta, M.<sup>2f</sup>, Fournet, M.B.<sup>1g\*</sup>

<sup>1</sup>Materials Research Institute, Athlone Institute of Technology, Athlone, Ireland

<sup>2</sup>Department of Science and Technology, Linköping University, Norrköping, Sweden

\*l.rodriguez@research.ait.ie, <sup>b</sup>e.lgarcia@research.ait.ie, <sup>c</sup>f.alwani@research.ait.ie,  
<sup>d</sup>ddevine@ait.ie, <sup>e</sup>marklynch@ait.ie, <sup>f</sup>miriam.huerta@liu.se, <sup>g</sup>mfournet@ait.ie

**Keywords:** Tissue scaffolds, extracellular matrix, fibronectin, triangular silver nanoplates, local surface plasmon resonance.

**Abstract.** Tissue scaffolds can be designed to mimic the native extracellular matrix (ECM), making them attractive for the development for a range of regenerative medicine applications. The macromolecules present in the ECM are critical for the provision of structural support to surrounding cells and signalling cues for the modulation of diverse processes including cell migration, proliferation and healing activation. Here, conformational and transitional behaviour of the ubiquitous ECM protein, fibronectin (Fn), in the presence of bone tissue regeneration scaffolds and living C2C12 myoblast cells is reported. Spectral monitoring of Fn functionalised high plasmonic resonance responsive gold-edge-coated triangular silver nanoplates (AuTSNP) is used to distinguish between compact and extended fibronectin conformations. Large spectral red shifts of ~20 to ~57 nm indicate Fn unfolding and fibril formation on incubation with C2C12 cells. The label-free nature, excellent sensitivity and straightforward application of the AuTSNP within cellular environments presents them as a powerful new tool to signature protein conformational activity in living cells and monitor essential protein activity for the assisted development of improved tissue scaffolds promoting enhanced tissue repair.

### Introduction

Chitosan is a promising crustacean derivative biomaterial prepared by the deacetylation of chitin and is abundant in nature. Chitosan has excellent biodegradability, biomimetic and biocompatibility properties for tissue engineering applications and the simulation of self-healing matrices and mimetic tissue repair scaffolds [1]. Here chitosan (CS) is combined with the bone ceramic hydroxyapatite (HAp) and photocrosslinked to form an osteoconductive and osteointegrative CS-HAp bone tissue regeneration scaffold as previously reported [2].

Tissue scaffolds mimic the native extracellular matrix (ECM), this critical component controls fundamental cellular processes and provides structural support to surrounding cells. The three-dimensional structure of the macromolecules present in the ECM is essential for the delivery of signalling cues for the modulation of diverse cell behaviours including cell-cell communication and promoting tissue repair [3].

ECM proteins are implicated in cancer and have active participation in tumor progression [3]. In particular, fibronectin (Fn), a critical ECM protein whose functions are governed by its conformational activity, is receiving increasing attention due to its participation in various phases of tumor proliferation. Fn can exhibit a compact soluble formation while circulating within the bloodstream [3]. Under conditions where Fn expression is altered, it can

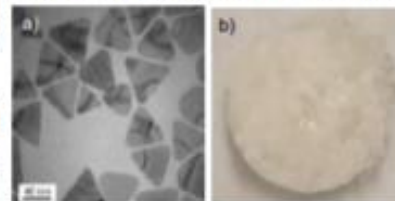


Fig. 1. (a) Transmission electron microscopy (TEM) of AuTSNP, b) CS-HAp bone tissue regeneration scaffold sample,

promote tumor cell invasion where upregulation and binding to cell-adhesion molecules and integrins, causes an activation of signaling pathways that promote tumorigenesis, metastasis and therapy resistance [3, 4]. Structurally Fn can experience conformational transitions induced by changes in the pH or temperature. Under physiological conditions (pH 7-7.4), Fn presents a folded compact shape, while at lower pH (pH 2.8- 4) it extends to enable fibril formation [5].

The potential for versatile in-situ real-time monitoring of protein activity and conformational behaviour is possible using high sensitivity localized surface plasmon resonance (LSPR) Triangular Silver Nanoplates (TSNPs) [6]. LSPR is an optical phenomenon where light interacting with nanoparticle surface electrons, observed as an extinction spectrum, exhibits measurable spectral shifts in response to surface interactions. These shifts are induced by local material and molecular interactions which alter the refractive index in the immediate vicinity of the nanoparticles [6]. This feature allows the TSNP to be used as a sensitive and straightforward tool to detect both the presence and conformation of proteins, and has previously been reported for real-time monitoring of conformational changes in Fn in the presence of live cells [7].

In this work we present the detection of conformational transitions and fibril formation activity of Fn in the presence of CS-HAP bone tissue regeneration scaffolds and C2C12 myoblast cells. Fn functionalised on to gold-edge-coated triangular silver nanoplates (AuTSNP), which exhibit some of the highest reported spectral shift responses to surface biomolecular interactions, are used to record in situ real time progression of the Fn behaviour [7].

#### Materials and Methods

High MW chitosan, fibronectin and chemicals for AuTSNP synthesis were obtained from Sigma Aldrich. C2C12 myoblast cell line was obtained from the European Collection of Authenticated Cell Cultures (ECACC). Extinction measurements were carried out using a UV-vis spectrometer (Synergy HT BioTek microplate reader). Scaffold sterilization was carried out using pulsed UV (Samtech Pulsed UV system).

##### Bone Tissue Regeneration Scaffold preparation

Chitosan- hydroxyapatite scaffolds (CS-HAP) were prepared using a previously reported novel one-step photocrosslinking reaction under the presence of UV light [2].

##### Gold-edge coated triangular silver nanoplates (AuTSNP) preparation

AuTSNP were synthesised using a previously described seed mediated approach [6]. TSNP growth was carried out by mixing 350  $\mu\text{L}$  of seed solution with ascorbic acid (AA) (75  $\mu\text{L}$ , 10mM), 4 mL of water and adding  $\text{AgNO}_3$  (3 mL, 0.5 mM) at a rate of 1 mL min<sup>-1</sup>. After synthesis, TSC (500  $\mu\text{L}$ , 25 mM) was added to the solution. Gold coating for 1 mL of TSNP solution was carried out by adding and mixing Gold (III) chloride trihydrate (20  $\mu\text{L}$ , 0.5 mM) and AA (18.9  $\mu\text{L}$ , 10 mM).

##### Protein conformational changes monitoring

Before monitoring Fn conformational changes in the presence of C2C12 myoblast cells, LSPR sensing of fibronectin activity was carried out at two different pH values (pH 7 and pH 4) to monitor and record conformational transitions of the protein in the presence of bone tissue regeneration scaffolds. After that, nanoplates were incubated with the C2C12 myoblast cell line and bone tissue regeneration scaffolds and monitored over 32 hours using UV-Vis spectrometry. Before carrying out the assays, nanoplates were coated with polyethylene glycol (PEG-Np) to provide a protective layer and minimise the direct contact between fibronectin and the nanoplates surface minimising the influence in the protein conformational behaviour [7]. PEG-Np and Fn PEG-Np, were incubated with the cells to monitor the conformational behaviour and interactions in the cellular and scaffold environments and observe any changes in cell morphology.

### Cell culture

Cells were cultured with phenol red-free supplemented DMEM (Dulbecco's Modified Eagle Medium, 10% fetal bovine serum, 5% penicillin–streptomycin, 5% L-glutamine) in a humidified atmosphere of 5% CO<sub>2</sub> at 37 °C. Cells were plated at an initial density of  $34 \times 10^4$  cells per mL in a 96 well plate and incubated for 24 h until confluence was reached. 600  $\mu$ L of PEG-Np were preincubated with 20  $\mu$ L of 1 mg/mL Fn. Before adding the nanoplates to the cells, media was changed to fresh media. Nanoplates and fibronectin-functionalised nanoplates were incubated with the cells in a PEG-Np - DMEM 1:1 ratio.

### Results and Discussion

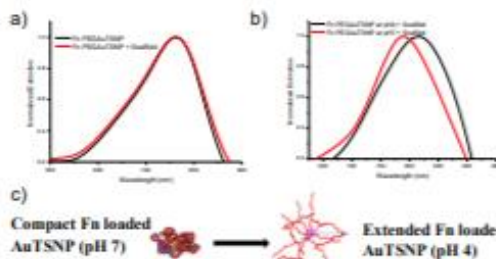


Fig. 2. a) UV-vis spectra of Fn functionalised PEG-Np with and without the presence of CS-HAp bone tissue regeneration scaffold. b) Spectral signatures of extended (black) and contracted (red) conformations of Fn at pH 4 and pH 7 respectively. c) Representation of Fn functionalised PEG-Np in compact and extended conformations.

In its contracted conformation, Fn has a hydrodynamic radius of the order of 23 nm which is exhibited when the pH is adjusted to 7. In the extended conformation at pH 4, the radius increases up to 130 nm for single Fn strands, however, it can become much larger as networks and fibrils are formed over time [7]. The LSPR extinction spectrum for Fn functionalised PEG-Np with and without the presence of CS-HAp bone tissue regeneration scaffolds is very similar indicating the strong attachment and insulating effect of the Fn on the AuTSNP surface from CS-HAp scaffold interactions. When no variation in pH is induced the LSPR spectrum shows no significant change with the LSPR<sub>max</sub> remaining constant, as shown in Fig. 2a. The minor broadening in the spectrum can be

associated with minimal interactions between the CS-HAp scaffold and the Fn functionalised PEG-Np. Upon pH adjustment from 7 to 4, the LSPR spectrum for Fn functionalised PEG-Np in the presence of the CS-HAp scaffold is observed to red shift by 27 nm, indicating the unfolding of the protein and its increased density in the vicinity of the AuTSNP (Fig. 2b) [7]. These large LSPR spectral differences distinguish between compact and extended Fn conformations due to induced refractive index changes local to the surface of the Au-TSNP. A red shift in the AuTSNP LSPR therefore provides a signature for Fn conformational transitioning from more compact to extended formats (Fig. 2c).

In order to observe Fn protein conformational transitions in the presence of CS-HAp bone tissue regeneration scaffolds and myoblast cells, Fn functionalised AuTSNP were incubated with C2C12 myoblast cells, CS-HAp scaffolds and monitored over time. Normal C2C12 myoblast morphology is shown for all treatments indicating that the AuTSNP have no observable detrimental effect on the cells (Fig 3).

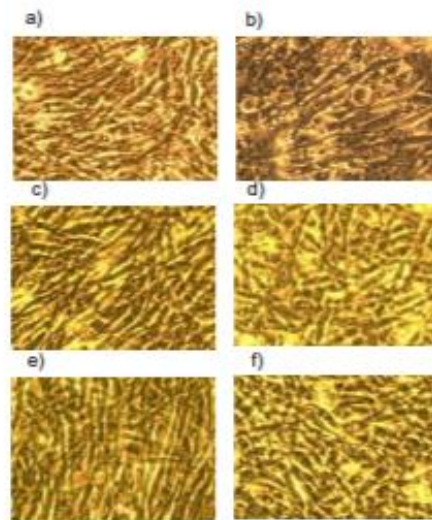


Fig. 3. Images of C2C12 cells taken after 32h of incubation with a) Fn, b) Fn and scaffold, c) Fn PEGNP, d) Fn PEGNP and scaffold, e) PEGNP, f) PEGNP and scaffold.

Fn PEG-NP in the presence of C2C12 myoblasts without the presence of the CS-HAP scaffolds, exhibit shifts of approximately  $\sim 20$  nm between 0h and 8h of incubation, while longer shifts of approximately  $\sim 57$  and  $\sim 50$  nm were measured from 24 h, as shown in figure 4 a). This can be associated with the expected increased unfolding and extension activity and the progressive fibrillar organization of the Fn within the cellular environment [8]. This is in keeping with reported evolution of Fn fibril formation at time points between 24h and 48h [9].

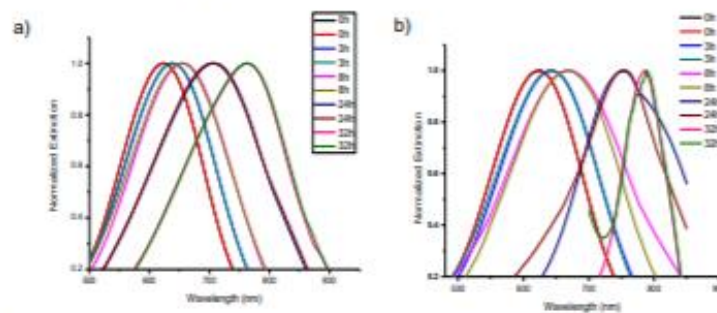


Fig. 4. LSPR spectra of a) Fn functionalised PEG-Np incubated with C2C12 over 32 hours, b) Fn PEG-Np incubated with C2C12 and tissue scaffolds over 32 hours.

The on-scaffold cellular incubated Fn-PEG-NP exhibited a similar behaviour with strong red shifts recorded overtime (Fig. 4b). These results correlate with the most recent models on Fn conformational activity within the cellular environment demonstrating the potential of the functionalised AuTSNP to detect dynamic protein conformational behaviour in living cells. Furthermore, this capacity to readily monitor critical on-scaffold protein behaviour has the potential to provide an essential tool for the development of advanced ECM mimetic tissue scaffolds for regenerative medicine applications.

### Conclusion

High sensitive LSPR Fn functionalised AuTSNP were used to monitor the conformation transitions of the ubiquitous ECM protein, Fn, in the presence of C2C12 myoblast cells. The conformational profile of Fn was investigated in a cellular environment with and without the presence of CS-HAp bone tissue regeneration scaffolds over time from 0 to 32h. As Fn unfolds from a compact conformation to form fibrils in which Fn displays a highly extended conformation, LSPR spectra exhibit large red shift shifts of ~20 nm generated over 32 hours. These results correlate directly with the most recent models on Fn conformational activity within the cellular environment, demonstrating the potential of the AuTSNP to provide critical detailed information on dynamic protein conformational response and behaviour. This highlights the capacity of the AuTSNP LSPR technique for straightforward, versatile non-labelling measurements of protein conformational dynamics in the high noise cellular environment and potential application in the development of advanced tissue scaffolds with improved regenerative and repair performance.



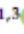
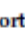
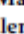

### References

- [1] Abdel-Fattah, W. I. et al. (2007) 'Synthesis, characterization of chitosans and fabrication of sintered chitosan microsphere matrices for bone tissue engineering', *Acta Biomaterialia*, 3(4), pp. 503–514. doi: 10.1016/j.actbio.2006.12.004.
- [2] Devine, D. M., Hctor, E., Hayes, J. S., Sheehan, E. & Evans, C. H. (2018) Extended release of proteins following encapsulation in hydroxyapatite/chitosan composite scaffolds for bone tissue engineering applications. *Mater. Sci. Eng. C* 84, 281–289.
- [3] Wang, J., & Hielscher, A. (2017). Fibronectin: How Its Aberrant Expression in Tumors May Improve Therapeutic Targeting. *Journal Of Cancer*, 8(4), 674-682. doi: 10.7150/jca.16901
- [4] Pankov, R., & Yamada, K. (2002). Fibronectin at a glance. *Journal Of Cell Science*, 115(20), 3861-3863. doi: 10.1242/jcs.00059
- [5] Tooney, N. M., Mosesson, M. W., Amrani, D. L., Hainfeld, J. F., & Wall, J. S. (1983). Solution and surface effects on plasma fibronectin structure. *The Journal of cell biology*, 97(6), 1686–1692. doi:10.1083/jcb.97.6.1686
- [6] Zhang, Y., Charles, D. E., Ledwith, D. M., Aherne D., Cunningham, S., Voisin, M., Blau, W. J., Gun'ko, Y. K., Kelly, J. M. & Brennan-Fournet, M. E. (2014) Wash-free highly sensitive detection of C-reactive protein using gold derivatized triangular silver nanoplates. *Royal Society of Chemistry*, 4, 29022-29031. Doi: 10.1039/c4ra04958f
- [7] Brennan-Fournet, M. E., Huerta, M., Zhang, Y., Malliaras, G. & Owens, R. M. (2015) Detection of fibronectin conformational changes in the extracellular matrix of live cells using plasmonic nanoplates. *J. Mater. Chem. B* 3, 9140–9147.
- [8] Rozario, T., Dzamba, B., Weber, G. F., Davidson, L. A., & DeSimone, D. W. (2009). The physical state of fibronectin matrix differentially regulates morphogenetic movements in vivo. *Developmental biology*, 327(2), 386–398. doi:10.1016/j.ydbio.2008.12.025
- [9] Antia, M., Baneyx, G., Kubow, K. and Vogel, V. (2008). Fibronectin in aging extracellular matrix fibrils is progressively unfolded by cells and elicits an enhanced rigidity response. *Faraday Discussions*, 139, p.229.



Article

# Biodegradation and Antimicrobial Properties of Zinc Oxide–Polymer Composite Materials for Urinary Stent Applications

Chaitra Venkatesh <sup>1,†</sup>, Marco Laurenti <sup>2,†</sup>, Marina Bandeira <sup>1,3</sup>, Eduardo Lanzagorta <sup>1</sup>, Lorenzo Lucherini <sup>2,4</sup>, Valentina Cauda <sup>2,\*</sup> and Declan M. Devine <sup>1</sup>

<sup>1</sup> Material Research Institute, Athlone Institute of Technology, Athlone, N37 HD68 Co. Westmeath, Ireland; c.venkatesh@research.ait.ie (C.V.); m.bandeira@research.ait.ie (M.B.); e.lgarcia@research.ait.ie (E.L.); ddevine@ait.ie (D.M.D.)

<sup>2</sup> Department of Applied Science and Technology, Politecnico di Torino, C.so Duca degli Abruzzi 24, 10129 Turin, Italy; marco.laurenti@polito.it (M.L.); lucherini.lorenzo@gmail.com (L.L.)

<sup>3</sup> Rua Francisco Getúlio Vargas, Universidade de Caxias do Sul, 1130, Caxias do Sul 95070-560, RS, Brazil

<sup>4</sup> Soil Mechanics Laboratory (LMS), École Polytechnique Fédérale de Lausanne (EPFL), Station 18, CH-1015 Lausanne, Switzerland

\* Correspondence: valentina.cauda@polito.it; Tel: +39-11-0907389

† These authors contributed equally to this work.

Received: 5 October 2020; Accepted: 18 October 2020; Published: 20 October 2020



**Abstract:** Research advancements in the field of urinary stents have mainly been in the selection of materials and coatings to address commonly faced problems of encrustation and bacterial adhesion. In this study, polylactic acid (PLA) and polypropylene (PP) were evaluated with zinc oxide (ZnO) coating to assess its ability to reduce or eliminate the problems of encrustation and bacteria adhesion. PLA and PP films were prepared via twin screw extrusion. ZnO microparticles were prepared using sol-gel hydrothermal synthesis. The as-prepared ZnO microparticles were combined in the form of a functional coating and deposited on both polymer substrates using a doctor blade technique. The ZnO-coated PP and PLA samples as well as their uncoated counterparts were characterized from the physicochemical standpoints, antibacterial and biodegradation properties. The results demonstrated that both the polymers preserved their mechanical and thermal properties after coating with ZnO, which showed a better adhesion on PLA than on PP. Moreover, the ZnO coating successfully enhanced the antibacterial properties with respect to bare PP/PLA substrates. All the samples were investigated after immersion in simulated body fluid and artificial urine. The ZnO layer was completely degraded following 21 days immersion in artificial urine irrespective of the substrate, with encrustations more evident in PP and ZnO-coated PP films than PLA and ZnO-coated PLA films. Overall, the addition of ZnO coating on PLA displayed better adhesion, antibacterial activity and delayed the deposition of encrustations in comparison to PP substrates.

**Keywords:** polylactic acid (PLA); polypropylene (PP); zinc oxide; antibacterial coatings; ureteral stents; bacteria biofilm; urine-derived encrustations

## 1. Introduction

Urinary stents are commonly used to drain retained urine after surgical procedures, in cases of urinary incontinence and in related issues to the urinary tract [1–3]. Although many improvements have been achieved so far, patients still face complications related to the insertion of urinary stents, especially when long-term usage is required. The main problems encountered in commercial urinary stents are friction, the release of substances, encrustation and bacterial adhesion that can cause adverse

effects to the patient, such as inflammation [1,4–6]. To date, work is still in progress on the development of a biocompatible, antimicrobial, antifouling and nonfrictional material potentially used for urinary stents to improve patients' quality of life by reducing the chances of postprocedure complications as well as to increase the lifetime of the stent [7–9].

Different materials have been employed to develop urinary stents. However, polymer-based materials are the most used due to their biocompatibility, biological inertness and low cost [7,10]. Moreover, several coatings technologies have been shown to improve biocompatibility, antimicrobial action and prevent encrustation, illustrating the potential of coatings to enhance the functionality of urinary stents [2,8,9,11] and even promoting the sustained delivery of pharmaceutically active compounds [12]. For example, antibiotics coatings were able to prevent biofilm formation and bacterial infections. However, many issues related to antibiotic resistance have been addressed, showing the loss of antimicrobial action after a few usages [8,13].

In this study, the performance of polylactic acid (PLA) and polypropylene (PP) as a material for urinary stents were evaluated. PLA is the most widely used aliphatic thermoplastic polymer. It is obtained from renewable agricultural resources such as starch from rice, corn, potatoes, beetroot, etc. and is used in various medical applications such as sutures, dermal fillers or stents [14]. PLA has been studied as a coating layer for antimicrobial applications by incorporation of nanoparticles such as silver [15], zinc oxide (ZnO) nanoparticles [16] or ZnO deposition on halloysite nanotubes and further incorporation into PLA [17]. PLA-ZnO nanocomposites have been produced by the method of melt compounding, and the resultant films were found to be amorphous and had antibacterial properties [18,19] and degradation process of the PLA was increased [20].

PP is a polymer from the family of polyolefins that has features such as low density, chemical inertness, and high melting temperature. Due to its high temperature resistance, it is used in various products in clinical environments [21]. It has been used for stenting in endoscopic dacryocystorhinostomy with successful and higher anatomic and functional efficacy [22,23]. Due to its excellent histocompatibility PP mesh has been studied as suitable stent material for airway strictures [24] and PP-silicone stent has been successfully evaluated for the treatment of benign esophageal strictures [25]. In order to enhance the properties of PP, different methodologies have been tested including reports by Zhao et al. who investigated the photodegradation resistance of PP to UV-irradiation by incorporation of ZnO and found significant improvements [26]. PP has been modified with ZnO to produce hybrid filter material and found to have high filtration efficiency [27]. Bojarska et al. investigated PP capillary membranes which were modified by ZnO nanowires. The use of plasma was found to improve the adhesion of ZnO nanowires on the PP membrane surface. Moreover, the resulting PP/ZnO membranes exhibited antibacterial properties against Gram-positive and Gram-negative bacteria [28].

This work aims to evaluate the use of ZnO as a novel coating material for the manufacturing of urinary stents. In particular, to achieve a material with superior antimicrobial property, both PLA and PP films were coated with a functional ZnO layer, as zinc oxide is well known for its antimicrobial action against both Gram-positive and Gram-negative bacteria [29,30]. Briefly, the mechanism of antimicrobial action involves the release of zinc ions, production of reactive oxygen species (ROS) and direct contact with the bacteria cell surface causing the rupture of the membrane and changes on the cell metabolism that can lead to cell death [31–34]. Thus, this research focused on the evaluation of the physical and mechanical properties, antimicrobial activity and adhesion of the zinc oxide coatings on PLA and PP substrates for urinary stents application. In particular, we show a different capability of these materials to react to artificial urine solution and another simulated physiological solution, which has a similar inorganic composition of the human plasma. The results indeed show that the behaviour of these ZnO-coated polymers can be efficiently modulated to get highly hydrophilic and biodegradable devices with further antimicrobial properties in the right urinary environment.

## 2. Materials and Methods

### 2.1. Preparation of PLA and PP Films

Poly(lactic acid) (PLA) obtained from Corbion, PLA LX175 (Total Corbion, Gorinchem, The Netherlands) and polypropylene (PP, Sigma Aldrich Ireland Ltd., Wicklow, Ireland) were used to produce the polymeric substrates. The PLA had a molecular weight ( $M_w$ ) of 24,000 g/mol and PP was isotactic with average  $M_w$  of ~250,000 g/mol. Both polymers were received in granular form.

Twin-screw extrusion was employed to process PLA and PP into films. Extrusion was performed by using an APV (Model MP19TC (35:1) APV Baker, Newcastle-under-Lyme, UK) twin-screw compounder with 19 mm diameter screws. The temperature profile was maintained (from die to feeder) at 200/190/180/170/160/110/50 °C. PLA was dried in the oven at 80 °C for 4 h. The dried PLA pellets were fed into the hopper of the extruder and extruded at a screw speed of 140 rpm. Extruded strands of the molten composite were then drawn through a three-roll calendar creating continuous films. Similarly, the PP pellets were processed by melt compounding under similar conditions for comparison. These films were used to punch out ASTM standard tensile test specimens by a physical punching process.

### 2.2. Synthesis of ZnO Microparticles

Zinc oxide microparticles were prepared via a sol-gel hydrothermal synthesis method as previously reported [35,36], using potassium hydroxide (KOH, Sigma Aldrich, Darmstadt, Germany) and zinc nitrate hexahydrate ( $Zn(NO_3)_2 \cdot 6H_2O$ , Sigma Aldrich) as precursors. All reagents were used as received. First, 5.58 g of potassium hydroxide and 14.8 g of zinc nitrate hexahydrate were dissolved separately in 100 mL of double-distilled water at room temperature. Afterwards, the zinc nitrate solution was added dropwise to the KOH solution under vigorous magnetic stirring conditions. The formed gel was treated at 70 °C for 4 h. Later, the precipitated ZnO powder was filtered from the basic solution and washed several times with demineralized water until pH neutralization and air dried in a muffle furnace at 60 °C overnight.

### 2.3. Deposition of ZnO Coating on Polymeric Substrates

Different methods were considered to coat PLA and PP substrates. First, a ZnO paste was prepared by adding zinc oxide powders in a 1:2 (*w/v*) ratio to a solution of acetic acid (1%, Sigma Aldrich), ethanol (67%, Sigma Aldrich) and water (33%). The paste was then stirred and sonicated to obtain a homogeneous dispersion of the particles. The prepared paste was deposited on the surface of both PP and PLA films using the doctor blade technique on a glass slide to obtain a uniform layer. Sodium hydroxide (Sigma Aldrich) and benzophenone (BP) (Sigma Aldrich) were also used for surface activation and grafting of the ZnO coatings to the polymer supports.

In this study three methods were employed:

1. For method 1, the coated PLA was thermally treated at 50 °C for 30 min and 60 °C for 15 min while coated PP films were treated at 70 °C for 15 min.
2. In method 2, ZnO paste was UV grafted onto the PLA substrate using the protocol developed by Shin et al. [37] with adaptations. For this, 20 mL of 10 wt.% acrylic acid aqueous solution was added to 20 mL of benzophenone 0.2 M and stirred under dark conditions. Then, ZnO paste containing 1 g of ZnO was added to the previous solution and stirred for 30 min in the absence of light. The final solution was poured in a glass petri dish containing the PLA films and exposed to UV light for five minutes at 40 W. After curing, samples were neutralized by immersion in a sodium bicarbonate (Sigma Aldrich) 0.1 M solution for 10 min, rinsed with distilled water and dried overnight at 40 °C.
3. In method 3, 1 g of ZnO powder was dispersed in 2 mL of ethanol and sonicated for 15 min. Different amounts of benzophenone 0.2 M ethanolic solution (0, 0.25 and 0.50 mL) were then

added to this solution and stirred until the solution became homogeneous. Then, PP and PLA were coated with ZnO + BP solution and exposed to UV light (0, 5 and 10 min), dried for 1 h at 37 °C and rinsed with water for removing excess reagents. All samples were dried overnight at 37 °C prior to analysis. For this method, PP was previously treated with a 0.1 M sodium hydroxide solution for 18 h for surface activation while PLA did not have any previous treatment.

Only the coatings produced using method 3 with 0.50 mL of BP and 5 min of UV treatment for PLA films and 0.50 mL of BP and no UV treatment for PP films showed good adhesion of the coatings (data not shown). Thus, only these set of samples (named ZnO@PP and ZnO@PLA) were fully characterized in this work.

#### 2.4. Characterization Setup

##### 2.4.1. Physicochemical Characterization

The morphology and chemical composition of the samples were investigated by means of field-emission scanning electron microscopy (FESEM, Merlin Carl Zeiss AG, Oberkochen, Germany) coupled with an energy dispersive x-ray (EDX) detector for chemical composition analyses. Before FESEM imaging, the surface of the samples was coated with a 5 nm-thick Pt coating. The crystalline structure was investigated with X-ray diffraction (XRD) using a Panalytical X'Pert PRO diffractometer (Malvern Panalytical S.r.l., Milan, Italy) in Bragg-Brentano configuration and equipped with a Cu K $\alpha$  monochromatic radiation ( $\lambda = 1.54059 \text{ \AA}$ ) as X-ray source. Fourier transform infrared spectroscopy (FTIR) in attenuated total reflectance (ATR) mode was performed with a Nicolet 5700 FTIR spectrometer (ThermoFisher, Waltham, MA, USA) equipped with diamond crystal. The ATR-IR spectra were background subtracted and acquired with  $2 \text{ cm}^{-1}$  resolution and 64 scans accumulation. Indexing of IR modes have been done according to Socrates [38].

Mechanical properties of the PLA and PP films were characterized by tensile tests, probing each different blend. Tensile testing was carried out on a Lloyd Lr10k tensometer (Ametek Ltd, West Sussex, UK) using a 2.5 kN load cell on ASTM standard test specimens at a strain rate of 50 mm/min. Data was recorded using Nexygen™ software (Ametek Ltd.). The tensile tests were carried out in adherence to ASTM D 882. Ten individual test specimens were analysed per group and before testing, the thickness of each sample was measured. The percentage strain at maximum load, stress at maximum load, stiffness, and Young's modulus of each sample were recorded.

The surface wettability of the composites was assessed using First Ten Angstroms' FTA32 goniometer (FTA Europe, Cambridge, UK). In this test, the sessile drop contact angle technique was utilized with distilled water as the probe liquid. Five measurements at various places on the films were taken.

Differential scanning calorimetry (DSC) was carried out using a DSC 2920 modulated DSC (TA Instruments, New Castle, DE, USA) with a nitrogen flow rate of 20 mL/min to prevent oxidation. Calibration of the instrument was performed using indium as standard. Test specimens weighing between 8 mg and 12 mg were measured on Sartorius scales (MC 210 P, Sartorius Lab Instruments GmbH & Co. KG, Goettingen, Germany), capable of being read to five decimal places. Samples were crimped in nonperforated aluminium pans, with an empty crimped aluminium pan used as the reference. The thermal history was removed by heating samples from 20 to 220 °C at the rate of 30 °C/min and then held isothermally at 220 °C for 10 min. The samples were then cooled down from 220 to 20 °C at 30 °C/min. Finally, the thermal properties of the samples were recorded by heating the samples from 20 to 220 °C at the rate of 10 °C/min, glass transition temperature, and melting temperature of each sample were recorded.

##### 2.4.2. Biodegradation Essays

Simulated body fluid (SBF) was prepared according to the method described by Kokubo and Takadama [39] with a final pH of 7.45. ZnO-coated PLA and PP films were then placed in the SBF

solution in a water bath at  $36.5 \pm 1$  °C. The SBF solution was replaced every two days and the adhesion of the films in SBF solution was monitored for seven days.

The artificial urine was prepared following the protocol described by Sarangapani et al. [40]. The solution was constituted basically by salts, urea ( $25 \text{ g}\cdot\text{L}^{-1}$ ) and creatinine ( $1.10 \text{ g}\cdot\text{L}^{-1}$ ). The final pH of the solution was 5.7. ZnO-coated films were placed in the artificial urine solution, which was kept at  $36.5 \pm 1$  °C, and monitored for 21 days regarding the adhesion and appearance of encrustation. Uncoated PLA and PP films were also placed in artificial urine for the same soaking time and used as control samples.

#### 2.4.3. Antibacterial Tests

The antimicrobial tests were performed using *Staphylococcus aureus* ATCC25923 (*S. aureus*) and *Escherichia coli* ATCC25922 (*E. coli*), tryptone soy broth (TSB, Neogen) and resazurin (Sigma Aldrich). *S. aureus* and *E. coli* were cultured and grown in an exponential phase in TSB medium at 37 °C. Bacterial cell viability when exposed to different polymer films was analysed in a 12-well plate according to the resazurin cell viability assay. Resazurin indicates cell viability by changing the solution colour from blue to pink when it is chemically reduced to resofurin due to the aerobic respiration that occurs with cell growth. Thus, the reduction of the dye is proportional to the viable cells present in the solution. Overnight cultures of the two bacteria strains were diluted to a concentration of approximately  $1.0 \times 10^4$  colony formation unit per millilitre (CFU·mL<sup>-1</sup>). Then, 500 µL of TSB and 25 µL of the diluted bacteria were added in each well. After this procedure, coated (10 mm × 10 mm) and noncoated polymer films were placed in the respective wells. A negative control without bacteria (500 µL of TSB) and positive control with live cells (500 µL of TSB and 25 µL of diluted bacteria solution) were also included in each plate. After overnight incubation at 37 °C, 75 µL of resazurin was added in every well, mixed thoroughly and incubated for 2 h at 37 °C under dark conditions. Then, the colour change of the solution and, consequently, the cell viability was evaluated by absorbance measurement at 600 nm in an ultraviolet-visible (UV-Vis) plate reader (Jenway 6300, Staffordshire, UK). The experiment was performed in triplicate and repeated independently three times.

#### 2.4.4. Statistical Analysis

Statistical analysis of the tensile test results, DSC measurements and the surface wettability measurements were carried out using general linear model (GLM) of two-way ANOVA in Minitab 17 Statistical Software (Minitab Ltd., Coventry, UK). All the values were considered at a 95% confidence interval, and *p*-values are considered significant when  $p \leq 0.05$ .

### 3. Results and Discussion

#### 3.1. Morphological, Structural and Chemical Characterization

Figures 1–3 show the FESEM images and EDX spectra of ZnO-coated PLA and PP substrates (ZnO@PLA and ZnO@PP). It can be observed that ZnO microparticles showing a flower-like morphology (Figure 2) have been successfully deposited atop of both the polymer surface types. Their presence is further corroborated by the detection of Zn traces by EDX analyses. The covering of the PLA substrate is superior with respect to the PP one. This is visible from the comparison of the FESEM images and of the semiquantitative analysis obtained by EDX spectroscopy. Actually, the Zn at.% changes from 31.90% for PLA support to 9.76% for PP, suggesting that ZnO is more abundant on PLA than on PP films.

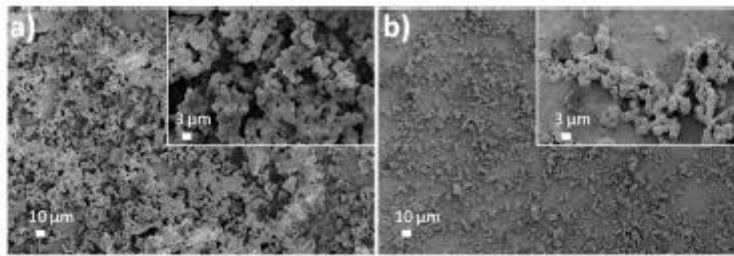


**Figure 1.** Field-emission scanning electron microscope (FESEM) images of ZnO microparticle coatings deposited on (a) polylactic acid (PLA) and (b) polypropylene (PP) polymeric supports.

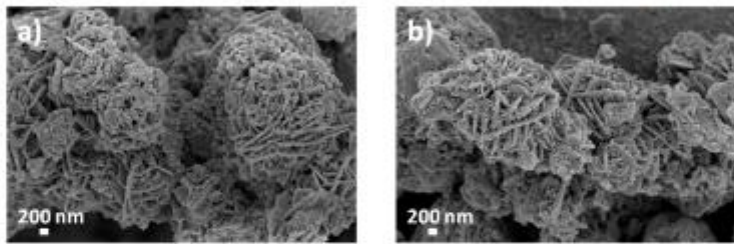


**Figure 2.** FESEM images showing the flower-like morphology of ZnO microparticle coatings deposited on (a) PLA and (b) PP polymeric supports.

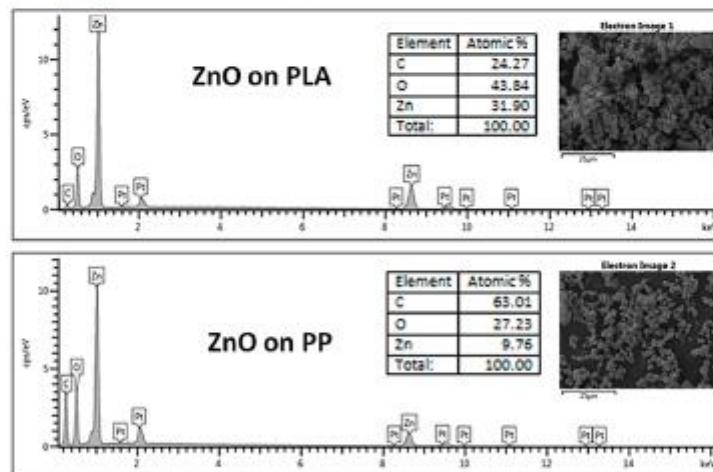


**Figure 3.** Energy dispersive X-ray (EDX) spectra of ZnO-coated PLA and PP supports.

Independently of the polymer, the presence of the ZnO coating after the fabrication process was confirmed also by the detection of the diffraction peaks belonging to wurtzite ZnO phase (Figure 4). The main ones are positioned at  $31.8^\circ$ ,  $34.4^\circ$  and  $36.2^\circ$ , and are ascribed to (100), (002) and (101) crystallographic planes according to the Joint Committee on Powder Diffraction Standards—International Centre for Diffraction Data (JCPDS-ICDD) database (Card No. 89-1397). Other minor reflections coming from additional crystal planes are also visible at higher  $2\theta$  angles.

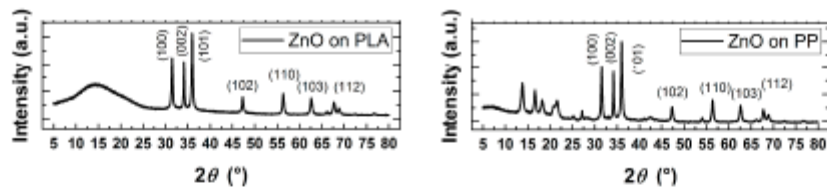


Figure 4. X-ray diffraction (XRD) pattern of sample ZnO@PLA and ZnO@PP.

Figure 5 shows the ATR-IR spectra for uncoated PLA and PP substrates as well as from the corresponding samples coated with ZnO microparticle film. The main IR modes are in the range  $3000\text{--}2900\text{ cm}^{-1}$  and near  $1450\text{ cm}^{-1}$  (both related to the C-H stretching/bending vibrations), at about  $1750\text{ cm}^{-1}$  (C=O stretching vibration), in the range  $1200\text{--}1150\text{ cm}^{-1}$  (C-O symm. stretch.) and three bands in the range  $1130\text{--}1040\text{ cm}^{-1}$  due to C-O-C symmetric stretching. These prominent modes of the spectrum are the characteristic peaks of PLA and PP [14,26,27]. When the ZnO microparticle coating is present, it is possible to observe a general reduction in intensity of the bands related to the polymeric materials underneath the ZnO materials. This effect is due to the micrometer thickness of the ZnO layer coating (more or less uniformly) the polymer. An additional broad band corresponding to H-O-H vibration of the ZnO hydrophilic surface is noticed in the range  $3500\text{--}3000\text{ cm}^{-1}$  for both kinds of ZnO-coated polymers. The presence of the ZnO coating is further confirmed by the presence of a broad band in the range  $950\text{--}850\text{ cm}^{-1}$  and due to Zn-OH mode. Similar presence of clear peak in the range  $400\text{--}700\text{ cm}^{-1}$  in PP/ZnO spectrum and absence in PP spectrum was observed in the study of ZnO nanowire growth via plasma activation by Bojarska et al. which could indicate the presence of zinc oxide [28].

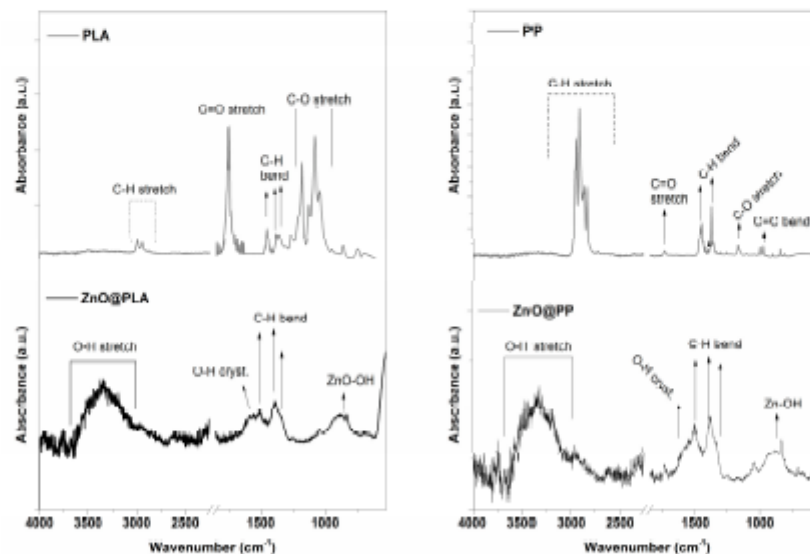
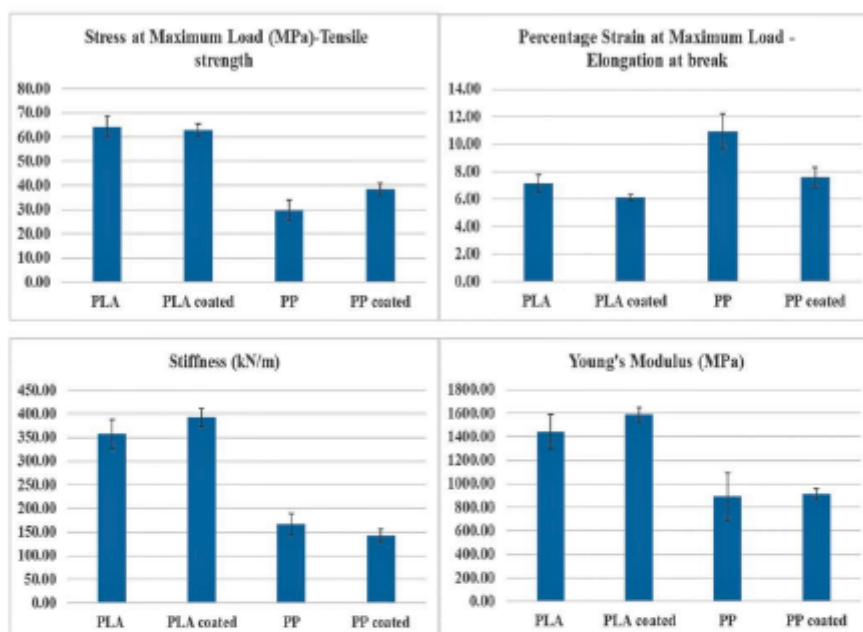


Figure 5. ATR-IR spectra of PLA and PP supports, with or without the presence of the ZnO coating.

### 3.2. Tensile Testing

The mechanical behaviour of PLA and PP polymers are analysed with and without the presence of the ZnO coating. The graphical representation of the mechanical properties are shown in Figure 6. In case of PLA and ZnO@PLA samples, no significant difference in the tensile strength, elongation at break, stiffness or Young's modulus ( $p \geq 0.05$ ) are observed. Similar results are obtained for PP and

ZnO@PP samples. This could be because the ZnO particles film is deposited on the polymer surface, which does not have any impact on the bulk polymer properties. However, various studies have shown a significant difference in mechanical properties when ZnO nanoparticles (NPs) are encapsulated into the polymer matrix [17,18,41–43].



**Figure 6.** Graphical representation of the mechanical properties of the polymers with and without ZnO coating. There is no significant difference between the coated samples (ZnO@PLA ZnO@PP) and their uncoated counterpart samples.

### 3.3. Surface Wettability

The surface wettability properties of all the coated and noncoated samples are shown in Figure 7. It was observed that there is a significant decrease in the contact angle of ZnO@PLA and ZnO@PP samples ( $p = 1 \times 10^{-3}$ ) when compared to bare PLA and PP substrates. The photomicrographs of the uncoated PLA surface has a contact angle of  $66^\circ$ , whereas a contact angle of  $24.07^\circ$  is achieved for the sample ZnO@PLA. The images of the uncoated PP has a contact angle of  $90.62^\circ$ , and ZnO@PP has a contact angle of  $44.55^\circ$ . With PP being hydrophobic and PLA being relatively hydrophobic, these results indicate that the presence of the ZnO coating increased the hydrophilicity of the surface. A similar reduction in contact angle values was observed when PLA films were surface-modified and bulk-modified by plasma polymerization/sputtering technique, where glycerol and ethylene glycol were used as additives [15]. In another work, PP film was treated by plasma discharge in order to enhance the surface wettability of PP and improve the adhesion of ZnO NPs [27].

### 3.4. Differential Scanning Calorimetry (DSC)

The thermal characteristics of the samples were analysed by DSC. The thermographs of the PLA, ZnO@PLA, PP and ZnO@PP samples are as shown in Figure 8. From the analysis of the thermographs, there is no evident difference between the coated and noncoated samples. However, in a study by Pantani et al. [18] the cold crystallization and melting temperature increased as ZnO NPs were incorporated into the PLA matrix by twin screw extrusion [18]. This confirms that the surface ZnO



coating of our work did not affect the bulk properties of the considered polymers, corroborating with the tensile test results.

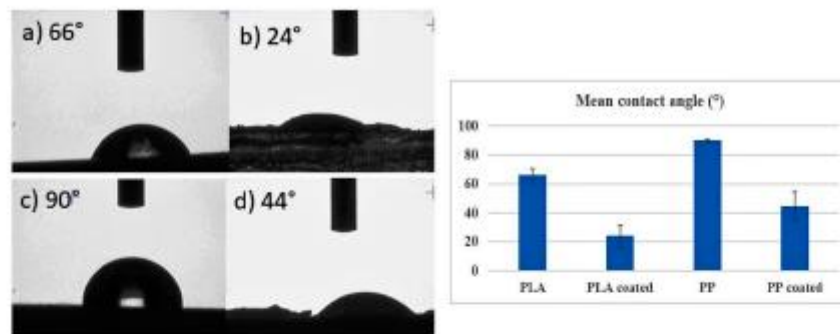


**Figure 7.** Surface wettability properties of the polymers with and without ZnO coating. With a  $p$ -value of 0.001, there is a significant decrease in the contact angle of ZnO@PLA and ZnO@PP when compared to the uncoated PLA and PP films. Water droplet on the surface of (a) PLA film, (b) ZnO@PLA, (c) PP film, and (d) ZnO@PP.

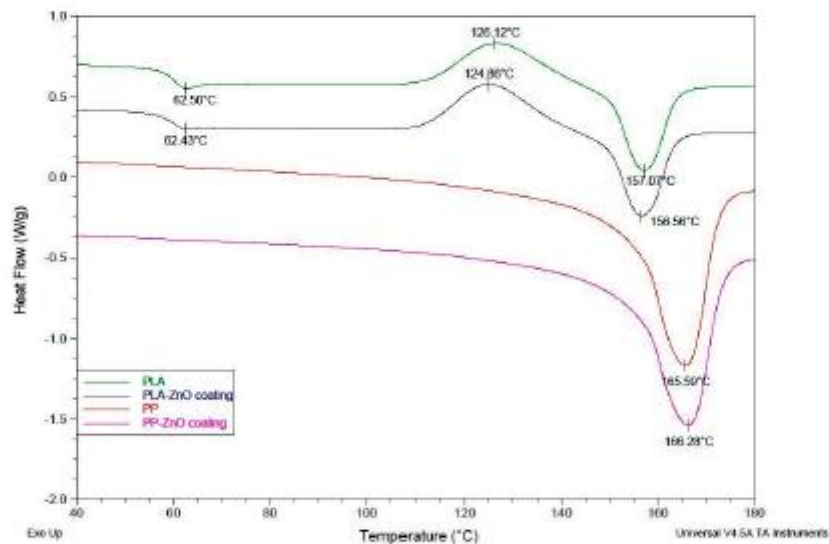


**Figure 8.** DSC thermographs of the PLA, ZnO@PLA, PP and ZnO@PP coated samples. No significant difference was observed between the coated and uncoated samples considering a  $p$ -value < 0.05.

### 3.5. Evaluation of the Biodegradation Properties in Biological Fluids

#### 3.5.1. Simulated Body Fluid (SBF)

ZnO@PLA and ZnO@PP samples were immersed in simulated body fluid (SBF) solution to test the adhesion of the ZnO coating to the polymer substrate. Figure 9 shows the pictures of ZnO@PLA and ZnO@PP samples after immersion in this solution for up to seven days. In the case of the PP substrate, the ZnO coating showed a considerable detachment after 2 h in contact with the SBF solution. However, no major changes occurred from 2 h to seven days. Interestingly, no significant alterations

were observed for ZnO@PLA samples over time, which indicates a higher adhesion of the ZnO coating to the PLA substrate in comparison to the PP one and well agrees with the results shown in Figure 1.

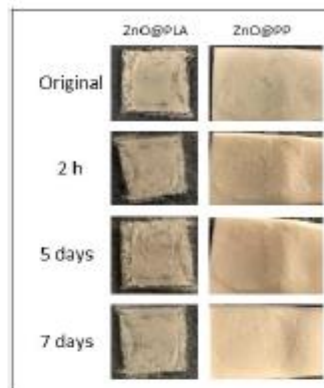


Figure 9. ZnO@PLA and ZnO@PP samples after different time intervals in SBF solution.

FESEM images reported in Figure 10a,c highlights that no visible changes in the morphology of the samples are present. The ZnO coating did not detach completely from the polymer supports and the flower-like ZnO microparticles preserve the original morphology. The presence of the ZnO coating is further confirmed by EDX measurements (Figure 10b,d). The compositional analyses also reveal the presence of P, Ca, Cl and Na, which are due to the prolonged contact of the samples with SBF solution. In particular, the abundance of Ca (around 1.9 at%) and P (around 2–3 at%) with respect to the other elements suggests the formation/precipitation of calcium phosphate compounds. This aspect is further supported by the IR spectroscopy results discussed in the following.

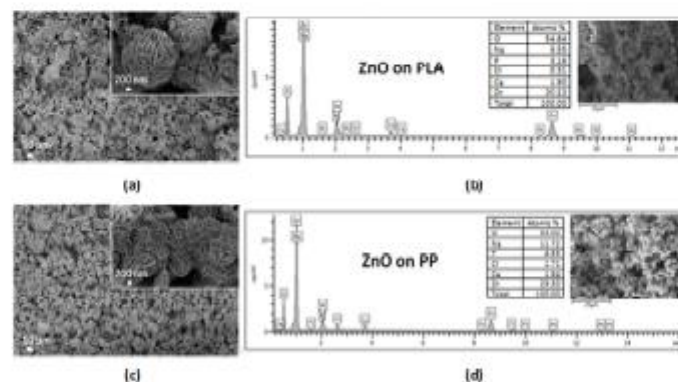
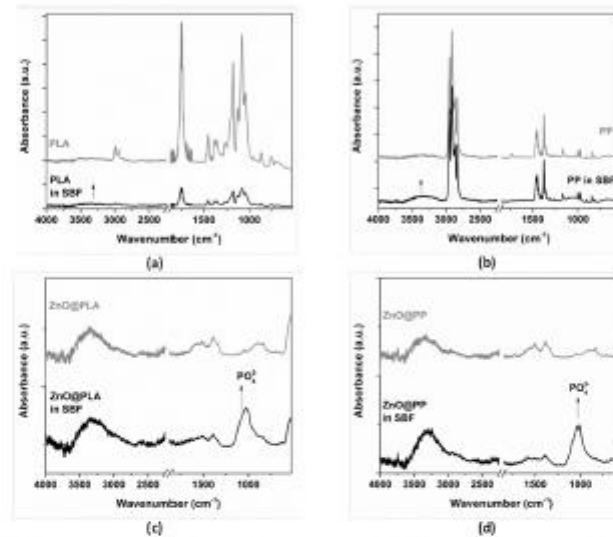


Figure 10. ZnO-coated PLA and PP supports soaked in SBF for 14 days: (a,c) FESEM images and (b,d) EDX spectra.

Figure 11 shows the IR spectra acquired after soaking all the sample typologies in SBF for 14 days. Panels a and b refer to the polymer substrates (PP and PLA) while panels c and d show the IR spectra acquired on ZnO@PLA and ZnO@PP samples, respectively. Considering the PLA and PP substrates, no changes are visible when compared to nonsoaked samples. This is likely related to the hydrophobic nature of the uncoated substrates. However, in the presence of the ZnO coating, a relatively intense band in the range  $1100\text{--}1000\text{ cm}^{-1}$  is observed due to the phosphate ( $\text{PO}_4^{3-}$ ) vibration modes (Figure 11c,d). This is due to the interaction between the ZnO surface and phosphate

groups present in SBF solution, which favours the formation of zinc phosphate and calcium phosphate compounds [44,45]. This aspect was also underlined by the corresponding EDX results of Figure 10. This indicates that the presence of the ZnO coating would allow for a more reactive surface able to induce the precipitation of an apatite-like functional layer. In general, an increase of the OH band intensity in the range  $3500\text{--}3000\text{ cm}^{-1}$  is observed, irrespectively of the presence of ZnO and due to the adsorption of water after the prolonged contact with SBF solution.



**Figure 11.** ATR-IR spectra of the samples after soaking in SBF for 14 days: (a) only PLA; (b) only PP; (c) ZnO@PLA; (d) ZnO@PP.

The XRD patterns of Figure 12a still show the presence of diffraction peaks belonging to wurtzite ZnO phase (indicated by arrows) and further witness the presence of the ZnO coating at the end of the biodegradation experiment in SBF.

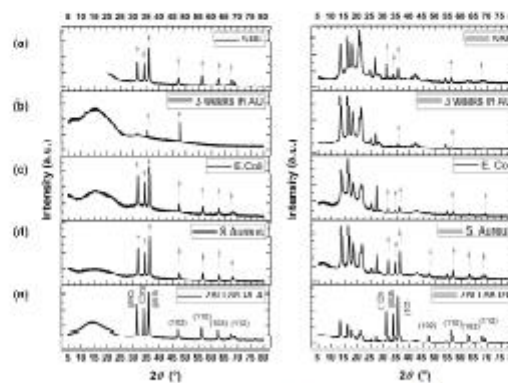


**Figure 12.** XRD pattern of samples ZnO@PLA and ZnO@PP: (a) after soaking in simulated body fluid solution for 14 days; (b) after immersion in artificial urine for 21 days; (c,d) at the end of the antimicrobial tests. XRD pattern of ZnO@PP and ZnO@PLA samples are also shown as reference in panel (e). Arrows indicate reflections coming from wurtzite ZnO phase.

### 3.5.2. Artificial Urine

When testing the coated polymer samples in artificial urine, a strikingly different behaviour was observed if compared to the SBF solution. As seen in Figure 13, ZnO@PLA samples show a considerable detachment of the ZnO layer after two days of immersion in artificial urine and a complete dissolution was observed after five days. Although the ZnO coatings on the PP supports are less uniform than on PLA, a slower dissolution was noticed when in contact with artificial urine. This might be related to the higher hydrophobicity of PP coated films that interact less with the solution in comparison to PLA films, as seen from the surface wettability analysis discussed in Section 3.3. Independently of the polymeric support, it can be noticed that the ZnO coating dissolved and/or detached faster in artificial urine than in SBF solution. This interesting feature can actually witness the fair tunability of our coated polymers, which selectively react differently upon the medium where they are immersed.

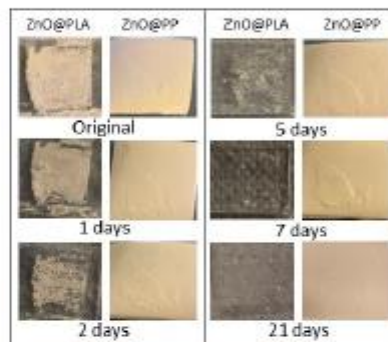


Figure 13. ZnO@PLA and ZnO@PP samples after different time intervals in artificial urine solution.

The biodegradation behaviour of ZnO@PLA and ZnO@PP samples was also evaluated in artificial urine solution for long time periods (21 days). Similarly, uncoated PLA and PP substrates were tested in the same experimental conditions, in order to evaluate any ability of ZnO to prevent the formation of encrustations in an artificial urine environment. If the uncoated PP and PLA supports are considered, the presence of precipitates with different morphologies and shapes can be observed (Figures 14 and 15): tabular-acicular surfaces, sheetlike, globular and spongelike structures are visible. In the case of the PP support (Figure 14), various type of encrustations can be found and in a more abundant way with respect to the PLA support (Figure 15).

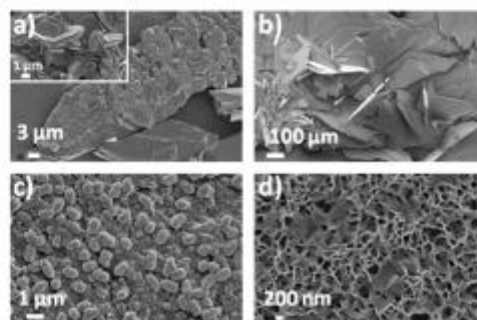


Figure 14. (a,b) FESEM images showing the formation of calcium phosphates precipitates and encrustations after immersion of PP support into artificial urine for 21 days. (c,d) Globular-shaped and spongelike morphology of hydroxyapatite precipitates.

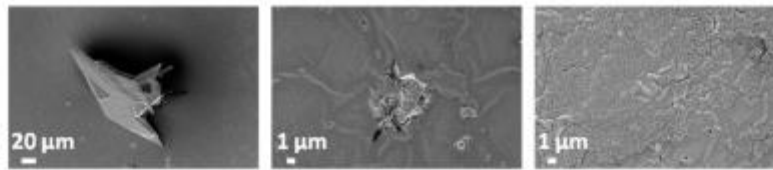


Figure 15. FESEM images of PLA support after immersion in artificial urine for 21 days.

By considering the morphology and the corresponding chemical composition summarized in Figures 16 and 17, calcium phosphate precipitates (Ca/P ratio around 0.9–1) are found for both the samples' types (Figure 14a,b and Figure 15) corresponding to brushite ( $\text{CaHPO}_4 \cdot 2\text{H}_2\text{O}$ ) or hydroxyapatite  $\text{Ca}_{10}(\text{PO}_4)_6(\text{OH})_2$ , the latter showing globular-shaped and spongelike morphology (Figure 14c,d) are detected only in the case of the PP support. For both PP and PLA supports, some traces of sodium chloride and potassium chloride are also present and due to the contact of the samples with artificial urine solution, while the presence of struvite  $(\text{NH}_4)\text{MgPO}_4 \cdot 6\text{H}_2\text{O}$ , corresponding to the crystalline prismatic deposits is also recognized (see the central Table in Figure 16). In Figure 15 (left panel), corresponding to the surface of the PLA sample, the typical crystalline structure of calcium oxalate  $\text{Ca}(\text{COO})_2$  is observed.

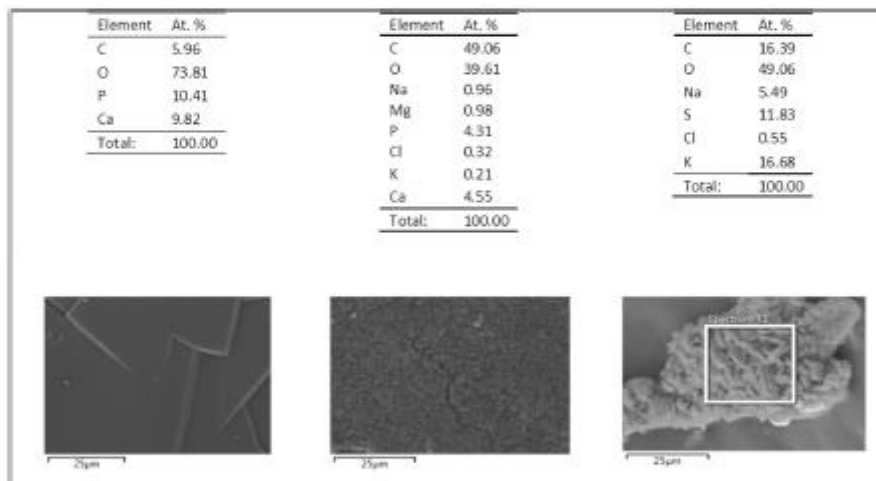


Figure 16. Chemical composition of three different precipitates formed at the surface of PP support after immersion in artificial urine for 21 days.

Differently from the previous case of SBF, the immersion of the ZnO-coated polymer substrates in artificial urine for 21 days negatively affected the ZnO morphology. A strong dissolution of the ZnO coating was observed through the corresponding FESEM images of Figures 18 and 19. There is an absence of the typical flowerlike microparticle morphology previously shown in Figure 1. The ZnO degradation is further supported by EDX analyses reported in Figures 20 and 21, showing small Zn traces in the case of sample ZnO@PP, while the amount of Zn is negligible for sample ZnO@PLA. Despite the degradation of the ZnO coating, a reduced amount of precipitates is observed for the ZnO@PLA support (Figure 19) with respect to the uncoated PLA counterpart. On the other hand, the presence of ZnO seems to not prevent the formation of encrustations in the case of the PP substrate (Figure 18), which could be related to the low level of ZnO coated onto the surface as observed in EDX. In particular, globular structures (peculiar of hydroxyapatite  $\text{Ca}_{10}(\text{PO}_4)_6(\text{OH})_2$ ), prismatic crystals of struvite  $(\text{NH}_4)\text{MgPO}_4 \cdot 6\text{H}_2\text{O}$  or brushite ( $\text{CaHPO}_4 \cdot 2\text{H}_2\text{O}$ ) and layered sheetlike structures are

observed on ZnO@PP sample, while similar prismatic needlelike structures of struvite or brushite are found at the surface of sample ZnO@PLA. Furthermore, and similar to the previous case, the presence of sodium chloride (NaCl) and potassium chloride (KCl) is noticed also for the ZnO-coated polymers and due to the prolonged interaction of the samples with artificial urine solution.

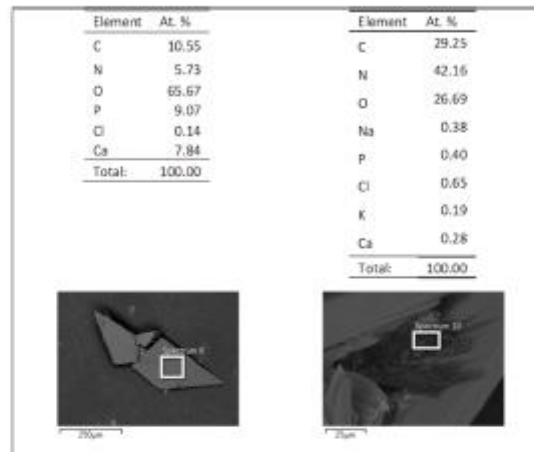


Figure 17. Chemical composition of three different precipitates formed at the surface of PLA support after immersion in artificial urine for 21 days.

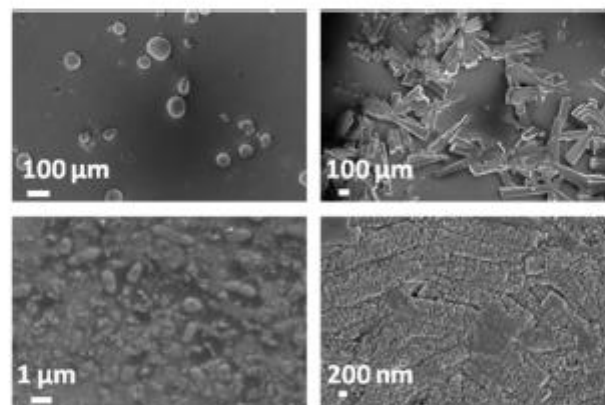


Figure 18. FESEM images of ZnO@PP sample after 21 days in artificial urine.

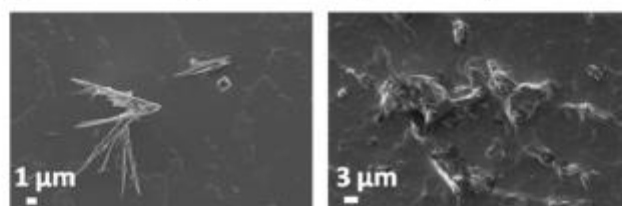
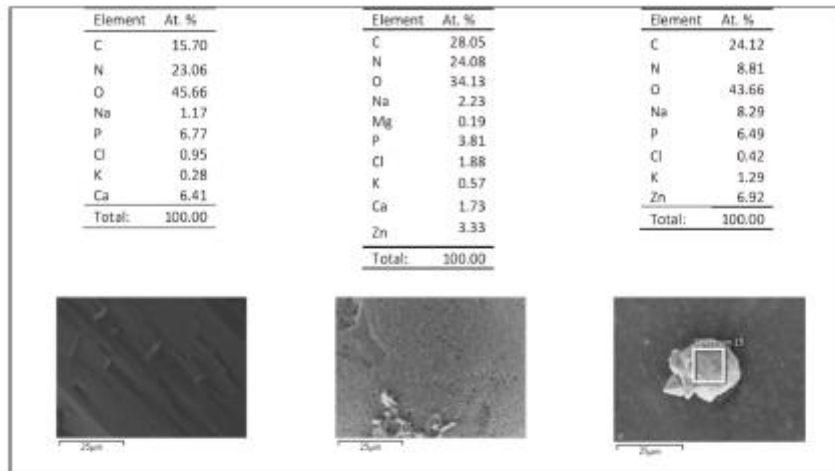
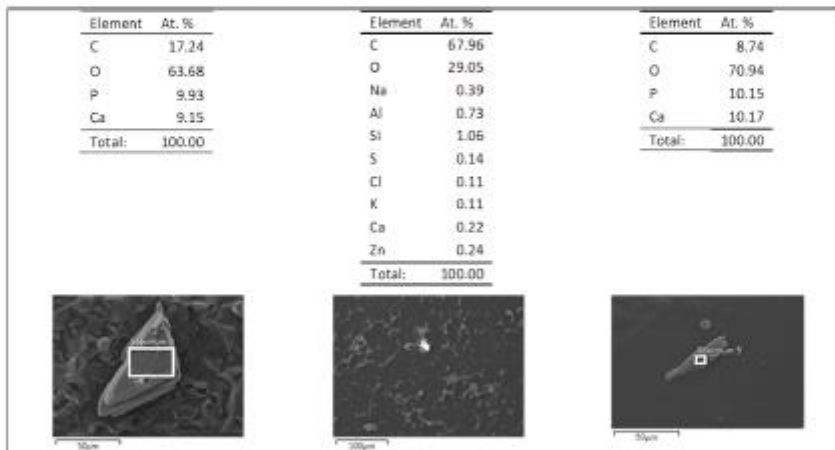


Figure 19. FESEM of ZnO@PLA sample after 21 days in artificial urine.



**Figure 20.** Chemical composition of three different precipitates formed at the surface of ZnO@PP sample after immersion in artificial urine for 21 days.



**Figure 21.** Chemical composition of three different precipitates formed at the surface of ZnO@PLA sample after immersion in artificial urine for 21 days.

Figure 12b shows the XRD pattern of ZnO@PLA and ZnO@PP substrates after the immersion in artificial urine for 21 days. In this case, the diffraction contribution coming from the ZnO microparticle film mostly disappear, with the (101) and (110) diffraction peaks being only slightly detectable. This aspect confirms the partial rather than complete degradation of the ZnO coating at the end of the experiment, as observed from FESEM analyses described previously.

ATR-IR analyses have been performed after soaking the sample in artificial urine for 21 days (Figure 22). Apart from the peaks characteristics of the polymer substrates, a strong change in the shape of the IR absorption band of  $3500\text{--}3000\text{ cm}^{-1}$  region is visible, and independent of the kind of polymer. In all the samples except ZnO@PLA, the presence of three distinct IR bands at  $3218$ ,  $3331$  and  $3440\text{ cm}^{-1}$  is noticed and confirms the formation of precipitates (mainly calcium phosphate compounds), as mentioned previously. These are due to stretching modes of vibration of water of crystallization as also to the N-H secondary stretching mode derived from urea. Additional IR modes

due to water of crystallization and N–H bending mode in the range 1670–1610  $\text{cm}^{-1}$  are detected as well. Such additional IR bands are barely detectable in sample ZnO@PLA and it confirms a reduced formation of encrustations and precipitates, as previously observed from the corresponding FESEM analyses. On the contrary, sample ZnO@PP shows additional IR bands with respect to the nonsoaked PP sample: the phosphate band in the 1100–1040  $\text{cm}^{-1}$  range and at 938  $\text{cm}^{-1}$ , carbonate ( $\text{CO}_3^{2-}$ ) bands in the range 1496–1434  $\text{cm}^{-1}$  and stretching mode of P–OH at around 866  $\text{cm}^{-1}$  [46].

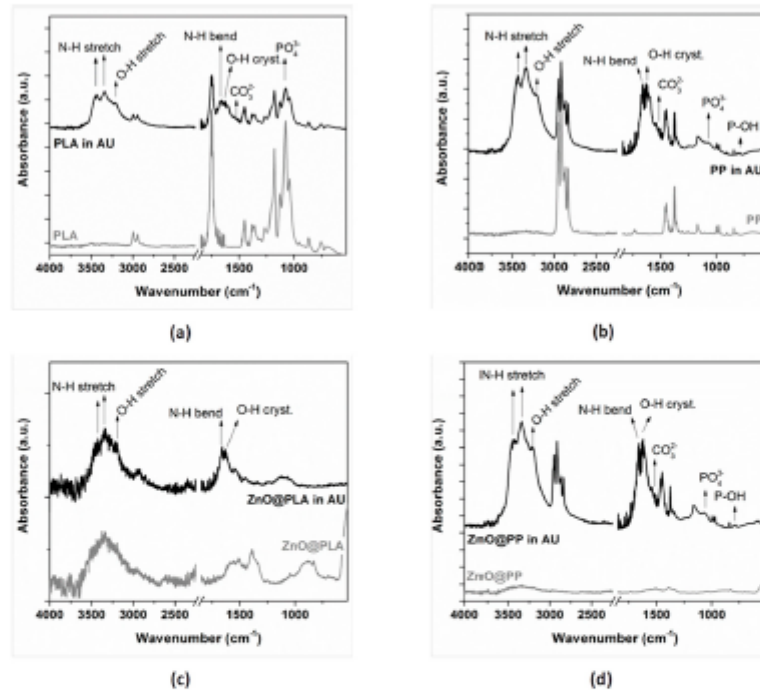


Figure 22. ATR-IR spectra of the samples after immersion in artificial urine for 21 days: (a) only PLA; (b) only PP; (c) ZnO@PLA; (d) ZnO@PP.

The strong degradation of the ZnO coating can be due to the acidic environment conditions of artificial urine, which induced ZnO dissolution. Actually, it is known that ZnO becomes more soluble as the pH of the solution decreases and dissolution increases significantly in pH values below 6.0 [47,48]. Thus, the different behaviours of the ZnO coating in both solutions and the faster dissolution of ZnO in artificial urine is probably related to its more acidic nature (pH 5.7) in comparison to the SBF solution (pH 7.45).

Another main issue related to urinary stents is the deposition of salts on the stent surface that can cause the blockage of liquid, inflammation and other complications [2,49]. In this study, encrustation was observed only after three weeks of immersion in artificial urine for ZnO-coated samples and two weeks for noncoated polymer supports. Hence, it can be concluded that the addition of the ZnO coating to both PLA and PP supports can be useful in preventing or at least delaying the deposition of encrustations.

### 3.6. Antimicrobial Tests

Bacteria cell viability was evaluated on a Gram-negative strain (*E. coli*) and a Gram-positive strain (*S. aureus*). The bacteria strains were incubated in the presence of noncoated PLA and PP films, and ZnO-coated PLA and PP films. Figure 23 shows the average growth percentages of each strain when incubated with the coated and noncoated films, considering the positive control as the reference



for 100% of cell viability, as it was incubated without the presence of any polymer. Cell viability shows a clear reduction when incubated in the presence of ZnO-coated films. In *E. coli*, incubation with noncoated PLA and PP reached 96% viability, while for the incubation with ZnO@PLA and ZnO@PP samples, the viability was reduced to 70% and 71% respectively. Similarly, *S. aureus* achieved 96% and 91% viability with PLA and PP, respectively, but it reached only 67% with ZnO@PLA and 66% with ZnO@PP. With a 95% confidence interval, it was concluded that there is an important difference in cell viability mean values between the ZnO-coated and noncoated samples, implicating successful antimicrobial activity exhibited by the ZnO microparticle film. In the same confidence interval, mean values for cell viability of *E. coli* and *S. aureus* showed no significant difference, suggesting that differences in cell wall structure did not affect the action mechanism of the ZnO particles in this case. Similar results with successful antimicrobial activity of polymer films with ZnO against *E. coli* and *S. aureus* strains were obtained in various studies [50,51].

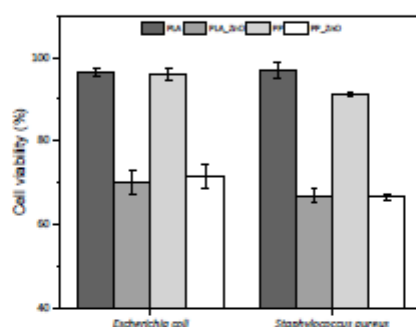


**Figure 23.** Bacteria cell viability after 24 h treatment with coated and noncoated PLA and PP films. There is no significant difference in the antimicrobial activity between *E. coli* and *S. aureus* ( $p < 0.05$ ).

Figure 24 shows the FESEM images of ZnO@PLA and ZnO@PP supports after the antimicrobial assays performed by culturing *E. coli* and *S. aureus* bacteria on both the samples typologies. In this case, the ZnO coating was still present, as further indicated by the presence of diffraction peaks belonging to ZnO (Figure 12c,d) as well as by the EDX compositional analyses reported in Table 1, which confirm the detection of Zn element in high amounts (around 15 at.%) for both PLA and PP supports. However, the morphology of the microparticles has changed from a flower-like structure to a more compact and round-shaped one. EDX data shown in Table 1 also underline the presence of other elements (Na, Ca, P, etc.) due to the interaction of the considered samples with the medium for bacteria culture.

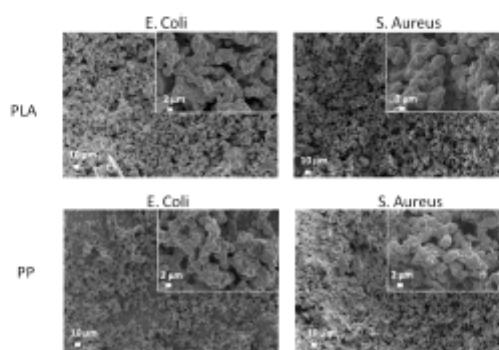


**Figure 24.** FESEM images of ZnO-coated PLA (top panels) and PP (bottom panels) samples after the antimicrobial assays performed by culturing *E. coli* (left panels) and *S. aureus* bacteria (right panels).

**Table 1.** Chemical composition at the surface of ZnO-coated PLA and PP supports after antimicrobial assays.

Element	<i>E. coli</i>		<i>S. aureus</i>	
	PLA/ZnO, at.%	PP/ZnO, at.%	PLA/ZnO, at.%	PP/ZnO, at.%
C	28.89	51.08	35.93	29.94
N	4.33	–	–	4.70
O	38.17	30.23	37.49	38.85
Na	7.69	4.97	7.21	7.36
P	3.17	2.12	2.86	2.75
Cl	1.14	0.69	1.26	0.79
K	0.92	0.91	0.92	0.74
S	–	0.13	–	–
Ca	–	0.35	–	–
Zn	15.69	9.52	14.33	14.87
Total.	100.00	100.00	100.00	100.00

#### 4. Conclusions

ZnO coatings were deposited on PLA and PP films by the doctor-blade technique. The ZnO functional layer was obtained starting from high-surface-area, flower-like ZnO microparticles prepared following a simple hydrothermal route. The resulting ZnO@PLA and ZnO@PP samples were studied from the morphological, compositional and structural standpoint. The biodegradation behaviour was investigated by considering the interaction of the considered samples with simulated body fluid and artificial urine solution for prolonged soaking times. Finally, the antimicrobial behaviour was studied as well against *S. aureus* and *E. coli*. It turned out that adhesion of the ZnO coating was better on PLA supports than on PP. The addition of the ZnO functional layer did not negatively influence the mechanical and thermal properties of both PLA and PP supports. Meanwhile, the surface wetting properties of the polymers changed after ZnO deposition and moved from the hydrophobic to the hydrophilic range. When both the samples typologies were soaked into SBF, ZnO dissolution was only partial and independent of the polymer substrate type. It was also found that both PP and PLA substrates prevent the precipitation/formation of phosphate compounds. The presence of the ZnO coating, in contrast, promoted the formation of phosphate compounds. On the contrary, a strong degradation of the ZnO functional coating was observed when the samples were soaked in artificial urine solution. After 21 days, all characterization results pointed out a complete degradation of the ZnO layer due to the acidic pH conditions of the artificial urine environment. The formation of precipitates/encrustations was observed mostly for PP and ZnO@PP, while it was limited on PLA and ZnO@PLA. The composition of the formed compounds was confirmed by compositional analysis and IR spectroscopy. The antimicrobial tests highlighted a good antibacterial activity against both the considered families of bacteria only in the presence of the functional ZnO coating. It is also worth mentioning that the ZnO coating was not affected by the medium for bacteria culture as it was still present after the bacteria culture.

**Author Contributions:** Conceptualization, V.C. and D.M.D.; investigation, C.V., M.L., M.B., E.L., and L.L.; data curation, C.V., M.L., and M.B.; writing—original draft preparation, C.V. and M.L.; writing—review and editing, all authors; supervision, M.L., V.C., and D.M.D. All authors have read and agreed to the published version of the manuscript.

**Funding:** This publication has emanated from research conducted with the financial support of Athlone Institute of Technology under the Presidents Seed Fund, Universidade de Caxias do Sul, grant number CAPES (PDSE - 88881.187620/2018-01) and European Network of Multidisciplinary Research to Improve the Urinary Stents (ENIUS) COST Action CA16217.

**Conflicts of Interest:** The authors declare no conflict of interest.

## References

- Lam, J.S.; Gupta, M. Update on ureteral stents. *Urology* **2004**, *64*, 9–15. [[CrossRef](#)] [[PubMed](#)]
- Yang, L.; Whiteside, S.; Cadieux, P.A.; Denstedt, J.D. Ureteral stent technology: Drug-eluting stents and stent coatings. *Asian J. Urol.* **2015**, *2*, 194–201. [[CrossRef](#)] [[PubMed](#)]
- Kim, H.-H.; Kim, K.-W.; Choi, Y.H.; Lee, S.B.; Baba, Y. Numerical analysis of urine flow with multiple sizes of double-j stents. *Appl. Sci.* **2020**, *10*, 4291. [[CrossRef](#)]
- Abdelaziz, A.Y.; Fouda, W.B.; Mosharafa, A.A.; Abelasoul, M.A.; Fayyad, A.; Fawzi, K. Forgotten ureteral stents: Risk factors, complications and management. *Afr. J. Urol.* **2018**, *24*, 28–33. [[CrossRef](#)]
- Liu, S.; Luo, G.; Sun, B.; Lu, J.; Zu, Q.; Yang, S.; Zhang, X.; Dong, J. Early removal of double-j stents decreases urinary tract infections in living donor renal transplantation: A prospective, randomized clinical trial. *Transplant. Proc.* **2017**, *49*, 297–302. [[CrossRef](#)]
- Ahalla, Y.; Khallouk, A.; Fassi, M.J.E.; Farid, M.H. Risk factor analysis and management of ureteral double-j stent complications. *Rev. Urol.* **2010**, *12*, e147–e151. [[CrossRef](#)]
- Forbes, C.; Scotland, K.B.; Lange, D.; Chew, B.H. Innovations in ureteral stent technology. *Urol. Clin.* **2019**, *46*, 245–255. [[CrossRef](#)]
- Singha, P.; Locklin, J.; Handa, H. A review of the recent advances in antimicrobial coatings for urinary catheters. *Acta Biomater.* **2017**, *50*, 20–40. [[CrossRef](#)]
- Cauda, F.; Cauda, V.; Fiori, C.; Onida, B.; Garrone, E. Heparin coating on ureteral double j stents prevents encrustations: An in vivo case study. *J. Endourol.* **2008**, *22*, 465–472. [[CrossRef](#)]
- Mosayyebi, A.; Vijayakumar, A.; Yue, Q.Y.; Bres-Niewada, E.; Manes, C.; Carugo, D.; Somani, B.K. Engineering solutions to ureteral stents: Material, coating and design. *Cent. Eur. J. Urol.* **2017**, *70*, 270–274. [[CrossRef](#)]
- Cauda, F.; Cauda, V.; Fiori, C. Coated ureteral stent. In *Biomaterials and Tissue Engineering in Urology*; Denstedt, J., Atala, A., Eds.; Woodhead Publishing Ltd.: London, UK, 2009; pp. 134–156.
- Laurenti, M.; Grochowicz, M.; Dragoni, E.; Carofiglio, M.; Limongi, T.; Cauda, V. Biodegradable and drug-eluting inorganic composites based on mesoporous zinc oxide for urinary stent applications. *Materials* **2020**, *13*, 3821. [[CrossRef](#)] [[PubMed](#)]
- Dave, R.N.; Joshi, H.M.; Venugopalan, V.P. Novel biocatalytic polymer-based antimicrobial coatings as potential ureteral biomaterial: Preparation and in vitro performance evaluation. *Antimicrob. Agents Chemother.* **2011**, *55*, 845–853. [[CrossRef](#)] [[PubMed](#)]
- Venkatesh, C.; Clear, O.; Major, I.; Lyons, J.G.; Devine, D.M. Faster release of lumen-loaded drugs than matrix-loaded equivalent in polylactic acid/halloysite nanotube. *Materials* **2019**, *12*, 1830. [[CrossRef](#)] [[PubMed](#)]
- Turalija, M.; Bischof, S.; Budimir, A.; Gaan, S. Antimicrobial PLA films from environment friendly additives. *Compos. Part B Eng.* **2016**, *102*, 94–99. [[CrossRef](#)]
- Zhang, H.; Hortal, M.; Jorda Beneyto, M.; Rosa, E.; Lara, M.; Lorente, I. ZnO-PLA nanocomposite coated paper for antimicrobial packaging application. *LWT-Food Sci. Technol.* **2016**, *78*, 250–257. [[CrossRef](#)]
- De Silva, R.T.; Pasbakhsh, P.; Lee, S.M.; Kit, A.Y. ZnO deposited/encapsulated halloysite–poly(lactic acid) (PLA) nanocomposites for high performance packaging films with improved mechanical and antimicrobial properties. *Appl. Clay Sci.* **2015**, *111*, 10–20. [[CrossRef](#)]
- Pantani, R.; Gorrasi, G.; Vigliotta, G.; Murariu, M.; Dubois, P. PLA-ZnO nanocomposite films: Water vapor barrier properties and specific end-use characteristics. *Eur. Polym. J.* **2013**, *49*, 3471–3482. [[CrossRef](#)]
- Marra, A.; Silvestre, C.; Duraccio, D.; Cimmino, S. Polylactic acid/zinc oxide biocomposite films for food packaging application. *Int. J. Biol. Macromol.* **2016**, *88*, 254–262. [[CrossRef](#)]
- Aržlovar, A.; Kržan, A.; Žagar, E. Degradation of PLA/ZnO and PHBV/ZnO composites prepared by melt processing. *Arab. J. Chem.* **2018**, *11*, 343–352. [[CrossRef](#)]
- Maddah, H.A. Polypropylene as a promising plastic: A review. *Am. J. Polym. Sci.* **2016**, *6*, 1–11. [[CrossRef](#)]
- Okuyucu, S.; Goru, H.; Oksuz, H.; Akoglu, E. Endoscopic dacryocystorhinostomy with silicone, polypropylene, and t-tube stents; randomized controlled trial of efficacy and safety. *Am. J. Rhinol. Allergy* **2015**, *29*, 63–68. [[CrossRef](#)] [[PubMed](#)]
- Viswanatha, B.; Vijayashree, M.S. Silicone stenting and polypropylene stenting in endoscopic dacryocystorhinostomy: A prospective comparative study. *Res. Otolaryngol.* **2015**, *4*, 49–53. [[CrossRef](#)]

24. Mitsuoka, M.; Hayashi, A.; Takamori, S.; Tayama, K.; Shirouzu, K. Experimental study of the histocompatibility of covered expandable metallic stents in the trachea. *Chest* **1998**, *114*, 110–114. [[CrossRef](#)] [[PubMed](#)]
25. Yuan, T.; Zheng, R.; Yu, J.; Edmonds, L.; Wu, W.; Cao, J.; Gao, F.; Zhu, Y.; Cheng, Y.; Cui, W. Fabrication and evaluation of polymer-based esophageal stents for benign esophagus stricture insertion. *RSC Adv.* **2016**, *6*, 16891–16898. [[CrossRef](#)]
26. Zhao, H.; Li, R.K.Y. A study on the photo-degradation of zinc oxide (ZnO) filled polypropylene nanocomposites. *Polymer* **2006**, *47*, 3207–3217. [[CrossRef](#)]
27. Jakubiak, S.; Tomaszewska, J.; Jackiewicz, A.; Michalski, J.; Kurzydowski, K.J. Polypropylene-zinc oxide nanorod hybrid material for applications in separation processes. *Chem. Process Eng.* **2016**, *37*, 393–403. [[CrossRef](#)]
28. Bojarska, M.; Nowak, B.; Skowroński, J.; Piątkiewicz, W.; Gradoń, I. Growth of ZnO nanowires on polypropylene membrane surface—characterization and reactivity. *Appl. Surf. Sci.* **2017**, *391*, 457–467. [[CrossRef](#)]
29. Mirzaei, H.; Darroudi, M. Zinc oxide nanoparticles: Biological synthesis and biomedical applications. *Ceram. Int.* **2017**, *43*, 907–914. [[CrossRef](#)]
30. Garino, N.; Sanvitale, P.; Dumontel, B.; Laurenti, M.; Colilla, M.; Izquierdo-Barba, I.; Cauda, V.; Vallet-Regi, M. Zinc oxide nanocrystals as a nanoantibiotic and osteoinductive agent. *RSC Adv.* **2019**, *9*, 11312–11321. [[CrossRef](#)]
31. Król, A.; Pomastowski, P.; Rafińska, K.; Railean-Plugaru, V.; Buszewski, B. Zinc oxide nanoparticles: Synthesis, antiseptic activity and toxicity mechanism. *Adv. Colloid Interface Sci.* **2017**, *249*, 37–52. [[CrossRef](#)]
32. Pasquet, J.; Chevalier, Y.; Pelletier, J.; Couval, E.; Bouvier, D.; Bolzinger, M.-A. The contribution of zinc ions to the antimicrobial activity of zinc oxide. *Colloids Surf. A Physicochem. Eng. Asp.* **2014**, *457*, 263–274. [[CrossRef](#)]
33. Dimapilis, E.A.S.; Hsu, C.-S.; Mendoza, R.M.O.; Lu, M.-C. Zinc oxide nanoparticles for water disinfection. *Sustain. Environ. Res.* **2018**, *28*, 47–56. [[CrossRef](#)]
34. Racca, L.; Canta, M.; Dumontel, B.; Ancona, A.; Limongi, T.; Garino, N.; Laurenti, M.; Canavese, G.; Cauda, V. Zinc oxide nanostructures in biomedicine. In *Smart Nanoparticles for Biomedicine*; Ciofani, G., Ed.; Elsevier: Amsterdam, The Netherlands, 2018; pp. 171–187.
35. Pugliese, D.; Bella, E.; Cauda, V.; Lamberti, A.; Sacco, A.; Tresso, E.; Bianco, S. A chemometric approach for the sensitization procedure of ZnO flowerlike microstructures for dye-sensitized solar cells. *ACS Appl. Mater. Interfaces* **2013**, *5*, 11288–11295. [[CrossRef](#)] [[PubMed](#)]
36. Cauda, V.; Stassi, S.; Lamberti, A.; Morello, M.; Fabrizio Pirri, C.; Canavese, G. Leveraging ZnO morphologies in piezoelectric composites for mechanical energy harvesting. *Nano Energy* **2015**, *18*, 212–221. [[CrossRef](#)]
37. Shin, J.; Liu, X.; Chikthimmah, N.; Lee, Y.S. Polymer surface modification using uv treatment for attachment of natamycin and the potential applications for conventional food cling wrap (ldpe). *Appl. Surf. Sci.* **2016**, *386*, 276–284. [[CrossRef](#)]
38. Socrates, G. *Infrared and Raman Characteristic Group Frequencies: Tables and Charts*; John Wiley & Sons: Chichester, UK, 2004.
39. Kokubo, T.; Takadama, H. How useful is SBF in predicting in vivo bone bioactivity? *Biomaterials* **2006**, *27*, 2907–2915. [[CrossRef](#)]
40. Sarangapani, S.; Cavedon, K.; Gage, D. An improved model for bacterial encrustation studies. *J. Biomed. Mater. Res.* **1995**, *29*, 1185–1191. [[CrossRef](#)]
41. Krueenate, J.; Tongpool, R.; Panyathanmaporn, T.; Kongrat, P. Optical and mechanical properties of polypropylene modified by metal oxides. *Surf. Interface Anal.* **2004**, *36*, 1044–1047. [[CrossRef](#)]
42. Jayaramudu, J.; Das, K.; Sonakshi, M.; Siva Mohan Reddy, G.; Aderibigbe, B.; Sadiku, R.; Sinha Ray, S. Structure and properties of highly toughened biodegradable polylactide/zno biocomposite films. *Int. J. Biol. Macromol.* **2014**, *64*, 428–434. [[CrossRef](#)]
43. Tang, Z.; Fan, F.; Chu, Z.; Fan, C.; Qin, Y. Barrier properties and characterizations of poly(lactic acid)/ZnO nanocomposites. *Molecules* **2020**, *25*, 1310. [[CrossRef](#)]
44. Laurenti, M.; Lamberti, A.; Genchi, G.G.; Roppolo, I.; Canavese, G.; Vitale-Brovvarone, C.; Ciofani, G.; Cauda, V. Graphene oxide finely tunes the bioactivity and drug delivery of mesoporous ZnO scaffolds. *ACS Appl. Mater. Interfaces* **2019**, *11*, 449–456. [[CrossRef](#)] [[PubMed](#)]
45. Laurenti, M.; Cauda, V. Gentamicin-releasing mesoporous ZnO structures. *Materials (Basel)* **2018**, *11*, 314. [[CrossRef](#)] [[PubMed](#)]
46. Salma, K.; Borodajenko, N.; Plata, A.; Berzina-Cimdina, L.; Stunda, A. Fourier transform infrared spectra of technologically modified calcium phosphates. In Proceedings of the 14th Nordic-Baltic Conference on Biomedical Engineering and Medical Physics, Riga, Latvia, 16–20 June 2008.

47. Richardson, J.J.; Lange, F.F. Controlling low temperature aqueous synthesis of ZnO. I. Thermodynamic analysis. *Cryst. Growth Des.* **2009**, *9*, 2570–2575. [[CrossRef](#)]
48. Sedlak, A.; Janusz, W. Specific adsorption of carbonate ions at the zinc oxide/electrolyte solution interface. *Physicochem. Probl. Miner. Process.* **2008**, *42*, 57–66.
49. Haleblan, G.; Kijvikai, K.; Rosette, J.d.L.; Preminger, G. Ureteral stenting and urinary stone management: A systematic review. *J. Urol.* **2008**, *179*, 424–430. [[CrossRef](#)]
50. Mizielińska, M.; Kowalska, U.; Jarosz, M.; Sumińska, P.; Landercy, N.; Duquesne, E. The effect of UV aging on antimicrobial and mechanical properties of PLA films with incorporated zinc oxide nanoparticles. *Int. J. Environ. Res. Public Health* **2018**, *15*, 794. [[CrossRef](#)]
51. Mania, S.; Cieslik, M.; Konzorski, M.; Święcikowski, P.; Nelson, A.; Banach, A.; Tylingo, R.T. The synergistic microbiological effects of industrial produced packaging polyethylene films incorporated with zinc nanoparticles. *Polymers* **2020**, *12*, 1198. [[CrossRef](#)]





**Publisher's Note:** MDPI stays neutral with regard to jurisdictional claims in published maps and institutional affiliations.



© 2020 by the authors. Licensee MDPI, Basel, Switzerland. This article is an open access article distributed under the terms and conditions of the Creative Commons Attribution (CC BY) license (<http://creativecommons.org/licenses/by/4.0/>).

Article

# Antimicrobial Active Bioplastics Using Triangular Silver Nanoplate Integrated Polycaprolactone and Polylactic Acid Films

Eduardo Lanzagorta Garcia <sup>\*</sup>, Olivia A. Attallah , Marija Mojicevic , Declan M Devine  and Margaret Brennan Fournet

Materials Research Institute, Athlone Institute of Technology, Athlone N37 HD68, Ireland; oadly@ait.ie (O.A.A.); mmojicevic@ait.ie (M.M.); ddevine@ait.ie (D.M.D.); mfournet@ait.ie (M.B.F.)

\* Correspondence: e.lanzagorta@research.ait.ie; Tel.: +353-083-352-7449

**Abstract:** An innovative antimicrobial technology for plastic surfaces is presented. We report the synthesis and scale-up of triangular silver nanoplates (TSNPs) and their integration into polycaprolactone (PCL) and polylactic acid (PLA) polymers through a solvent-casting technique. The TSNPs have a high geometric aspect ratio and strong local surface plasmon resonance (LSPR) response, which provides an effective tool for monitoring their integrity during processing and integration with the biodegradable plastics. An aqueous-based seed-mediated chemical method was used to synthesize the TSNPs, and characterisation was carried out using TEM and UV (Ultraviolet)-VIS (Visible) spectroscopy to measure LSPR profiles. The UV-VIS spectra of silver seeds and TSNPs exhibited characteristic peaks at 395 and 600 nm respectively. Synthesized TSNPs were coated with thiol-terminated polyethylene glycol (SH-PEG) and transferred into chloroform in order to effect compatibility with PCL and PLA. TSNP/PCL and TSNP/PLA composite films were prepared by solvent casting. The morphological structure, thermal, mechanical, and antimicrobial properties of the TSNP-incorporated composite films were evaluated. Results showed the TSNP-treated films had a rougher surface than the bare films. Insignificant changes in the thermal properties of TSNP-treated films compared to bare ones were also observed, which indicated the thermal stability of the composite films. The tensile strength and antimicrobial properties of the composite films were increased after TSNP incorporation. TSNP/PCL and TSNP/PLA films exhibited improved antimicrobial activity against *Escherichia coli* and *Staphylococcus aureus* with antimicrobial effect (AE) values ranging between 0.10 and 0.35. The obtained results and demonstrated TSNP production scalability validate the TSNP treated PCL and PLA films as a composite material with desirable antimicrobial effect for wide-ranging surface applications.

**Keywords:** polycaprolactone; polylactic acid; antibacterial; triangular silver nanoplates; composite films



Citation: Garcia, E.L.; Attallah, O.A.; Mojicevic, M.; Devine, D.M.; Brennan Fournet, M. Antimicrobial Active Bioplastics Using Triangular Silver Nanoplate Integrated Polycaprolactone and Polylactic Acid Films. *Materials* 2021, 14, 1132. <https://doi.org/10.3390/ma14051132>

Academic Editor: Lubomira Tashva

Received: 22 January 2021

Accepted: 20 February 2021

Published: 28 February 2021

**Publisher's Note:** MDPI stays neutral with regard to jurisdictional claims in published maps and institutional affiliations.



Copyright © 2021 by the authors. Licensee MDPI, Basel, Switzerland. This article is an open access article distributed under the terms and conditions of the Creative Commons Attribution (CC BY) license (<http://creativecommons.org/licenses/by/4.0/>).

## 1. Introduction

Surfaces, in particular common synthetic surfaces, are a frequent source of contamination and/or transmission of microbiological organisms and a critical aspect of disease and infection containment. This can be especially problematic at sites such as healthcare facilities, food industries, and public environments, among others, where pathogens can easily spread and lead to disease acquisition and transmission. Furthermore, antibiotic resistance in microorganisms is rising globally and severely compromising our ability to prevent and treat common infectious diseases [1].

The development of new antibiotic drugs is a long and investment-intensive process, with costs averaging USD 800 million and durations of 10 years or more required [2,3]. Additionally, there is no guarantee that a given drug will be legally approved for use or will generate sufficient profits, making it unattractive for pharmaceutical companies, hence there is a notable decrease in the release of approved antibiotics during the last decades. Thus, to address the growing problem of antimicrobial resistance, there is an

urgent need for the development of novel and innovative alternative approaches. These new technologies must enable a reduced dependence on antibiotic drugs and deliver reduced risks of infection. As a result, researchers are focusing on new strategies such as including novel molecules and using informatics and nanotechnology for the development of novel anti-infection technologies.

Progress in nanoscience has provided a range of advanced functional nanomaterials that are paving the way to improved solutions for human well-being in several different fields. The applications of functional nanomaterials vary from energy to electronics to sensors, environmental, and drug delivery [4]. Metallic nanoparticles (NPs) such as copper oxide (CuO), titanium dioxide (TiO<sub>2</sub>), gold (Au), and iron oxide (Fe<sub>2</sub>O<sub>3</sub>) NPs have demonstrated significant antimicrobial potential [5]. Nevertheless, silver (Ag) remains one of the most attractive metals for the synthesis of NPs, because of the wide applications derived from its unique properties. Attributes like Ag's malleability, conductivity, optical profile, and antimicrobial properties underpin its value and convenience for several functionalities and human requirements, through ancient and modern times [6,7].

Despite the numerous advantages and applications for Ag NPs, environmental risks are also a concern as the number of products using them increases rapidly. This will inevitably increase human and environmental exposure. Although the effects that nanomaterials could have on the environment are not fully understood yet, there is concern that some NPs could accumulate in target organs of the respiratory, cardiovascular, reproductive, urinary, and central nervous systems in exposed species [8]. Therefore, further studies are required to determine the extent of environmental risk, and to implement preventive measures accordingly. Humans are generally exposed to Ag from several sources, including jewelry, functional textiles, coins, tableware, deodorants, catheters, antibacterial treatments, coatings in refrigerators, etc. [9]. Several factors influence the cytotoxic level of Ag NPs, including size/shape of the nanoparticle, concentration, dose, surface chemistry and coatings on the NPs, the environment in which they interact and reside, and agglomeration [10]. Hence, more information is still required to correctly assess the hazards of chronic exposure to nano-silver and its ions, both for humans and the environment. For biomedical applications, it was found that the optimum particle size of Ag NPs to exert acceptable antimicrobial activity is in the range of 15–50 nm [11].

Triangular silver nanoplates (TSNPs) and other non-spherical Ag nanostructures with sharp geometries have been postulated to possess highly controllable optical properties related to strong electric-field enhancement that are especially pronounced in Ag nanostructures with tips [12]. TSNPs have been reported to exhibit higher antimicrobial activity, attributed to a rate of Ag<sup>+</sup> ion release five times larger, compared to spherical NPs. As Ag<sup>+</sup> ion release is caused by oxidation, the increased ion release of TSNPs is a consequence of their sharp edges and corners, which make them more susceptible to oxidation [13–17]. It is also recognised that larger surface-to-volume ratio possessed by smaller NPs compared to larger ones allows smaller particles to release more Ag<sup>+</sup> ions. These results support the suitability of TSNPs to deliver antimicrobial activity for devices and surfaces.

Integration of Ag NPs into biodegradable polymers as polycaprolactone (PCL) and polylactic acid (PLA) for composite-film fabrication has been explored, and significant improvement was noticed in the antimicrobial properties of the Ag NP-treated composite films [18–21]. Nevertheless, one of the major challenges for the incorporation of Ag NPs in polymers is the nonhomogeneous distribution of NPs in the polymer matrix. Such insufficient dispersion, caused by NP agglomeration, leads to the deterioration of the optical and mechanical properties of the polymer nanocomposites [22]. Generally, the synthesis of Ag NPs is usually performed in aqueous systems due to the poor solubility of Ag ion salts in organic solvents, and also due to the increased environmental favourability of aqueous-based chemistries. Aqueous conditions, however, strongly hinder the compatibility of Ag NPs with hydrophobic polymer matrices during blending [23]. Therefore, to increase such compatibility strategies including surface modification, ultrasonic oscillations, and mechanical alloying have been proposed [24].

In the specific case of TSNPs, only a limited number of reports for their incorporation as fillers in composites to improve composites' antimicrobial properties are reported. The functionalization of TSNPs on bulk glass surfaces designed to impart an antibacterial effect based on the release of  $\text{Ag}^+$  has been studied in [4]. A report by Vukoje et al. (2014) discussed the incorporation of TSNPs in cotton fabrics pretreated with chitosan for improvement of the antimicrobial properties of the fabrics. Results showed that the TSNPs were able to increase the antibacterial activity against Gram-negative *E. coli*, Gram-positive *S. aureus*, and yeast *Candida albicans* with a bactericidal percentage of 99% [25]. Furthermore, despite the diversity of TSNPs' applications and their incorporation into polymers for the improvement of their electrical and thermal conductivity [26–30], there is a lack of information about TSNP integration into bioplastics for antimicrobial purposes. Combining the urgent need to develop innovative antimicrobial technologies that combine environmental sustainability and plastic-circularity principles, here we present antimicrobial biodegradable plastics based on TSNPs incorporated into PCL and PLA films. Furthermore, the polyester nature of PCL and PLA plastics is showing promise for closed-loop circularity developments, making these polymers, upon the incorporation of antimicrobial TSNPs, highly lucrative as biodegradable antimicrobial plastics. This study describes a solvent-casting technique for the preparation of TSNP-integrated polymer films with improved antimicrobial properties using PCL and PLA as model polymers for film processing. The morphological structure, thermal behavior, and mechanical properties of the fabricated films were characterized in detail. The antibacterial activity of TSNP-treated films was evaluated against *Escherichia coli* and *Staphylococcus aureus* strains. A new scaled-up TSNP production methodology is demonstrated, validating the industrial-scale applicability to this antimicrobial technology. This demonstration of antimicrobial active TSNP-integrated PCL and PLA bioplastics, which combine cost-effectivity with industrial scalability, is antibiotic-free and highly relevant, particularly given the current Covid-19 pandemic.

## 2. Materials and Methods

### 2.1. Materials

The HPLC-grade water (34877-2.5L), sodium citrate tribasic (C8532-100G) [TSC], poly(sodium 4-styrenesulfate) (434574-5G) [PSSS], sodium borohydride (213462-25G) [ $\text{NaBH}_4$ ], silver nitrate (204390-10G) [ $\text{AgNO}_3$ ] and L-ascorbic acid (A92902-25G) [AA] were obtained from Sigma-Aldrich Ireland Ltd. (Arklow, Ireland). An FRX pump from Syrris (Royston, UK) was used for the addition of  $\text{AgNO}_3$ . O-[2-(3-mercaptopropionylamino)ethyl]-O'-methylpolyethylene glycol (11124-1G-F) The [SH-PEG] was obtained from Sigma-Aldrich Ireland Ltd. The PCL CAPA 6250 [MW 25,000] was obtained from Perstorp (Malmö, Sweden). The PLA Ingeo 4044D was obtained from NatureWorks LLC (Minnetonka, MN, USA).

### 2.2. Synthesis of Triangular Silver Nanoplates (TSNPs)

The TSNP synthesis was performed using a seed-mediated approach, adapted from [31]. This method involved two steps: seed production and TSNP growth. For the seed production, 5 mL of TSC (2.5 mM), 0.25 mL of PSSS (500 mg/L), and 0.3 mL of  $\text{NaBH}_4$  (10 mM) were mixed, followed by the addition of 5 mL of  $\text{AgNO}_3$  (0.5 mM) at the rate of 2 mL/min with constant stirring. TSNP growth was carried out in 4 mL of distilled water (DW), 0.075 mL of AA (10 mM), and 0.35 mL of seed solution (25.56 ppm of Ag), with the addition of 3 mL of  $\text{AgNO}_3$  (0.5 mM) at a rate of 1 mL/min. Finally, 0.5 mL of TSC (25 mM) was added. The finished reaction resulted in a final Ag concentration of 21.34 ppm.

### 2.3. Scale-Up of TSNP Production

Scaling up the TSNP synthesis was achieved by increasing all the reactants' volumes from the adapted method proportionally to reach a final volume of 200 mL. An Ag seed volume of 20 mL was prepared by mixing 8.53 mL DW, 0.95 mL TSC (25 mM), 0.47 mL PSSS (500 mg/mL), and 0.57 mL  $\text{NaBH}_4$  (10 mM). A volume of 9.48 mL of  $\text{AgNO}_3$  (0.5 mM) was

added at a rate of 3.79 mL/min. After 4 hours, the preparation of the seeds was complete and 8.75 mL of seed solution (25.56 ppm) was mixed with 100 mL of DW and 1.87 mL of AA (10 mM). 75 mL of AgNO<sub>3</sub> (0.5 mM) was added at a rate of 25 mL/min, followed by 12.5 mL of TSC (25 mM) after the reaction was finished.

#### 2.4. Transfer of TSNP to Chloroform

The prepared TSNP solution was concentrated with thermal evaporation at 40 °C for 8 days in an oven, to obtain an estimated final concentration of 43 ppm. The transfer of TSNP into chloroform was performed based on a previously reported method [23] with slight modification. Briefly, the TSNPs were coated with thiol-terminated polyethylene glycol (SH-PEG) where an amount of 4 mg of SH-PEG per milliliter of TSNP solution was stirred for a couple of minutes. Afterwards, the treated TSNPs were mixed with chloroform in a 1:1 proportion and centrifuged at 16.162 rcf for 45 minutes, and the supernatant was discarded.

#### 2.5. TSNP Integration into PCL and PLA Biopolymers via Solvent-Casting Technique

The solvent-casting procedure for the PCL and PLA included the dissolution of 800 mg of polymer pellets in 15 mL of chloroform at room temperature, then 5 mL of TSNPs in chloroform were mixed with polymer solutions separately, and each mixture was poured in a Petri dish and dried overnight in an airtight oven at 40 °C. The treated films had a final concentration of 0.026 wt % of TSNPs. Bare films of PCL and PLA were prepared using the same procedure without the addition of TSNPs for further analysis comparisons.

#### 2.6. Antimicrobial Activity

The antimicrobial activity of casted films was evaluated against *Escherichia coli* ATCC 9001 (LGC Standards, Middlesex, UK) and *Staphylococcus aureus* ATCC 25923 (LGC Standards, Middlesex, UK) in Luria-Bertani broth (10 g/L tryptone, 10 g/L NaCl, 5 g/L yeast extract, pH 7.2) using adapted standard broth microdilution assay for bacteria that grow aerobically, as recommended by the CLSI (Clinical and Laboratory Standards Institute 2015). Prepared films (1 cm<sup>2</sup>) were used as samples, with bare films as a negative control and tested microorganisms as a positive control. Growth of the respective test organisms (10<sup>5</sup> CFU/mL) after 24 h at 37 °C was measured as optical density (OD) at 600 nm using a Biotek Synergy HT Microplate Reader (Biotek Instruments GmbH, Bad Friedrichshall, Germany). Serial dilution of cultivated broth was plated and incubated (30 °C, 24 h), and the number of colonies (CFU/mL) developed on the bare and treated films was calculated.

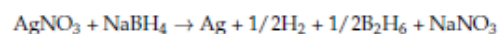
#### 2.7. Instrumentation

The equipment used for the characterization of the TSNPs and prepared films are discussed in detail in Supplementary Materials.

### 3. Results and Discussion

#### 3.1. TSNP Synthesis

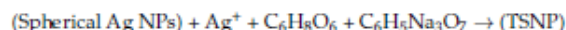
The TSNP synthesis was performed using a seed-mediated approach adapted from [31]. The method involved two steps; seed production and TSNP growth. NaBH<sub>4</sub> was used for the reduction of AgNO<sub>3</sub> and seed formation. The chemical reaction occurred as follows [32]:



TSC and PSSS were used as stabilizers for seed production, and both have been reported to aid the formation of nanoplates. It is postulated that citrate ions and PSSS (being a charged polymer) bind to the surface of the [111] facet of seed particles, and promote the growth of the NPs into a triangular plate shape [31,33].

During the growth step, the spherical Ag seeds reacted with new Ag<sup>+</sup> ions in the presence of AA and citrate ions, forming the TSNP as follows [34]:





It was found that upon the addition of  $\text{AgNO}_3$ , the colour changed from yellow to shades of orange, then shades of red and purple, and finally a dark blue colour of TSNPs was obtained. The normalized UV-VIS spectrum of the seeds and the TSNPs prepared using 350  $\mu\text{L}$  of seeds are shown in Figure 1. The spectrum of the seeds had a localized surface plasmon resonance (LSPR) peak at 395 nm and a full width at half maximum (FWHM) of 79 nm (435–356 nm). The TSNP curve had a peak at 601 nm and an FWHM of 150 nm (663–513 nm). These results are in accordance with the results obtained by the original method, indicating the successful production of TSNPs [31].

The remarkably strong local surface plasmon resonance (LSPR) of these TSNPs has previously been reported in [35]. The LSPR of these TSNPs provides a highly effective tool for monitoring the processing of the TSNPs, providing a means to directly follow the geometric evolution of the TSNPs, interactions at their surfaces, and compatibility with matrices in which they are embedded [36,37]. The LSPR response is hence available to provide a direct readout of the preservation of the TSNP integrity through the processing steps involved in the preparation of TSNP antimicrobial biodegradable plastic films.

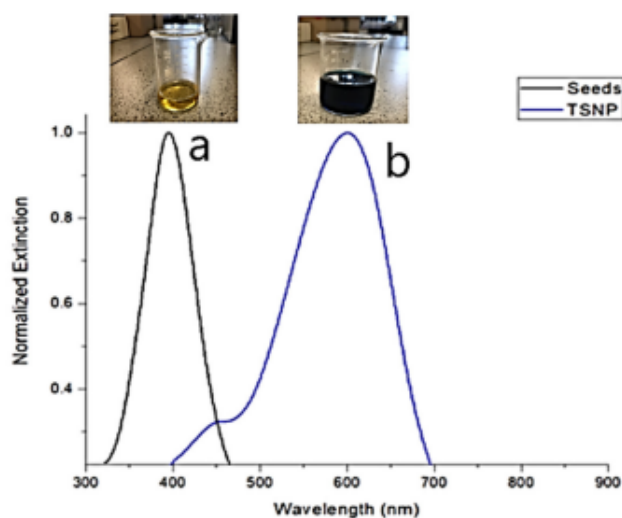
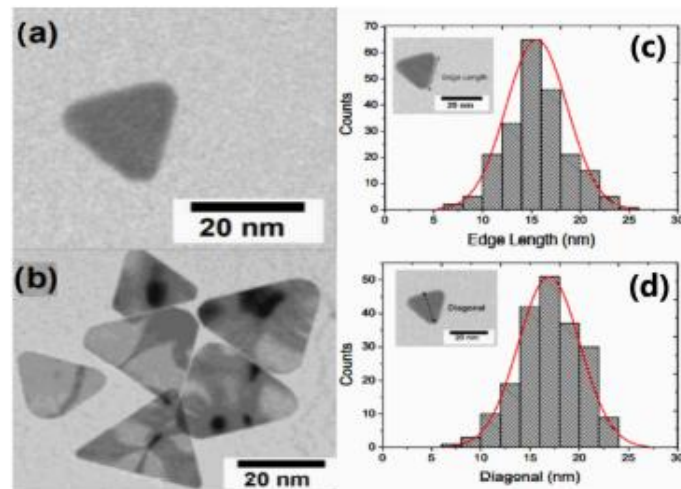


Figure 1. UV-VIS spectrum of (a) Ag seeds and (b) TSNPs.

As shown in Figure 2, transmission electron microscope (TEM) analysis confirmed the presence of triangular plates, with defined sharp corners having a mean edge length of  $15 \pm 4$  nm and a mean diagonal of  $17 \pm 6$  nm. While in the case of equilateral triangles, to which the TSNP can be approximated, the edge length was greater than the diagonal length, which was also true for the TSNPs, given the relatively high error in the measurement of the mean diagonal lengths.



**Figure 2.** TEM images of (a) single TSNP, (b) multiple TSNP, (c) Edge length and (d) diagonal size distribution of TSNP.

The scaling up of the TSNP production was performed to evaluate the efficiency of the synthesis technique in the production of large volumes of TSNPs. As shown in Figure S1, the LSPR peak wavelength of the scaled-up TSNP batch was 584, with an FWHM of 112 nm (635–523 nm). An insignificant blue shift in the peak and a small reduction in FWHM was observed in comparison to that of smaller prepared volumes of TSNP.

A concentrated solution of TSNPs (43 ppm) was then obtained via thermal evaporation, as previously described. Figure 3 shows the UV-VIS spectrum of the TSNPs (21.34 ppm) before evaporation, with an LSPR peak wavelength of 633 nm suffering a small blue shift to 617 nm after thermal evaporation. The FWHM also exhibited a change, from 153 nm (706–553 nm) to 179 nm (723–544 nm) after evaporation. These differences between both LSPR spectral profiles were indicative of a slight broadening in the homogeneity of the TSNPs, with the minor blue shift and consistent spectral profile confirming that the triangular shape of the TSNP was preserved [35]. The scale-up process, therefore, did not significantly affect the geometric profile of the TSNPs, and hence was not an inhibitory process for the antimicrobial performance of the TSNPs.

In the current study, a solvent-casting technique was selected for demonstration of TSNP-incorporated biodegradable plastic film fabrication. One of the advantages of this technique is that it does not involve high temperatures, which can result in the fast oxidation of TSNPs. Nevertheless, the dissolution of all the film's components in a single solvent is an essential requirement of the solvent-casting technique. The selected model biodegradable polymers (PCL and PLA) for the film production are hydrophobic polymers that have very poor solubility in water. TSNPs were therefore transferred from the aqueous phase to an organic phase. Chloroform was chosen as the organic solvent due to its high solubility for the model polymers, and SH-PEG was used to assist the transfer of TSNPs from the aqueous solution to chloroform [38]. UV-VIS spectra of the TSNPs before and after coating with SH-PEG, and after the transfer in chloroform, are presented in Figure 3. LSPR peak wavelengths were 596 nm for SH-PEG-coated TSNPs and 650 nm after transfer to chloroform, which was indicative of increased local refractive index at the TSNP surfaces due to the accumulation of SH-PEG. In comparison to the LSPR of concentrated TSNP, a blue shift of 21 nm occurred after coating the concentrated TSNP with SH-PEG, indicating that these TSNPs were, to a minor degree, more susceptible to oxidation following the concentration process. A subsequent red shift of 54 nm occurred for the concentrated

SH-PEG-coated TSNPs upon transferring them to chloroform, indicating the preserved integrity of the TSNP geometries under these conditions. The FWHM was shifted to 197 nm (514–711 nm) for SH-PEG-coated and 168 nm (565–733 nm) for the chloroform solution. Noticeably, the most drastic shift in the LSPR and FWHM was observed during the transfer step. After transferring to chloroform, and contrary to the other shifts, a red shift occurred. Such a result can be attributed to the higher refractive index of chloroform (1.44) than water (1.33), which led to the production of red shifts in the LSPR of the TSNPs [39–41].

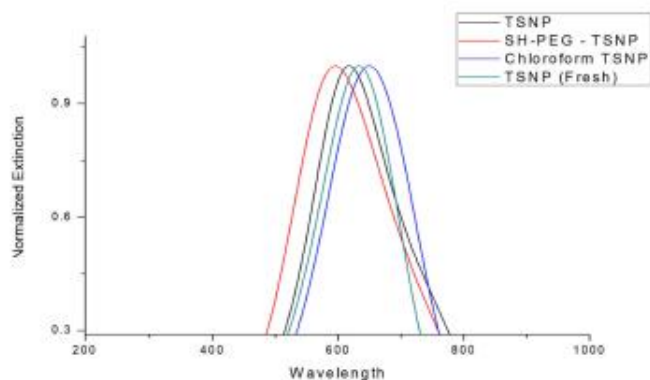


**Figure 3.** UV-VIS spectra of nonconcentrated TSNPs, concentrated TSNPs, SH-PEG-coated TSNPs, and TSNPs after transfer to chloroform.

### 3.2. TSNP-Treated Polymer Films

Solvent casting was evaluated as a film-processing technique. Two model biodegradable polymers, PCL and PLA, were selected for the fabrication of TSNP-integrated composite films. Chloroform was used to dissolve the polymers and as suspension media for the SH-PEG-coated TSNPs. This resulted in better protection for the TSNPs from the air after solvent evaporation, allowing the films to maintain the blue colour of the TSNPs as shown in Figure 4. As mentioned before, the blue colour was an observable feature directly related to the LSPR properties of the TSNPs, serving as a straightforward indicator of the geometric integrity, as drastic changes in the geometry, would also lead to observable change or loss of colour. A similar example has been previously reported, in which blue TSNP-integrated cotton fabrics changed to yellow after autoclave sterilization, showing that agglomeration or transformation of the nanoplates into nanodiscs occurred [25].

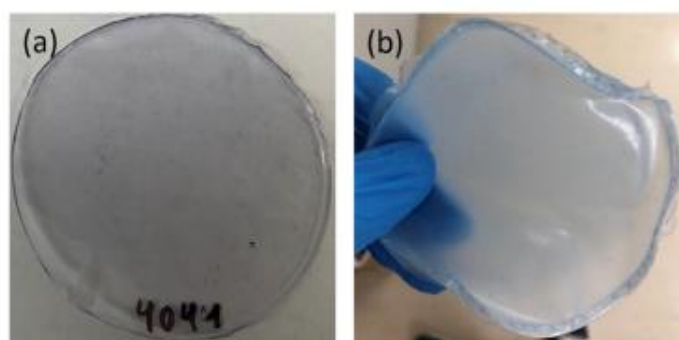


**Figure 4.** Photographic picture of (a) TSNP/PLA and (b) TSNP/PCL films.

### 3.2.1. Scanning Electron Microscopy

A Scanning electron microscope (SEM) analysis was performed for the investigation of TSNP distribution in PCL and PLA films. The morphology of all the films is shown in Figure 5. The illustrative SEM images of the pure PCL and PLA films presented a good compact structure, with a smooth appearance. The images of TSNP-treated PCL (Figure 5b) and TSNP-treated PLA (Figure 5d) films showed rougher surfaces. On the whole, the TSNP had some tendency of aggregation in the PCL and PLA films. Such behaviour can be attributed to the high surface energy that TSNPs possess, which is affected by changes in the size of the NPs and environmental factors such as pH and ionic strength [42].

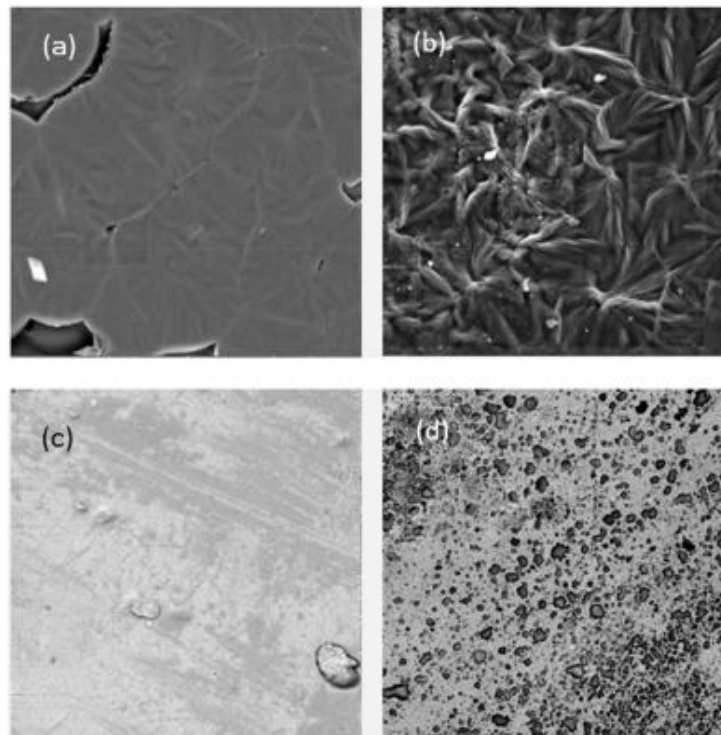


Figure 5. SEM images of (a) PCL, (b) TSNP/PCL, (c) PLA, and (d) TSNP/PLA films (1000 $\times$  magnification).

### 3.2.2. Differential Scanning Calorimetry (DSC)

The typical DSC curves of the bare and TSNP-treated PCL and PLA films are shown in Figure 6a,b, respectively. The glass transition ( $T_g$ ), cold crystallization peak ( $T_c$ ), melting process ( $T_m$ ), and degree of crystallinity ( $X_c$ ) data are summarized in Table 1. Noticeably, TSNPs had a limited effect on the thermal transitions of the treated polymers. For instance, compared to the bare PCL film, the addition of TSNPs did not affect the  $T_m$  (56  $^{\circ}\text{C}$ ) and  $T_c$  (27  $^{\circ}\text{C}$ ) of the PCL. Additionally, in treated PLA films, the values of  $T_g$  and  $T_m$  did not vary significantly from the bare PLA film, for which a change by 1–2  $^{\circ}\text{C}$  was only observed. This can be attributed to the rearrangements of the PCL and PLA chains promoted by the TSNPs, which resulted in the lowering of  $T_m$  by 1–2  $^{\circ}\text{C}$  [43]. These results were in accordance with previous reports in which the addition of Ag NPs did not result in obvious

changes in the  $T_m$  values of PCL films [44]. Another study by Mróz et al. also found that nano-silver did not significantly affect the thermal transitions of treated PLA films [45].

Moreover, as listed in Table 1, the addition of the TSNPs led to an increase in the degree of crystallinity in PLA films of up to 27%, but no significant effect was observed in PCL films ( $X_c = 47\%$ ). In the case of treated PLA films, the resultant increase in the percentage of  $X_c$  can be explained by the phenomenon of heterogeneous nucleation. A similar result was obtained by Chu et al., where the  $X_c$  of PLA was increased as a result of addition of Ag NPs [46].

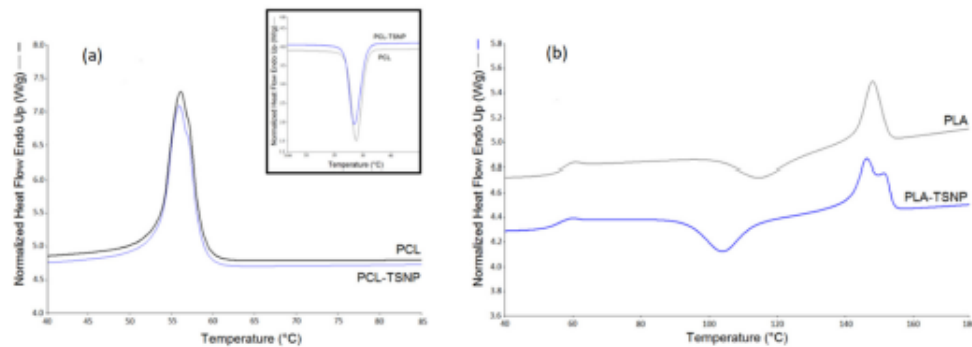


Figure 6. DSC curves for (a) bare and treated PCL films and (b) bare and treated PLA films.

Table 1. Thermal characteristics of the pure and TSNP-treated films.

Sample	$T_g$ (°C)	$T_m$ (°C)	$T_c$ (°C)	$X_c$ (%)
PCL	-	56.06	27.75	47.9
TSNP/PCL	-	55.92	27.36	47.6
PLA	56.7	148.1	114.86	21.5
TSNP/PLA	55.1	146.25	104	27.4

### 3.2.3. Thermogravimetric Analysis (TGA)

A TGA analysis was carried out to study the thermal stability of the prepared films. The TGA curves of the bare and TSNP-treated PCL films are shown in Figure 7a, while Figure 7b demonstrates the TGA curves of the bare and TSNP-treated PLA films. From the thermogravimetric curves, it can be observed that the bare and TSNP-treated films had a relatively good thermal stability, since all the maximum mass losses occurred between 400 and 500 °C. As shown in Figure 7a, the onset degradation temperature ( $T_{onset}$ ) of pure PCL was approximately 439 °C, and the degradation was complete at about 550 °C. In PLA films, the  $T_{onset}$  was 380 °C, and complete degradation was observed at 475 °C. Both the  $T_{onset}$  and the completed degradation temperature of the TSNP-treated PLA and PCL films were not significantly different when compared with their pure films. Therefore, we can conclude that the addition of TSNPs obviously maintained the thermal stability of the PCL and PLA films. These results were in accordance with previously published studies in which no significant difference in thermal stability was observed upon the addition of nano-silver-coated chitosan to PLA films [47,48]. Similarly, the addition of different silver concentrations did not change the thermogravimetric behaviour of PLA samples after 7 days in composting conditions, as reported by [47]. On the other hand, Cerkez et al. (2017) and Leonés et al. (2017) concluded that PCL films and PCL electrospun fibers did not show a significant difference in thermal decomposition when treated with Ag NPs [49,50].

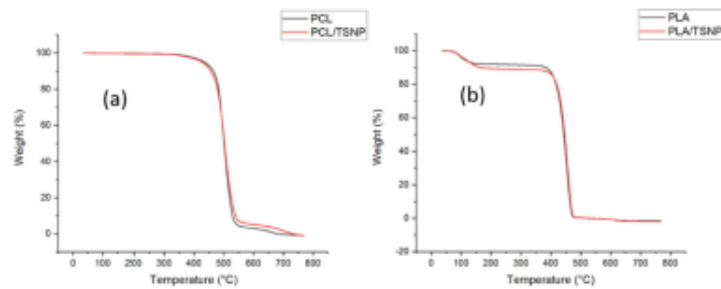


Figure 7. TGA curves of (a) bare and TSNP-treated PCL films, and (b) bare and TSNP-treated PLA films.

### 3.2.4. Mechanical Properties

Tensile strength (TS), elastic modulus (EM), and elongation at break ( $\epsilon$ ) of the fabricated films were calculated as illustrated in Figure 8. The pure films of PCL and PLA exhibited a lower tensile strength (TS = 13.97 MPa for PCL and 21.99 MPa for PLA) and a higher percentage of elongation at break ( $\epsilon = 11.07\%$  for PCL and 4.84% for PLA) values compared to the TSNP-treated films. This was in accordance with Augustine et al. (2016), who reported that electrospun PCL membranes either maintained TS and EM values or exhibited an increase in those parameters at a higher percentage of added Ag NPs [51]. For PLA films, similar results were obtained by Ali et al. (2014), as they observed an increase in TS after the addition of Ag NPs to PLA [52]. Similarly, an increase in TS was also reported by Szymanska-Chargot et al. (2020) after fabricating a PLA composite containing Ag NPs and nanocellulose from carrot pomace [53]. In the current study, the increase of TS of PCL and PLA films after being mixed with the TSNPs can be attributed to the high compatibility between TSNPs and the model polymers. However, the TSNP-treated PCL films suffered a significant decrease in the elongation at break percentage, resulting in the formation of a very brittle film. Such a result might be due to TSNP stacking (as observed in SEM images), which reduced the mobility of the polymer chains. A similar outcome was also reported by Abdelaziz et al. (2020) as a result of adding hydroxyapatite nanoparticles to PCL composites [54].

Concerning the EM of the fabricated films, it was found that the incorporation of TSNPs led to an increase in the EM of the PLA film due to the high stiffness of the TSNPs as fillers compared to pure PLA. An increase in the EM as a result of Ag NP addition was also reported by Liu et al. (2017) and Szymanska-Chargot et al. (2020) [53,55]. Alternatively, there was no significant difference between the bare and TSNP-treated PCL films. A similar trend was also observed by Augustine et al. (2016), in which nanocomposites containing a small concentration of Ag NPs did not show a significant change in the elastic modulus of PCL composites [51].

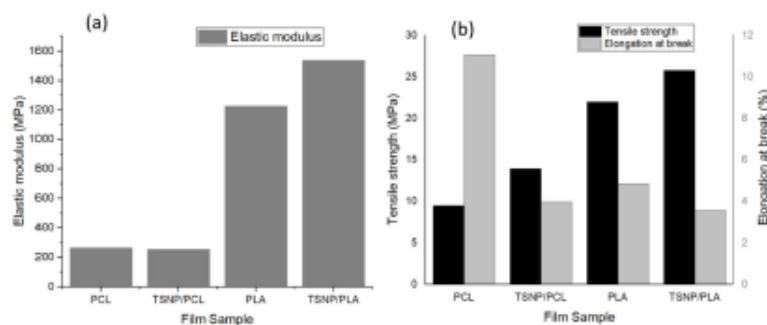


Figure 8. (a) Elastic modulus, (b) Tensile strength and Elongation at break of treated and bare PCL and PLA films

### 3.3. Antimicrobial Activity

Dispersion of nanoparticles inside a polymer matrix can influence the mechanical and barrier properties, but also it can change its antimicrobial nature. As previously mentioned, TSNPs are proven to possess considerable antimicrobial activities, and as such the incorporation of TSNP in PCL and PLA films can improve the composites' antibacterial characteristics. In our present study, both Gram-positive (*S. aureus* ATCC 25923) and Gram-negative (*E. coli* ATCC 9001) bacteria were used to assess the antimicrobial properties of TSNP-treated PCL and PLA composite films with respect to bare films. These bacterial strains were chosen as representatives of common harmful microorganisms occurring in various biomedical related products [56,57]. The antimicrobial effects (AE) of bare and TSNP-treated PCL and PLA composite films were then calculated using the following formula [4].

$$AE = \log NC - \log NE$$

where NC is the number of CFU/mL developed on the bare films, and NE is the number of CFU/mL counted after exposure to TSNP-treated films.

As shown in Table 2, all TSNP-treated films exerted an acceptable inhibitory effect against the tested Gram-positive and Gram-negative bacterial strains. Such antimicrobial activity was attributed to the TSNPs incorporated in the composite films since the bare PCL and PLA films showed no antibacterial activity. Additionally, solvent-casted TSNP/PLA films demonstrated higher AE values than TSNP/PCL films against both *S. aureus* and *E. coli*, which can be attributed to the easiness of  $Ag^+$  ions to be released from the surface of the PLA rather than the PCL matrix. Such results were in accordance with Ahi et al. (2019), who demonstrated that PLA films treated with a microbicidal compound such as propolis had a higher antimicrobial activity than PCL films did against *S. aureus* [58].

It is also worth mentioning that the TSNP-treated films showed increased antibacterial activity against Gram-negative bacteria than towards Gram-positive ones. This was due to the scarce thickness of the cell wall in the Gram-negative bacteria, making them more susceptible to the action of  $Ag^+$  ions released by the TSNPs in the treated films [59,60].

**Table 2.** Antimicrobial effect (AE) values \* for TSNP-treated films.

Bacterial Strain	TSNP/PCL Films	TSNP/PLA Films
<i>E. coli</i> ATCC 9001	0.10	0.35
<i>S. aureus</i> ATCC 25923	0.11	0.28

\*Values were obtained as the average of three measurements.  $AE = \log N_C - \log N_E$

## 4. Conclusions

In this study, a solvent-casting technique for the incorporation of in-house fabricated TSNPs in PCL and PLA polymers was developed. The effect of TSNPs on the morphological structure, thermal properties, mechanical properties, and antimicrobial activity of PCL and PLA films was investigated. An SEM analysis showed the cross-section of the TSNP-treated films had a rougher surface than the bare films. The DSC curves confirmed that TSNPs had no effect on  $T_c$  and  $T_m$  values, but had an enhancing effect on the  $X_c$  percentage, especially for PLA. With the addition of TSNPs, TGA results showed maintenance in the thermal stability of the treated films. We found that with the incorporation of TSNPs in the model polymers, the composite films had a higher TS and lower elongation of break ( $\epsilon$ ). The EM of PLA films was also improved upon the addition of TSNPs, while no significant effect was observed on the EM of treated PCL films. Concerning the antimicrobial activity, the treated PCL and PLA films showed an enhanced growth inhibition for both *E. coli* and *S. aureus* strains, which was attributed to the bacterial inhibition ability of the TSNPs.

In conclusion, the obtained results clearly showed that these PCL and PLA films with incorporated TSNPs have considerable potential as bioplastics, with acceptable antimicrobial activity for surface and biomedical applications. Future work will constitute the

optimization of TSNP-treated films to maximize their antimicrobial activity. In addition, a comparative study will be carried out to demonstrate the advantage of TSNPs over other morphologies of Ag NPs with respect to the antimicrobial activity of treated polymer films.

**Supplementary Materials:** The following are available online at <https://www.mdpi.com/1996-1944/14/5/1132/s1>, Instrumentation, Figure S1. UV-VIS spectrum of Scaled-Up TSNPs (300 mL).

**Author Contributions:** Conceptualization, M.M. and M.B.F.; methodology, E.L.G., O.A.A. and M.M.; validation, M.M.; formal analysis, O.A.A.; investigation, E.L.G. and O.A.A.; resources, E.L.G., D.M.D. and M.B.F.; data curation, E.L.G.; writing—original draft preparation, E.L.G.; writing—review and editing, O.A.A., M.M. and M.B.F.; visualization, E.L.G. and O.A.A.; supervision, M.B.F.; project administration, D.M.D. and M.B.F.; funding acquisition, D.M.D. and M.B.F. All authors have read and agreed to the published version of the manuscript.

**Funding:** This project received funding from the European Union's Horizon 2020 research and innovation programme under grant agreement No. 870292 (BioICEP) and was supported by the National Natural Science Foundation of China (grant numbers: Institute of Microbiology, Chinese Academy of Sciences: 31961133016; Beijing Institute of Technology: 31961133015; Shandong University: 31961133014). This project also received funding from a part of the Interreg VB NWE Programme, project number NWE1058 (CURCOL).

**Data Availability Statement:** All data generated or analysed during this study are included in the article (and its Supplementary Information Files).

**Acknowledgments:** The authors acknowledge the guidance and support received from the research institute at the Athlone Institute of Technology.

**Conflicts of Interest:** The authors declare no conflict of interest.

## References

1. Michael, C.A.; Dominey-Howes, D.; Labbate, M. The antimicrobial resistance crisis: Causes, consequences, and management. *Front. Public Health* **2014**, *2*, 1–8. [CrossRef] [PubMed]
2. Conly, J.M.; Johnston, B.L. Where are all the new antibiotics. *Can. J. Infect. Dis. Med. Microbiol.* **2005**, *16*, 159–160. [CrossRef] [PubMed]
3. Wouters, O.J.; McKee, M.; Luyten, J. Estimated Research and Development Investment Needed to Bring a New Medicine to Market, 2009–2018. *JAMA J. Am. Med. Assoc.* **2020**, *323*, 844–853. [CrossRef]
4. D'Astino, A.; Taglietti, A.; Desando, R.; Bini, M.; Patrini, M.; Dacarro, G.; Cucca, L.; Pallavicini, P.; Grisoli, P. Bulk surfaces coated with triangular silver nanoplates: Antibacterial action based on silver release and photo-thermal effect. *Nanomaterials* **2017**, *7*, 7. [CrossRef]
5. Baptista, P.V.; McCusker, M.P.; Carvalho, A.; Ferreira, D.A.; Mohan, N.M.; Martins, M.; Fernandes, A.R. Nano-strategies to fight multidrug resistant bacteria—“A Battle of the Titans”. *Front. Microbiol.* **2018**, *9*, 1–26. [CrossRef]
6. Lee, S.H.; Jun, B.H. Silver nanoparticles: Synthesis and application for nanomedicine. *Int. J. Mol. Sci.* **2019**, *20*, 865. [CrossRef]
7. Renziye, G.; Erdal, G. Synthesis of Silver Nanoparticles. In *Silver Nanoparticles: Fabrication, Characterization and Applications*; IntechOpen: London, UK, 2018. [CrossRef]
8. Erdogan, O.; Kara, M. Analytical approach to the waste management of nanomaterials in developing countries. *Front. Drug Chem. Clin. Res.* **2019**, *2*, 1–5. [CrossRef]
9. Hadrup, N.; Sharma, A.K.; Loeschner, K. Toxicity of silver ions, metallic silver, and silver nanoparticle materials after in vivo dermal and mucosal surface exposure: A review. *Regul. Toxicol. Pharmacol.* **2018**, *98*, 257–267. [CrossRef] [PubMed]
10. Akter, M.; Sikder, M.T.; Rahman, M.M.; Ullah, A.K.M.A.; Hossain, K.F.B.; Banik, S.; Hosokawa, T.; Saito, T.; Kurasaki, M. A systematic review on silver nanoparticles-induced cytotoxicity: Physicochemical properties and perspectives. *J. Adv. Res.* **2018**, *9*, 1–16. [CrossRef] [PubMed]
11. Raza, M.A.; Kanwal, Z.; Rauf, A.; Sabri, A.N.; Riaz, S.; Naseem, S. Size and shape-dependent antibacterial studies of silver nanoparticles synthesized by wet chemical routes. *Nanomaterials* **2016**, *6*, 74. [CrossRef] [PubMed]
12. Kelly, K.L.; Coronado, E.; Zhao, L.L.; Schatz, G.C. The Optical Properties of Metal Nanoparticles: The Influence of Size, Shape, and Dielectric Environment. *J. Phys. Chem. B* **2003**, *107*, 668–677. [CrossRef]
13. Lu, W.; Yao, K.; Wang, J.; Yuan, J. Ionic liquids-water interfacial preparation of triangular Ag nanoplates and their shape-dependent antibacterial activity. *J. Colloid Interface Sci.* **2015**, *437*, 35–41. [CrossRef]
14. Pal, S.; Tak, Y.K.; Song, J.M. Does the antibacterial activity of silver nanoparticles depend on the shape of the nanoparticle? A study of the gram-negative bacterium *Escherichia coli*. *Appl. Environ. Microbiol.* **2007**, *73*, 1712–1720. [CrossRef] [PubMed]
15. Van Dong, P.; Ha, C.H.; Binh, L.T.; Kasbohm, J. Chemical synthesis and antibacterial activity of novel-shaped silver nanoparticles. *Int. Nano Lett.* **2012**, *2*, 9. [CrossRef]



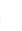





16. Flores-López, L.Z.; Espinoza-Gómez, H.; Somanathan, R. Silver nanoparticles: Electron transfer, reactive oxygen species, oxidative stress, beneficial and toxicological effects. Mini review. *J. Appl. Toxicol.* **2019**, *39*, 16–26. [\[CrossRef\]](#)
17. Vo, Q.K.; Phung, D.D.; Nguyen, Q.N.V.; Thi, H.H.; Thi, N.H.N.; Thi, P.P.N.; Bach, L.G.; Tan, L.V. Controlled synthesis of triangular silver nanoplates by gelatin-chitosan mixture and the influence of their shape on antibacterial activity. *Processes* **2019**, *7*, 873. [\[CrossRef\]](#)
18. Binkley, D.M.; Lee, B.E.J.; Saem, S.; Moran-Mirabal, J.; Grandfield, K. Fabrication of polycaprolactone electrospun nanofibers doped with silver nanoparticles formed by air plasma treatment. *Nanotechnology* **2019**, *30*, 215101. [\[CrossRef\]](#)
19. Thomas, R.; Soumya, K.R.; Mathew, J.; Radhakrishnan, E.K. Electrospun Polycaprolactone Membrane Incorporated with Biosynthesized Silver Nanoparticles as Effective Wound Dressing Material. *Appl. Biochem. Biotechnol.* **2015**, *176*, 2213–2224. [\[CrossRef\]](#) [\[PubMed\]](#)
20. Shamel, K.; Ahmad, M.B.; Yunus, W.Z.; Ibrahim, N.A.; Rahman, R.A.; Jokar, M.; Darroudi, M. Silver/poly (lactic acid) nanocomposites: Preparation, characterization, and antibacterial activity. *Int. J. Nanomedicine* **2010**, *5*, 573–579. [\[CrossRef\]](#)
21. Sonseca, A.; Madani, S.; Rodríguez, G.; Hevilla, V.; Echeverría, C.; Fernández-García, M.; Muñoz-Bonilla, A.; Charef, N.; López, D. Multifunctional PLA blends containing chitosan mediated silver nanoparticles: Thermal, mechanical, antibacterial, and degradation properties. *Nanomaterials* **2020**, *10*, 1065. [\[CrossRef\]](#)
22. Kango, S.; Kalia, S.; Celli, A.; Njuguna, J.; Habibi, Y.; Kumar, R. Surface modification of inorganic nanoparticles for development of organic-inorganic nanocomposites—A review. *Prog. Polym. Sci.* **2013**, *38*, 1232–1261. [\[CrossRef\]](#)
23. Park, J.O.; Cho, S.H.; Lee, J.S.; Lee, W.; Lee, S.Y. A foolproof method for phase transfer of metal nanoparticles via centrifugation. *Chem. Commun.* **2016**, *52*, 1625–1628. [\[CrossRef\]](#)
24. Müller, K.; Bugnicourt, E.; Latorre, M.; Jorda, M.; Sanz, Y.E.; Lagaron, J.M.; Miesbauer, O.; Bianchin, A.; Hankin, S.; Bözl, U.; et al. Review on the processing and properties of polymer nanocomposites and nanocoatings and their applications in the packaging, automotive and solar energy fields. *Nanomaterials* **2017**, *7*, 74.
25. Vukoje, I.; Lazić, V.; Vodnik, V.; Mitrić, M.; Jokić, B.; Ahrenkiel, S.P.; Nedeljković, J.M.; Radetić, M. The influence of triangular silver nanoplates on antimicrobial activity and color of cotton fabrics pretreated with chitosan. *J. Mater. Sci.* **2014**, *49*, 4453–4460. [\[CrossRef\]](#)
26. Knauer, A.; Csáki, A.; Fritzsche, W.; Serra, C.A.; Lederer, N.; Michael Köhler, J. Micro continuous flow-through synthesis of triangular silver nanoprisms and their incorporation in complexly composed polymer microparticles. *Chem. Eng. J.* **2013**, *227*, 191–197. [\[CrossRef\]](#)
27. Audoit, J.; Laffont-dantras, L.; Lonjon, A.; Dantras, E.; Audoit, J.; Laffont-dantras, L.; Lonjon, A.; Dantras, E.; Percolative, C.L. Percolative silver nanoplates/PVDF nanocomposites: Bulk and surface electrical conduction. *Polymer* **2016**, *78*, 104–110. [\[CrossRef\]](#)
28. Zhang, J.; Sun, Y.; Zhang, H.; Xu, B.; Zhang, H.; Song, D. Preparation and application of triangular silver nanoplates/chitosan composite in surface plasmon resonance biosensing. *Anal. Chim. Acta* **2013**, *769*, 114–120. [\[CrossRef\]](#)
29. Reynoso-García, P.J.; Guizado-Rodríguez, M.; Barba, V.; Ramos-Ortiz, G.; Martínez-Gutiérrez, H. Stabilization of Silver Nanoparticles with a Dithiocarbamate Ligand and Formation of Nanocomposites by Combination with Polythiophene Derivative Nanoparticles. *Adv. Condens. Matter Phys.* **2018**, *2018*, 4376051. [\[CrossRef\]](#)
30. Kudryashov, M.; Logunov, A.; Gogova, D.; Mashin, A.; De Filpo, G. Ag/PVP/PAN nanocomposites with triangular nanoprisms of silver synthesized by UV-induced polymerization: Morphology manipulation and optical properties tuning. *Opt. Mater.* **2020**, *101*, 109746. [\[CrossRef\]](#)
31. Aherne, D.; Ledwith, D.M.; Gara, M.; Kelly, J.M. Optical properties and growth aspects of silver nanoprisms produced by a highly reproducible and rapid synthesis at room temperature. *Adv. Funct. Mater.* **2008**, *18*, 2005–2016. [\[CrossRef\]](#)
32. Solomon, S.D.; Bahadory, M.; Jeyarajasingam, A.V.; Rutkowsky, S.A.; Boritz, C.; Mulfinger, L. Synthesis and study of silver nanoparticles. *J. Chem. Educ.* **2007**, *84*, 322–325.
33. Kelly, J.M.; Keegan, G.; Brennan-Fournet, M.E. Triangular silver nanoparticles: Their preparation, functionalisation and properties. *Acta Phys. Pol. A* **2012**, *122*, 337–345. [\[CrossRef\]](#)
34. Etacheri, V.; Georgekutty, R.; Seery, M.K.; Pillai, S.C. Single step morphology-controlled synthesis of silver nanoparticles. *Mater. Res. Soc. Symp. Proc.* **2010**, *1217*, 7–13. [\[CrossRef\]](#)
35. Charles, D.E.; Aherne, D.; Gara, M.; Ledwith, D.M.; Gun, Y.K.; Kelly, J.M.; Blau, W.J.; Brennan-fournet, M.E. Versatile Solution Phase Triangular Silver Nanoplates for Highly Sensitive Plasmon Resonance Sensing. *ACS Nano* **2010**, *4*, 55–64. [\[CrossRef\]](#) [\[PubMed\]](#)
36. Zhang, Y.; Charles, D.E.; Ledwith, D.M.; Aherne, D.; Cunningham, S.; Voisin, M.; Blau, W.J.; Gun'ko, Y.K.; Kelly, J.M.; Brennan-Fournet, M.E. Wash-free highly sensitive detection of C-reactive protein using gold derivatised triangular silver nanoplates. *RSC Adv.* **2014**, *4*, 29022–29031. [\[CrossRef\]](#)
37. Brennan-Fournet, M.E.; Huerta, M.; Zhang, Y.; Malliaras, G.; Owens, R.M. Detection of fibronectin conformational changes in the extracellular matrix of live cells using plasmonic nanoplates. *J. Mater. Chem. B* **2015**, *3*, 9140–9147. [\[CrossRef\]](#) [\[PubMed\]](#)
38. Shephard, J.J.; Soper, A.K.; Callear, S.K.; Imberti, S.; Evans, J.S.O.; Salzmann, C.G. Polar stacking of molecules in liquid chloroform. *Chem. Commun.* **2015**, *51*, 4770–4773. [\[CrossRef\]](#) [\[PubMed\]](#)
39. Bashkatov, A.N.; Genina, E.A. Water refractive index in dependence on temperature and wavelength: A simple approximation. *Proc. SPIE Int. Soc. Opt. Eng.* **2003**, *5068*, 393–395.

40. Samoc, A. Dispersion of refractive properties of solvents: Chloroform, toluene, benzene, and carbon disulfide in ultraviolet, visible, and near-infrared. *J. Appl. Phys.* **2003**, *94*, 6167–6174. [\[CrossRef\]](#)
41. Aherne, D.; Charles, D.E.; Brennan-Fournet, M.E.; Kelly, J.M.; Gun'ko, Y.K. Etching-resistant silver nanoprisms by epitaxial deposition of a protecting layer of gold at the edges. *Langmuir* **2009**, *25*, 10165–10173. [\[CrossRef\]](#)
42. Shuaib, U.; Hussain, T.; Ahmad, R.; Zakaullah, M.; Mubarak, F.E.; Muntaha, S.T.; Ashraf, S. Plasma-liquid synthesis of silver nanoparticles and their antibacterial and antifungal applications. *Mater. Res. Express* **2020**, *7*, 035015. [\[CrossRef\]](#)
43. Li, W.; Zhang, C.; Chi, H.; Li, L.; Lan, T.; Han, P.; Chen, H.; Qin, Y. Development of antimicrobial packaging film made from poly (lactic acid) incorporating titanium dioxide and silver nanoparticles. *Molecules* **2017**, *22*, 1170. [\[CrossRef\]](#)
44. Benhacine, F.; Hadj-Hamou, A.S.; Habi, A. Development of long-term antimicrobial poly ( $\epsilon$ -caprolactone)/silver exchanged montmorillonite nanocomposite films with silver ion release property for active packaging use. *Polym. Bull.* **2016**, *73*, 1207–1227. [\[CrossRef\]](#)
45. Mróz, P.; Bialas, S.; Mucha, M.; Kaczmarek, H. Thermogravimetric and DSC testing of poly (lactic acid) nanocomposites. *Thermochim. Acta* **2013**, *573*, 186–192. [\[CrossRef\]](#)
46. Chu, Z.; Zhao, T.; Li, L.; Fan, J.; Qin, Y. Characterization of antimicrobial poly (lactic acid)/ nano-composite films with silver and zinc oxide nanoparticles. *Materials* **2017**, *10*, 659. [\[CrossRef\]](#) [\[PubMed\]](#)
47. Gorraasi, G.; Sorrentino, A.; Pantani, R. Modulation of Biodegradation Rate of Poly (lactic acid) by Silver Nanoparticles. *J. Polym. Environ.* **2015**, *23*, 316–320. [\[CrossRef\]](#)
48. Nootsuwan, N.; Sukthavorn, K.; Wattanathana, W.; Jongrungruangchok, S.; Veranitisagul, C.; Koonsaeng, N.; Laobuthee, A. Development of antimicrobial hybrid materials from polylactic acid and nano-silver coated chitosan. *Orient. J. Chem.* **2018**, *34*, 683–692. [\[CrossRef\]](#)
49. Cerkez, I.; Sezer, A.; Bhullar, S.K. Fabrication and characterization of electrospun poly( $\epsilon$ -caprolactone) fibrous membrane with antibacterial functionality. *R. Soc. Open Sci.* **2017**, *4*, 160911. [\[CrossRef\]](#) [\[PubMed\]](#)
50. Leonés, A.; Mujica-García, A.; Arrieta, M.P.; Salari, V.; Lopez, D.; Kenny, J.M.; Peponi, L. Organic and inorganic PCL-based electrospun fibers. *Polymers* **2020**, *12*, 1325. [\[CrossRef\]](#)
51. Augustine, R.; Kalarikkal, N.; Thomas, S. Electrospun PCL membranes incorporated with biosynthesized silver nanoparticles as antibacterial wound dressings. *Appl. Nanosci.* **2016**, *6*, 337–344. [\[CrossRef\]](#)
52. Ali, N.A.; Tariq, F.; Noori, M. Crystallinity, Mechanical, and Antimicrobial properties of Polylactic acid/microcrystalline cellulose/Silver Nanocomposites. *Int. J. Appl. Innov. Eng. Manag.* **2014**, *3*, 77–81.
53. Szymańska-Chargot, M.; Chylińska, M.; Pieczywek, P.M.; Walkiewicz, A.; Pertile, G.; Frac, M.; Cieślak, K.J.; Zdunek, A. Evaluation of nanocomposite made of polylactic acid and nano-cellulose from carrot pomace modified with silver nanoparticles. *Polymers* **2020**, *12*, 812. [\[CrossRef\]](#)
54. Abdelaziz, D.; Hefnawy, A.; Al-Wakeel, E.; El-Fallal, A.; El-Sherbiny, I.M. New biodegradable nanoparticles-in-nanofibers based membranes for guided periodontal tissue and bone regeneration with enhanced antibacterial activity. *J. Adv. Res.* **2020**. [\[CrossRef\]](#)
55. Liu, C.; Shen, J.; Yeung, K.W.K.; Tjong, S.C. Development and Antibacterial Performance of Novel Poly(lactic acid)-Graphene Oxide-Silver Nanoparticle Hybrid Nanocomposite Mats Prepared by Electrospinning. *ACS Biomater. Sci. Eng.* **2017**, *3*, 471–486. [\[CrossRef\]](#)
56. Lu, H.; Zhu, J.; Li, J.; Chen, J. Effectiveness of Active Packaging on Control of *Escherichia Coli* O157:H7 and Total Aerobic Bacteria on Iceberg Lettuce. *J. Food Sci.* **2015**, *80*, M1325–M1329. [\[CrossRef\]](#) [\[PubMed\]](#)
57. González-Fandos, E.; Giménez, M.; Olarte, C.; Sanz, S.; Simón, A. Effect of packaging conditions on the growth of micro-organisms and the quality characteristics of fresh mushrooms (*Agaricus bisporus*) stored at inadequate temperatures. *J. Appl. Microbiol.* **2000**, *89*, 624–632. [\[CrossRef\]](#)
58. Ahi, Z.B.; Renkler, N.Z.; Gul Seker, M.; Tuzlakoglu, K. Biodegradable Polymer Films with a Natural Antibacterial Extract as Novel Periodontal Barrier Membranes. *Int. J. Biomater.* **2019**. [\[CrossRef\]](#)
59. Pazos-Ortiz, E.; Roque-Ruiz, J.H.; Hinojos-Márquez, E.A.; López-Esparza, J.; Donohué-Cornejo, A.; Cuevas-González, J.C.; Espinosa-Cristóbal, L.E.; Reyes-López, S.Y. Dose-Dependent Antimicrobial Activity of Silver Nanoparticles on Polycaprolactone Fibers against Gram-Positive and Gram-Negative Bacteria. *J. Nanomater.* **2017**. [\[CrossRef\]](#)
60. Abbaszadegan, A.; Ghahramani, Y.; Gholami, A.; Hemmateenejad, B.; Dorostkar, S.; Nabavizadeh, M.; Sharghi, H. The Effect of Charge at the Surface of Silver Nanoparticles on Antimicrobial Activity against Gram-Positive and Gram-Negative Bacteria: A Preliminary Study. *J. Nanomater.* **2015**. [\[CrossRef\]](#)

Review

## Macro and Micro Routes to High Performance Bioplastics: Bioplastic Biodegradability and Mechanical and Barrier Properties

Olivia A. Attallah <sup>1</sup>, Marija Mojicevic <sup>1,\*</sup>, Eduardo Lanzagorta Garcia <sup>1</sup>, Muhammad Azeem <sup>1</sup>,  
Yuanyuan Chen <sup>1</sup>, Shumayl Asmawi <sup>2</sup> and Margaret Brenan Fournet <sup>1</sup>

<sup>1</sup> Materials Research Institute, Athlone Institute of Technology, N37 HD68 Athlone, Ireland; oadly@ait.ie (O.A.A.); e.lgarcia@research.ait.ie (E.L.G.); m.azeem@research.ait.ie (M.A.); yuanyuanchen@ait.ie (Y.C.); mfournet@ait.ie (M.B.F.)

<sup>2</sup> Fundamental and Applied Science Department, Universiti Teknologi PETRONAS, Bandar Seri Iskandar 32610, Perak Darul Ridzuan, Malaysia; muhammad\_24531@utp.edu.my

\* Correspondence: mmojicevic@ait.ie



**Citation:** Attallah, O.A.; Mojicevic, M.; Garcia, E.L.; Azeem, M.; Chen, Y.; Asmawi, S.; Brenan Fournet, M. Macro and Micro Routes to High Performance Bioplastics: Bioplastic Biodegradability and Mechanical and Barrier Properties. *Polymers* **2021**, *13*, 2155. <https://doi.org/10.3390/polym13132155>

Academic Editors: José Miguel Ferré, Vicent Fombuena Borrás and Miguel Fernando Aldás Carrasco

Received: 29 May 2021

Accepted: 25 June 2021

Published: 30 June 2021

**Publisher's Note:** MDPI stays neutral with regard to jurisdictional claims in published maps and institutional affiliations.



Copyright © 2021 by the authors. Licensee MDPI, Basel, Switzerland. This article is an open access article distributed under the terms and conditions of the Creative Commons Attribution (CC BY) license (<https://creativecommons.org/licenses/by/4.0/>).

**Abstract:** On a score sheet for plastics, bioplastics have a medium score for combined mechanical performance and a high score for biodegradability with respect to counterpart petroleum-based plastics. Analysis quickly confirms that endeavours to increase the mechanical performance score for bioplastics would be far more achievable than delivering adequate biodegradability for the recalcitrant plastics, while preserving their impressive mechanical performances. Key architectural features of both bioplastics and petroleum-based plastics, namely, molecular weight ( $M_w$ ) and crystallinity, which underpin mechanical performance, typically have an inversely dependent relationship with biodegradability. In the case of bioplastics, both macro and micro strategies with dual positive correlation on mechanical and biodegradability performance, are available to address this dilemma. Regarding the macro approach, processing using selected fillers, plasticisers and compatibilisers have been shown to enhance both targeted mechanical properties and biodegradability within bioplastics. Whereas, regarding the micro approach, a whole host of bio and chemical synthetic routes are uniquely available, to produce improved bioplastics. In this review, the main characteristics of bioplastics in terms of mechanical and barrier performances, as well as biodegradability, have been assessed—identifying both macro and micro routes promoting favourable bioplastics' production, processability and performance.

**Keywords:** biomaterials; biodegradation; bioplastics; mechanical performance; barrier performance; processability

### 1. Introduction

Pervasive plastics are leaving an indelible imprint on our planet. As high performance and energy-saving materials, plastics are ubiquitous and central to socio-economic advancement. Current mainstay plastics are processed from fossil fuel resources, with production requirements expected to double over the next 20 years. After use, these recalcitrant plastics are contributing to waste stockpiles and alarming pollution. Recycling technologies, which primarily include mechanical and thermochemical approaches, does not meet the efficiency levels required to safeguard the planet and adequately revalorise plastics as new products. The current linear economic model of resource mining, use and discarding, is now widely recognised as unsustainable. A circular approach, where resources are repurposed cyclically, akin to biological lifecycles, is essential in achieving a sustainable socio-economic ecosystem.

Nature readily operates elegant and efficient regenerative cycles for natural polymers and end of life bio-based materials. Such biodegradation and bio-regeneration processes

involve microbial, enzymatic and biocatalytic activities for depolymerisation and repolymerisation. Petroleum-based plastics, with their smooth surface topographies, extensive hydrophobic chains and lack of bio-accessible organic chemical groups, are strongly bio-inert and largely incompatible with bioprocessing, leading to their persistence over century timescales within land and water environments. Biomass provides a wealth of renewable and bio-waste resources for bioplastics synthesis. Many of these bio-based plastics, encompass capacities for biodegradation and bioprocessing with high performance features akin to petroleum-based plastics. The realisation of bioplastics that exhibit a complete set of mechanical and biodegradability, hold the promise of delivering material of ecologically sustainable, low carbon footprint circularity.

Bioplastics to date, however, have not achieved wide acceptability by the industry. Incompatibility with existing sorting infrastructures and high temperature mechanical recycling implemented for fossil-based plastics, along with raised production costs, are limiting factors. Technical shortcomings, such as brittleness, lower gas barrier functions and processing performances, have also played a role in keeping current market penetration levels in the region at just 2%. Combining high performance for consumer applications and continuous low carbon closed loop regeneration within plastics poses considerable challenges. At a fundamental structural level, polymeric features associated with good mechanical and fluid barrier properties are typically prohibitive to biodegradability. Petroleum-based plastics achieve the required degrees of high mechanical strength combined with flexibility and strong liquid and gas barrier properties by packing their sleek chemically structured chains into signature crystalline and amorphous regional arrangements. The tight alignment of chemically simple chains at high degrees of crystallinity also renders these plastics largely incompatible with biodegradation processes that require bioactivities, including enzymatic hydrolysis. Bioplastics, in contrast, by the very fact that they are generated from bio-based resources, are inherently more complex with more elaborate chemical structures. This provides both a means to progress their mechanical performance properties and provides amenability to bioactivity with higher levels of hydrolysable groups available for post use biodegradation and biodepolymerisation. To date, equivalent results are readily achievable, and in cases, results outperform particular mechanical properties for polylactic acid (PLA) and polyhydroxyalkanoates (PHA) bioplastics compared with conventional fossil-based thermoplastics. The potential to address performance limitations by a combination of bottom up and top-down approaches using considered chemical structure modifications and blending and composite formations, holds the promise of framing a new generation of bioplastics that encompass sustainability with performance.

In this review, the sustainability/performance triangulation between the biodegradability, mechanical and barrier properties of bioplastics is discussed. Approaches to overcoming the gap between industrially required mechanical and barrier performances and biodegradability are overviewed and related to the potential to build a new generation of high-performance sustainable plastics.

## 2. Bioplastic Production

Biopolymers can be obtained directly from biomass, as in the case of proteins and polysaccharides and synthetic biopolymers, such as PLA. Biodegradable polymers, including polycaprolactone (PCL), polyglycolic acid (PGA) and polybutylene succinate-co-adipate (PBSA), are primarily synthesised from petrochemicals. Microbial fermentation of biopolymers, including PHA and bacterial cellulose (BC), operates under relatively benign low energy conditions, and hence, is a highly favourable sustainable production route. Various microorganisms can accumulate PHAs as storage materials when cultivated under different nutrient and environmental conditions. This ability allows their survival under stressful conditions. The number and size of the PHA granules, the monomer composition, macromolecular structure and physico-chemical properties vary, depending on the producing microorganisms, the feedstock supplied and the operation conditions [1–3]. On the other hand, some bacteria can produce BC. This exopolysaccharide is a naturally occurring,

chemically pure, free of hemicellulose, lignin and pectin, which is why BC purification is an easy process demanding low energy consumption. Nevertheless, production yields are very low, cultivation times are extensive, and thickness of layers is limited, which are major drawbacks in the conventional BC production process, affecting the range of possible applications [4]. For the industrial production of bioplastics, three limitations are very important. These include requirements of specialised growth conditions, expensive precursors, and high recovery costs. Building an increased body of knowledge on producing microbes' metabolism, biosynthetic pathways and their regulation is essential in overcoming these limitations [1,5].

### 3. Biosynthesised Plastics

In recent years, PHA polymers have emerged as one of the most promising biodegradable materials. Unlike commonly used fossil-based plastics or PLA, which requires the additional step of lactic acid polymerisation, PHAs are the product of bacterial metabolism and have a function of cytoplasmic inclusions. These materials, thanks to the over 150 monomer units, can have a variety of polymer properties that can compete with commonly used plastics, such as polyethylene or polypropylene [6]. Monomer composition is connected to the substrate specificity of PHA synthase, hence the type of derived PHA is highly connected to the microorganism used for its production. For example, biosynthesis of short-chain length PHAs (SCL-PHAs) consisting of poly-3-hydroxybutyrate P(3HB) homopolymers is a three-step process regulated by 3-ketothiolase, acetoacetyl-CoA reductase and the SCL PHA synthase [7,8]. Bacteria, such as *Aeromonas caviae* and *Pseudomonas stutzeri*, are proven producers of PHA synthases with wide substrate specificity. Moreover, these enzymes have been identified after recombinant expression in *Ralstonia eutropha*, previously PHA negative. These PHA synthases can produce copolymers of SCL- and medium-chain length PHAs (MCL-PHA) [9]. It has been reported that combinatorial mutations in *P. aeruginosa*, *P. oleovorans*, and *P. putida* resulted in their ability to synthesise PHAs with 3-hydroxybutyrate (3HB), 3-hydroxyhexanoate (3HHx), 3-hydroxyoctanoate (3HO), 3-hydroxydecanoate (3HD), or 3-hydroxydodecanoate (3HDD) monomers [10–13]. These structures are presented in Table 1. The development of recombinant strains and using genetic engineering techniques can lead to improved mechanical and thermal characteristics of PHA materials. These properties are highly dependent on various factors during upstream and downstream processes. Modification of PHAs chemical structure, such as the introduction of functional groups or producing blends and copolymers, can also affect the quality of these materials [14]. Traditional chemical synthesis techniques have been successfully used for creating block copolymers with PHA materials. For example, block copolymers, including PHB blocks balancing with other materials (poly(6-hydroxyhexanoate), poly(3-hydroxyoctanoate), monomethoxy-terminated poly(ethylene glycol) (mPEG), and poly(ethylene glycol) (PEG)), have been reported. These structures are presented in Table 2 [8,15].

**Table 1.** Chemical structures of monomers described as units of PHA copolymer producing strains.

3-Hydroxyacids	Structure
butyric (3HB)	
hexanoic (3HHx)	
octanoic (3HO)	
decanoic (3HD)	
dodecanoic (3HDD)	

**Table 2.** Chemical structures of polymers commonly found as building blocks in PHA related block copolymers.

Polymer	Structure
poly(6-hydroxyhexanoate)	
poly(3-hydroxyoctanoate)	
monomethoxy-terminated poly(ethylene glycol) (mPEG)	
poly(ethylene glycol)	

PHAs can also be derived from various substrates, including industrial waste streams [16], food waste [17], supplemented solid biodiesel waste, plant oils [7]. Besides these, seaweeds were found to be great feedstock for PHAs productions [18]. These materials can be produced using different strategies, including batch, fed-batch and continuous processes, and various conditions could be used for their conduction. Batch cultivations are easy and simple to operate, but production yields are very low. On the other hand, fed-batch cultivation can provide higher product and cell concentrations (no substrate inhibition) [19].

Continuous cultivation are also considered to be a viable strategy, providing required concentrations of limiting substrates, such as fatty acids and their derivatives [20]. Nevertheless, large scale application is still impractical with this type of production. Another strategy used for PHA production is solid state fermentation (SSF)—microbial cultivation on solid support made of appropriate substrates. SSF can be performed with inexpensive cultivation media, such as substrates, based on agro-industrial residues. This strategy provides disposing of waste, while valuable compounds are being produced at the same time [21]. There are few additional advantages of SSF over submerged fermentation: Easier aeration, higher substrate concentration, as well as reduced downstream processing steps. However, keeping conditions constant during the process is the biggest drawback to the market-ready production of PHAs using this strategy [22].

Bacteria from the genus *Komagataeibacter* (former *Gluconacetobacter*) synthesises another interesting, biosynthesised bioplastic—bacterial cellulose (BC). The BC production is a multi-step, strictly regulated process that involves regulatory proteins, few enzymes and catalytic complexes. The formation of 1,4- $\beta$ -glucan chains is the first step in BC synthesis. This process, together with chains' assembly and crystallisation, occurs intracellularly. The second step involves extracting cellulose chains from the cells and their assembly in fibrils [4,23]. The yield and properties of the resulting material highly depend on the used bacterial strain and conditions of the conducted process, including medium composition, aeration, shaking, etc. Morphological and physical properties of the resulting material are in correlation to the cultivation broth composition. BC production can be improved using genetically modified producing strains, isolating novel strains with the ability to produce BC, and investigating process parameters and their significance. Florea et al. isolated *Komagataeibacter rhaeticus* strain able to produce a high yield of BC, while growing in low nitrogen level medium [24]. In order to increase BC production in limited oxygen conditions, genetically engineered strains have been developed [25]. Hungund et al. reported using ethyl methanesulfonate and ultraviolet radiation for *Gluconacetobacter xylinus* NCIM 2526 strain improvement that resulted in a significantly higher yield of BC (30%) [26].

Different strategies can be used to produce BC, including aerated submerged cultivation, static culture and airlift bioreactors [27]. Effects of these conditions on cellulose mechanical properties are presented in Figure 1.

Tensile strength, polymerisation degree and crystallinity index are highly influenced by BC structure. Produced in static conditions, BC forms pellicles on the surface of the medium. This gelatinous membrane can vary in thickness up to few centimetres depending on substrates' availability. Produced like this, BC has a significantly higher crystallinity index and tensile strength than the BC produced in agitated culture. Supply of air in agitated cultures will result in pellets with a higher crystallinity index. Crucial factors in BC production are the design of the reactor and proper control of conditions and process. These parameters highly affect the yield and quality of the resulting material. No matter which strategy is used, pH, oxygen supply, and temperature are essential conditions that should be carefully monitored. These parameters are mostly strain-dependent, but it was shown that the optimal pH value for cell growth and BC production is usually between 4.0 and 7.023, while the optimal temperature is in the range 28–30 °C [28].

Despite the great mechanical properties of the resulting material, static culture cannot provide uniformity of the cultivation broth; hence, cells are not equally exposed to nutrients and the thickness of the BC layer can be uneven. Additionally, productivity achieved in this strategy is very low, and it demands an extensive period of cultivation [29,30]. To improve the productivity of this process, the fed-batch strategy was developed, and a constant BC production rate was achieved for 30 days [31]. Submerged cultivations with agitation provide uniformity of nutrients, especially oxygen, resulting in higher yields in comparison to the static cultivations and making the production process cost-effective. Products of agitated fermentation depend on applied agitation speed and may include various forms of cellulose: Spheres, pellets, fibrous suspension [32]. As previously mentioned, higher

productivity is the biggest advantage of submerged compared to static cultivation, but drawbacks, such as products' shape consistency and limited mechanical properties, are issued to overcome [33]. Another problem that can limit BC yield in aerated cultivation is a synthesis of gluconic acid. Due to the high agitation rates and hydrostatic stresses, the production of the secondary, protective metabolites is favoured over cellulose. Nevertheless, submerged cultivation of BC was implemented in different types of bioreactors, such as airlift, stirred tank and rotating disk. Production of this material on a large scale is still an issue, and designing new or improving existing equipment for this purpose is an important subject of research [34].

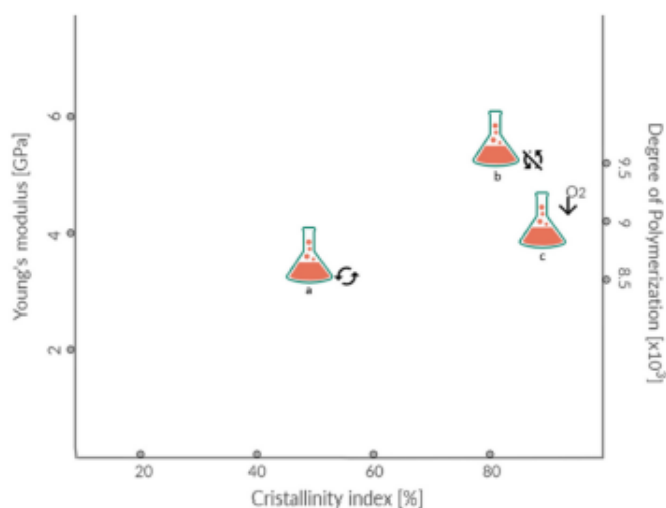


**Figure 1.** Young's modulus, crystallinity index and degree of polymerisation of BC depending on cultivation conditions: a—with shaking, b—without shaking, c—with additional oxygen supply.

### 3.1. Bioplastic Mechanical Performance

Bio-based polyesters (PLA, and PHAs) exhibit similar mechanical properties and can even exceed conventional plastic performances. Figure 2 demonstrates the Maximum Tensile Strength (MPa) and maximum Tensile Elongation (%) of bioplastics compared to petroleum-derived plastics. PLA is one of the most prominent bioplastics in terms of global consumption. It possesses several desirable properties, such as biocompatibility, biodegradability, composability and low toxicity to humans. The mechanical properties of PLA are greatly affected by the degree of PLA crystallinity. PLA derived from 93%, or more L-lactic acid can be semi-crystalline, while it is strictly amorphous when derived from 50–93% L-lactic acid. Thus, high tensile strength can be observed in films of high L-lactide content. Tensile strength and impact resistance are also influenced by the degree of crosslinking and the annealing of L-PLA, which increases the stereoregularity of the chain [35]. Comparison of mechanical properties between poly(98% L-lactide) and poly(94% L-lactide) showed a slightly greater elongation at yield for 98% than 94% L-lactide. However, poly(94% L-lactide) has an elongation at the break seven times greater than poly(98% L-lactide), indicating more plastic behaviour with 94% of L-lactide [35].



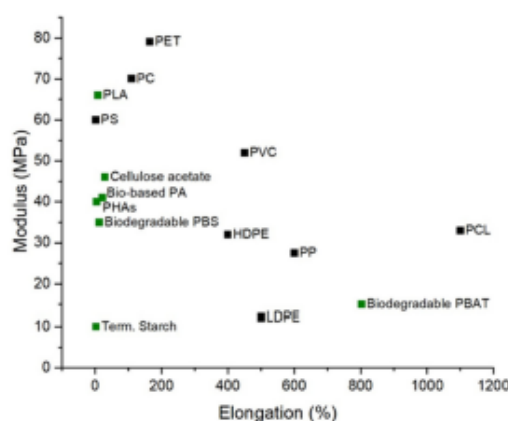
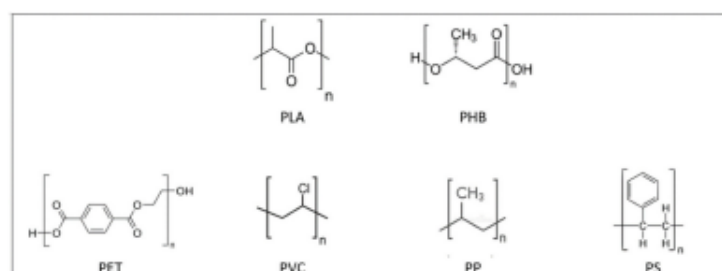


Figure 2. Maximum Tensile Strength (MPa) and Maximum Tensile Elongation (%) of bioplastics compared to petroleum-derived plastics, Data from Ref. [36].

For racemic mixtures, a study by Chen et al. demonstrated that polymerisation of 50% D-Lactide and 50% L-Lactide usually results in forming an amorphous polymer of poly (DL-lactide) [37].

As a packaging material, PLA offers high stiffness (greater than polyethylene terephthalate (PET) and polystyrene (PS)), good clarity (similar to PET), relatively low processing temperatures, excellent resistance to fats and grease, and good breathability suitable for fruits and vegetable storage. Such characteristics make PLA a potential candidate to replace PS, polyethylene (PE) and polypropylene (PP) in the fabrication of disposable cups, salad boxes and cold food packaging [38]. Nevertheless, PLA brittleness with less than 10% elongation at the break renders it unsuitable as a pure material for applications that require plastic deformations at higher stress levels [39]. Additionally, PLA's poor gas moisture permeability performance make it unsuitable for many beverage bottle applications [38].

On the other hand, PHAs gained considerable interest as a green alternative to petrochemically derived plastics, as they are biocompatible, biodegradable and synthesised from renewable resources [40,41]. PHB is the only polymer from the PHAs family to be produced in large quantities. This material is considered an aliphatic polyester with a linear polymer chain, composed of monomers of 3-hydroxybutyrate with a chromophoric carbonyl group. Being a member of the PHAs, PHB is also characterised by having a methyl ( $\text{CH}_3$ ) as an alkyl replacing group, which provides it with a hydrophobic charge. The regularity of the polymerised PHB chain has a direct influence on its degree of crystallinity that, in turn, is influenced by the synthesis route used. Isotactic PHB, which has chiral carbon in absolute configuration R, is obtained through bacterial fermentation, while syndiotactic PHB is synthesised through a synthetic route from monomers with setting R and S. As isotactic PHB presents a more regular structure, it will allow a higher crystallinity than syndiotactic [42]. Favourable PHB properties in terms of melting point, strength, modulus and barrier properties promotes it as a substitute for PP, low density polyethylene (LDPE), polyvinyl chloride (PVC) and PET in packaging applications. Differences in chemical structures between PLA, PHB and previously mentioned commonly used plastics are shown in Figure 3.



**Figure 3.** Chemical structures of biodegradable: Polylactic acid (PLA) and polyhydroxybutyrate (PHB); and nonbiodegradable polymers: Polyethylene terephthalate (PET), polyvinyl chloride (PVC), polypropylene (PP), polystyrene (PS).

Nevertheless, as a bioplastic, PHB has drawbacks, such as being brittle, hard and thermally unstable, making it challenging to use for applications like injection moulding in food industries [43,44]. As a pure material, PHB is highly crystalline (around 80%), resulting in the previously mentioned brittle nature and low elongations. The brittle nature of PHB is associated with a secondary crystallisation of the amorphous phase at ambient temperature. Another important issue is the glass temperature ( $T_g$ ) of PHB. The  $T_g$  is close to room temperature resulting in secondary crystallisation taking place during storage, which, combined with a low nucleation density feature, leads to large spherulite formations which can grow over long durations leading to inter-spherulitic cracks [43]. Generally, spherulites are formed when PHB is crystallised from the melt, with band spacing between them depending on the crystallisation temperature [45]. Cracks are always present within spherulites in melt-crystallised PHB, and subsequent growth of the cracks leads to failure of the polymer. Two distinct types of crack exist in PHB spherulites, which can run either radially or circumferentially within the spherulites. Radial cracks occur more frequently in films crystallised at lower temperatures, while circumferential cracks occur when PHB is crystallised at high temperatures [46]. Another problem with PHB processing is the narrow processing window. The melting temperature of PHB is around 180 °C, therefore, processing temperature should be at least 190 °C. However, thermal degradation at this point happens rapidly, drastically reducing the acceptable residence time in the processing equipment to a few minutes only [47].

However, notwithstanding the limitations of PLA and PHAs, these bioplastic polymers have the potential to be fine-tuned to extend their application range comparable to fossil-based thermoplastics.

### 3.2. Bioplastic Barrier Performance

Inadequate fluid and gas barrier properties strongly impedes the utilisation of biopolymers in applications, such as the food-packaging sector. The established utilisation of PET and polyolefin family polymers in packaging applications is due to their combination of low cost, transparency, good barrier (to oxygen and water vapours), and mechanical characteristics. The oxygen permeability of PET (0.04 barrer) is much stronger than that of the recently developed biopolymers [48]. Among previously mentioned biopolymers, the most widely used—PHB stand apart having significant gas barrier properties (0.01 barrer), which are comparable to benchmark polymers, such as PET [49]. However, PHB's brittle mechanical nature precludes its suitability for food packaging applications. PLA, while having tunable mechanical properties, has oxygen permeability levels in the region of 0.26 barrer, restricting its use within several food-packaging applications [50]. As an approach to overcoming these barrier limitations, the addition of fillers to block the gas and moisture molecular pathways through the polymers, on a nano-micro scale level, is an attractive option [51].

An ideal filler should have a high surface area, aspect ratio and suitable chemical compatibility to provide enhanced mechanical and gas barrier properties at low filler content. The filler geometrical characteristics are an important factor in reducing gas permeability. The higher the aspect ratio, the greater the surface activity, which leads to an increase in mechanical properties, as well as gas barrier properties of the polymer matrix.

In terms of the orientation of fillers inside the polymer matrix, the Nielson model is commonly used. This is an ideal case where the orientation of the filler is perpendicular to the direction of diffusion and is generally not readily achievable. The modified version of the Nielson model is proposed by Bharadwaj by introducing the orientation parameter ( $S$ ) [52]. If  $S = 0$ , designates perfect orientation and the Bharadwaj model will be reduced to the Nielson model, and maximum permeability reduction will be observed as indicated in Figure 4. Different models based on volume fraction and aspect ratio have also been developed to compare theoretical data with experimentally investigated gas barrier results [53].

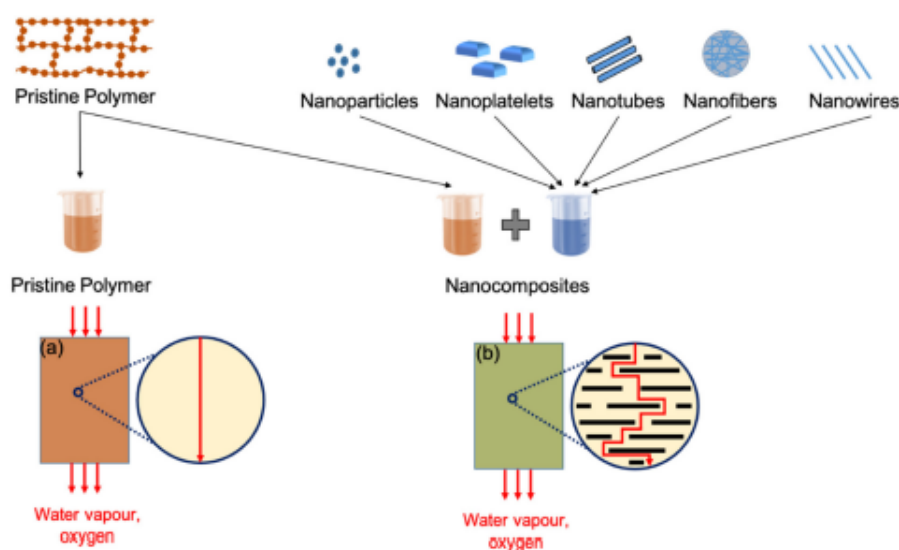


**Figure 4.** Effect of filler addition on gas barrier properties of nanocomposites: (a) Poor barrier properties in pristine polymer, due to direct diffusion pathways for gas molecules, (b) improved barrier properties in nanocomposites due to longer diffusion pathways.

Another aspect to be considered while studying the bioplastics' barrier properties is the dispersion and interchain compatibility of fillers within the bioplastics' matrices. Well exfoliated nano-fillers in polymer matrices give optimal reinforcement and contribute to other material performance characteristics [51]. A major issue with the dispersion of fillers in polymers is their hydrophilic nature, which causes inefficient compatibility with the hydrophobic polymer phase. Therefore, treatments are adopted to promote better interactions and good dispersion between the polymer phase and the fillers [54]. Moreover, the structural characteristics of the filler define the contribution imparted to the mechanical and gas barrier properties of polymers. The structural format of fillers dramatically impacts the gas barrier properties of their host polymers [55]. This is due to the higher crystallinity, which increases the effective path of diffusion and impedes the passage of gas molecules through the polymers rendering them suitable for packaging applications.

Figure 5 demonstrates the effect of fillers addition on the barrier properties, especially

the oxygen ( $O_2$ ) permeability of commonly used petroleum-based plastics and biopolymers. The data is compiled by converting oxygen permeability values from different units into a single unit (barrer). The addition of smaller amounts of fillers in biopolymers has drastically reduced the permeability of oxygen, fulfilling the criteria of ideal gas barrier material (LDPE, PET, and high density polyethylene (HDPE)). Among biopolymers, PHAs showed more hindrance to the passage of gas molecules in their pristine polymers as compared to mentioned petroleum-based polymers. Functionalised graphene oxide (Gr-O) proved to be the best filler. The impressive reduction of oxygen permeability by Gr-O could be related to the strong interfacial adhesion between Gr-O and PHA polymer matrix [56].

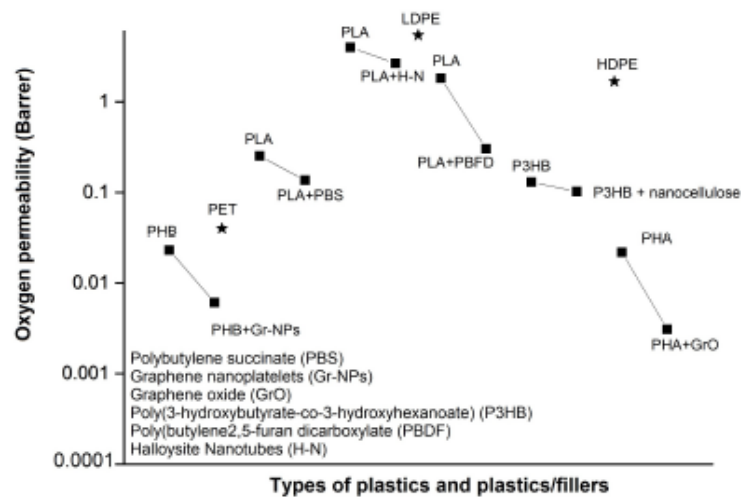


Figure 5. Effect of nanofillers on oxygen permeability of various biopolymers.

### 3.3. Bioplastic Processing and Formulation

Blending and composite formation is an established route for achieving improved technical and processing performance within polymer engineering. Blending PHAs, in particular, PHB with other polymers, offers opportunities to improve processability by lowering the processing temperature and reducing the brittle nature of these biopolymers. The physical, chemical and molecular architectural aspects dictate the enhancement of the polymer blend achievable through compounding techniques and introduced additives. Plasticiser additives can improve polymer viscosity and improve chain mobility during processing. Thermal stabilising additives can be used to eliminate premature degradation of polymers during processing, such as antioxidants, which guard against the presence of oxygen in the processing environment. Compatibiliser additives can improve miscibility between polymers by inducing flexible physical dipole-dipole interactions, or hydrogen bonding [57]. Nanocomposite additives, such as nanocrystals and nanofibres, can significantly improve the mechanical strength and gas barrier properties of the polymers if they are well dispersed in the biopolymer matrices. Natural fibres as an example of nanocomposite have been recently introduced as the main component in fibre reinforced biopolymer composites [58]. The intermolecular hydrogen bonds connecting the polymer chains of natural fibres provide a linear crystalline structure with a tensile strength reaching 15 GPa [59]. Such great strength is also accompanied by other advantages, as low cost, abundance, biodegradability, easy recyclability and fabrication of low weight composite materials [58]. All these properties made natural fibres perfect candidates as fillers in biopolymer composites and can compete with glass or carbon fibres. Accordingly, several studies were performed to evaluate the effect of incorporating natural fibres in biopolymer

composites to improve the composite's mechanical and barrier properties. Among natural fibres, cellulose [60–66], hemp [67–73], kenaf [74–78] and flax [79–88] were the most studied ones. It is worth mentioning that nanocomposites of natural fibres or crystals added as fillers without plasticiser or compatibiliser, results in their poor dispersion and decrease the quality of polymer composite. Alternatively, plasticisers of hydrophilic nature, when mixed with biopolymers or their blends, tend to increase the wettability and O<sub>2</sub> permeability and deteriorate the barrier properties of the polymer composite.

Thus, to obtain better performance of nanocomposites with plasticisers or compatibilisers in biopolymer composites, both additives should be used together. The addition of nanocomposites with plasticisers improves the interfacial adhesion between the nanocomposites and the polymer matrix, allowing better dispersion and consequently provides a more tortuous path for gas and water and increase the barrier properties. Other approaches were introduced to improve the dispersion of the nanocomposites of natural fibres or crystals in polymer matrices. These include physical and chemical treatments of the nanocomposites before mixing with biopolymers. Bio-based coatings were also applied to natural fibres reinforced biocomposites as a means of inducing the hydrophobicity, and thus, improve the barrier properties of the biocomposite.

### 3.3.1. Blends and Composites

As previously mentioned, the processability and formability of PHB represent a drawback in industrial applications; blending with PLA provides a potential route to facilitating its introduction in the market, while also improving PLA properties at the same time. Several studies on PLA-PHB blends have been conducted in recent years, with the results typically showing a slightly higher Young's modulus than neat PHB and neat PLA [89]. Blends with PHB content of 50% or higher have shown lower values of tensile stress and elongation at the break in comparison to pure PLA [90]. However, above 60% PLA content has been reported to increase elongation at the break by up to 12%, with values even comparable to typical thermoplastics achieved on the addition of plasticisers [57,89,91–93]. Furthermore, the PLA-PHB 75:25 blend demonstrated higher mechanical performance than neat PLA, and greater impact resistance than the homopolymers on their own [89,94]. Jandras et al. reported the incorporation of PHB within PLA matrix in different ratios resulting in intermediate properties for the blends. The ductility of PLA increased consistently as PHB concentrations increased from 10 to 30 wt%. The maximum increase in percentage elongation was observed in the 70:30 ratio, suggesting some degree of molecular interaction between the macromolecules of PLA and PHB within the blend (Figure 6). However, tensile modulus and tensile strength were considerably decreased in the case of the blends, compared to pure PLA, as well as a corresponding decrease in stiffness. Blends prepared at 70:30 ratio were used for trial with compatibilisers and preparation of blend composites, due to the optimum elongation at the break and impact strength exhibited [57].

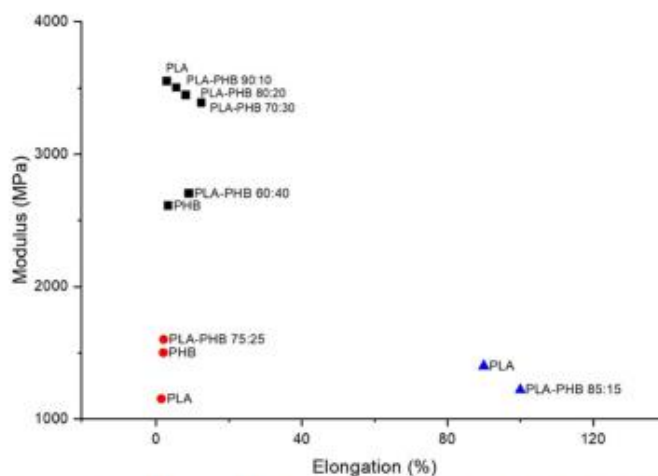


**Figure 6.** Young's Modulus (MPa) vs. elongation at the break (%) of PLA, PHB and their blends, reported by Jandas et al. (black squares), Data from Ref. [57], Armentano et al. (blue triangles), Data from Ref. [91] and Arrieta et al. (red circles), Data from Ref. [94].

### 3.3.2. Compatibilisers and Plasticisers

Facilitation of processability and improved flexibility in PLA/PHB blends is achievable using plasticisers [94]. Plasticisers are available as cost-effective, readily available materials on the market and are also generally of natural origin and include: Oxypropylated glycerin (or laprol), glycerol, glycerol triacetate, 4-nonylphenol, 4,40-dihydroxydiphenylmethane, acetyl tributyl citrate, salicylic ester, acetylsalicylic acid ester, soybean oil, epoxidised soybean oil, dibutyl phthalate, triethyl citrate, dioctyl phthalate, dioctyl sebacate, acetyl tributyl citrate, di-2-ethylhexylphthalate, tri(ethylene glycol)-bis(2-ethylhexanoate), triacetate, and fatty alcohols with or without glycerol fatty esters. Blends of PEG (2–5%) and PHB produced by solvent casting technique has been demonstrated to increase the elongation at the break by up to about four times compared with the original neat PHB. This behaviour was attributed to a plasticising effect of PEG, which acts to weaken the intermolecular forces between the adjacent polymer chains. The changes in free volume reduced the melting temperatures of the system and are also associated with an accompanying reduction in tensile strength [95].

As shown in Figure 7, compatibilisers, such as maleic anhydride, have been applied to PLA and PLA/PHB blends to impart additional flexibility and improve the blend's young's modulus by the induction of flexible physical interactions, including dipole-dipole or hydrogen bonding [57]. For industrial purposes, considerable attention needs to be paid to the selection of suitable plasticisers or compatibilisers as most tend to negatively impact other mechanical properties, such as lowering barrier properties of bioplastic blends, which can restrict their use in packaging applications [89].

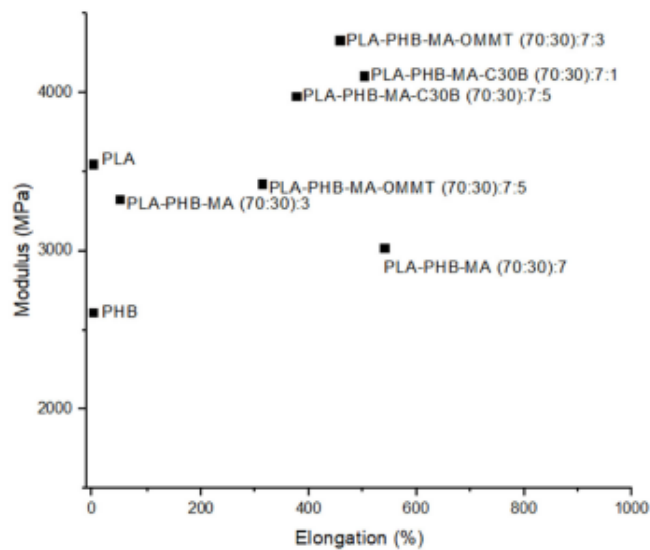


Figure 7. Young's Modulus (MPa) vs. Elongation (%) of PLA, PHB and their blends using MA as a compatibiliser, together with OMMT and C30B nanoclays, Data from Ref. [57].

### 3.3.3. Natural Fillers

The use of naturally sourced fibre-based fillers, with their considerable tensile strength and high sustainability, presents a key route to facilitating polymer circularity. The hydrophilic nature of bare natural fibres with no surface treatment requires an address, due to the incompatibility with hydrophobic biopolymer. Biopolymer composites reinforced with untreated natural fibres typically exhibit non-uniform fibre dispersion with interfaces promoting crack formation. These material defects can lead to premature mechanical failure of the composites [58,59,96]. These defects are attributable to the natural fibre hydrophilicity, which hinders proper mixing with the biopolymer hydrophobic matrix causing poor fibre/matrix interfacial bonding [59]. While high susceptibility of moisture absorption by the hydrophilic natural fibres can support the growth of fungi and bacteria and deteriorate the physical and mechanical properties of the biocomposites [58], this fact can be a highly useful feature that can be availed of post use for achieving biocyclability.

Different approaches are available to enhance the interfacial adhesion between the fibres and matrix, resulting in the fabrication of biocomposites with better mechanical and barrier properties. Among these solutions is the surface modification of natural fibres. Surface modification can result in increasing the sites of reaction, offering new functionality to the fibre surface and enhancing surface roughness by removing impurities [59]. Such modification will lead eventually to the improvement in mechanical properties and reduction of the water absorption of the fabricated biocomposite. The techniques applied to modify the natural surface fibres before inclusion in biopolymer matrices include physical, chemical, biological treatments and their combinations. Some examples of physical treatment techniques are calendaring, stretching, hybrid yarns production and thermal treatments; while chemical techniques include, alkali swelling, silane modifications, graft copolymerisation, and treatment with isocyanate, mercerisation [97].

A representative selection of the recently applied surface modifications for natural fibres reinforced biocomposites are given in Table 3.

Table 3. Surface treatment of natural fibres reinforced bio-composites.

Process	Natural Fibre Used	Biopolymer Matrix	Outcomes			Ref.
			Interfacial Adhesion	Mechanical Properties	Barrier Properties	
Treatment with compatibilisers; Polyglycerol polyglycidyl ether (SR-4GL), Trimethylol propane polyglycidyl ether (SR-TMP), and Polyglycerol polypropyleneoxide (SC-P1000)	Cellulose fibres	PLA	Improved interfacial adhesion between fibres and PLA and		Inhibited degradation of the PLA matrix	[65]
STEFAC TM 8170, surfactant modification	Cellulose fibres	PLA/PHB		Enhanced mechanical performance	Improved water resistance, reduced oxygen and UV-light transmission, as well as appropriate disintegration in compost	[94]
Alkali treatment	Kenaf fibre	PHB			Reduction in the crystallinity of PHB (up to 6% reduction), making it more ductile, and improvement of the flexural modulus by up to 11%.	[75]
Silane treatment	Flax fibre	PLA	Improvement to fibre/matrix adhesion with 2% w/w silane content, yet further improvement of the fibre-matrix interface can be partially resolved by silane/alkali treatment combination.	Improved mechanical properties		[80]
Alkali treatment	Flax fibres	PLA			$T_g$ values of fabricated bio-composites were lowered by 10 °C for 10% NaOH treatment and 15 °C for 30% NaOH treatment	[82]
Treatment with ethylene plasma	Flax fibres	PHB	Improved interfacial adhesion strength in the bio-composite		Improved thermal resistance	[88]



Combinations of natural materials with petroleum-based plastics is an option that is also under development. While facilitating the high mechanical performance, considerations are required when using this approach as further dilemma's may be posed regarding factors, such as continued resource depletion dependencies and degradation and biodegradation pathways, which potentially lead to increased microplastics production.

#### 3.3.4. Bio-Coatings

The application of bio-based coatings to biocomposites and natural fibre reinforced biocomposites is a promising approach proposed to overcome the significant water uptake propensities of natural fibres and increase the moisture resistance of bioplastics for fluid barrier property application requirements. Exposure to long term environmental/hygroscopic ageing necessitates the induction of a higher level of hydrophobicity in chemically modified natural fibre reinforced bio-composites and bioplastics in general. Introducing bio-based coatings to natural fibres reinforced biocomposites, ensures the environmentally friendly and biodegradable nature of fibres. Besides, bio-based coatings are obtained from renewable resources and have superior hydrophobic characteristics [62]. For instance, polyurethane (PU) coatings were first introduced as bio-based coating resins in the 1950s [98]. PU coatings mainly provide their composites with high solvent resistance, hydrolytic stability, resistance to acid–base conditions and weather-ability [62]. Currently, most of the industrially produced PUs are petroleum-based polyols. Thus, renewable resources, such as vegetable oil [99–101], canola oil [102], soybean oil [103–105] and castor oil [106–108], are thoroughly investigated and were able to produce PU coating of competing properties to that of petroleum-based ones.

Polyfurfuryl alcohol (PFA) is another attractive type of bio-based coatings that can be used for barrier property application requirements. PFA has a low cost manufacturing process and can be obtained from natural resources as the agricultural residue of wheat, birch wood, hazelnut shells, corn, rice hulls, oat and sugar cane [62]. In addition, PFA's hydrophobicity, great heat distortion temperature and resistance to chemical erosion make it an excellent candidate as a coating material for bioplastics and natural fibres reinforced biocomposites.

Despite such potentials of PU and PFA as bio-based coatings, there is almost no work presented in the literature on the application of PU and PFA as coatings for natural fibre reinforced composites or biocomposites, except for a recent study done by Mokhothu et al. [109]. This study proposed using PU and PFA as bio-based coatings to composites containing flame-retardant treated natural fibres (flax) and phenolic resin. For three days, uncoated and coated samples were subjected to 90 °C and 90% relative humidity. Analysis was performed to the relative moisture content and mechanical properties and compared with the commercially available water-resistant product (FIRESHELL<sup>®</sup> (FIE)). Concerning the mechanical properties, PFA coated samples showed the highest modulus value (1.93 GPa) after being subjected to environmental conditioning with respect to uncoated (1.59 GPa); PU (1.05 GPa) and FIE (0.98 GPa) coated composites. Besides, the PFA and PU coated samples showed high stress at the break and a decreased elongation at the break in comparison to FIE coated ones. The moisture content of the conditioned PFA and PU coated composites was significantly reduced by 75% and 30%, respectively, when compared to uncoated and FIE coated composites [109].

#### 4. Bioplastics Biodegradability

There is an important distinction between degradable polymers and biodegradable polymers. Degradable polymers are defined as polymers that can be depolymerised or recycled under controlled conditions and processes. According to the American Society for Testing and Materials (ASTM) definition, biodegradable polymers are polymers that can undergo decomposition into carbon dioxide, methane, water, inorganic compounds, or biomass, which can be measured by standardised tests, in a specified period, reflecting available disposal conditions (ASTM standard D6813). The mechanism of biodegrada-

tion is that the molecular weight of biodegradable polymers reduced, due to hydrolysis and oxidation, followed by breaking down into natural elements, such as water and carbon dioxide, via microorganisms. Aliphatic polyesters are the most economically viable biodegradable polymers, with PHB being among the most mechanically promising. The structural changes to the polymer molecules can be described in terms of three main categories of actions or mechanisms, namely, chain depolymerisation, random chain scission, and substituent reactions [110]. As defined by the IUPAC, depolymerisation is the process of converting a polymer into a monomer or a mixture of monomers/oligomers. Therefore, chain depolymerisation means the chain reaction is responding to the transformation of the macromolecular polymer chain into its constituent micromolecular monomers. Random scission is defined in the IUPAC Gold Book as a chemical reaction resulting in the breaking of skeletal bonds. It is also defined as a degradation mechanism that assumes a random cleavage of bonds along the macromolecular polymer chains [111]. This leads to the production of fragments that steadily decrease in length, which may eventually be small enough to allow for the removal of micromolecules. Substituent reactions refer to the kinetic reactions carried out by the constituent monomers of a polymer chain, which differ between polymers. According to Ghosh (1990), each kind of substituent has a characteristic chemical nature and reactivity [112]. However, as substituent reactions can only be observed at relatively low temperatures, substituent reactions only assume prominence when initiated and accomplished at temperatures lower than those of the breaking temperature of main chain bonds of a polymer.

Several factors affect the degradability of a polymer. In general, the surface conditions, the first-order structures, and the high order structures of a polymer play a major role in determining the rate of degradation. Surface conditions, such as hydrophilicity and surface area, directly correspond with the overall degradability of a polymer. Additionally, external environmental factors, such as humidity and temperature, also affect the overall degradability. Humidity introduces water molecules to a polymer and may result in a hydrolysis process, depending on the susceptibility or hydrophobicity of the polymer. Furthermore, the crystallinity of a polymer is also proportional to the degradability of a polymer, so that the lower the degree of crystallinity, the higher the degradability of the polymer. According to Tokiwa et al. (2009), this can be attributed to the fact that enzymes generally interact with the amorphous regions within a polymer, which are loosely packed together as compared to the crystalline regions. Moreover, the melting temperature ( $T_m$ ) of polyesters greatly affects their enzymatic degradation. This is evident from the fact that aliphatic polyesters and polycarbonates with low  $T_m$  have a greater biodegradability than aliphatic polyurethanes and polyamides, which have higher  $T_m$  [113]. This is due to the large melting enthalpy change values of the latter, which can be attributed to the presence of hydrogen bonds among the polymer chains. The introduction of heat into a polymer matrix generally weakens the intermolecular bonds, resulting in an increased rate of degradation. With biodegradation specifically, the microbial species introduced to the polymer, directly correlates with the level of microbial activity, which in turn determines the rate of degradation of a biodegradable polymer [114]. The degree of microbial activity is also heavily influenced by nutrient and oxygen content in the biodegradation environment.

As described earlier, selected microorganisms can produce and store PHAs. The ability to synthesise these molecules does not imply the capacity to also degrade them, in the case where extracellular hydrolases capable of converting polymers are also expressed [115,116]. Under nutrient-limited conditions, degradation occurs when the limitation is removed. Currently, six hundred PHA depolymerases from various microorganisms have been identified and categorised within eight families [117]. The degradation of these polymers is affected by many factors, such as type of enzyme, temperature, moisture, and nutrients composition [118]. Degradation rates of PHAs are also related to the microbial population density. It was shown that during degradation of P(3HB-co-3HV) copolymer, microbes at first attach to the polymer and then begin secreting degrading enzymes. Although PHA producing/degrading microbes usually express high specificity towards

P(3HB), many microbes have been identified with wide substrate specificity. *Xanthomonas* spp., for example, has the ability to produce enzymes for PHAs with aromatic side chain degradation and can also degrade P(3HB), P(3HO), and poly-3-hydroxy-5-phenylvalerate (P(3HPV)) [119]. The type of polymer also plays an important role in degradability. In addition to the presence of side chains, length and composition are also significant factors. Manna et al. report that homopolymers have higher degradation rates in comparison with copolymers of PHAs [120]. Other studies have demonstrated opposing results [118], which may be explained because, in these cases, the experiments were conducted in natural environments where previously mentioned factors (nutrients, moisture, temperature etc.) were non-controllable. Kusaka et al. showed that PHAs degradation ability is negatively correlated to the  $M_w$  and crystallinity [121]. The format and shape of the polymer material is also a significant factor for PHAs degradation, with thin films degrading faster than thicker films. Soil and climatic conditions are further factors that can affect the PHA degradation rate [28,118]. Boyandin et al. examined PHA films degradation response and reported that humid and the hot Vietnamese climate facilitated degradation of PHA [122].

Additives, such as fillers, are another factor that can affect the biodegradability of the bioplastic in which they are added, as demonstrated in Figures 8 and 9. There is no general guarantee that the addition of fillers will enhance or inhibit biodegradability as the effect of fillers on a polymer is mainly dependent on its chemical and physical aspects, such as size, geometry, surface area, and the surface energy of its particles [123] (Murphy, 2001). These aspects directly affect the overall degradation ability of a polymer. In general, the effect of additives on the biodegradability of a polymer is largely dependent on the properties of the additives, such as hydrophobicity and amenability to bacterial growth on the surface.

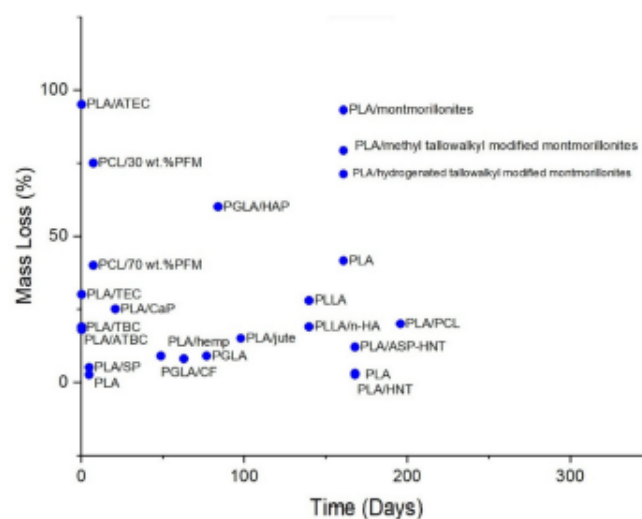
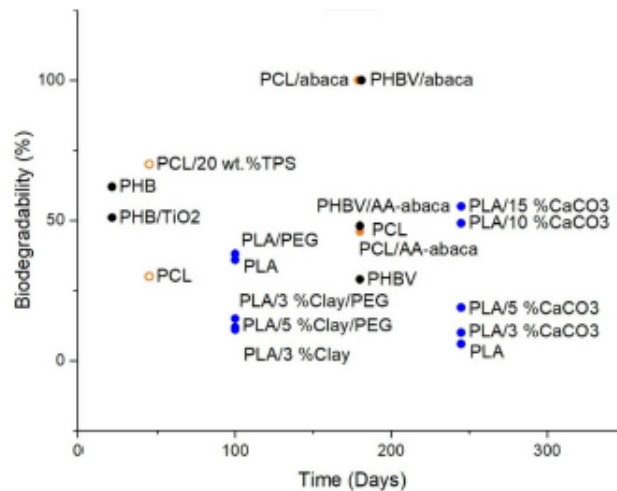


Figure 8. Mass Loss percentage of composites in various hydrolytic degradation environments.



**Figure 9.** Biodegradability of PLA, PCL and PHB with the addition of various fillers and plasticisers in various soil burial degradation environments.

Aframehr et al. report a study on the effect of calcium carbonate ( $\text{CaCO}_3$ ) in soil burial biodegradation where the  $\text{CaCO}_3$  fillers, act to increase the biodegradability of PLA. The weight loss of  $\text{CaCO}_3$  nanocomposites is approximately two times higher than other nanocomposites, with a weight loss of around 55% for PLA/15%  $\text{CaCO}_3$ , 49% for PLA/10%  $\text{CaCO}_3$ , 19% for PLA/5%  $\text{CaCO}_3$ , 10% for PLA/3%  $\text{CaCO}_3$ , and around 6% for neat PLA after a soil exposure time of 35 weeks [124]. A study by Teramoto et al. investigated the effect of treated and untreated abaca fibre filler on the biodegradability of poly(3-hydroxybutyrate-co-3-hydroxyvalerate) (PHBV) after being subjected to a soil-burial environment for a duration of 180 days. Neat PHBV exhibited the least biodegradability at only around 29% weight loss, followed by PHBV/AA-abaca at around 48% weight loss, and lastly, PHBV/untreated abaca with the highest biodegradability, which can be seen in the high degree of fragmentation after 60 days [125].

Altaee et al. conducted a study on the biodegradation of PHB and titanium oxide (PHB- $\text{TiO}_2$ ) composites in a soil burial environment with pH 7.30 and a humidity of 80% at 30 °C and found that PHB- $\text{TiO}_2$  exhibits a lower weight loss of only ~51% after three weeks as compared to ~62% weight loss of neat PHB through the same duration [126]. Paul et al. (2005) studied the degradation of nanocomposites of PLA with unmodified and organo-modified montmorillonites and found that montmorillonites filler enhances hydrolytic degradation. PLA with unmodified montmorillonites exhibited the greatest decrease in  $M_w$  after 23 weeks of hydrolytic degradation with a 93.1% loss in  $M_w$ . These results were followed by PLA with montmorillonites treated with bis-(2-hydroxyethyl) methyl tallowalkyl ammonium cations and PLA with montmorillonites treated with dimethyl-2-ethylhexyl (hydrogenated tallowalkyl) ammonium cations at 79.2% and 71.2%  $M_w$  loss, respectively. In comparison, unfilled PLA is found to only have a 41.6%  $M_w$  decrease compared to its initial value [127]. Chen et al. found that PLA with halloysite nanotubes (HNTs) as filler has a greater rate of hydrolytic degradation as compared to neat PLA as shown from the mass reduction of 3.1% for PLA/HNT as compared to that of neat PLA at only 2.6% in an in vitro environment in SBF at 37 °C by the end of the 24th week of degradation. It was also reported that PLA with HNTs surface treated with 3-aminopropyltriethoxysilane (ASP) has an even greater hydrolytic degradation, due to better interfacial adhesion between PLA and HNTs, which is evident from the mass reduction of 12.1% [128]. A study by Navarro et al. (2005) investigated the effect of the addition of calcium phosphate (CaP)

glass to PLA on its hydrolytic degradability. During the first three weeks of the degradation, PLA/CaP composites experienced a greater weight loss than neat PLA, but an increase of weight of the PLA/CaP composite was reported after three weeks. This may be credited to forming hydrated calcium phosphate precipitate on the composite. The maximum weight loss exhibited by week 3 is 25%, and a final weight loss percentage of about 22% on week 6. In a comparison, the weight loss of neat PLA is around 1% from week 3 through week 5 [129]. Moreover, a study by Huang et al. (2013) investigated the hydrolytic degradability of poly(L-lactic acid) (PLLA)/nanohydroxyapatite (n-HA) and found that the rate of degradation of PLLA/n-HA composite was slower than neat PLLA. This is evident from the weight loss of only around 19% for PLLA/n-HA composite and about 28% for neat PLLA after 20 weeks in a PBS environment with an initial pH of around 7.4 [130]. A study by Valapa et al. (2016) investigated the hydrolytic degradation behaviour of sucrose palmitate (SP) reinforced PLA (PLA-SP) nanocomposites in acidic (pH 2), basic (pH 12), and neutral (pH 7) hydrolytic degradation environments and found that the rate of degradation is increased with the addition of sucrose palmitate. This can be seen in the mass loss percentage of about 5.1% for PLA-SP as compared to only around 2.6% mass loss percentage of neat PLA in a pH7 degradation solution at 35 °C after 115 h [131].

Alternatively, the alterations proposed by the addition of plasticisers and compatibilisers to bioplastics directly affect their degradability since plasticisers and compatibilisers decrease the glass transition temperature ( $T_g$ ) of the polymers they are blended with, as shown in Figures 8 and 9 [132]. Like fillers, there is no general guarantee that the addition of plasticisers will positively or negatively impact biodegradation as it is highly dependent on the properties of the plasticisers used. Some of the more common forms of plasticisers include citrate esters and phthalates (phthalate, isophthalate, terephthalate), the latter being biodegradable as degradation by microorganisms is considered as the most effective method of degradation for phthalates plasticisers [133]. A study by Labrecque et al. (1997) researched using triethyl citrate (TEC), tributyl citrate (TBC), acetyl triethyl citrate (ATEC) and acetyl tributyl citrate (ATBC) as plasticisers for PLA and their effect on enzyme-catalysed hydrolytic degradation. The study found that all citrate esters enhanced the degradability of PLA. At a concentration of 20%, ATEC plasticised PLA has the highest weight loss of around 95%, followed by neat PLA at around 48%, and a decreased rate of degradation in TEC, TBC, and ATBC with weight losses of around 30%, 19%, and 18%, respectively, after a degradation period of 6 h [134]. A 2009 study by Ozkoc and Kemaloglu found that the addition of PEG and clay plasticisers to PLA decreases the rate of biodegradation after exposure to the composting environment for 100 days. This is evident from the weight loss percentage values of about 15%, 12%, and 11% for PLA/3%Clay/PEG, PLA/5%Clay/PEG, and PLA/3%Clay, respectively, in comparison to that of neat PLA with a 36% weight loss. However, the weight loss percentage of PLA/PEG shows a slight increase as compared to neat PLA with a value of around 38% weight loss [135].

Careful selection and monitoring of additives and composite formation, hence, has the potential for exploitation both to enhance the target mechanical properties and simultaneously promote biodegradation.

## 5. Conclusions

The fundamental many-faceted aspects of biopolymer architectures afford greater versatility for configuration and exploitation compared with the main ubiquitous recalcitrant synthetic petroleum-based plastics. This is a pivotal trait that is available for harnessing to enable bioplastics to meet both the high mechanical and barrier performances of their petroleum-based counterparts together with full sustainable biodegradability and circularity. Their very bio-nature means bioplastics are inherently more elaborate at a structural level. This increases accessibility to bio-interactions for enzymatic biodegradation, biodepolymerisation and biorepolymerisation, as well as supporting routes to improving mechanical and barrier performances. While several bioplastics have already achieved certain mechanical and barrier performance criteria, which are equivalent and even ex-

ceed those of corresponding petroleum-based plastics, courses of action for resolving the remaining limitations are becoming increasingly accessible.

Here, avenues for the advancement of the performance of bioplastics with respect to mechanical and barrier properties alongside biodegradability are discussed. The key architectural features properties are  $M_w$  and crystallinity, which typically exhibit an inversely dependent relationship with mechanical performance and biodegradability for both bioplastics and petroleum-based plastics. Increasing  $M_w$  and crystallinity are generally associated with higher mechanical performance and decreased biodegradability as lower crystallinity corresponds to looser chain packing, facilitating enzyme access.

Both macro and micro strategies have the potential for dual positive correlation on the mechanical and biodegradability performances of bioplastics. Regarding the macro approach, new possibilities are afforded, such as harnessing intricate bioplastic structures and formats, which include microfibrillar frameworks and combination with advanced methods, such as in situ polymerisation. Blending and compounding with additives as selected fillers, plastisizers and compatibilisers are also being demonstrated for improved mechanical features, without decreasing biodegradability.

Whereas, regarding the micro approach, expanding PHAs families and large numbers for possible monomer units, present the potential to engineer biodegradable plastics with equivalent target petroleum plastic performances without associated environmental pollution. Further routes include metabolic pathway alteration, design of high specificity substrates, intricate copolymer and block copolymer and genetic modification to produce strains to achieve next-generation multifunctional biopolymers.

In these respects, bioplastic polymers, in contrast to Petroleum-based plastics, have not yet been tailored or even adequately explored to establish their capacities for current and future applications. Given the range and diversity of options available for bioplastics development, there are excellent prospects to extend their application range on a comparable scale to fossil-based thermoplastics and beyond. Further innovations can be expected as the knowledge and new capacities for the manipulation of biopolymers advances, and spawns outputs in related and novice disciplines. The realisation of high performance plastics, without recalcitrance, pollution or resource depletion and switching to regenerative low carbon circularity, has the potential to both safeguard and promote future prosperity for the planet and its inhabitants.

**Author Contributions:** O.A.A. Conceptualization, Data curation, Investigation, Writing—original draft; E.L.G. Investigation, Data curation, Formal analysis; Writing—original draft; M.A. Investigation, Data curation; S.A. Investigation, Data curation; Y.C. Data curation, Formal analysis; Writing—original draft; M.B.F. Supervision, Validation, Writing—original draft; M.M. Investigation, Visualization, Writing—original draft, Writing—review & editing. All authors have read and agreed to the published version of the manuscript.

**Funding:** This project has received funding from the European Union's Horizon 2020 research and innovation programme under grant agreement No 870292 (BioICEP).

**Institutional Review Board Statement:** Not applicable.

**Informed Consent Statement:** Not applicable.

**Data Availability Statement:** The data presented in this study are available on request from the corresponding author.

**Acknowledgments:** This project has received funding from the European Union's Horizon 2020 research and innovation programme under grant agreement No 870292 (BioICEP) and is supported by the National Natural Science Foundation of China (grant numbers: Institute of Microbiology, Chinese Academy of Sciences: 31961133016, Beijing Institute of Technology: 31961133015, Shandong University: 31961133014).

**Conflicts of Interest:** The authors declare no conflict of interest.

## References

- Madison, L.L.; Huisman, G.W. Metabolic Engineering of Poly(3-Hydroxyalkanoates): From DNA to Plastic. *Microbiol. Mol. Biol. Rev.* **1999**, *63*, 21–53. [CrossRef] [PubMed]
- Koller, M.; Maršálek, L.; Dias, M.M.D.S.; Braunegg, G. Producing microbial polyhydroxyalkanoate (PHA) biopolyesters in a sustainable manner. *New Biotechnol.* **2017**, *37*, 24–38. [CrossRef] [PubMed]
- Koller, M. A Review on Established and Emerging Fermentation Schemes for Microbial Production of Polyhydroxy-alkanoate (PHA) Biopolyesters. *Fermentation* **2018**, *4*, 30. [CrossRef]
- Rajwade, J.M.; Paknikar, K.; Kumbhar, J.V. Applications of bacterial cellulose and its composites in biomedicine. *Appl. Microbiol. Biotechnol.* **2015**, *99*, 2491–2511. [CrossRef]
- Sudesh, K.; Abe, H.; Doi, Y. Synthesis, structure and properties of polyhydroxyalkanoates: Biological polyesters. *Prog. Polym. Sci.* **2000**, *25*, 1503–1555. [CrossRef]
- Muneer, F.; Rasul, I.; Azeem, E.; Siddique, M.H.; Zubair, M.; Nadeem, H. Microbial Polyhydroxyalkanoates (PHAs): Efficient Replacement of Synthetic Polymers. *J. Polym. Environ.* **2020**, *28*, 2301–2323. [CrossRef]
- Ciesielski, S.; Mozejko-Ciesielska, J.; Pisutpaisal, N. Plant oils as promising substrates for polyhydroxyalkanoates production. *J. Clean. Prod.* **2015**, *106*, 408–421. [CrossRef]
- Shuai, X.-T.; Jedlinski, Z.; Luo, Q.; Farhod, N. Synthesis of novel block copolymers of poly(3-hydroxybutyric acid) with poly(ethylene glycol) through anionic polymerisation. *Chin. J. Polym. Sci.* **2000**, *18*, 19–23.
- Fu, J.; Sharma, P.; Spicer, V.; Krokhin, O.V.; Zhang, X.; Fristensky, B.; Wilkins, J.A.; Cicek, N.; Sparling, R.; Levin, D.B. Effects of impurities in biodiesel-derived glycerol on growth and expression of heavy metal ion homeostasis genes and gene products in *Pseudomonas putida* LS46. *Appl. Microbiol. Biotechnol.* **2015**, *99*, 5583–5592. [CrossRef]
- Noda, I.; Lindsey, S.B.; Caraway, D. Nodax™ Class PHA Copolymers: Their Properties and Applications. In *Beneficial Microorganisms in Food and Nutraceuticals*; Springer Science and Business Media LLC: Berlin/Heidelberg, Germany, 2010; pp. 237–255.
- Kunioka, M.; Doi, Y. Thermal degradation of microbial copolyesters: Poly(3-hydroxybutyrate-co-3-hydroxyvalerate) and poly(3-hydroxybutyrate-co-4-hydroxybutyrate). *Macromolecules* **1990**, *23*, 1933–1936. [CrossRef]
- Avella, M.; Martuscelli, E.; Raimo, M. Review Properties of blends and composites based on poly(3-hydroxy)butyrate (PHB) and poly(3-hydroxybutyrate-hydroxyvalerate) (PHBV) copolymers. *J. Mater. Sci.* **2000**, *35*, 523–545. [CrossRef]
- Qiu, Y.-Z.; Han, J.; Guo, J.-J.; Chen, G.-Q. Production of Poly(3-hydroxybutyrate-co-3-hydroxyhexanoate) from Gluconate and Glucose by Recombinant *Aeromonas hydrophila* and *Pseudomonas putida*. *Biotechnol. Lett.* **2005**, *27*, 1381–1386. [CrossRef]
- McAdam, B.; Fournet, M.B.; McDonald, P.; Mojicevic, M. Production of Polyhydroxybutyrate (PHB) and Factors Impacting Its Chemical and Mechanical Characteristics. *Polymers* **2020**, *12*, 2908. [CrossRef]
- Ravenelle, E.; Marchessault, R.H. One-Step Synthesis of Amphiphilic Diblock Copolymers from Bacterial Poly([R]-3-hydroxybutyric acid). *Biomacromolecules* **2002**, *3*, 1057–1064. [CrossRef]
- Amaro, T.M.M.M.; Rosa, D.; Comi, G.; Iacumin, L. Prospects for the Use of Whey for Polyhydroxyalkanoate (PHA) Production. *Front. Microbiol.* **2019**, *10*, 992. [CrossRef]
- Colombo, B.; Favini, F.; Scaglia, B.; Sciarria, T.P.; D'Imporzano, G.; Pognani, M.; Alekseeva, A.; Eisele, G.; Cosentino, C.; Adani, F. Enhanced polyhydroxyalkanoate (PHA) production from the organic fraction of municipal solid waste by using mixed microbial culture. *Biotechnol. Biofuels* **2017**, *10*, 1–15. [CrossRef] [PubMed]
- Rajendran, N.; Sharanya, P.; Sneha Raj, M.; Ruth Angeeleena, B.; Rajam, C. Seaweeds can be a new source for bio-plastics. *J. Pharm. Res.* **2012**, *5*, 1476–1479.
- Chee, J.Y.; Tan, Y.; Samian, R.; Sudesh, K. Isolation and Characterization of a *Burkholderia* sp. USM (JCM15050) Capable of Producing Polyhydroxyalkanoate (PHA) from Triglycerides, Fatty Acids and Glycerols. *J. Polym. Environ.* **2010**, *18*, 584–592. [CrossRef]
- Koller, M.; Salerno, A.; Dias, M.; Reiterer, A.; Braunegg, G. Modern biotechnological polymer synthesis: A review. *Food Technol. Biotechnol.* **2010**, *48*, 255–269.
- Pandey, A. Solid-state fermentation. *Biochem. Eng. J.* **2003**, *13*, 81–84. [CrossRef]
- Sindhu, R.; Pandey, A.; Binod, P. Solid-state fermentation for the production of Poly(hydroxyalkanoates). *Chem. Biochem. Eng. Q.* **2015**, *29*, 173–181. [CrossRef]
- Reiniati, I.; Hymak, A.N.; Margaritis, A. Recent developments in the production and applications of bacterial cellulose fibers and nanocrystals. *Crit. Rev. Biotechnol.* **2017**, *37*, 510–524. [CrossRef]
- Florea, M.; Hagemann, H.; Santosa, G.; Abbott, J.; Micklem, C.; Spencer-Milnes, X.; Garcia, L.D.A.; Paschou, D.; Lazenbatt, C.; Kong, D.; et al. Engineering control of bacterial cellulose production using a genetic toolkit and a new cellulose-producing strain. *Proc. Natl. Acad. Sci. USA* **2016**, *113*, E3431–E3440. [CrossRef] [PubMed]
- Liu, M.; Li, S.; Xie, Y.; Jia, S.; Hou, Y.; Zou, Y.; Zhong, C. Enhanced bacterial cellulose production by *Gluconacetobacter xylinus* via expression of *Vitreoscilla* hemoglobin and oxygen tension regulator. <http://www.ncbi.nlm.nih.gov/pubmed/27247386>
- Hungund, B.; Gupta, S. Strain improvement of *Gluconacetobacter*. *Biotechnol.* **2010**, *9*, 32.
- Neves, N.M.; Reis, R.L. (Eds.) *Biomaterials from Nature for Advanced Devices and Therapies*; Wiley: Hoboken, NJ, USA, 2016; pp. 384–399.

28. Volova, T.G.; Prudnikova, S.; Sukovaty, A.G.; Shishatskaya, E. Production and properties of bacterial cellulose by the strain *Komagataeibacter xylinus* B-12068. *Appl. Microbiol. Biotechnol.* **2018**, *102*, 7417–7428. [CrossRef] [PubMed]
29. Lin, S.-P.; Calvar, I.L.; Catchmark, J.M.; Liu, J.-R.; Demirci, A.; Cheng, K.-C. Biosynthesis, production and applications of bacterial cellulose. *Cellulose* **2013**, *20*, 2191–2219. [CrossRef]
30. Shah, N.; Ul-Islam, M.; Khattak, W.A.; Park, J.K. Overview of bacterial cellulose composites: A multipurpose advanced material. *Carbohydr. Polym.* **2013**, *98*, 1585–1598. [CrossRef] [PubMed]
31. Hsieh, J.-T.; Wang, M.-J.; Lai, J.-T.; Liu, H.-S. A novel static cultivation of bacterial cellulose production by intermittent feeding strategy. *J. Taiwan Inst. Chem. Eng.* **2016**, *63*, 46–51. [CrossRef]
32. Ul-Islam, M.; Khan, S.; Ullah, M.W.; Park, J.K. Bacterial cellulose composites: Synthetic strategies and multiple applications in bio-medical and electro-conductive fields. *Biotechnol. J.* **2015**, *10*, 1847–1861. [CrossRef] [PubMed]
33. Singhsa, P.; Narain, R.; Manuspiya, H. Physical structure variations of bacterial cellulose produced by different *Komagataeibacter xylinus* strains and carbon sources in static and agitated conditions. *Cellulose* **2018**, *25*, 1571–1581. [CrossRef]
34. Parte, F.G.B.; Santoso, S.P.; Chou, C.-C.; Verma, V.; Wang, H.-T.; Ismadji, S.; Cheng, K.-C. Current progress on the production, modification, and applications of bacterial cellulose. *Crit. Rev. Biotechnol.* **2020**, *40*, 397–414. [CrossRef] [PubMed]
35. Auras, R.; Harte, B.; Selke, S. An Overview of Polylactides as Packaging Materials. *Macromol. Biosci.* **2004**, *4*, 835–864. [CrossRef]
36. Zhao, X.; Comish, K.; Vodovotz, Y. Narrowing the Gap for Bioplastic Use in Food Packaging: An Update. *Environ. Sci. Technol.* **2020**, *54*, 4712–4732. [CrossRef]
37. Chen, S.-Q.; Lopez-Sanchez, P.; Wang, D.; Mikkelsen, D.; Gidley, M.J. Mechanical properties of bacterial cellulose synthesised by diverse strains of the genus *Komagataeibacter*. *Food Hydrocol.* **2018**, *81*, 87–95. [CrossRef]
38. Jem, K.J.; Tan, B. The development and challenges of poly (lactic acid) and poly (glycolic acid). *Adv. Ind. Eng. Polym. Res.* **2020**, *3*, 60–70. [CrossRef]
39. Farah, S.; Anderson, D.G.; Langer, R. Physical and mechanical properties of PLA, and their functions in widespread applications—A comprehensive review. *Adv. Drug Deliv. Rev.* **2016**, *107*, 367–392. [CrossRef] [PubMed]
40. Visakh, P.M. CHAPTER 1. Polyhydroxyalkanoates (PHAs), their Blends, Composites and Nanocomposites: State of the Art, New Challenges and Opportunities. In *Polyhydroxyalkanoate (PHA) Based Blends, Composites and Nanocomposites*; Green Chemistry Series; Royal Society of Chemistry: Cambridge, UK; 2014; pp. 1–17. [CrossRef]
41. Goh, L.-K.; Purama, R.K.; Sudesh, K. Enhancement of Stress Tolerance in the Polyhydroxyalkanoate Producers without Mobilization of the Accumulated Granules. *Appl. Biochem. Biotechnol.* **2014**, *172*, 1585–1598. [CrossRef]
42. Dos Santos, A.J.; Valentina, L.V.O.D.; Schulz, A.A.H.; Duarte, M.A.T. From Obtaining to Degradation of PHB: Material Properties. Part I. *Ing. Cienc.* **2017**, *13*, 269–298. [CrossRef]
43. El-Hadi, A.M.; Schnabel, R.; Straube, E.; Müller, G.; Henning, S. Correlation between degree of crystallinity, morphology, glass temperature, mechanical properties and biodegradation of poly (3-hydroxyalkanoate) PHAs and their blends. *Polym. Test.* **2002**, *21*, 665–674. [CrossRef]
44. Smith, M.K.M.; Paleri, D.M.; Abdelwahab, M.; Mielewski, D.F.; Misra, M.; Mohanty, A.K. Sustainable composites from poly(3-hydroxybutyrate) (PHB) bioplastic and agave natural fibre. *Green Chem.* **2020**, *22*, 3906–3916. [CrossRef]
45. Barham, P.J.; Keller, A.; Otun, E.L.; Wills, H.H.; Holmes, P.A. Crystallization and morphology of a bacterial thermoplastic Poly-3-hydroxybutyrate. *J. Mater. Sci.* **1984**, *19*. [CrossRef]
46. Barham, P.J.; Keller, A. The relationship between microstructure and mode of fracture in polyhydroxybutyrate. *J. Polym. Sci. Part B Polym. Phys.* **1986**, *24*, 69–77. [CrossRef]
47. Janigová, I.; Laciák, I.; Chodák, I. Thermal degradation of plasticized poly(3-hydroxybutyrate) investigated by DSC. *Polym. Degrad. Stab.* **2002**, *77*, 35–41. [CrossRef]
48. Shim, S.H.; Kim, K.T.; Lee, J.U.; Jo, W.H. Facile Method to Functionalize Graphene Oxide and Its Application to Poly(ethylene terephthalate)/Graphene Composite. *ACS Appl. Mater. Interfaces* **2012**, *4*, 4184–4191. [CrossRef] [PubMed]
49. Papadopoulou, E.L.; Bassett, P.; Paul, U.C.; Marras, S.; Ceseracciu, L.; Roy, I.; Athanassiou, A. Green Composites of Poly(3-hydroxybutyrate) Containing Graphene Nanoplatelets with Desirable Electrical Conductivity and Oxygen Barrier Properties. *ACS Omega* **2019**, *4*, 19746–19755. [CrossRef] [PubMed]
50. Dhar, P.; Gaur, S.S.; Soundararajan, N.; Gupta, A.; Bhasney, S.M.; Milli, M.; Kumar, A.; Katiyar, V. Reactive Extrusion of Polylactic Acid/Cellulose Nanocrystal Films for Food Packaging Applications: Influence of Filler Type on Thermomechanical, Rheological, and Barrier Properties. *Ind. Eng. Chem. Res.* **2017**, *56*, 4718–4735. [CrossRef]
51. Azeem, M.; Jan, R.; Farrukh, S.; Hussain, A. Improving gas barrier properties with boron nitride nanosheets in poly-mer-composites. *Results Phys.* **2019**, *12*, 1535–1541. [CrossRef]
52. Bharadwaj, R.K. Modeling the Barrier Properties of Polymer-Layered Silicate Nanocomposites. *Macromolecules* **2001**, *34*, 9189–9192. [CrossRef]
53. Moggridge, G.; Lape, N.K.; Yang, C.; Cussler, E. Barrier films using flakes and reactive additives. *Prog. Org. Coat.* **2003**, *46*, 231–240. [CrossRef]
54. Cui, Z.; Martínez, A.P.; Adamson, D.H. PMMA functionalized boron nitride sheets as nanofillers. *Nanoscale* **2015**, *7*, 10193–10197. [CrossRef]



55. Gitari, B.; Chang, B.P.; Misra, M.; Navabi, A.; Mohanty, A.K. A comparative study on the mechanical, thermal, and water barrier properties of PLA nanocomposite films prepared with bacterial nanocellulose and cellulose nanofibrils. *BioResources* **2019**, *14*, 1867–1889.
56. Xu, P.; Yang, W.; Niu, D.; Yu, M.; Du, M.; Dong, W.; Chen, M.; Lemstra, P.J.; Ma, P. Multifunctional and robust polyhydroxyalkanoate nanocomposites with superior gas barrier, heat resistant and inherent antibacterial performances. *Chem. Eng. J.* **2020**, *382*, 122864. [CrossRef]
57. Jandas, P.J.; Mohanty, S.; Nayak, S.K. Morphology and Thermal Properties of Renewable Resource-Based Polymer Blend Nanocomposites Influenced by a Reactive Compatibilizer. *ACS Sustain. Chem. Eng.* **2013**, *2*, 377–386. [CrossRef]
58. Kick, T.; Gnethe, T.; Mahltig, B. A Natural Based Method for Hydrophobic Treatment of Natural Fiber Material. *Acta Chim. Slov.* **2017**, *64*, 373–380. [CrossRef] [PubMed]
59. Lu, N.; Oza, S.; Tajabadi, M.G. Surface Modification of Natural Fibers for Reinforcement in Polymeric Composites. In *Surface Modification of Biopolymers*; John Wiley & Sons, Inc.: Hoboken, NJ, USA, 2015; pp. 224–237.
60. Zhijiang, C.; Yi, X.; Haizheng, Y.; Jia, J.; Liu, Y. Poly(hydroxybutyrate)/cellulose acetate blend nanofiber scaffolds: Preparation, characterization and cytocompatibility. *Mater. Sci. Eng. C* **2016**, *58*, 757–767. [CrossRef]
61. Panaitescu, D.M.; Nicolae, C.A.; Gabor, A.R.; Trusca, R. Thermal and mechanical properties of poly(3-hydroxybutyrate) reinforced with cellulose fibers from wood waste. *Ind. Crop. Prod.* **2020**, *145*, 112071. [CrossRef]
62. Mokhothu, T.H.; John, M.J. Review on hygroscopic aging of cellulose fibres and their biocomposites. *Carbohydr. Polym.* **2015**, *131*, 337–354. [CrossRef]
63. Joffe, R.; Pupure, L.; Berthold, E.; Varna, J. Micro-structure and Mechanical Properties in PLA Reinforced with Cellulosic Fiber Sheets Made by Wet Forming Method. In Proceedings of the 8th International Conference on Composites Testing and Model Identification (CompTest 2017), Leuven, Belgium, 5–7 April 2017.
64. Masmoudi, F.; Bessadok, A.; Dammak, M.; Jaziri, M.; Ammar, E. Biodegradable packaging materials conception based on starch and polylactic acid (PLA) reinforced with cellulose. *Environ. Sci. Pollut. Res.* **2016**, *23*, 20904–20914. [CrossRef]
65. Kyutoku, H.; Maeda, N.; Sakamoto, H.; Nishimura, H.; Yamada, K. Effect of surface treatment of cellulose fiber (CF) on durability of PLA/CF bio-composites. *Carbohydr. Polym.* **2019**, *203*, 95–102. [CrossRef]
66. Piekarska, K.; Sowinski, P.; Piorowska, E.; Haque, M.M.U.; Praeilla, M. Structure and properties of hybrid PLA nanocomposites with inorganic nanofillers and cellulose fibers. *Compos. Part A Appl. Sci. Manuf.* **2016**, *82*, 34–41. [CrossRef]
67. Hu, R.; Lim, J.-K. Fabrication and Mechanical Properties of Completely Biodegradable Hemp Fiber Reinforced Polylactic Acid Composites. *J. Compos. Mater.* **2007**, *41*, 1655–1669. [CrossRef]
68. Pomet, M.; Juntaro, J.; Heng, J.; Mantalaris, A.; Lee, A.; Wilson, K.; Kalinka, G.; Shaffer, M.S.P.; Bismarck, A. Surface Modification of Natural Fibers Using Bacteria: Depositing Bacterial Cellulose onto Natural Fibers To Create Hierarchical Fiber Reinforced Nanocomposites. *Biomacromolecules* **2008**, *9*, 1643–1651. [CrossRef]
69. Xu, Z.; Yang, L.; Ni, Q.; Ruan, F.; Wang, H. Fabrication of high-performance green hemp/poly(lactic acid) fibre composites. *J. Eng. Fibers Fabr.* **2019**, *14*. [CrossRef]
70. Michel, A.; Billington, S. Characterization of poly-hydroxybutyrate films and hemp fiber reinforced composites exposed to accelerated weathering. *Polym. Degrad. Stab.* **2012**, *97*, 870–878. [CrossRef]
71. Keller, A. Compounding and mechanical properties of biodegradable hemp fibre composites. *Compos. Sci. Technol.* **2003**, *63*, 1307–1316. [CrossRef]
72. Sawpan, M.A.; Pickering, K.L.; Fernyhough, A. Characterisation of hemp fibre reinforced Poly(Lactic Acid) composites. *Int. J. Mater. Prod. Technol.* **2009**, *36*, 229. [CrossRef]
73. Smoca, A.; Kukle, S.; Zelca, Z. Properties of Hemp Fibres Reinforced PLA Composites. *Key Eng. Mater.* **2019**, *800*, 205–209. [CrossRef]
74. Avella, M.; Buzarovska, A.; Errico, M.E.; Gentile, G.; Grozdanov, A.; Bogoeva-Gaceva, G. Poly(3-hydroxybutyrate-co-3-hydroxyvalerate)-based biocomposites reinforced with kenaf fibers. *J. Appl. Polym. Sci.* **2007**, *104*, 3192–3200. [CrossRef]
75. Hassan, A.; Isa, M.R.M.; Ishak, Z.A.M. Improving the thermal and mechanical properties of injection moulded Kenaf Fibre-reinforced Polyhydroxy-butyrates composites through fibre surface treatment. *BioResources* **2019**, *14*, 3101–3116.
76. Buzarovska, A.; Bogoeva-Gaceva, G.; Grozdanov, A.; Avella, M. Crystallization behavior of polyhydroxybutyrate in model composites with kenaf fibers. *J. Appl. Polym. Sci.* **2006**, *102*, 804–809. [CrossRef]
77. Graupner, N.; Müssig, J. A comparison of the mechanical characteristics of kenaf and lyocell fibre reinforced poly(lactic acid) (PLA) and poly(3-hydroxybutyrate) (PHB) composites. *Compos. Part A Appl. Sci. Manuf.* **2011**, *42*, 2010–2019. [CrossRef]
78. Kuciel, S.; Liber-Krec, A. Biocomposites based on PHB filled with wood or kenaf fibers. *Polimery* **2011**, *56*, 218–223. [CrossRef]
79. Bayart, M.; Gauvin, F.; Foruzanmehr, M.R.; Elkoun, S.; Robert, M. Mechanical and moisture absorption characterization of PLA composites reinforced with nano-coated flax fibers. *Fibers Polym.* **2017**, *18*, 1288–1295. [CrossRef]
80. Georgiopoulos, P.; Kontou, E.; Georgousis, G. Effect of silane treatment loading on the flexural properties of PLA/flax unidirectional composites. *Compos. Commun.* **2018**, *10*, 6–10. [CrossRef]
81. Karali, N.G.; Aytac, A. Properties of alkali treated short flax fiber reinforced poly(lactic acid)/polycarbonate composites. *Fibers Polym.* **2014**, *15*, 2607–2612. [CrossRef]
82. Aydın, M.; Tozlu, H.; Kemalolu, S.; Aytac, A.; Ozkoc, G. Effects of Alkali Treatment on the Properties of Short Flax Fibre-Poly(Lactic Acid) Eco-Composites. *J. Polym. Environ.* **2011**, *19*, 11–17. [CrossRef]

83. Shanks, R.A.; Hodzic, A.; Ridderhof, D. Composites of poly(lactic acid) with flax fibers modified by interstitial polymerization. *J. Appl. Polym. Sci.* **2006**, *99*, 2305–2313. [\[CrossRef\]](#)
84. Foruzanmehr, M.; Vuillaume, P.; Elkoun, S.; Robert, M. Physical and mechanical properties of PLA composites reinforced by TiO<sub>2</sub> grafted flax fibers. *Mater. Des.* **2016**, *106*, 295–304. [\[CrossRef\]](#)
85. Ventura, H.; Claramunt, J.; Rodríguez-Pérez, M.; Ardanuy, M. Effects of hydrothermal aging on the water uptake and tensile properties of PHB/flax fabric biocomposites. *Polym. Degrad. Stab.* **2017**, *142*, 129–138. [\[CrossRef\]](#)
86. Chilali, A.; Assarar, M.; Zouari, W.; Kebir, H.; Ayad, R. Mechanical characterization and damage events of flax fabric-reinforced biopolymer composites. *Polym. Polym. Compos.* **2019**, *28*, 631–644. [\[CrossRef\]](#)
87. Rytlewski, P.; Stepczyńska, M.; Moraczewski, K.; Malinowski, R.; Karasiewicz, T.; Sikorska, W.; Żenkiewicz, M. Flax fibers reinforced polycaprolactone modified by triallyl isocyanurate and electron radiation. *Polym. Compos.* **2019**, *40*, 481–488. [\[CrossRef\]](#)
88. Lee, S.G.; Choi, S.-S.; Park, W.H.; Cho, D. Characterization of surface modified flax fibers and their biocomposites with PHB. *Macromol. Symp.* **2003**, *197*, 089–100. [\[CrossRef\]](#)
89. Arrieta, M.P.; Samper, M.D.; Aldas, M.; López, J. On the Use of PLA-PHB Blends for Sustainable Food Packaging Applications. *Materials* **2017**, *10*, 1008. [\[CrossRef\]](#)
90. Zhang, M.; Thomas, N.L. Blending polylactic acid with polyhydroxybutyrate: The effect on thermal, mechanical, and biodegradation properties. *Adv. Polym. Technol.* **2011**, *30*, 67–79. [\[CrossRef\]](#)
91. Armentano, I.; Fortunati, E.; Burgos, N.; Dominici, F.; Luzi, F.; Fiori, S.; Jimenez, A.; Yoon, K.; Ahn, J.; Kang, S.; et al. Processing and characterization of plasticized PLA/PHB blends for biodegradable multiphase systems. *Express Polym. Lett.* **2015**, *9*, 583–596. [\[CrossRef\]](#)
92. Armentano, I.; Fortunati, E.; Burgos, N.; Dominici, F.; Luzi, F.; Fiori, S.; Jiménez, A.; Yoon, K.; Ahn, J.; Kang, S.; et al. Bio-based PLA/PHB plasticized blend films: Processing and structural characterization. *LWT* **2015**, *64*, 980–988. [\[CrossRef\]](#)
93. Abdelwahab, M.; Flynn, A.; Chiou, B.-S.; Imam, S.; Orts, W.; Chiellini, E. Thermal, mechanical and morphological characterization of plasticized PLA-PHB blends. *Polym. Degrad. Stab.* **2012**, *97*, 1822–1828. [\[CrossRef\]](#)
94. Arrieta, M.P.; Samper, M.D.; Lopez, J.; Jiménez, A. Combined Effect of Poly(hydroxybutyrate) and Plasticizers on Polylactic acid Properties for Film Intended for Food Packaging. *J. Polym. Environ.* **2014**, *22*, 460–470. [\[CrossRef\]](#)
95. Rodrigues, J.A.F.R.; Parra, D.E.; Lugão, A.B. Crystallization on films of PHB/PEG blends. *J. Therm. Anal. Calorim.* **2005**, *79*, 379–381. [\[CrossRef\]](#)
96. Ali, A.; Shaker, K.; Nawab, Y.; Jabbar, M.; Hussain, T.; Milityk, J.; Baheti, V. Hydrophobic treatment of natural fibers and their composites—A review. *J. Ind. Text.* **2018**, *47*, 2153–2183. [\[CrossRef\]](#)
97. Lalit, R.; Mayank, P.; Ankur, K. Natural Fibers and Biopolymers Characterization: A Future Potential Composite Material. *Stroj. Cas.* **2018**, *68*, 33–50. [\[CrossRef\]](#)
98. Awasthi, S.; Agarwal, D. Influence of cycloaliphatic compounds on the properties of polyurethane coatings. *J. Coat. Technol. Res.* **2007**, *4*, 67–73. [\[CrossRef\]](#)
99. Alagi, P.; Choi, Y.J.; Hong, S.C. Preparation of vegetable oil-based polyols with controlled hydroxyl functionalities for thermoplastic polyurethane. *Eur. Polym. J.* **2016**, *78*, 46–60. [\[CrossRef\]](#)
100. Miao, S.; Wang, P.; Su, Z.; Zhang, S. Vegetable-oil-based polymers as future polymeric biomaterials. *Acta Biomater.* **2014**, *10*, 1692–1704. [\[CrossRef\]](#) [\[PubMed\]](#)
101. Deka, H.; Karak, N. Bio-based hyperbranched polyurethanes for surface coating applications. *Prog. Org. Coat.* **2009**, *66*, 192–198. [\[CrossRef\]](#)
102. Kong, X.; Liu, G.; Curtis, J.M. Novel polyurethane produced from canola oil based poly(ether ester) polyols: Synthesis, characterization and properties. *Eur. Polym. J.* **2012**, *48*, 2097–2106. [\[CrossRef\]](#)
103. Tan, S.; Abraham, T.; Ference, D.; Macosko, C.W. Rigid polyurethane foams from a soybean oil-based Polyol. *Polymer* **2011**, *52*, 2840–2846. [\[CrossRef\]](#)
104. Ismail, E.A.; Motawie, A.; Sadek, E.; Ismail, E.A.; Motawie, A.; Sadek, E. Synthesis and characterization of polyurethane coatings based on soybean oil-polyester polyols. *Egypt. J. Pet.* **2011**, *20*, 1–8. [\[CrossRef\]](#)
105. Datta, J.; Głowińska, E. Effect of hydroxylated soybean oil and bio-based propanediol on the structure and thermal properties of synthesized bio-polyurethanes. *Ind. Crop. Prod.* **2014**, *61*, 84–91. [\[CrossRef\]](#)
106. Fu, C.; Zheng, Z.; Yang, Z.; Chen, Y.; Shen, L. A fully bio-based waterborne polyurethane dispersion from vegetable oils: From synthesis of precursors by thiol-ene reaction to study of final material. *Prog. Org. Coat.* **2014**, *77*, 53–60. [\[CrossRef\]](#)
107. Thakur, S.; Karak, N. Castor oil-based hyperbranched polyurethanes as advanced surface coating materials. *Prog. Org. Coat.* **2013**, *76*, 157–164. [\[CrossRef\]](#)
108. Guranathan, T.; Mohanty, S.; Nayak, S.K. Isocyanate terminated castor oil-based polyurethane prepolymer: Synthesis and characterization. *Prog. Org. Coat.* **2015**, *80*, 39–48. [\[CrossRef\]](#)
109. Mokhothu, T.H.; John, M.J. Bio-based coatings for reducing water sorption in natural fibre reinforced composites. *Sci. Rep.* **2017**, *7*, 1–8. [\[CrossRef\]](#)
110. Van Krevelen, D.W.; Te Nijenhuis, K. *Properties of Polymers: Their Correlation with Chemical Structure; Their Numerical Estimation and Prediction from Additive Group Contributions*; Elsevier: Amsterdam, The Netherlands, 2009.
111. Sanchez, P.; A Perez-Maqueda, L.; Perejon, A.; Criado, J.M. A new model for the kinetic analysis of thermal degradation of polymers driven by random scission. *Polym. Degrad. Stab.* **2010**, *95*, 733–739. [\[CrossRef\]](#)

112. Ghosh, P. *Polymer Science and Technology*; Tata McGraw-Hill Education: New York, NY, USA, 1990.
113. Tokiwa, Y.; Calabia, B.P.; Ugwu, C.U.; Aiba, S. Biodegradability of Plastics. *Int. J. Mol. Sci.* **2009**, *10*, 3722–3742. [\[CrossRef\]](#)
114. Bernard, M. Industrial Potential of Polyhydroxyalkanoate Bioplastic: A Brief Review. *USURJ: Univ. Sask. Undergrad. Res. J.* **2014**, *1*. [\[CrossRef\]](#)
115. Muhammadi, S.; Afzal, M.; Hameed, S. Bacterial polyhydroxyalkanoates-eco-friendly next generation plastic: Production, biocompatibility, biodegradation, physical properties and applications. *Green Chem. Lett. Rev.* **2015**, *8*, 56–77. [\[CrossRef\]](#)
116. Ahmed, T.; Shahid, M.; Azeem, F.; Rasul, L.; Shah, A.A.; Noman, M.; Hameed, A.; Manzoor, N.; Manzoor, I.; Muhammad, S. Biodegradation of plastics: Current scenario and future prospects for environmental safety. *Environ. Sci. Pollut. Res.* **2018**, *25*, 7287–7298. [\[CrossRef\]](#) [\[PubMed\]](#)
117. Knoll, M.; Hamm, T.M.; Wagner, F.; Martinez, V.; Pleiss, J. The PHA Depolymerase Engineering Database: A systematic analysis tool for the diverse family of polyhydroxyalkanoate (PHA) depolymerases. *BMC Bioinform.* **2009**, *10*, 89. [\[CrossRef\]](#)
118. Mergaert, J.; Webb, A.; Anderson, C.; Wouters, A.; Swings, J. Microbial degradation of poly(3-hydroxybutyrate) and poly(3-hydroxybutyrate-co-3-hydroxyvalerate) in soils. *Appl. Environ. Microbiol.* **1993**, *59*, 3233–3238. [\[CrossRef\]](#)
119. Jendrossek, D.; Handrick, R. Microbial Degradation of Polyhydroxyalkanoates. *Annu. Rev. Microbiol.* **2002**, *56*, 403–432. [\[CrossRef\]](#)
120. Manna, A.; Paul, A. Degradation of microbial polyester poly(3-hydroxybutyrate) in environmental samples and in culture. *Biodegradation* **2000**, *11*, 323–329. [\[CrossRef\]](#) [\[PubMed\]](#)
121. Kusaka, S.; Iwata, T.; Doi, Y. Properties and biodegradability of ultra-high-molecular-weight poly[(R)-3-hydroxybutyrate] produced by a recombinant *Escherichia coli*. *Int. J. Biol. Macromol.* **1999**, *25*, 87–94. [\[CrossRef\]](#)
122. Boyandin, A.N.; Prudnikova, S.; Filipenko, M.L.; Khrapov, E.A.; Vasil'Ev, A.D.; Volova, T. Biodegradation of polyhydroxyalkanoates by soil microbial communities of different structures and detection of PHA degrading microorganisms. *Appl. Biochem. Microbiol.* **2011**, *48*, 28–36. [\[CrossRef\]](#)
123. Murphy, J. Chapter 4—Modifying Specific Properties: Mechanical Properties—Fillers. In *Additives for Plastics Handbook*, 2nd ed.; Murphy, J., Ed.; Elsevier Science: Amsterdam, The Netherlands, 2001; Volume 1, pp. 19–35.
124. Aframehr, W.M.; Molki, B.; Heidarian, P.; Behzad, T.; Sadeghi, M.; Bagheri, R. Effect of calcium carbonate nanoparticles on barrier properties and biodegradability of polylactic acid. *Fibers Polym.* **2017**, *18*, 2041–2048. [\[CrossRef\]](#)
125. Teramoto, N.; Urata, K.; Ozawa, K.; Shibata, M. Biodegradation of aliphatic polyester composites reinforced by abaca fiber. *Polym. Degrad. Stab.* **2004**, *86*, 401–409. [\[CrossRef\]](#)
126. Altae, N.; El-Hiti, G.A.; Fahdil, A.; Sudesh, K.; Yousif, E. Biodegradation of different formulations of polyhydroxybutyrate films in soil. *SpringerPlus* **2016**, *5*, 1–12. [\[CrossRef\]](#)
127. Paul, M.-A.; Delcourt, C.; Alexandre, M.; Degée, P.; Monteverde, E.; Dubois, P. Polylactide/montmorillonite nanocomposites: Study of the hydrolytic degradation. *Polym. Degrad. Stab.* **2005**, *87*, 535–542. [\[CrossRef\]](#)
128. Chen, Y.; Murphy, A.; Scholz, D.; Geever, L.M.; Lyons, J.G.; Devine, D.M. Surface-modified halloysite nanotubes reinforced poly(lactic acid) for use in biodegradable coronary stents. *J. Appl. Polym. Sci.* **2018**, *135*, 46521. [\[CrossRef\]](#)
129. Navarro, M.; Ginebra, M.; Planell, J.; Barrias, C.; Barbosa, M. In vitro degradation behavior of a novel bioresorbable composite material based on PLA and a soluble CaP glass. *Acta Biomater.* **2005**, *1*, 411–419. [\[CrossRef\]](#)
130. Huang, J.; Xiong, J.; Liu, J.; Zhu, W.; Wang, D. Investigation of the in vitro degradation of a novel polylactide/nanohydroxyapatite composite for artificial bone. *J. Nanomater.* **2013**, *2013*, 3. [\[CrossRef\]](#)
131. Valapa, R.B.; Pugazhenti, G.; Katiyar, V. Hydrolytic degradation behaviour of sucrose palmitate reinforced poly(lactic acid) nanocomposites. *Int. J. Biol. Macromol.* **2016**, *89*, 70–80. [\[CrossRef\]](#) [\[PubMed\]](#)
132. Jamarani, R.; Erythropel, H.C.; Nicell, J.A.; Leask, R.L.; Marić, M. How Green is Your Plasticizer? *Polymers* **2018**, *10*, 834. [\[CrossRef\]](#)
133. Boll, M.; Geiger, R.; Junghare, M.; Schink, B. Microbial degradation of phthalates: Biochemistry and environmental implications. *Environ. Microbiol. Rep.* **2020**, *12*, 3–15. [\[CrossRef\]](#) [\[PubMed\]](#)
134. Labrecque, L.V.; Kumar, R.A.; Gross, R.A.; McCarthy, S.P. Citrate esters as plasticizers for poly(lactic acid). *J. Appl. Polym. Sci.* **1997**, *66*, 1507–1513. [\[CrossRef\]](#)
135. Ozkoc, G.; Kemaloglu, S. Morphology, biodegradability, mechanical, and thermal properties of nanocomposite films based on PLA and plasticized PLA. *J. Appl. Polym. Sci.* **2009**, *114*, 2481–2487. [\[CrossRef\]](#)

# Appendix 16. Review paper published in MDPI International Journal of Molecular Sciences 2022

(<https://doi.org/10.3390/ijms232012198>)



International Journal of  
Molecular Sciences



Article

## Enhanced Antimicrobial Activity of Biocompatible Bacterial Cellulose Films via Dual Synergistic Action of Curcumin and Triangular Silver Nanoplates

Eduardo Lanzagorta Garcia <sup>1</sup>, Marija Mojicevic <sup>1,\*</sup>, Dusan Milivojevic <sup>2</sup>, Ivana Aleksic <sup>2</sup>, Sandra Vojnovic <sup>2</sup>, Milena Stevanovic <sup>2</sup>, James Murray <sup>1</sup>, Olivia Adly Attallah <sup>1</sup>, Declan Devine <sup>1</sup> and Margaret Brennan Fournet <sup>1</sup>

<sup>1</sup> Materials Research Institute, Technological University of the Shannon: Midlands Midwest, N37 HD68 Athlone, Ireland

<sup>2</sup> Institute of Molecular Genetics and Genetic Engineering, University of Belgrade, Vojvode Stepe 444a, 11000 Belgrade, Serbia

\* Correspondence: mmojicevic@ait.ie; Tel.: +353-877-772-272



Citation: Garcia, E.L.; Mojicevic, M.; Milivojevic, D.; Aleksic, I.; Vojnovic, S.; Stevanovic, M.; Murray, J.; Attallah, O.A.; Devine, D.; Fournet, M.B. Enhanced Antimicrobial Activity of Biocompatible Bacterial Cellulose Films via Dual Synergistic Action of Curcumin and Triangular Silver Nanoplates. *Int. J. Mol. Sci.* **2022**, *23*, 12198. <https://doi.org/10.3390/ijms232012198>

Academic Editor: Ayae Sugawara-Narutaki

Received: 30 August 2022

Accepted: 10 October 2022

Published: 13 October 2022

**Publisher's Note:** MDPI stays neutral with regard to jurisdictional claims in published maps and institutional affiliations.



Copyright © 2022 by the authors. Licensee MDPI, Basel, Switzerland. This article is an open access article distributed under the terms and conditions of the Creative Commons Attribution (CC BY) license (<https://creativecommons.org/licenses/by/4.0/>).

**Abstract:** Curcumin and triangular silver nanoplates (TSNP)-incorporated bacterial cellulose (BC) films present an ideal antimicrobial material for biomedical applications as they afford a complete set of requirements, including a broad range of long-lasting potency and superior efficacy antimicrobial activity, combined with low toxicity. Here, BC was produced by *Komagataeibacter medellinensis* ID13488 strain in the presence of curcumin in the production medium (2 and 10%). TSNP were incorporated in the produced BC/curcumin films using ex situ method (21.34 ppm) and the antimicrobial activity was evaluated against *Escherichia coli* ATCC95922 and *Staphylococcus aureus* ATCC25923 bacterial strains. Biological activity of these natural products was assessed in cytotoxicity assay against lung fibroblasts and in vivo using *Caenorhabditis elegans* and *Danio rerio* as model organisms. Derived films have shown excellent antimicrobial performance with growth inhibition up to 67% for *E. coli* and 95% for *S. aureus*. In a highly positive synergistic interaction, BC films with 10% curcumin and incorporated TSNP have shown reduced toxicity with 80% MRC5 cells survival rate. It was shown that only 100% concentrations of film extracts induce low toxicity effect on model organisms' development. The combined and synergistic advanced anti-infective functionalities of the curcumin and TSNP incorporated in BC have a high potential for development for application within the clinical setting.

**Keywords:** bacterial cellulose; silver nanoparticles; curcumin; antimicrobial properties; biopolymers; zebrafish

### 1. Introduction

Bacterial cellulose (BC) has gained great attraction from several research and industrial sectors due to its high purity, absence of lignin and hemicellulose commonly found in plant cellulose, and its exclusive properties [1]. The crystalline structure of BC is naturally composed of randomly assembled nanofibrils aggregated in bundles. Such arrangement allows a great surface area that provides BC with high liquid holding capacity, flexibility, mouldability, and high mechanical strength in the wet state [1–3]. Furthermore, BC is considered a biocompatible material which renders it suitable for a wide range of applications, especially in the biomedical field, such as wound healing systems [4], BC-based biosensors [5], tissue regeneration [6], scaffolds [7], and transdermal applications [2,3]. However, BC still shows high challenges regarding interactions and functionalization for constructing uniform functional materials. Pristine BC lacks the adhesive sites necessary for migration and cell signaling which can be improved by further modifications such as crosslinking with metal ions [8].

The production process of BC is regarded as one of the crucial steps that controls the properties of the resulting material. Various species of bacteria, including Gram-

negative and Gram-positive, and different substrates can be used for BC production. Such variety results in different morphologies, structures, properties, and applications of the produced BC [9]. Process of BC production involves several biochemical reactions and it was revealed that specific operons are in control of biosynthesis, transportation through cells and supramolecular assembly of cellulose fibrils. However, molecular mechanism, more specifically: transport of acyl groups from the Krebs's cycle to the periplasm, transport of glucan chains from the cell and polymerization of glucose are yet to be determined [10].

Between Gram-positive bacteria only few species have been reported to produce BC, such as: *Bacillus* sp. [11], *Leifsonia* sp. [12], *Lactobacillus* sp. [13], and *Rhodococcus* sp. [14]. In contrast, the number of Gram-negative BC producers is significantly higher. Species belonging to *Pseudomonas* [15], *Escherichia* [16], *Alcaligenes* [17], *Enterobacter* [18], *Salmonella* [19], *Acetobacter* [20], and *Komagataeibacter* genera have been reported as BC producers in the literature. On the other hand, bio-cellulose can be synthesized in a cell-free system in the presence of appropriate enzymatic machinery after disrupting bacterial cell walls [21].

Recently, one of the most attractive genera that has been studied for BC production is *Komagataeibacter*. Species belonging to this genera are well-recognized, exceptionally efficient BC producers known for its phenotype diversity manifested by preference of the carbon source, BC structure and production rate depending on the strain. Several species from this genus have been identified as strong cellulose producers, including *Komagataeibacter xylinus*, *Komagataeibacter medellinensis*, *Komagataeibacter oboediensis*, *Komagataeibacter pomacei*, *Komagataeibacter nataicola*, *Komagataeibacter rhaeticus* [1].

The utilization of other compounds as substrates for BC production, together with glucose has been recently evaluated as an approach for improving the properties of resulting BC, as a final product [22]. Such an approach can also be extended to enhance the antimicrobial activity of BC, given its wide range of applications in the biomedical field. Improvement of polymers' antimicrobial properties is a popular research topic [23]. Different additives have been proposed to produce BC with enhanced antimicrobial properties. These include the addition of antibiotics [24], inorganic antimicrobials such as metallic nanoparticles [25], carbon nanomaterials [26] and organic antimicrobials such as bioactive substances [27] or synthetic compounds [28]. Moreover, based on reported literature, it was proved that associating two antimicrobial agents with a single composite can have great benefits due to the synergistic action of both compounds to overcome microbial resistance [29,30].

Curcumin is a polyphenolic pigment obtained from the turmeric root plant. It displays a broad-spectrum of antibacterial, antifungal, and antiviral properties which rendering it an attractive candidate for enhancing BC antimicrobial properties [31,32]. Fabrication of curcumin-loaded BC hydrogels has been explored as wound dressing material [33–37] with favorable results of biocompatibility and successful growth inhibition of Gram-negative and Gram-positive strains. Other studied applications include the treatment of melanoma in skin cancer cells [38] and active packaging materials [39]. Studies by Adamczak et al. showed that curcumin clearly has stronger effect against Gram-positive in comparison to Gram-negative bacteria. Curcumin has very selective antimicrobial activity, its effect strongly depends on the microorganism itself, not only genus related, but on the strain level as well [40].

Silver nanoparticles (Ag NPs) are another widely used broad-spectrum antimicrobials that have been incorporated into BC to boost their antimicrobial properties. Different approaches have been undertaken for the fabrication of BC-Ag NPs composites, focusing mainly on in situ methods for the synthesis of the nanoparticles within the BC [41–45], as well as immersion of BC in Ag NPs solution for impregnation of the nanoparticles into the BC matrix [46–48]. Wang et al. used chemical oxidation method to prepare silver oxide powder and combined it with cellulose nanofibrils to improve antimicrobial properties of this material [49]. The variation of incorporated Ag NPs morphologies also showed great potential in providing additional or differential properties for BC which can further

broaden its applications. For instance, silver nanowires have been incorporated into BC to boost its antimicrobial effects thanks to the higher length-to-diameter ratio of the nanowires, which also prevents blocking the BC pores and allows air circulation for wound dressing applications [50]. Despite such potential of the different shapes of Ag NPs, the fabrication of BC composites using other Ag NP shapes, such as TSNP, which have exhibited higher antimicrobial activity compared to spherical NPs [51–54], has not been yet explored.

Considering previously stated, and the rising interest of the scientific community and manufacturing sectors, it is clear that there is still room for BC properties improvements. One of the most promising approaches includes designing BC-based composites with superior characteristics, important from the perspective of the desired application field. This study aimed to assess the biocompatibility and antibacterial characteristics of the BC materials produced in the presence of curcumin with *ex situ* incorporated TSNP.

## 2. Results

### 2.1. Production of BC

*Komagataeibacter medellinensis* ID13488 bacterial strain was used to produce BC in HS medium, and HS medium that was supplemented with 2% and 10% of curcumin (*w/v*) (Figure 1). The BC films exhibited clear color differences due to curcumin supplementation using visual inspection. The intensity of the acquired orange color is notably greater for the sample supplemented with 10% curcumin (BC-Cur10%), than the one with 2% (BC-Cur2%).

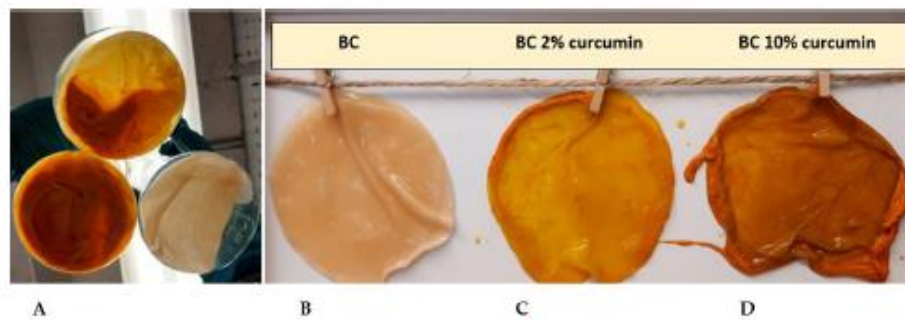


**Figure 1.** (A): Difference between BC pellicles in HS and curcumin-modified HS media after 14 days of incubation; (B): BC produced in HS medium; (C): BC produced in 2% curcumin supplemented HS medium; (D): BC produced in 10% curcumin supplemented HS medium.

After 14 days of incubation, the produced BC was dried and weighed. Due to the presence of curcumin, BC pellicles resulted in higher mass compared to the non-supplemented medium (Figure 2). Differences in weights are also a result of curcumin incorporation. UV-Visible spectral measurements showed that BC films absorbed 27.8% and 41% of curcumin during the two-week incubation period.

### 2.2. Characterization of Produced BC Films

#### 2.2.1. Scanning Electron Microscopy (SEM) and Energy Dispersive X-ray Spectroscopy (EDS)

SEM micrographs of the dried BC films grown in the presence of curcumin are shown in Figure 3. A smooth surface was observed in bare BC films (Figure 3A), while samples with incorporated curcumin showed crystal particles on the materials' surface (Figure 3C,E). The presence of curcumin crystals indicates their strong interaction with the nanofibril matrix of BC [55].

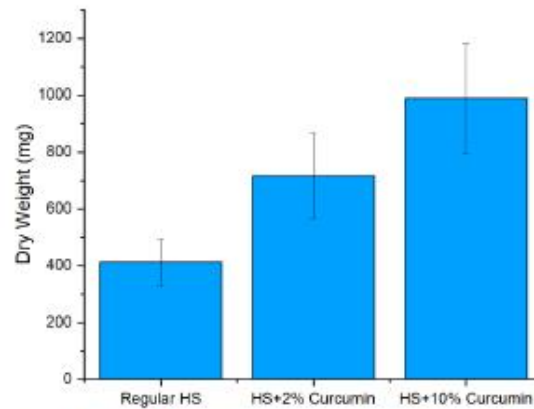


Figure 2. Dry weight of BC and curcumin-supplemented BC with 2% and 10%.

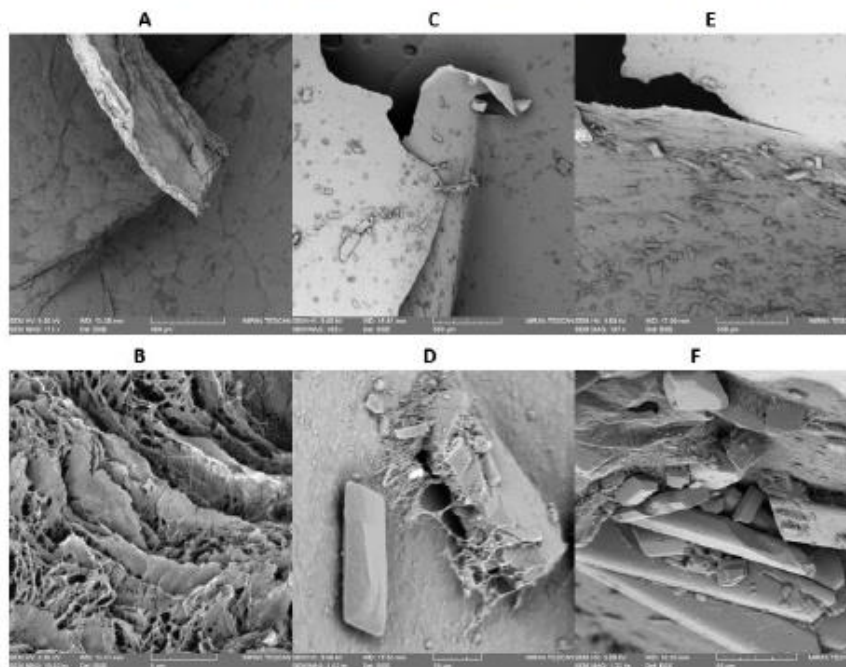
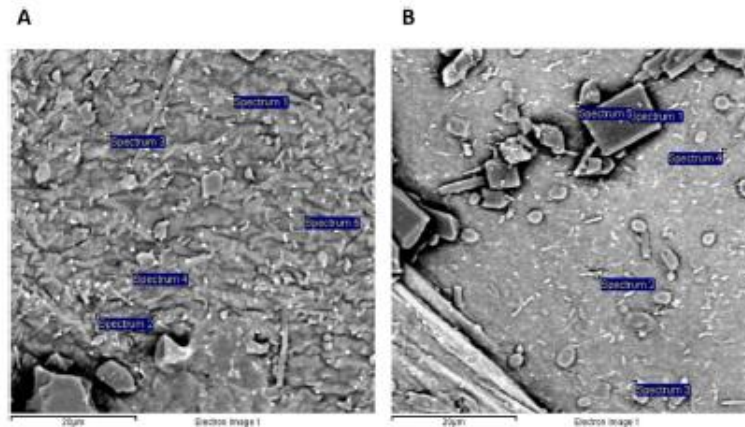


Figure 3. SEM micrographs of BC film 100 $\times$  (A) and 10k $\times$  (B); BC-Cur2% 100 $\times$  (C) and 3.5k $\times$  (D); BC-Cur10% 100 $\times$  (E) and 1.2k $\times$  (F).

The distribution of TSNP appearing as bright white dots on the surface of BC films is illustrated in Figure 4. The percentage of TSNP within the BC films was determined with the help of EDS analysis, 5 different white dots were randomly selected and analyzed. The presence of silver (Ag) was confirmed for all the selected spots in tested samples (BC-TSNP-Cur2%, BC-TSNP-Cur10%). EDS analysis revealed a strong signal in the silver region with the average percentages of 80.56 and 63.9% for examined materials, respectively.



**Figure 4.** SEM micrographs of examined materials with spots selected for EDS analysis: BC-TSNP-Cur2% (A) and BC-TSNP-Cur10% (B).

### 2.2.2. Thermal Gravimetric Analysis (TGA)

The TGA analysis was carried out to study the thermal stability of the fabricated BC films. The TGA curves of bare BC and BC-Cur and BC-Cur-TSNP films are shown in Figure 5. All the films started gradually losing mass below 100 °C, which could be attributed to the moisture content in the BC films. Maximum mass loss occurred between 200 °C and 600 °C. For most samples, the onset degradation temperature ( $T_{onset}$ ) was around 213 °C, and the degradation rate was stabilized at 600 °C. Furthermore, it can be indicated that the incorporation of curcumin and TSNP did not significantly affect the BC films' thermal stability, and this outcome follows the reported literature [25,56].

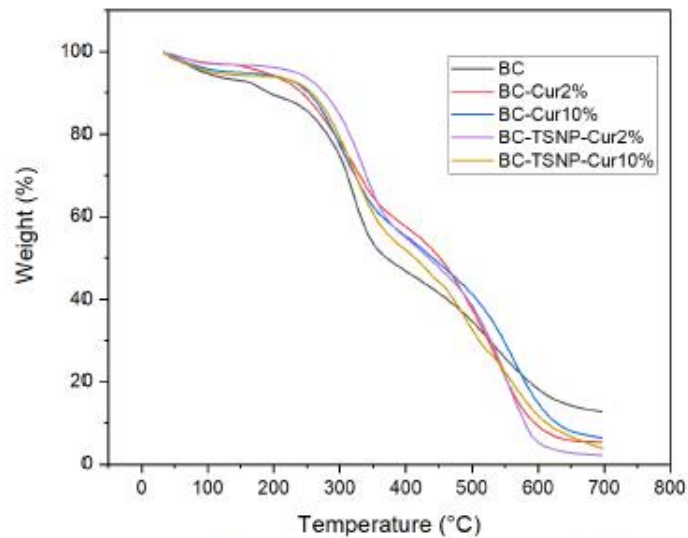


**Figure 5.** TGA curves of BC, Cur-treated BC, and Cur-TSNP-treated BC films.



### 2.2.3. Fourier Transform Infrared Spectroscopy (FTIR)

FTIR analysis was performed to obtain a comparative view of the functional groups in BC and their changes after the addition of curcumin and TSNP. The resulting FTIR spectra for the BC specimens are shown in Figure 6. The spectrum of bare BC showed characteristic peaks at  $3277\text{ cm}^{-1}$  (O-H stretching vibration),  $2918\text{ cm}^{-1}$  (C-H stretching),  $1626\text{ cm}^{-1}$ ,  $1535\text{ cm}^{-1}$  (protein amide II absorption),  $1156\text{ cm}^{-1}$  (C-O-C asymmetric bending/stretching),  $1055\text{--}1033\text{ cm}^{-1}$  (bending of C-O-H bond of carbohydrates), and  $665\text{ cm}^{-1}$  (C-OH out of plane bending) [57,58]. The spectrum for curcumin allowed to identify characteristic peaks at  $3504\text{ cm}^{-1}$  (O-H stretching vibration),  $1600\text{ cm}^{-1}$  (benzene ring stretching vibration),  $1503\text{ cm}^{-1}$  (C=O and C=C vibrations),  $1426\text{ cm}^{-1}$  (olefinic C-H bending vibrations),  $1272\text{ cm}^{-1}$  (aromatic C-O stretching vibrations), and  $1026\text{ cm}^{-1}$  [59–62].

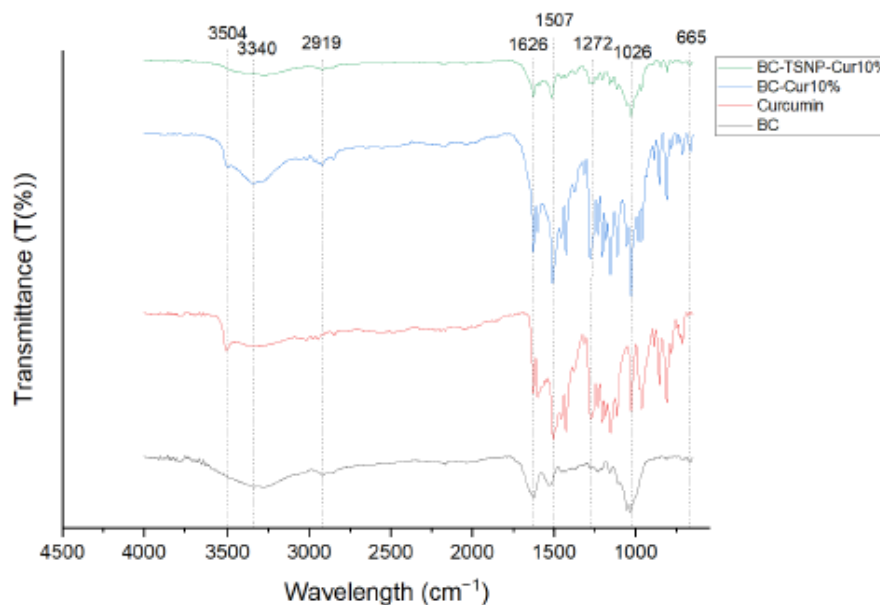


**Figure 6.** FTIR spectra for BC, curcumin, BC-Cur10%, BC-TSNP, and BC-TSNP-Cur10%.

Spectrum of BC-Cur10% shows characteristic peaks from both, BC and curcumin. As shown in Figure 6, the peak assigned to OH stretching vibration of BC exhibited a shift from  $3340\text{ cm}^{-1}$  to  $3346\text{ cm}^{-1}$ , and the peak assigned to C=O and C=C vibrations of curcumin, shifted from  $1503\text{ cm}^{-1}$  to  $1507\text{ cm}^{-1}$ . A weak peak at  $1279\text{ cm}^{-1}$  was attributed to C-H bending in the spectrum of BC [63], while it was much stronger in the same wavelength for BC-Cur10%. The small peaks that showed from  $1550\text{ cm}^{-1}$  to  $1100\text{ cm}^{-1}$  in the BC spectrum were masked by larger curcumin peaks in the spectrum of BC-Cur10%. The rest of the peaks either remained in the same wavelength or had a small shift of  $1\text{--}2\text{ cm}^{-1}$  only, when compared to BC or curcumin spectra. Thus, the obtained results confirm the incorporation of curcumin into the BC matrix and suggest a chemical interaction with the cellulose fibrils. A similar tendency was observed by Sajjad et al. after incorporating curcumin into BC sheets, where additional peaks appeared, and the characteristic peaks of BC suffered small shifts [36].

In the spectrum obtained for BC-TSNP-Cur10%, a shift from  $3340$  to  $3277\text{ cm}^{-1}$  was observed in the OH peak. The C=O and C=C vibrations peak was also shifted from  $1503$  to  $1512\text{ cm}^{-1}$  concerning the curcumin spectrum. Additionally, when compared to the

spectrum of BC-Cur10%, several peaks showed reduced intensities between 1500 and 1000  $\text{cm}^{-1}$ , which are estimated to occur due to the impregnation of TSNP within the matrix of BC-Cur films.

#### 2.2.4. Weathering Testing

When combined with humidity, the color of an organic pigment can fade much more quickly than due to light alone. For this reason, weather testing is often carried out to measure irradiation effects with humidity. Curcumin is a very light-fast material and its color fades quickly when exposed to such conditions. Even with the addition of UV absorbers and hindered amine light stabilizers, curcumin remains relatively unstable.

Figure 7 shows warping occurred in all five samples after weather testing. This indicates that the combination of UV and moisture caused structural changes to the BC film, presumably due to reduced chain length from photocoxidative degradation on the exposed surface, which was more than that on the rear of the samples. The weathering cycles caused embrittlement of samples containing curcumin, without TSNP. Large deposits of curcumin were present on the surface of the samples, indicating that perhaps much of the curcumin is rejected from the wafer as the solution dries. The degree of incompatibility between the BC and curcumin was less pronounced in the samples containing TSNP. While it is not clear from Figure 7, spectrophotometry measurements showed color fading in all samples. The values for color changes due to weathering exposure are presented in Table 1 as  $\Delta E^*$  to calculate color difference. Due to the initial color differences between samples, it is not fair to directly compare  $\Delta E^*$  values between cases; however, it is clear that none of the materials is UV stable. Not only is there a significant color change for each case, but the embrittlement and disintegration of the material indicates a likely deterioration in mechanical properties due to UV light exposure. Such behavior will be addressed and resolved in future work.

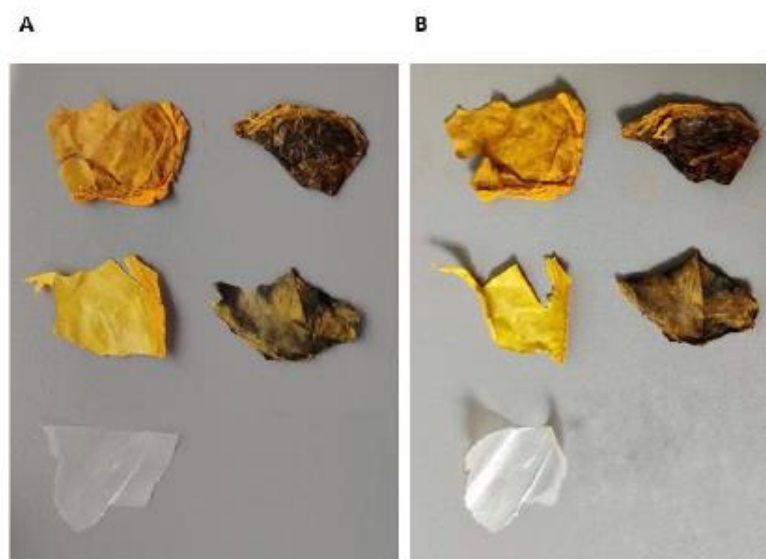


**Figure 7.** Samples before (A) and after (B) weather testing. From left-to-right, top-to-bottom: BC-Cur10%, BC-TSNP-Cur10%, BC-Cur2%, BC-TSNP-Cur2% and BC.

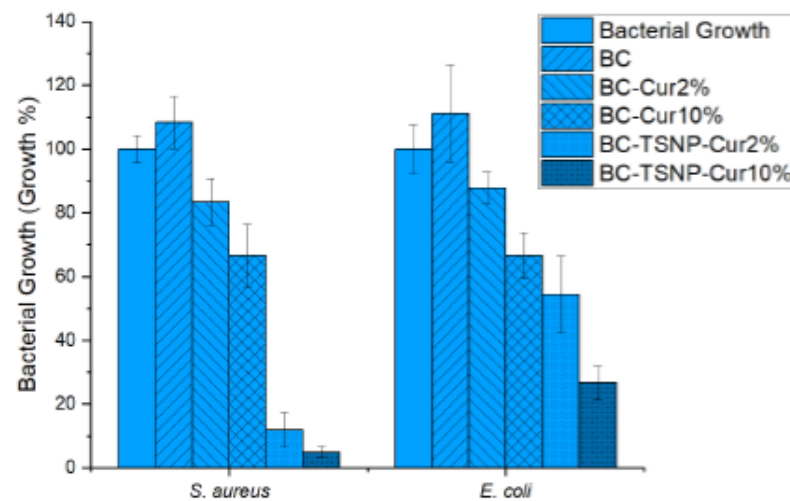
**Table 1.** Color change,  $\Delta E^*$  for each sample case due to weather testing.

Samples	$\Delta E^*$
BC	2.83
BC-Cur2%	12.74
BC-Cur10%	6.40
BC-TSNP-Cur2%	4.69
BC-TSNP-Cur10%	6.87

### 2.3. Biological Evaluations

#### 2.3.1. Antimicrobial Activity

Antimicrobial activity of derived BC films was evaluated against *S. aureus* and *E. coli*, as representatives of Gram-positive and Gram-negative bacteria, respectively. Results are displayed in Figure 8 as bacterial growth percentage. Pure BC film did not affect the growth of the tested strains in the desired fashion; on the contrary, the growth was enhanced by approximately 10% in both bacterial strains. Nevertheless, the antimicrobial performance of the BC films was significantly enhanced in the presence of curcumin, reducing the growth by approximately 15% in BC-Cur2% film, and up to 33% with BC-Cur10% films. Additional incorporation of TSNP in BC-Cur films resulted in further inhibition of *E. coli* growth (up to 67% of reduction) and even greater inhibition against *S. aureus* (up to 95% of growth reduction). The statistical analysis by ANOVA-Dunnett ( $\alpha = 0.05$ ) showed that for *E. coli*, all the groups are significantly different to the control, with the exception of BC and BC-Cur2%. Meanwhile, in the case of *S. aureus*, the only group that did not result to be significantly different to the control, was the bare BC.

**Figure 8.** Antimicrobial activity of derived BC films measured as absorbance rate at 630 nm.

#### 2.3.2. Cytotoxicity Assay

Cytotoxicity was evaluated by using a human fibroblasts cell line (MRC5) exposed to BC film extracts of different concentrations, previously prepared in RPMI medium under dynamic conditions. The viability of MRC5 cells was assessed using a standard MTT assay. The results presented in Figure 9 indicate that more than 80% of cells survived after being in contact with 100% concentrations of BC film extracts, indicating their low toxicity. According to the literature, materials are considered safe when the cells viability is over 70% [64]. It was also shown that only 100% concentrations of BC-Cur2% and BC-Cur10%

film extracts induce a significant decrease in MRC5 cells viability after 48 h treatments. Significant toxicity was related to 100% and 50% concentrations of both BC-TSNP and BC-TSNP-Cur2%. Interestingly, the increased amounts of curcumin in BC-TSNP-Cur10% film extract resulted in considerably reduced toxicity since more than 80% of cells survived after being in contact with the highest concentration of this extract. The statistical analysis by ANOVA-Tukey ( $\alpha = 0.05$ ) showed that for the extracts in a concentration of 100%, showed a significant difference of all the materials against the bare BC survival growth, except for the BC-TSNP-Cur10% group. Meanwhile, in the 50% extracts, the groups of BC-TSNP and BC-TSNP-Cur2% were the only ones that showed a statistical significance.

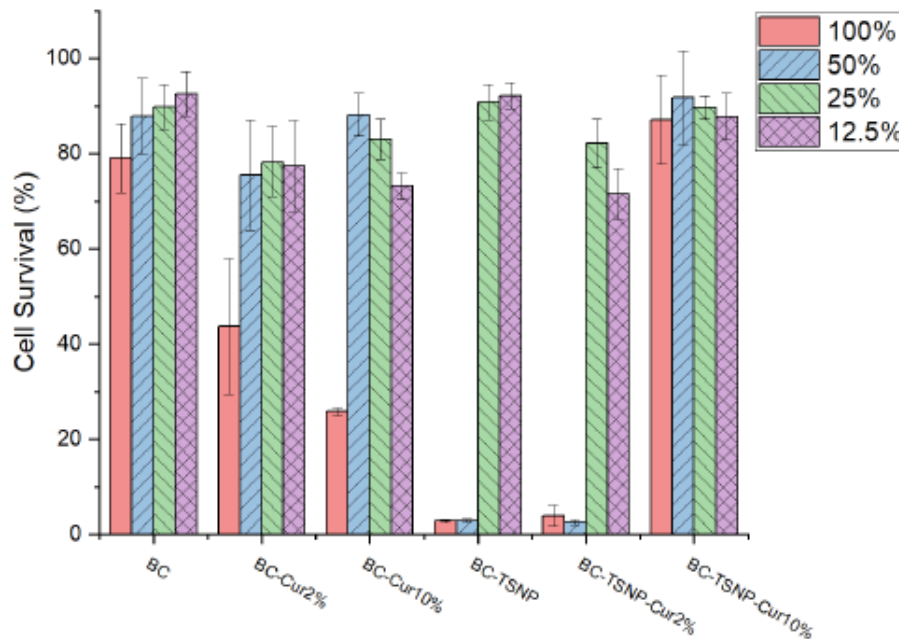


**Figure 9.** Survival rate of cell line (MRC5) after exposure to BC film extracts of different concentrations.

### 2.3.3. *Danio Rerio* Embryotoxicity Assay

The effects of BC materials were examined on zebrafish embryos in 12.5%, 10%, 5%, and 2.5% concentrations (Figure 10).

As presented in Figure 11, control material BC was not significantly toxic, while BC-TSNP in the highest tested concentration (50%) was toxic, with the teratogenic effects such as microcephaly and hepatotoxicity. Supplementation of BC with curcumin in two concentrations causes toxic effects on zebrafish, mostly heart and liver toxicity, while BC-TSNP-Cur2% and BC-TSNP-Cur10% did not have any toxic or teratogen effects on zebrafish embryos.

### 2.3.4. *Caenorhabditis elegans* Survival Assay

In order to confirm previous results, the effects of BC materials were examined on *C. elegans* model system in four different concentrations: 50, 25, 12.5, and 6.25  $\mu\text{g mL}^{-1}$  and the results are presented in Figure 12. *C. elegans* has been widely used to evaluate biological activity and interactions of nanoparticles and natural products with different targets in organisms [65,66]. Overall BC materials showed little to no toxicity, with only around 10% dead at the highest concentration for BC-TSNP-Cur2%, BC-TSNP, and BC-Cur10%.

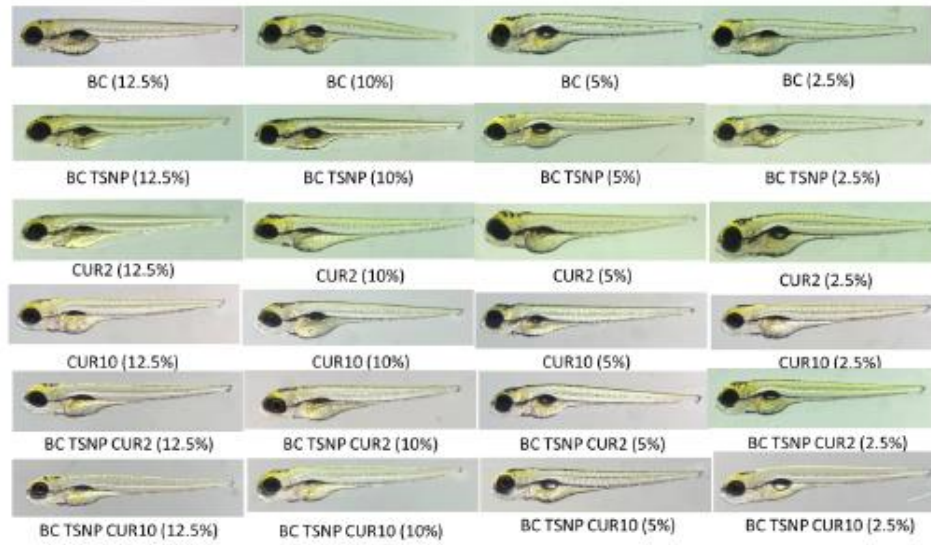


Figure 10. Effect of BC materials on development of zebrafish embryos, images of zebrafish embryos at 120 hpf treated with different extracts concentrations and untreated as a control.

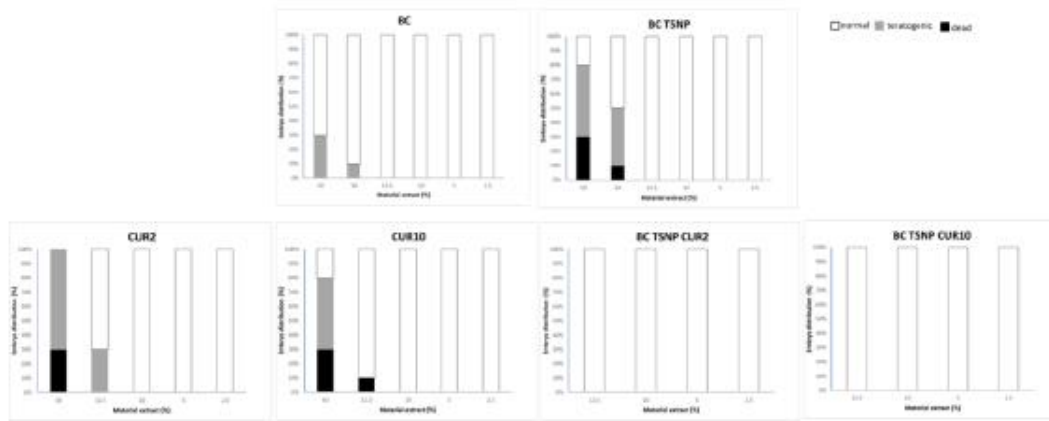


Figure 11. Diagrams for each tested material extract with the percentages of live, dead, and teratogenic embryos.

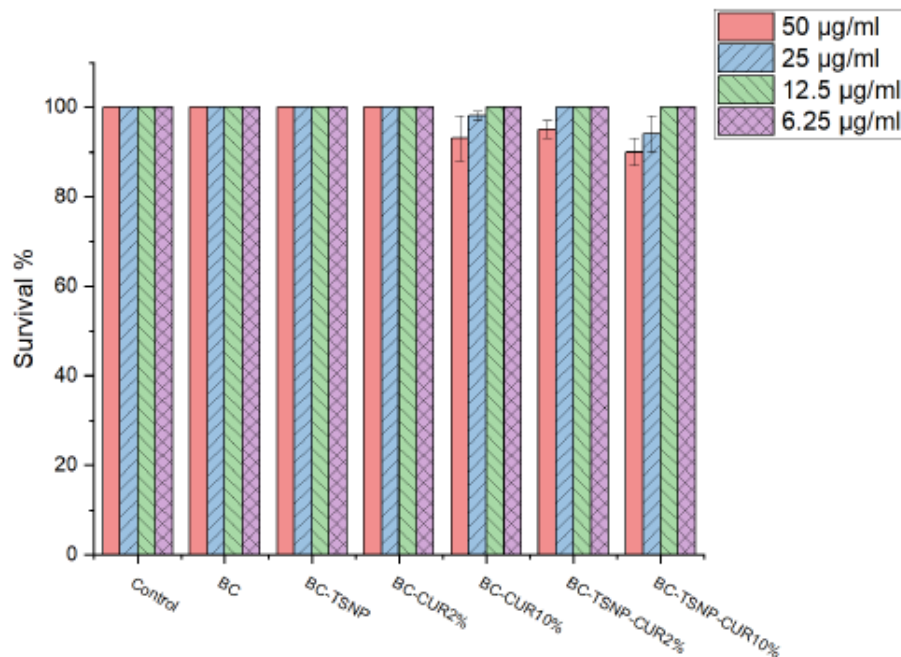


Figure 12. *C. degans* survival rate in the presence of examined BC materials after 24 h.

### 3. Discussion

Advanced anti-infective biomedical materials which meet the stringent requirement for applications in clinical settings are urgently required [67]. BC is a sustainable biopolymer with unique physical properties leading to its expansive potential in the biomedical field. Effectively harnessing and integrating the functional properties of natural materials for synergistic performance, development has the potential to deliver high-performance biomaterials. Here a series of high-impact results have been delivered by developing enhanced antimicrobial curcumin and TSNP-incorporated BC films.

First, the production of BC in the presence of curcumin resulted in a higher product yield, up to 200% in the case where 10% of curcumin was used in the medium. This result is highly significant considering the current multiple inhibiting factors within BC production and consumption. Moreover, the addition of curcumin has improved the antimicrobial characteristics of the resulting material. Such results could be attributed to the antimicrobial activity of curcumin itself, which boosted the overall antimicrobial activity of the BC-Cur films. The antimicrobial activity was also concentration dependent since it increased with the increase in curcumin amount added during the cultivation of BC. These observations coincide with previously published results by Sajjad et al. (2020) [36]. This antimicrobial effect was enhanced further again with the incorporation of TSNP, resulting in inhibition of *E. coli* growth up to 67% and even greater inhibition against *S. aureus* (up to 95% of growth reduction). Contrary to our results, Gupta et al. (2020) observed higher growth inhibition against the Gram-negative strain than the Gram-positive, when testing the antimicrobial activity for ex situ curcumin-loaded BC [68]. Nonetheless, curcumin has previously been demonstrated to exhibit a higher antimicrobial effect toward Gram-positive strains than Gram-negative. Minimal inhibitory concentration of crude curcumin against *S. aureus* was found to be  $\sim 100 \mu\text{g mL}^{-1}$ , while for Gram-negative *E. coli* this concentration

increases four-fold. This suggests that the activity of curcumin is predominant in the case of Cur-TSNP-loaded BC films against Gram-positive strains [32,40,69].

In a highly positive synergistic interaction, BC films with 10% curcumin and incorporated TSNP have shown reduced toxicity with an 80% cells survival rate. Achievement of this feature is important because the material can be characterized as safe once cells viability is over 70%, and it can be concluded that modified BC is a biocompatible material [64]. In vivo tests further confirmed these results. In the case of the zebrafish model system, supplementation of BC with curcumin in both used concentrations caused heart and liver toxicity, while BC films with curcumin and TSNP did not have any toxic or teratogen effects on zebrafish embryos. Previously published study, where curcumin was tested separately on zebrafish embryos, showed the severe toxicity of this compound, with some of the teratogenic effects including bent or hook-like tails, spinal column curving, edema in pericardial sac, retarded yolk sac resorption, and shorter body length in the examined concentration of  $7.5 \mu\text{mol L}^{-1}$  [70]. While in a different study, tested in lower dosages ( $1\text{--}6 \mu\text{mol L}^{-1}$ ), curcumin had a moderate acute toxicity effect on zebrafishes with no obvious morphological abnormalities according to their score based on the degree of morphological anomalies (2–4 minor toxic effects) [71]. In addition, silver nanoparticles are toxic for zebrafish development; one study revealed that nanoparticle treatments resulted in concentration-dependent toxicity, typified by phenotypes that had abnormal body axes, twisted notochord, slow blood flow, pericardial edema, and cardiac arrhythmia [72]. Our study suggests that combining curcumin and TSNP in BC does not show high toxicity on zebrafish development in the examined conditions. The synergetic effect of these natural compounds leading to improved biological activity of the BC films obtained in this study will be further addressed in the future. In the case of *C. elegans*, previous studies on curcumin itself reported that this compound can prolong lifespan and influence age-related biomarkers in this model organism [73]. On the other hand, nanoparticles, especially silver, have shown significant toxic effects on this model organism [74]. Our results imply that the concentration of TSNP incorporated in BC films was insufficient to affect *C. elegans* under examined conditions significantly.

BC is a biomaterial of growing importance with a rising application spectrum and its developments are very significant. Further studies will include improvement of mechanical characteristics of these materials that will potentially result in designing products suitable for various packaging and biomedical applications. This study has effectively demonstrated that integrating curcumin in a production medium with ex situ TSNP incorporation leads to safe, biocompatible, antimicrobial BC films.

## 4. Materials and Methods

### 4.1. Materials

The HPLC-grade water (34877-2.5L), sodium citrate tribasic (C8532-100G) [TSC], poly(sodium 4-styrenesulfate) (434574-5G) [PSSS], sodium borohydride (213462-25G) [ $\text{NaBH}_4$ ], silver nitrate (204390-10G) [ $\text{AgNO}_3$ ], L-ascorbic acid (A92902-25G) [AA] and citric acid (C2404-500G) were obtained from Sigma-Aldrich Ireland Ltd. (Arklow, Ireland). LP-BT100-1F Peristaltic Dispensing Pump with YZIII15 pump head and Tygon LMT-55 Tubing #17 were obtained from Drifton (Hvidovre, Denmark). Curcumin (FC09321) was obtained from Biosynth Carbosynth (Thal, Switzerland). Glucose (NCM0241A), yeast extract (NCM0218A), and balanced peptone No. 1 (NCM0257A) were manufactured by Neogen (Lansing, MI, USA) and distributed by Cruinn Diagnostics (Dublin, Ireland). Sodium phosphate dibasic dodecahydrate (71650) [ $\text{Na}_2\text{HPO}_4$ ] was obtained from Fluka Analytical.

### 4.2. Synthesis of TSNPs

TSNP were synthesized by a previously described seed-mediated approach [75]. Briefly,  $\text{NaNH}_4$  (0.57 mL, 10 mM) was used for the reduction of  $\text{AgNO}_3$  (9.48 mL, 0.5 mM), using TSC (9.5 mL, 2.5 mM) and PSSS (0.47 mL, 500 mg/L) as stabilizers for the formation of the seeds. TSNP were afterwards grown from the seeds (8.75 mL,

25.56 ppm), with the addition of 100 mL of distilled water,  $\text{AgNO}_3$  (75 mL, 0.5 mM) and using AA (1.87 mL, 10 mM) as a reducing agent. TSC (12.5 mL, 25 mM) was added at the end of the reaction to provide stabilization to the TSNP.

#### 4.3. Production of BC Films Using Curcumin as a Supplement

The BC was produced using *Komagataeibacter medellinensis* ID13488. Pre-culture of the bacteria was prepared in Hestrin and Schramm (HS) liquid medium (2% glucose, 0.5% yeast extract, 0.27%  $\text{Na}_2\text{HPO}_4$  and 0.15% citric acid) as previously reported [76], and the incubation was carried out for 2 days at 30 °C on a rotary shaker with the agitation rate of 180 rpm. BC production was performed in HS medium supplemented with 2% and 10% curcumin (*w/v*). BC films grown in HS medium without additives were used as a negative control for further assessments.

Different media batches were inoculated with 100  $\mu\text{L mL}^{-1}$  from pre-culture (10% *v/v* inoculum), and incubated statically at 30 °C for 14 days. After incubation, BC hydrogels were removed from liquid media. Bare BC films were washed in a 0.5 M potassium hydroxide (KOH) solution in the water bath (1 h, 100 °C) and neutralized with distilled water. In order to prevent degradation of curcumin, BC films produced with the addition of curcumin were immersed in distilled water and autoclaved (121 °C, 15 min). After washing process, films were dried overnight at 60 °C.

#### Estimation of Curcumin Absorption from Media

The UV-visible spectral measurements were performed in a UV 1280 Shimadzu (Kyoto, Japan) spectrophotometer using 10 mm path length matched quartz cuvettes [77]. The measurements were taken in the wavelength range of 200–700 nm. In aqueous solution, curcumin had a peak at 427 and a shoulder at 360 nm. Peak area was used for estimation of curcumin incorporation via comparison between non-inoculated media and media after 14 days of incubation.

#### 4.4. Preparation of TSNP Incorporated BC Films

A total of 20 mg of each examined BC films (BC with 2% of curcumin, BC with 10% of curcumin) were immersed into 5 mL of TSNP solution (21.34 ppm) and incubated overnight at 30 °C with shaking on horizontal platform (100 rpm). Afterwards, films were removed from the solution and dried overnight at 60 °C.

#### 4.5. Characterisation of Derived BC Films

##### 4.5.1. Morphological Characterization and Estimation of TSNP Absorption

Scanning electron microscopy (SEM) images were obtained using Mira XMU SEM (Tescan™, Brno, Czech Republic) in back scattered electron mode for surface analysis. The accelerating voltage used was 9 kV. Prior to analysis, tested samples were placed on an aluminum stub and sputtered with a thin layer of gold using Baltec SCD 005 for 110 s at 0.1 mbar vacuum. Energy dispersive X-ray spectroscopy (EDS) was used to confirm the presence of silver in the samples immersed in TSNP solution. Data were gathered by an X-Max E.D.S. system (Oxford Instruments, Oxford, UK) with Inca software.

##### 4.5.2. Thermogravimetric Analysis (TGA)

Thermal stability of the BC films was evaluated using a Pyris TGA 1 thermogravimetric analyzer (Perkin Elmer, Washington, DC, USA) with software Pyris 1. The film samples were taken in a standard aluminum pan and heated from 30 to 700 °C at the rate of 10 °C  $\text{min}^{-1}$  under a nitrogen flow of 50  $\text{mL min}^{-1}$ .

##### 4.5.3. Fourier Transforms Infrared (FTIR) Spectroscopy

A Perkin-Elmer Spectrum One FTIR spectrometer (Perkin Elmer Inc., Washington, DC, USA) fitted with a universal ATR sampling accessory and Perkin Elmer software, was used



to record the spectra of dried BC films. The spectral resolution was  $4\text{ cm}^{-1}$  and 20 scans were acquired for each spectrum ( $4000\text{--}650\text{ cm}^{-1}$ ).

#### 4.5.4. Evaluation of BC Films Stability via Weathering Tests

Weather testing was carried out on the BC films to determine their stability against UV irradiation using a QUV/se accelerated weather tester from Q-Lab (Westlake, OH, USA) in compliance with the ISO 4892 test standard. Fluorescent UV-A lamps with a radiant emission range of 365 nm down to 295 nm were used to simulate sunlight exposure. A set temperature of  $40\text{ }^{\circ}\text{C}$  was used in the chamber and UV irradiance of  $0.76\text{ W m}^{-2}$ . Samples were exposed to moisture spray and UV light cyclically in 4-h increments. In total, the samples were exposed for 20 h in each condition.

To quantify the effects of weathering, spectrophotometry was used before and after exposure to measure the degree of color change in samples. A CM-3610A bench-top spectrophotometer from Konica Minolta (Tokyo, Japan) with an  $8^{\circ}$  observant angle was used to measure the color change in specimens. Procedures followed the ISO 11664-4 test standard and the  $\Delta E^*$  (CIEDE2000) metric was used to calculate color difference.

#### 4.5.5. Biological Evaluations

##### Antibacterial Activity of BC Films

All the dried BC films' antimicrobial activity was evaluated against *Escherichia coli* ATCC 95922 and *Staphylococcus aureus* ATCC 25923 in Luria-Bertani (LB) broth ( $10\text{ g L}^{-1}$  tryptone,  $10\text{ g L}^{-1}$  NaCl,  $5\text{ g L}^{-1}$  yeast extract, pH 7.2). Overnight cultures of the bacteria were diluted to a concentration of  $10^8\text{ CFU mL}^{-1}$  to be used as pre-culture. Dried BC films (10 mg of each specimen) were immersed in fresh LB broth and inoculated with 1% (v/v) from pre-culture, for a final concentration of  $10^6\text{ CFU mL}^{-1}$  of bacteria. Untreated BC films were used as negative control. After incubation for 24 h at  $37\text{ }^{\circ}\text{C}$  and 100 rpm, BC films were removed from the cultures and optical density (OD) of the cultivated broth was measured at 630 nm using a Biotek Synergy HT Microplate Reader (Biotek Instruments GmbH, Bad Friedrichshall, Germany). Growth percentage was calculated using the following equation (Equation (1)).

$$\text{Growth Percentage} = \left( \frac{\text{Absorbance of tested sample}}{\text{Absorbance of positive control}} \right) \times 100 \quad (1)$$

##### Cytotoxicity Assay

The cytotoxicity of BC films was evaluated by testing against the human fibroblasts (MRC-5) obtained from ATCC. BC films were sterilized under UV light for 20 min and then immersed into RPMI (Roswell Park Memorial Institute) medium ( $5\text{ mg mL}^{-1}$ ). The samples were incubated at  $37\text{ }^{\circ}\text{C}$ , 180 rpm for 48 h. After incubation, samples were centrifuged (5000 rpm, 15 min), and sterilized by filtering using  $0.22\text{ }\mu\text{m}$  pore size filters.

Cells were plated into a flat-bottom 96-well plate at a concentration of  $1 \times 10^4$  cells per well in RPMI medium supplemented with  $100\text{ }\mu\text{g mL}^{-1}$  streptomycin,  $100\text{ U mL}^{-1}$  penicillin, and 10% (v/v) fetal bovine serum (FBS) and incubated for 24 h at  $37\text{ }^{\circ}\text{C}$  to allow the formation of a monolayer. After 24 h of cells incubation, RPMI medium was substituted with decreasing concentrations of BC extracts: 100%, 50%, 25%, and 12.5% (v/v) while the control samples contained only RPMI medium. The incubation at  $37\text{ }^{\circ}\text{C}$ , 5%  $\text{CO}_2$  continued for 48 h and the cytotoxicity was determined afterwards using 3-(4,5-dimethylthiazol-2-yl)-2,5-diphenyltetrazoliumbromide (MTT) reduction assay [78].

The extent of MTT reduction to formazan was measured spectrophotometrically at 540 nm using a Tecan Infinite 200 Pro multiplate reader (Tecan Group Ltd., Mannedorf, Switzerland). The results were presented as percentage of the control (untreated cells) that was arbitrarily set to 100%.

#### *Danio rerio* Embryotoxicity Assay

BC materials were incubated in embryo water ( $100 \text{ mg mL}^{-1}$ ) 24 h at  $30^\circ\text{C}$  with shaking on horizontal platform (180 rpm), and that extract was used for toxicology assessment. In vivo toxicity evaluation was carried out on the zebrafish (*Danio rerio*) model, and the general rules of the OECD Guidelines for the testing of chemicals were followed while zebrafish embryotoxicity assay was performed [79]. Briefly, zebrafish embryos were produced by mating of adult females and males (ratio 1:2), collected, washed from detritus and distributed into 24-well plates containing 10 embryos per well in 1 mL embryo water ( $0.2 \text{ g L}^{-1}$  of Instant Ocean® Salt in distilled water), and incubated at  $28^\circ\text{C}$ . Experiments were performed in triplicate using 30 embryos per each tested concentration. Non-treated embryos were used as a negative control. Embryos were examined under the stereomicroscope (SMZ143-N2GG, Motic, Germany) every 24 h for five days, counting and discarding dead embryos and observing teratogenic effects. After the assay embryos were killed by freezing at  $-20^\circ\text{C}$  for 24 h. All experiments involving zebrafish were performed in compliance with the European directive 2010/63/EU and the ethical guidelines of the Guide for Care and Use of Laboratory Animals of the Institute of Molecular Genetics and Genetic Engineering, University of Belgrade.

#### *Caenorhabditis elegans* Survival Assay

The nematode *Caenorhabditis elegans* AU37, obtained from the Caenorhabditis Genetics Center (CGC), University of Minnesota, Minneapolis, Minnesota, US. *C. elegans* AU37 (glp-4; sek-1), was used to establish the toxicity of BC materials.

For this assay 25 mg of each BC films was suspended in 2.5 mL of M9 medium (45 mL of 5xM9 salt, 50 mL of glucose solution 50% (w/v), 500  $\mu\text{L}$  of 1 M  $\text{MgSO}_4$ , 25  $\mu\text{L}$  of 1 M  $\text{CaCl}_2$ , 250  $\mu\text{L}$  vitamins, 250  $\mu\text{L}$  of trace elements solution, 125  $\mu\text{L}$  of ampicillin  $50 \mu\text{g mL}^{-1}$ , and final volume adjusted to 250 mL with double distilled water). Samples were incubated at  $37^\circ\text{C}$ , with shaking on horizontal platform at 180 rpm for 24 h. After incubation, BC films were removed from the suspension and extracts were prepared in the following concentrations:  $50 \mu\text{g mL}^{-1}$ ,  $25 \mu\text{g mL}^{-1}$ ,  $12.5 \mu\text{g mL}^{-1}$ , and  $6.25 \mu\text{g mL}^{-1}$ .

The worm was propagated under standard conditions, synchronized by hypochlorite bleaching, and cultured on a nematode growth medium using *E. coli* OP50 as a food source, as described previously [80]. The *C. elegans* AU37 survival assay followed the standard procedure [81] with some minor modifications. Briefly, synchronized worms (L4 stage) were suspended in a medium containing 95% M9 buffer (3.0 g of  $\text{KH}_2\text{PO}_4$ , 6.0 g of  $\text{Na}_2\text{HPO}_4$ , 5.0 g of NaCl, and 1 mL of 1 M  $\text{MgSO}_4 \cdot 7\text{H}_2\text{O}$  in 1 L of water), 5% LB broth (Oxoid, Basingstoke, UK), and  $10 \mu\text{g mL}^{-1}$  of cholesterol (Sigma-Aldrich, Munich, Germany). The experiment was carried out in 96-well flat-bottomed microtiter plates (Sarstedt, Nümbrecht, Germany) with a final volume of 100  $\mu\text{L}$  per well. The wells were filled with 50  $\mu\text{L}$  of the suspension of nematodes (25–35 nematodes) and 50  $\mu\text{L}$  of tested BC film suspension. Subsequently, the plates were incubated at  $25^\circ\text{C}$  for 48 h. The fraction of dead worms was determined after 48 h by counting the number of dead worms and the total number of worms in each well, using a stereomicroscope (SMZ143-N2GG, Motic, Germany). All BC films suspensions were tested three times in each assay, and each assay was repeated two times ( $n = 6$ ). As a negative control experiment, nematodes were exposed to the medium containing 1% DMSO.

#### 4.6. Statistical Analysis

Statistical analysis for the in vitro cytotoxic evaluation was performed using one-way analysis of variance (ANOVA) and grouped using the Tukey method with a 95% confidence interval. Statistical analysis for the antimicrobial evaluation was performed using ANOVA, paired with the Dunnett method and a 95% confidence interval. The software used to perform these analyses was Minitab (Version 20.2) for Windows (64-bit). All data collected for this study were expressed as mean  $\pm$  standard deviation. A sample size of four was used for each concentration tested in the cytotoxicity evaluation, and a sample size of three was used for the antimicrobial evaluation.

**Author Contributions:** Conceptualization, E.L.G. and M.M.; methodology, E.L.G., D.M., S.V., I.A., J.M. and M.S.; validation, E.L.G. and M.M.; formal analysis, E.L.G., D.M., I.A. and S.V.; writing—original draft, E.L.G., M.M. and O.A.A.; writing—review and editing, M.M. and M.B.F.; supervision, M.M., M.B.F. and D.D.; funding acquisition, M.B.F. All authors have read and agreed to the published version of the manuscript.

**Funding:** This project received funding from the European Union’s Horizon 2020 research and innovation programme under grant agreement No. 870292 (BioICEP) and was supported by the National Natural Science Foundation of China (grant numbers: Institute of Microbiology, Chinese Academy of Sciences: 31961133016; Beijing Institute of Technology: 31961133015; Shandong University: 31961133014). This project also received funding from a part of the Interreg VB NWE Programme, project number NWE1058 (CURCOL).

**Institutional Review Board Statement:** Not applicable.

**Informed Consent Statement:** Not applicable.

**Data Availability Statement:** Not applicable.

**Conflicts of Interest:** The authors declare no conflict of interest.

## References

- Gorgieva, S.; Trček, J. Bacterial Cellulose: Production, Modification and Perspectives in Biomedical Applications. *Nanomaterials* **2019**, *9*, 1352. [\[CrossRef\]](#)
- Silva, S.S.; Fernandes, E.M.; Pina, S.; Silva-Correira, J.; Vieira, S.; Oliveira, J.M.; Reis, R.L. 2.11 Polymers of Biological Origin. *Compr. Biomater. II* **2017**, *2*, 228–252. [\[CrossRef\]](#)
- Sharma, C.; Bhardwaj, N.K. Bacterial Nanocellulose: Present Status, Biomedical Applications and Future Perspectives. *Mater. Sci. Eng. C* **2019**, *104*, 109963. [\[CrossRef\]](#)
- de Amorim, J.D.P.; da Silva Junior, C.J.G.; de Medeiros, A.D.M.; do Nascimento, H.A.; Sarubbo, M.; de Medeiros, T.P.M.; Costa, A.F.d.S.; Sarubbo, L.A. Bacterial Cellulose as a Versatile Biomaterial for Wound Dressing Application. *Molecules* **2022**, *27*, 5580. [\[CrossRef\]](#)
- Torres, F.G.; Troncoso, O.P.; Gonzales, K.N.; Sari, R.M.; Gea, S. Bacterial Cellulose-based Biosensors. *Med. Devices Sens.* **2020**, *3*, e10102. [\[CrossRef\]](#)
- Hickey, R.J.; Pelling, A.E. Cellulose Biomaterials for Tissue Engineering. *Front. Bioeng. Biotechnol.* **2019**, *7*, 45. [\[CrossRef\]](#)
- Zhang, C.; Salick, M.R.; Cordie, T.M.; Ellingham, T.; Dan, Y.; Turng, L.S. Incorporation of Poly(Ethylene Glycol) Grafted Cellulose Nanocrystals in Poly(Lactic Acid) Electrospun Nanocomposite Fibers as Potential Scaffolds for Bone Tissue Engineering. *Mater. Sci. Eng. C* **2015**, *49*, 463–471. [\[CrossRef\]](#)
- Zander, N.E.; Dong, H.; Steele, J.; Grant, J.T. Metal Cation Cross-Linked Nanocellulose Hydrogels as Tissue Engineering Substrates. *ACS Appl. Mater. Interfaces* **2014**, *6*, 18502–18510. [\[CrossRef\]](#)
- Wang, J.; Tavakoli, J.; Tang, Y. Bacterial Cellulose Production, Properties and Applications with Different Culture Methods—A Review. *Carbohydr. Polym.* **2019**, *219*, 63–76. [\[CrossRef\]](#)
- Jacek, P.; Dourado, F.; Gama, M.; Bielecki, S. Molecular Aspects of Bacterial Nanocellulose Biosynthesis. *Microb. Biotechnol.* **2019**, *12*, 633–649. [\[CrossRef\]](#) [\[PubMed\]](#)
- Bagewadi, Z.K.; Bhavikatti, J.S.; Muddapur, U.M.; Yaraguppi, D.A.; Mulla, S.I. Statistical Optimization and Characterization of Bacterial Cellulose Produced by Isolated Thermophilic *Bacillus Licheniformis* Strain ZBT2. *Carbohydr. Res.* **2020**, *491*, 107979. [\[CrossRef\]](#) [\[PubMed\]](#)
- Velmurugan, P.; Myung, H.; Govarthanan, M.; Yi, Y.J.; Seo, S.K.; Cho, K.M.; Lovanh, N.; Oh, B.T. Production and Characterization of Bacterial Cellulose by *Leifsonia* Sp. CBNU-EW3 Isolated from the Earthworm, *Eisenia Fetida*. *Biotechnol. Bioprocess Eng.* **2015**, *20*, 410–416. [\[CrossRef\]](#)
- Khan, H.; Kadam, A.; Dutt, D. Studies on Bacterial Cellulose Produced by a Novel Strain of *Lactobacillus* Genus. *Carbohydr. Polym.* **2020**, *229*, 115513. [\[CrossRef\]](#) [\[PubMed\]](#)
- Tanskul, S.; Amornthatree, K.; Jaturonlak, N. A New Cellulose-Producing Bacterium, *Rhodococcus* sp. MI 2: Screening and Optimization of Culture Conditions. *Carbohydr. Polym.* **2013**, *92*, 421–428. [\[CrossRef\]](#) [\[PubMed\]](#)
- Arrebola, E.; Carrión, V.J.; Gutiérrez-Barranquero, J.A.; Pérez-García, A.; Rodríguez-Palenzuela, P.; Cazorla, F.M.; de Vicente, A. Cellulose Production in *Pseudomonas Syringae* Pv. *Syringae*: A Compromise between Epiphytic and Pathogenic Lifestyles. *FEMS Microbiol. Ecol.* **2015**, *91*, fiv071. [\[CrossRef\]](#) [\[PubMed\]](#)
- Monteiro, C.; Saxena, I.; Wang, X.; Kader, A.; Bokranz, W.; Simm, R.; Nobles, D.; Chromek, M.; Brauner, A.; Brown, R.M.; et al. Characterization of Cellulose Production in *Escherichia Coli* Nissle 1917 and Its Biological Consequences. *Environ. Microbiol.* **2009**, *11*, 1105–1116. [\[CrossRef\]](#)
- Cannon, R.E.; Anderson, S.M. Biogenesis of Bacterial Cellulose. *Crit. Rev. Microbiol.* **1991**, *17*, 435–447. [\[CrossRef\]](#)

18. Hungund, B.S.; Gupta, S.G. Production of Bacterial Cellulose from *Enterobacter Amnigenus* GH-1 Isolated from Rotten Apple. *World J. Microbiol. Biotechnol.* **2010**, *26*, 1823–1828. [CrossRef]
19. Römling, U.; Lünsdorf, H. Characterization of Cellulose Produced by *Salmonella Enterica* Serovar Typhimurium. *Celulose* **2004**, *11*, 413–418. [CrossRef]
20. Aswini, K.; Gopal, N.O.; Uthandi, S. Optimized Culture Conditions for Bacterial Cellulose Production by *Acetobacter Senegalensis* MA1. *BMC Biotechnol.* **2020**, *20*, 46. [CrossRef]
21. Ullah, M.W.; Ul-Islam, M.; Khan, S.; Kim, Y.; Park, J.K. Innovative Production of Bio-Cellulose Using a Cell-Free System Derived from a Single Cell Line. *Carbohydr. Polym.* **2015**, *132*, 286–294. [CrossRef]
22. Żywicka, A.; Junka, A.F.; Szymczyk, P.; Chodaczek, G.; Grzesiak, J.; Sedghizadeh, P.P.; Fijałkowski, K. Bacterial Cellulose Yield Increased over 500% by Supplementation of Medium with Vegetable Oil. *Carbohydr. Polym.* **2018**, *199*, 294–303. [CrossRef]
23. Comini, S.; Scutera, S.; Sparti, R.; Banche, G.; Coppola, B.; Bertea, C.M.; Bianco, G.; Gatti, N.; Cuffini, A.M.; Palmero, P.; et al. Combination of Poly ( $\epsilon$ -Caprolactone) Biomaterials and Essential Oils to Achieve Anti-Bacterial and Osteo-Proliferative Properties for 3D-Scaffolds in Regenerative Medicine. *Pharmaceutics* **2022**, *14*, 1873. [CrossRef]
24. Lemnaru, G.M.; Truşcă, R.D.; Ilie, C.I.; Țiplea, R.E.; Fica, D.; Oprea, O.; Stoica-Guzun, A.; Fica, A.; Diţu, L.M. Antibacterial Activity of Bacterial Cellulose Loaded with Bacitracin and Amoxicillin: In Vitro Studies. *Molecules* **2020**, *25*, 4069. [CrossRef]
25. Pal, S.; Nisi, R.; Stoppa, M.; Licciulli, A. Silver-Functionalized Bacterial Cellulose as Antibacterial Membrane for Wound-Healing Applications. *ACS Omega* **2017**, *2*, 3632–3639. [CrossRef] [PubMed]
26. Miyashiro, D.; Hamano, R.; Umamura, K. A Review of Applications Using Mixed Materials of Cellulose, Nanocellulose and Carbon Nanotubes. *Nanomaterials* **2020**, *10*, 186. [CrossRef] [PubMed]
27. Bodea, I.M.; Cătunescu, G.M.; Pop, C.R.; Fit, N.I.; David, A.P.; Dudesu, M.C.; Stănilă, A.; Rotar, A.M.; Beteg, E.I. Antimicrobial Properties of Bacterial Cellulose Films Enriched with Bioactive Herbal Extracts Obtained by Microwave-Assisted Extraction. *Polymers* **2022**, *14*, 1435. [CrossRef] [PubMed]
28. Zheng, L.; Li, S.; Luo, J.; Wang, X. Latest Advances on Bacterial Cellulose-Based Antibacterial Materials as Wound Dressings. *Front. Bioeng. Biotechnol.* **2020**, *8*, 593768. [CrossRef]
29. Bush, K. Synergistic Antibiotic Combinations. *Top. Med. Chem.* **2017**, *25*, 169–244. [CrossRef]
30. Guo, C.; Cheng, F.; Liang, G.; Zhang, S.; Duan, S.; Fu, Y.; Marchetti, F.; Zhang, Z.; Du, M. Multimodal Antibacterial Platform Constructed by the Schottky Junction of Curcumin-Based Bio Metal—Organic Frameworks and  $Ti_3C_2T_x$  MXene Nanosheets for Ef Fi Cient Wound Healing. *Adv. NanoBiomed Res.* **2022**, *2*, 2200064. [CrossRef]
31. Praditya, D.; Kirchhoff, L.; Brüning, J.; Rachmawati, H.; Steinmann, J.; Steinmann, E. Anti-Infective Properties of the Golden Spice Curcumin. *Front. Microbiol.* **2019**, *10*, 912. [CrossRef]
32. Zorofchian Moghadamtousi, S.; Abdul Kadir, H.; Hassandarvish, P.; Tajik, H.; Abubakar, S.; Zandi, K. A Review on Antibacterial, Antiviral, and Antifungal Activity of Curcumin. *Biomed. Res. Int.* **2014**, *2014*, 186864. [CrossRef]
33. Chiaoprakobkij, N.; Suwanmajo, T.; Sanchavanakit, N. Curcumin-Loaded Bacterial Cellulose/Alginate/Gelatin. *Mol. Impr. Sens.* **2020**, *25*, 3800. [CrossRef]
34. Gupta, A.; Keddie, D.J.; Kannappan, V.; Gibson, H.; Khalil, I.R.; Kowalczyk, M.; Martin, C.; Shuai, X.; Radecka, I. Production and Characterisation of Bacterial Cellulose Hydrogels Loaded with Curcumin Encapsulated in Cyclodextrins as Wound Dressings. *Eur. Polym. J.* **2019**, *118*, 437–450. [CrossRef]
35. Khamrai, M.; Banerjee, S.L.; Paul, S.; Samanta, S.; Kundu, P.P. Curcumin Entrapped Gelatin/Ionically Modified Bacterial Cellulose Based Self-Healable Hydrogel Film: An Eco-Friendly Sustainable Synthesis Method of Wound Healing Patch. *Int. J. Biol. Macromol.* **2019**, *122*, 940–953. [CrossRef]
36. Sajjad, W.; He, F.; Ullah, M.W.; Ikram, M.; Shah, S.M.; Khan, R.; Khan, T.; Khalid, A.; Yang, G.; Wahid, F. Fabrication of Bacterial Cellulose-Curcumin Nanocomposite as a Novel Dressing for Partial Thickness Skin Burn. *Front. Bioeng. Biotechnol.* **2020**, *8*, 553037. [CrossRef]
37. Shefa, A.A.; Sultana, T.; Park, M.K.; Lee, S.Y.; Gwon, J.G.; Lee, B.T. Curcumin Incorporation into an Oxidized Cellulose Nanofiber-Polyvinyl Alcohol Hydrogel System Promotes Wound Healing. *Mater. Des.* **2020**, *186*, 108313. [CrossRef]
38. Subtaweessin, C.; Woraham, W.; Taokaew, S.; Chiaoprakobkij, N.; Senemasapun, A.; Phisalaphong, M. Characteristics of Curcumin-Loaded Bacterial Cellulose Films and Anticancer Properties against Malignant Melanoma Skin Cancer Cells. *Appl. Sci.* **2018**, *8*, 1188. [CrossRef]
39. Xu, Y.; Liu, X.; Jiang, Q.; Yu, D.; Xu, Y.; Wang, B.; Xia, W. Development and Properties of Bacterial Cellulose, Curcumin, and Chitosan Composite Biodegradable Films for Active Packaging Materials. *Carbohydr. Polym.* **2021**, *260*, 117778. [CrossRef]
40. Adamczak, A.; Ożarowski, M.; Karpiński, T.M. Curcumin, a Natural Antimicrobial Agent with Strain-Specific Activity. *Pharmaceutics* **2020**, *13*, 153. [CrossRef]
41. Barud, H.S.; Regiani, T.; Marques, R.E.C.; Lustr, W.R.; Messaddeq, Y.; Ribeiro, S.J.L. Antimicrobial Bacterial Cellulose-Silver Nanoparticles Composite Membranes. *J. Nanomater.* **2011**, *2011*, 721631. [CrossRef]
42. Fadakar Sarkandi, A.; Montazer, M.; Harifi, T.; Mahmoudi Rad, M. Innovative Preparation of Bacterial Cellulose/Silver Nanocomposite Hydrogels: In Situ Green Synthesis, Characterization, and Antibacterial Properties. *J. Appl. Polym. Sci.* **2021**, *138*, 49824. [CrossRef]
43. Stanisławska, A. Bacterial Nanocellulose as a Microbiological Derived Nanomaterial. *Adv. Mater. Sci.* **2016**, *16*, 67. [CrossRef]

44. Kalantari, K.; Afifi, A.M.; Moniri, M.; Moghaddam, A.B.; Kalantari, A.; Izadiyan, Z. Autoclave-Assisted Synthesis of AgNPs in *Z. Officinale* Extract and Assessment of Their Cytotoxicity, Antibacterial and Antioxidant Activities. *IET Nanobiotechnology* **2019**, *13*, 262–268. [\[CrossRef\]](#)
45. Wu, J.; Zheng, Y.; Wen, X.; Lin, Q.; Chen, X.; Wu, Z. Silver Nanoparticle/Bacterial Cellulose Gel Membranes for Antibacterial Wound Dressing: Investigation In Vitro and In Vivo. *Biomed. Mater.* **2014**, *9*, 035005. [\[CrossRef\]](#)
46. Nicomrat, D. Silver Nanoparticles Impregnated Bio-cellulose Produced by Sweet Glutinous Rice Fermentation with the Genus *Acetobacter*. *E3S Web Conf.* **2020**, *141*, 03003. [\[CrossRef\]](#)
47. Maneerung, T.; Tokura, S.; Rajaravani, R. Impregnation of Silver Nanoparticles into Bacterial Cellulose for Antimicrobial Wound Dressing. *Carbohydr. Polym.* **2008**, *72*, 43–51. [\[CrossRef\]](#)
48. Pourali, P.; Yahyaee, B.; Ajoudanifaz, H.; Taheri, R.; Alavi, H.; Hoseini, A. Impregnation of the Bacterial Cellulose Membrane with Biologically Produced Silver Nanoparticles. *Curr. Microbiol.* **2014**, *69*, 785–793. [\[CrossRef\]](#)
49. Wang, C.; Liu, W.; Cao, H.; Jia, L.; Liu, P. Cellulose Nanofibers Aerogels Functionalized with Ag<sub>0</sub>: Preparation, Characterization and Antibacterial Activity. *Int. J. Biol. Macromol.* **2022**, *194*, 58–65. [\[CrossRef\]](#)
50. Wan, Y.; Yang, S.; Wang, J.; Gan, D.; Gama, M.; Yang, Z.; Zhu, Y.; Yao, B.; Luo, H. Scalable Synthesis of Robust and Stretchable Composite Wound Dressings by Dispersing Silver Nanowires in Continuous Bacterial Cellulose. *Compos. Part B Eng.* **2020**, *199*, 108259. [\[CrossRef\]](#)
51. Lu, W.; Yao, K.; Wang, J.; Yuan, J. Ionic Liquids-Water Interfacial Preparation of Triangular Ag Nanoplates and Their Shape-Dependent Antibacterial Activity. *J. Colloid Interface Sci.* **2015**, *437*, 35–41. [\[CrossRef\]](#) [\[PubMed\]](#)
52. Pal, S.; Tak, Y.K.; Song, J.M. Does the Antibacterial Activity of Silver Nanoparticles Depend on the Shape of the Nanoparticle: A Study of the Gram-Negative Bacterium *Escherichia coli*. *Appl. Environ. Microbiol.* **2007**, *73*, 1712–1720. [\[CrossRef\]](#) [\[PubMed\]](#)
53. Van Dong, P.; Ha, C.H.; Binh, L.T.; Kasbohm, J. Chemical Synthesis and Antibacterial Activity of Novel-Shaped Silver Nanoparticles. *Int. Nano Lett.* **2012**, *2*, 9. [\[CrossRef\]](#)
54. Vo, Q.K.; Phung, D.D.; Nguyen, Q.N.V.; Thi, H.H.; Thi, N.H.N.; Thi, P.P.N.; Bach, L.G.; Tan, L. Van Controlled Synthesis of Triangular Silver Nanoplates by Gelatin-Chitosan Mixture and the Influence of Their Shape on Antibacterial Activity. *Processes* **2019**, *7*, 873. [\[CrossRef\]](#)
55. Akrami-Hasan-Kohal, M.; Tayebi, L.; Ghorbani, M. Curcumin-Loaded Naturally-Based Nanofibers as Active Wound Dressing Mats: Morphology, Drug Release, Cell Proliferation, and Cell Adhesion Studies. *New J. Chem.* **2020**, *44*, 10343–10351. [\[CrossRef\]](#)
56. Miñano, J.; Puiggali, J.; Franco, L. Effect of Curcumin on Thermal Degradation of Poly(Glycolic Acid) and Poly( $\epsilon$ -Caprolactone) Blends. *Thermochim. Acta* **2020**, *693*, 178764. [\[CrossRef\]](#)
57. Gea, S.; Reynolds, C.T.; Roohpour, N.; Wirjosentono, B.; Soykeabkaew, N.; Bilotti, E.; Peijs, T. Investigation into the Structural, Morphological, Mechanical and Thermal Behaviour of Bacterial Cellulose after a Two-Step Purification Process. *Bioresour. Technol.* **2011**, *102*, 9105–9110. [\[CrossRef\]](#)
58. Wang, S.S.; Han, Y.H.; Chen, J.L.; Zhang, D.C.; Shi, X.X.; Ye, Y.X.; Chen, D.L.; Li, M. Insights into Bacterial Cellulose Biosynthesis from Different Carbon Sources and the Associated Biochemical Transformation Pathways in *Komagataeibacter* sp. W1. *Polymers* **2018**, *10*, 963. [\[CrossRef\]](#)
59. Chen, X.; Zou, L.Q.; Niu, J.; Liu, W.; Peng, S.F.; Liu, C.M. The Stability, Sustained Release and Cellular Antioxidant Activity of Curcumin Nanoliposomes. *Molecules* **2015**, *20*, 14293–14311. [\[CrossRef\]](#)
60. Ismail, E.H.; Sabry, D.Y.; Mahdy, H.; Khalil, M.M.H. Synthesis and Characterization of Some Ternary Metal Complexes of Curcumin with 1,10-Phenanthroline and Their Anticancer Applications. *J. Sci. Res.* **2014**, *6*, 509–519. [\[CrossRef\]](#)
61. Nandiyanto, A.B.D.; Wiryani, A.S.; Rusli, A.; Purnamasari, A.; Abdullah, A.G.; Ana; Widiaty, I.; Hurriyati, R. Extraction of Curcumin Pigment from Indonesian Local Turmeric with Its Infrared Spectra and Thermal Decomposition Properties. *Mater. Sci. Eng.* **2017**, *755*, 012136. [\[CrossRef\]](#)
62. Gunasekaran, S.; Natarajan, R.K.; Natarajan, S.; Rathikha, R. Structural Investigation on Curcumin. *Asian J. Chem.* **2008**, *20*, 2903–2913.
63. Wang, S.S.; Han, Y.H.; Ye, Y.X.; Shi, X.X.; Xiang, P.; Chen, D.L.; Li, M. Physicochemical Characterization of High-Quality Bacterial Cellulose Produced by *Komagataeibacter* sp. Strain W1 and Identification of the Associated Genes in Bacterial Cellulose Production. *RSC Adv.* **2017**, *7*, 45145–45155. [\[CrossRef\]](#)
64. Andreani, T.; Nogueira, V.; Pinto, V.V.; Ferreira, M.J.; Rasteiro, M.G.; Silva, A.M.; Pereira, R.; Pereira, C.M. Influence of the Stabilizers on the Toxicity of Metallic Nanomaterials in Aquatic Organisms and Human Cell Lines. *Sci. Total Environ.* **2017**, *607–608*, 1264–1277. [\[CrossRef\]](#)
65. Ha, N.M.; Tran, S.H.; Shim, Y.H.; Kang, K. *Caenorhabditis Elegans* as a Powerful Tool in Natural Product Bioactivity Research. *Appl. Biol. Chem.* **2022**, *65*, 18. [\[CrossRef\]](#)
66. Li, Y.; Zhong, L.; Zhang, L.; Shen, X.; Kong, L.; Wu, T. Research Advances on the Adverse Effects of Nanomaterials in a Model Organism, *Caenorhabditis Elegans*. *Environ. Toxicol. Chem.* **2021**, *40*, 2406–2424. [\[CrossRef\]](#)
67. Hooshmand, S.E.; Ebadati, A.; Hosseini, E.S.; Vahabi, A.H.; Oshaghi, M.; Rahighi, R.; Orooji, Y.; Jahromi, M.A.M.; Varma, R.S.; Hamblin, M.R.; et al. Antibacterial, Antibiofilm, Anti-Inflammatory, and Wound Healing Effects of Nanoscale Multifunctional Cationic Alternating Copolymers. *Bioorg. Chem.* **2022**, *119*, 105550. [\[CrossRef\]](#)

68. Gupta, A.; Briffa, S.M.; Swingler, S.; Gibson, H.; Kannappan, V.; Adamus, G.; Kowalczyk, M.; Martin, C.; Radecka, I. Synthesis of Silver Nanoparticles Using Curcumin-Cyclodextrins Loaded into Bacterial Cellulose-Based Hydrogels for Wound Dressing Applications. *Biomacromolecules* **2020**, *21*, 1802–1811. [\[CrossRef\]](#) [\[PubMed\]](#)
69. Tyagi, P.; Singh, M.; Kumari, H.; Kumari, A.; Mukhopadhyay, K. Bactericidal Activity of Curcumin I Is Associated with Damaging of Bacterial Membrane. *PLoS ONE* **2015**, *10*, 0121313. [\[CrossRef\]](#)
70. Wu, J.Y.; Lin, C.Y.; Lin, T.W.; Ken, C.F.; Wen, Y. Der Curcumin Affects Development of Zebrafish Embryo. *Biol. Pharm. Bull.* **2007**, *30*, 1336–1339. [\[CrossRef\]](#)
71. Gao, X.P.; Feng, E.; Zhang, X.Q.; Liu, X.X.; Wang, Y.B.; She, J.X.; He, Z.H.; He, M.F. Toxicity Assessment of 7 Anticancer Compounds in Zebrafish. *Int. J. Toxicol.* **2014**, *33*, 98–105. [\[CrossRef\]](#) [\[PubMed\]](#)
72. Asharani, P.V.; Lian Wu, Y.; Gong, Z.; Valiyaveetil, S. Toxicity of Silver Nanoparticles in Zebrafish Models. *Nanotechnology* **2008**, *19*, 255102. [\[CrossRef\]](#) [\[PubMed\]](#)
73. Liao, V.H.C.; Yu, C.W.; Chu, Y.J.; Li, W.H.; Hsieh, Y.C.; Wang, T.T. Curcumin-Mediated Lifespan Extension in *Caenorhabditis Elegans*. *Mech. Ageing Dev.* **2011**, *132*, 480–487. [\[CrossRef\]](#) [\[PubMed\]](#)
74. Yang, X.; Gondikas, A.P.; Marinakos, S.M.; Auffan, M.; Liu, J.; Hsu-kim, H.; Meyer, J.N. Mechanism of Silver Nanoparticle Toxicity Is Dependent on Dissolved Silver and Surface Coating in *Caenorhabditis Elegans*. *Environ. Sci. Technol.* **2012**, *46*, 1119–1127. [\[CrossRef\]](#)
75. Garcia, E.L.; Attallah, O.A.; Mojovic, M.; Devine, D.M.; Fournet, M.B. Antimicrobial Active Bioplastics Using Triangular Silver Nanoplate Integrated Polycaprolactone and Poly(lactic Acid) Films. *Materials* **2021**, *14*, 1132. [\[CrossRef\]](#)
76. Molina-ramirez, C.; Enciso, C.; Torres-taborada, M.; Zuluaga, R.; Gañán, P.; Rojas, O.J.; Castro, C. Effects of Alternative Energy Sources on Bacterial Cellulose Characteristics Produced by *Komagataeibacter Medellinensis*. *Int. J. Biol. Macromol.* **2018**, *117*, 735–741. [\[CrossRef\]](#)
77. Mondal, S.; Ghosh, S.; Moulik, S.P. Stability of Curcumin in Different Solvent and Solution Media: UV-Visible and Steady-State Fluorescence Spectral Study. *J. Photochem. Photobiol. B Biol.* **2016**, *158*, 212–218. [\[CrossRef\]](#) [\[PubMed\]](#)
78. Hansen, M.B.; Nielsen, S.E.; Berg, K. Re-Examination and Further Development of a Precise and Rapid Dye Method for Measuring Cell Growth/Cell Kill. *J. Immunol. Methods* **1989**, *119*, 203–210. [\[CrossRef\]](#)
79. OECD. Test No. 236: Fish Embryo Acute Toxicity (FET) Test. In *OECD Guidelines for the Testing of Chemicals*; Section 2; OECD: Paris, France, 2013; ISBN 9789264203709.
80. Sternagle, T. Maintenance of *C. Elegans*. *WormBook* **2006**, *1*, 1–11. [\[CrossRef\]](#)
81. Brackman, G.; Cos, P.; Maes, L.; Nelis, H.J.; Coenye, T. Quorum Sensing Inhibitors Increase the Susceptibility of Bacterial Biofilms to Antibiotics In Vitro and In Vivo. *Antimicrob. Agents Chemother.* **2011**, *55*, 2655–2661. [\[CrossRef\]](#)